Advances for Urban Planning in Highly Dynamic Environments through very High-Resolution Remote Sensing Approaches

Dissertation

der Mathematisch-Naturwissenschaftlichen Fakultät

der Eberhard Karls Universität Tübingen

zur Erlangung des Grades eines

Doktors der Naturwissenschaften

(Dr. rer. nat.)

vorgelegt von

M. Sc. Gebhard Warth

aus Kirchheim unter Teck

Tübingen

2022

Gedruckt mit Genehmigung der Mathematisch-Naturwissenschaftlichen Fakultät der Eberhard Karls Universität Tübingen.

Tag der mündlichen Qualifikation:	17.02.2022
Dekan:	Prof. Dr. Thilo Stehle
1. Berichterstatter/-in:	Prof. Dr. Volker Hochschild
2. Berichterstatter/-in:	Prof. Dr. Michael Peterek

Content

Tables

Figures

Abbreviations

AI	Artificial intelligence
BT	Building-types
CIAM	Congrès Internationaux d'Architecture Moderne
DL	deep learning
DSM	digital surface model
EO	earth observation
ESA	European Space Agency
EU	European Union
FOR	fields of roof
GI	green infrastructure
GNI	gross national income
GSD	ground sample distance
GUF	Global Urban Footprint
IPCC	International Panel on Climate Change
IWM	Integrated water management
LiDAR	light detection and ranging
LULC	Land use/Land cover
MDG	Millennium Development Goals
MDP	Municipal Development Plan
MFBT	multifamily building-type
MSWM	Municipal solid waste management
NASA	National Aeronautics and Space Administration
nDSM	normalized DSM
NREL	National Renewable Energy Laboratory
NSRDB	National Solar Radiation Database
NUA	New Urban Agenda
OBIA	Object-based image analysis
OSM	OpenStreetMap
PV	Photovoltaic
RS	Remote Sensing
SDG	Sustainable Development Goals
SES	socioeconomic status
SEC	socioeconomic class
SEP	Socioeconomic points
SFBT	single-family building-type
UGI	Urban green spaces
UHI	urban heat island
VHR	very high-resolution

Zusammenfassung

Die fortschreitende Urbanisierung und der Klimawandel stellen Städte und Stadtplanung vor große Herausforderungen. Der Lebensraum für die Bewohner und die Infrastruktur müssen entsprechend den Klimaschutzanforderungen angepasst werden, zudem muss die Resilienz urbaner Räume gegenüber Klimawandelwandelfolgen erhöht werden. Ziel der urbanen Planung und urbanen Infrastrukturplanung ist vor diesem Hintergrund im Auftrag der Gesellschaft Lösungen zu finden, um diesen Anforderungen der Zukunft gerecht zu werden und um lebenswerte Städte mit allen städtischen Funktionen zu gewährleisten. Zudem müssen durch Planer ökonomische und ökologisch geeignete Vorschläge für die Bereitstellung urbaner Infrastruktur gefunden werden, um Grundbedürfnisse zu erfüllen und Slums zurückzudrängen. Gute Planungspraxis erfordert dafür die Entwicklung von Planungsszenarien für angemessene, erfolgreiche und integrierte Lösungen, wobei eine Datenbasis als Entscheidungsgrundlage dienen muss, die durch Datenkonsistenz, -qualität und -aktualität als Evidenz für Szenarienentwicklung herangezogen werden kann.

In dieser Dissertationsschrift wird durch drei Studien gezeigt, dass die Disziplin der Fernerkundung durch die Verwendung sehr hochaufgelöster Erdbeobachtungsdaten einen Beitrag für erfolgreiche urbane Planung und urbane Infrastrukturplanung leisten kann, indem der Informationsgehalt bisheriger Fernerkundungsansätze unter Verwendung anwendungsfreundlicher Ansätze erhöht werden kann und direkt planungsrelevante Informationen als Evidenz für die Entscheidungsfindung bereitgestellt werden kann.

In den hochdynamischen Städten Da Nang (VN) und Belmopan (BZ) konnte an dieser Thematik gearbeitet werden. Durch die Differenzierung photogrammetrisch abgeleiteter Höhenmodelle in sehr hoher Auflösung wurden in Da Nang anstatt flächenhafter Änderungen urbaner Gebiete Dynamiken innerhalb des Gebäudebestands bestimmt und evaluiert. Der Gebäudetyp kann, wie in Belmopan gezeigt, als geeignetes Mittel für Abschätzung sozioökonomischer Indikatoren dienen, die in Zusammenhang mit spezifischen Verbräuchen stehen. Mit der Verwendung von Drohnendaten wurde die Bestimmung der Gebäudetypen verbessert und zudem der Zusammenhang zwischen Gebäudetyp und Stromverbrauch gezeigt, wodurch eine Photovoltaikenergie-Bilanzierung auf Einzelgebäudeebene durchgeführt werden konnte.

Abstract

Ongoing urbanization and climate change pose major challenges for cities and urban planning. The living space for residents and the infrastructure must be adapted to meet climate protection requirements, and the resilience of urban areas to the effects of climate change must be increased. Against this background, the aim of urban planning and urban infrastructure planning is to find solutions on behalf of society to meet these future requirements and to ensure livable cities with all urban functions. In addition, planners must find economically and ecologically appropriate solutions for the provision of urban infrastructure to meet basic needs and reduce slums. Good planning practice requires the development of planning scenarios for appropriate, successful and integrated solutions, using a database as a foundation for decision-making that can be used as evidence for scenario development through data consistency, quality and timeliness.

In this dissertation paper, it is shown through three studies that the discipline of remote sensing can contribute to improve urban planning and urban infrastructure planning through the use of very high-resolution earth observation data by increasing the information content of previous remote sensing applications using application-friendly approaches and directly providing planning-relevant information as evidence for decision making.

In the highly dynamic cities of Da Nang (VN) and Belmopan (BZ), work could be accomplished on this topic. By differentiating through photogrammetrically derived elevation models in very high spatial resolution, instead of areal changes of urban areas, dynamics within the building stock were determined and evaluated in Da Nang. Building-type, as shown in Belmopan, can serve as a suitable instrument for estimating socioeconomic indicators related to specific consumptions. With the use of drone data, the determination of the building-type was improved compared to satellite imagery and, in addition, the relationship between building-type and electricity consumption was shown, making it possible to perform photovoltaic energy balancing at the individual building level.

Publication List for the Dissertation

a) Accepted publications as first author:

1. **Warth, G.**, Braun, A., Bödinger, C., Hochschild, V. and Bachofer, F. (2019) 'DSM-Based Identification of Changes in Highly Dynamic Urban Agglomerations', *European Journal of Remote Sensing*, vol. 52, no. 1, pp. 322–334.

2. **Warth, G.**, Braun, A., Assmann, O., Fleckenstein, K. and Hochschild, V. (2020) 'Prediction of Socioeconomic Indicators for Urban Planning Using VHR Satellite Imagery and Spatial Analysis', *Remote Sensing*, vol. 12, no. 11, p. 1730.

b) Submitted manuscripts as first author:

3. **Warth, G.**, Assmann, O., Fleckenstein, K., Braun, A. and Hochschild, V. (2021) 'Photovoltaic Energy Balancing in Belmopan Based on Building-Types, UAV Aerial Imagery and Household Data', *Geography and Sustainability (under review)*.

Related Work through Scientific Contributions

Warth, G., Braun, A., Bachofer, F. and Hochschild, V. (2018) 'Urban Structure Mapping and change Analysis in Highly Dynamic Urban Areas Based on Spectral and Three-Dimensional Analysis of VHR Remote Sensing Imagery' *Mapping Urban Areas from Space (MUAS),* Frascati.

- Study cities: Kigali, Rwanda & Da Nang, Vietnam
- Research question: Presenting the capabilities of remote sensing applications to provide information on urban characteristics and planning relevant information.
- Data & methods: Determination of urban structure types and the relevance of urban structure types using very high-resolution WorldView data in order to generating an understanding for urban areas and urban morphology.

Braun, A., Warth, G., Bachofer, F. and Hochschild, V. (2019) 'Identification of Roof Materials in High-Resolution Multispectral Images for Urban Planning and Monitoring' *Joint Urban Remote Sensing Event (JURSE)*, Vannes. doi: 10.1109/JURSE.2019.8809026.

- Study city: Kigali, Rwanda

- Research question: Using single building footprints as spatial reference and Sentinel-2 and WorldView-4 satellite imagery in order to extract roof material information from multi- and hyperspectral information.
- Data & Methods: Application of the spectral unmixing method WorldView-4 imagery with 16 spectral bands to detect and locate roof materials as indicator of socioeconomic status.

Vetter-Gindele, J., Braun, A., Warth, G., Bui, T.T.Q., Bachofer, F., Eltrop, L. (2019) 'Assessment of Household Solid Waste Generation and Composition by Building-type in Da Nang, Vietnam' *Resources*, vol. 8, no. 171. https://doi.org/10.3390/resources8040171

- Study City: Da Nang, Vietnam
- Research question: Assessment of household solid waste production for five building types in Da Nang.
- Data & methods: Building type determination accomplished by means of satellite image analysis, household solid waste analysis through on the basis of empirical data collected through household surveys in Da Nang.

Braun, A., Warth, G., Bachofer, F., Quynh Bui, T.T., Tran, H., Hochschild, V. (2020) 'Changes in the Building Stock of Da Nang between 2015 and 2017'. *Data*, vol. 5, no. 42. https://doi.org/10.3390/data5020042

- Study City: Da Nang, Vietnam
- Research demand: Generation and provision of a building reference dataset for Da Nang and change analysis on a single building level.
- Data & methods: A single building dataset of Da Nang for 2015 was generated using very high-resolution Pléiades imagery, on which subsequently, changes were identified by visual interpretation and comparison with a Pléiades acquisition of 2017.

Matabishi, J.-G., Warth, G., Braun, A. (2021, under review): 'MESMA Of DESIS Data to Identify Rooftops in Kigali City' *1st DESIS User Workshop*, Munich

- Study city: Kigali, Rwanda
- Research question: Evaluation of the suitability of hyperspectral imagery from DESIS to determine specific roof materials.
- Data & methods: DESIS imagery from February 2020 with 235 spectral bands between 400 and 1,000 nanometers, rooftop materials collected in Kigali: sheet metal, corrugated metal, clay tiles in different designs and conditions.

Foreword

Ongoing urbanization and unclear effects of the climate change challenge urban planning and urban infrastructure planning, especially in developing countries where a scarcity of well-trained planners and established planning routines exist. Through the work within the BMBF funded RapidPlanning project I got in touch with this discipline in which an interdisciplinary team developed approaches to bring forward evidence-based planning for supply and disposal infrastructure. Remote sensing in this framework has a major relevance to contribute in this process by providing planning relevant base data. According to my conviction that remote sensing could provide information for the process of planning urban supply and disposal infrastructure going beyond describing urban characteristics, the studies for this doctoral thesis were designed to show the ability to provide planning-ready data for the planning processes.

First of all, I hereby want give thanks to Prof. Dr. Volker Hochschild, who offered me the possibility to join the RapidPlanning project in early 2018. Through his leap of trust into my work, I could contribute to the projects with own ideas and develop several project proposals our partners. I do not take it for granted that he always has an open door for us and is a contact person. In the same way I want to give my thanks to Prof. Dr. Michael Peterek not only for his willingness to supervise and accompany this thesis, but as well the very good and pleasant cooperation in the research projects. Special thanks to Dr. Oliver Assmann, with whom I developed and discussed ideas for hours and who offered me a non-geographer view on the work. Dr. Andreas Braun and Dr. Christian Sommer always are always open to discuss ideas and to share their knowledge, for which I cannot give enough thanks. I extent these thanks to our complete work group to Christian B., Jörg, Lizzy, Zara, Silvia, Sandy and Tamara, but as well as the former colleagues Hans, Adel, Felix, Geraldine, Janine, and Alice, who always a nice and motivating atmosphere. Special thanks to Hanna Usbeck-Frei and Carolyn Duffy for their language edits. Last but not least I want to thank my family and especially my wife Elisa and for their support and encouragement during the past time.

Besides all lessons learnt on remote sensing techniques, spatial data analysis, integrated urban infrastructure planning and international collaboration I was very much impressed by the passion of our local partners in the project cities Kigali, Da Nang and Belmopan and their motivation to

contribute to progress and growing wealth in their home towns and countries. At the same time, on of the biggest problems in urban infrastructure planning and city administration became apparent: Once administration employees get qualified through training, they often get poached or moved to other positions. Such processes prevent stability in the planning departments and knowledge concentration. Accordingly, planning procedures in such environments must be reduced in complexity and offer low obstacle subprocesses. In this context my personal motivation in the context of this doctoral thesis emerged to study comprehensible approaches that could be implemented in the local planning practice.

In this thesis I present my research to address the challenge for the development of approaches to support urban infrastructure planning by providing data and information from very high-resolution remote sensing data. In the first section, I give an introduction into the thematic context of urbanization, urban planning and infrastructure planning. Furthermore, by giving an overview on the recent literature on remote sensing research in the urban context, I present the state of the arts and derive the research deficit in the face of ongoing urbanization. After defining the objectives of my work, the three research papers for this thesis are presented in the results section. The thesis concludes with the discussion section and the further outlook.

1. Introduction

This doctoral thesis summarizes, concludes and discusses three research papers which adress improving data provision approaches for urban planning, especially urban infrastructure planning in highly dynamic urban systems. In order to present the relevance of this thesis, the following chapters provide the thematic frame. By introducing the topic of urbanization, urban planning, and presenting the state of the art of remote sensing applications to support urban planning, the relevance and necessity for urban planning is being underlined. Furthermore, deficits and challenges in urban planning, and the potential of remote sensing applications to support it are highlighted.

1.1. The Urbanized Planet

Urbanization as the process of increasing the share of the urban dwelling population, challenges cities and administrations to meet its residents demands on quality of life and to provide urban functions for all groups of the society. Although the largest urbanization rates have been observed in the second half of the 20th century (UNDESA, 2019), the process begins very early in history. It can be categorized into four major phases (Kraas et al., 2016). The first pre-historic and antique epoch of urbanization started in Mesopotamia, from where the process continued over the Fertile Crescent, the Nile Valley, and the Mediterranean region (Mumford, 1956). The second main phase of urbanization was during the high medieval phase, where cities in Europe evolved and city foundations were intentionally supported by the rulers (Jöchner, 2011). The third phase of urbanization accompanied the period of industrialization starting in the middle of the 19th century. The need of labor forces and the specialization of the businesses caused migration from the rural areas to the industrial regions and resulted in massive growth in urban population (McNeill and Engelke, 2013). The fourth and present phase of urbanization is a phase of global urbanization, in which urbanization processes occur on the global scale (Kraas et al., 2016). Developed countries entered this phase after World War II, when the agricultural sector went through an intensive transition into a highly mechanized and almost industrialized sector and progress in transportation systems enabled global distribution of goods. In the meantime, processes of urban shrinking can be observed in some developed countries (UNDESA, 2015). In developing countries, especially in Asia and Africa, the growth of the urbanized population is very fast. The "urban turning point" in 2007

marked a very important date in this steady process of urbanization, with more than 50 % of the global population living in cities (UN-Habitat, 2006). In 2022, 57 % of the global population is expected be urbanized. According to UN data, 60.4 % of the global population will be living in cities and 68.4 % in 2050 (UNDESA, 2019).

The main requirement for the formation of cities and urban structure is the food supply. Agriculture therefore needs to have developed such a productivity, that the urban population, which is not part of the agricultural sector, can sufficiently be supplied with food. Additionally, food transportation into the city must be ensured (Teuteberg, 1987). The growing agricultural productivity also resulted in labor efficiency and consequently, less need of labor forces, which enabled the rural population to leave the agricultural sector. Political, economic, and societal reasons were the drivers for urbanization through all epochs. Initially, cities offered security from external threats through fortification systems and stationed military. The gained security and consistency enabled urban development into economic centers through trade and proximity to political leaders. The following economic growth led to growing numbers of jobs for migrating population from rural areas (Kraas et al., 2016). To this day, economic reasons are one of the main factors for urbanization. Cities and urban areas promise income and wealth. UN data from 2011 shows that more than 90 % of the global GDP is earned in urban areas (Fragkias et al., 2013). The transformation in the social order lead to social innovation, such as production specialization, technological innovations, but as well social innovations like class-structured societies, law bases, and government in social structures which resulted in higher social complexity (Elmqvist et al., 2013). Besides economic reasons, social factors are very import for urbanization, as well. Access to secondary schools and universities, hospitals and other health care institutions, public institutions, culture, architecturally inspiring ambience, creative urban milieus and liberal lifestyles are found in cities. Therefore, cities served as models for social development from the beginning. Besides these pulling factors that entail migration, demographic dynamics caused by birth surpluses or reclassification of administrative units play an important role in urbanization as well (Kraas et al., 2016).

Megacities are characterized through either more than 10 million inhabitants (UNDESA, 2015) or 5 million inhabitants and a population density of larger than 2,000 inhabitants/km^2 (Bronger, 2004). Additionally, qualitative criteria have to be considered which confirm global relevance of

the city. In 2016, 28 cities worldwide were characterized as megacities, the number is expected to increase to 41 in 2030 Megacities will then be home to 14 % of the global urban population (Kraas et al., 2016). 9 % will live in 63 "*Emerging megacities*", which are defined by a population of 5-10 million inhabitants. The largest increase of population will have taken place in the *medium-sized cities*, defined through a population of 1-5 million inhabitants, from 128 million inhabitants in 1950 to 1.13 billion inhabitants in 2030. The share of the global population living in cities between 0.5 and 1 million inhabitants will remain almost stable between 1950 and 2030, the share is estimated to slightly increase from 8.8 % to 10.1 %. Although the share of the population living in smaller settlements with less than 300,000 inhabitants, as categorized by the UN (UNDESA, 2019), is expected to decrease from 60 % in 1950 to 38 % in 2030, 1.9 billion people will live in this city category which implicates the largest absolute numbers of growth in urban population (Seto et al., 2013). The expected population distribution within the presented city categories make clear that not only megacities or emerging megacities have to be in focus of urban planning and political decisions. Most of the urban population will live in small cities (Seto et al., 2013), which makes planning concepts for these cities essential increase living conditions for a large part of the global population.

As mentioned before, the year 2007 marked the urban turning point, in 2018 the UN estimated 55.3 % of the global population living in cities (UNDESA, 2019). The annual urbanization rate of 1.9 % results in growth of urbanized population. As shown in Figure 1, the process of urbanization is predicted by the UN to be ongoing for the next decades, although the non-uniform process of urbanization shows significant differences when comparing statistics on the continents. While Europe and Northern America have below-average urbanization rates, Africa and Asia are well above average. These regions, unlike Europe and North America, are currently comparably low urbanized. According to UN DESA data, Africa is 43.5 % urbanized and Asia is 51.1 % urbanized. Even though the urbanization rates on the global scale appear to evolve at a low level, the absolute number of urbanized population will still be growing. Since the largest increase in population is predicted for Africa and Asia (UNDESA, 2019), the will be facing major challenges for the urban sphere.

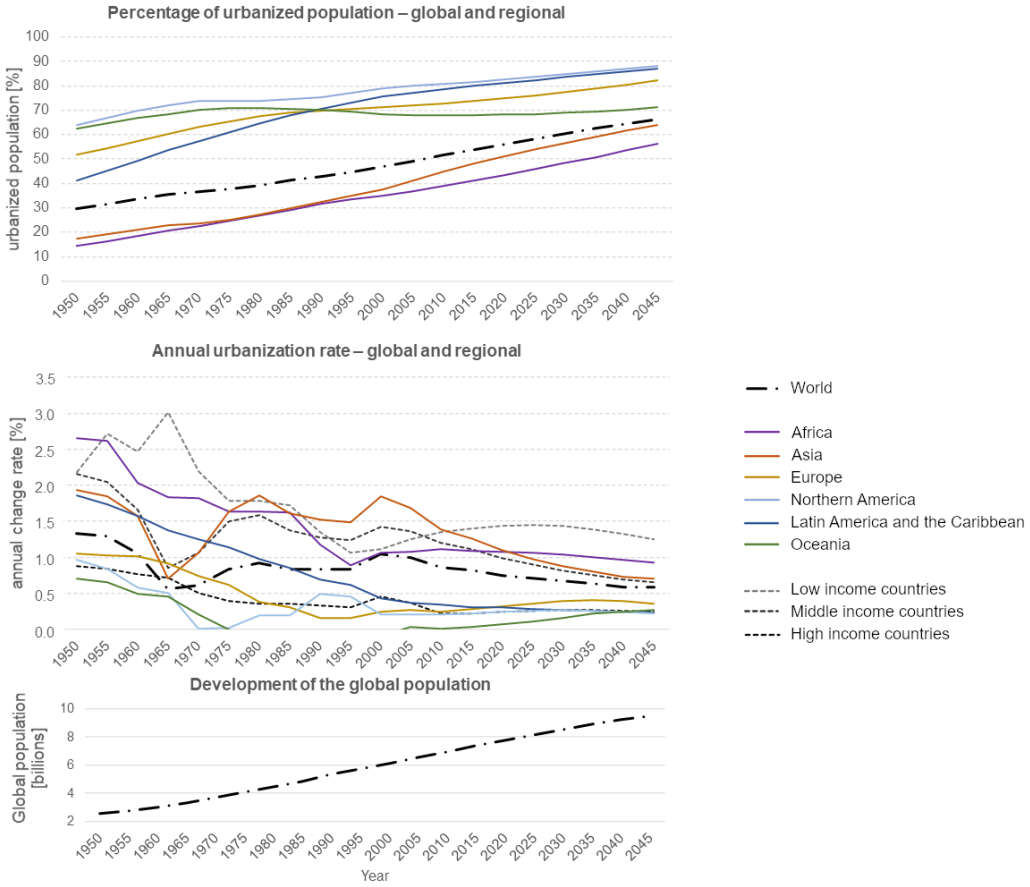

Figure 1: *Global and regional overview on urbanized population, urbanization rates and the global population according to individual city definitions by each country (United Nations, 2018).*

When interpreting UN DESA data, one must consider that no globally consistent definition of 'city' is applied for the statistics, but the definition of the respective country. Table 1 gives a comparison between the UN urbanization statistics and the percentage of the global population living in urban agglomerations with more than 300,000 inhabitants. This ensures a data comparability, albeit the threshold value of 300,000 is certainly not set ideally, because 85 of all capital cities do not even reach this population (UNDESA, 2019).

Table 1: *Comparison of percentage of urbanized population according to countries definitions and population living in urban agglomerations with more than 300,000 inhabitants (data: UN DESA 2019).*

	1950	1960	1970	1980	1990	2000	2010	2020	2030	2035
Urbanized population	30 %	34 %	37 %	39 %	43 %	47 %	52 %	56 %	60 %	63 %
Population in urban agglomerations >300,000 inhabitants	17 %	19 %	21 %	22 %	24 %	27 %	30 %	33 %	36 %	37 %

For further detailed statistics on urbanization, refer to the Word Urbanization Prospects: The 2018 revision (UNDESA, 2019).

The term "city" itself is very heterogeneously defined with large regional differences. For the 233 countries, UN-Habitat counted 104 different definitions for 'city' using a single criterion, such as administrative function, population size/density or urban characteristics (UN-Habitat, 2020c). Further 337 definitions were found in which multiple criteria form the definition.

In order to establish a uniform term and find a globally consistent measure to compare cities, UN-Habitat took up the multi-criteria city definitions from the New York University and the European Commission (European Commission, 2020; UN-Habitat, 2020c) (see Table 2). Both definitions base on a 1 km^2 raster, through which the definition can be applied through earth observation techniques on a global scale. Thus, independency from statistical information and census information is given and cities can be monitored transparently.

Besides positive effects of urbanization and the described factors of cities on page 2 being nuclei of economic and social development, urbanization causes negative consequences, especially through expansion of urban land use and urban sprawl. Projections indicate an increase in global urban land cover over 200 % between 2000 and 2030, global urban population on the other hand will grow by 70 % (Seto et al., 2013) and 88 % of protected areas will be effected by urban expansion through ecological and climatological effects (McDonald et al., 2008). Also, social challenges

Table 2: *City class definitions according to the New York University and the European Commission*

New York University: ***City as defined by its urban extent***		**European Commission:** ***Degree of urbanization***	
Urban built-up	1 km^2 units with built-up density >50 %	**High density cluster**	cluster of contiguous 1 km^2 units with >1,500 inhabitants/km^2 and a minimum population of 50,000
Suburban built-up	1 km^2 units with built-up densities between 25-50 %	**Urban cluster**	cluster of contiguous 1 km^2 units with >300 inh./km^2 and a min. population of 5,000
Rural built-up	1 km^2 units with built-up densities <25 %	**Rural grid cell**	1 km^2 cell outside of high-density and urban cluster

still remain dominant in the urban sphere. Even though the number of global urban population living in slum areas decreased significantly from 33 % in 2009 to 24 % in 2018 (Ritchie and Roser, 2018), the absolute number of slum dwellers increased by 42.9 % in the same period (Kraas et al., 2016).

This condensed description of ecological and social challenges already makes the need for proper urban planning very evident, in order to establish a socially and ecologically fair city development while also considering the upcoming challenges due to climate change and economic competitiveness.

1.2. Urban Planning

Urban planning is the endeavor to arrange urban areas to establish a spatial order considering the populations demands (Albers, 1988). Besides the needs of the population, economic, social, and environmental aspects have to be taken into account to ensure sustainable urban development. A large variety of different approaches, planning practices and activities does not allow for a single and unique definition. This in turn prevents from defining conventions for the urban planning process (Levin-Keitel et al., 2019). Good practice in urban planning however requires the cognitive anticipation of future acting, conditions and environment (Pahl-Weber and Schwartze, 2018). As a consequence, data, knowledge or evidence must be the main foundation and basis for accurate scenario development to support decision making in the urban planning process (Streich, 2011).

Initially urban planners focused on creative and esthetic design, yet post-world war II urban planning was in need of addressing sociological problems. Towards the end of the 20th century, environmental awareness in society had an impact in urban planning. Eventually participative and communicative methods achieved transparent planning as demanded by the society. This development explains the interdisciplinary character of urban planning, where different needs are met in architecture or engineering, but also ecological, social and economic aspects are handled (Pahl-Weber and Schwartze, 2018). Urban planning is an administrative task, which is set in between the

level of politics and the level of specialized disciplines (Pahl-Weber and Schwartze, 2018). Therefore, urban planners are service providers, independent from single interests and committed to the community and common interest (Levin-Keitel et al., 2019).

Though following interdisciplinary approaches, urban planning was strongly influenced by leading visions. The Athens Charter, mainly influenced by Le Corbusier and proclaimed by the Congrès Internationaux d'Architecture Moderne IV (CIAM IV) in 1933 (Mumford, 2002), was the guideline for planning cities as a 'Functional City'. After it became clear that the motor vehicle would replace the previous modes of transportation for goods and passengers, urban planning had to be adapted to this new perspective. Transportation infrastructure and city design were now planned in a car-oriented approach to reduce inner-city chaos through separating the functions of living, recreation, working and transport, considering traffic integration (Knie and Marz, 1997). Thus, the concept of the city machine or machine-centered functionalism was created (Knie and Marz, 1997). This charter dominated urban planning during the post-world-war-II era and enabled strong economic growth during this period, but also led to heavy land consumption at the expense of the natural environment.

In context of the sustainability debate, the negative developments of the Charter's approach were recognized and taken up by the Leipzig Charter from 2007, at least in the European Union's (EU) sphere of influence to support the EU Sustainable Development Strategy (BMUB, 2007). The focus of the Leipzig Charter lies on the approach of integrated urban planning, the development of a European polycentric urban structure to relieve transportation, the modernization of infrastructure and energy efficiency improvements, as well as the involvement of public, administrative, commercial and private stakeholders (BMUB, 2007).

As cities are the habitat for majority of global population since 2007, urban spaces offer the opportunity to reach the majority of the population, but urban planning is as well challenged to provide suitable planning for the business sector, addressing ecological issues and for different groups of the society. When urban planning does not address the concerns and needs of all socioeconomic groups, consequences are uncontrolled construction development, missing public infrastructure, congested road network, social fragmentation, poverty, unemployment, crime or

ecological degradation (Taubenböck and Dech, 2010a), which is often revealed through the formation of slum areas. The socioeconomic status (SES) hereby is a combined measure of economic and social status which considers education, income and occupation (Baker, 2014). Initially referred to in medical studies to explain health in residential groups (Schell and Denham, 2003; Winkler and Stolzenberg, 1998), the SES has recently been brought in connection with household waste production (Khan et al., 2016; Oribe-Garcia et al., 2015) and electricity consumption (Jones et al., 2015). The slum topic will be addressed in detail in section 1.3.

Subsequent to the Millennium Development Goals (MDG), which since 2000 defined the goals on the reduction of poverty and hunger, increase of education, health and environmental protection to be reached by 2015 (United Nations, 2015b), the 2030 Agenda for Sustainable Development extended the perspective through defining the 17 SDGs. These in part recall some MDGs but add topics like sustainability, climate action and specify social topics (United Nations, 2015a) in order to respond to the risks of climate change and environmental degradation as well as to reduce social and economic inequalities. As the majority of the global population since the global urban turning point in 2007 lives in cities, it can be reached through urban planning. Therefore, urban planning has the challenge and the opportunity to contribute strongly to the achievement of the SDGs. Figure 2 highlights goals, which can be addressed by urban planning.

Figure 2: *Sustainable Development Goals in the context of urban planning highlighted in color: SDG 3: Good health and well-being, SDG 4: Quality education, SDG 6: Clean water and sanitation, SDG 7: Affordable energy, SDG 9: Industry, innovation and infrastructure, SDG 10: Reduced inequalities, SDG 11: Sustainable cities and communities, SDG 13: Climate action and SDG 17: Partnerships for the goals (United Nations, 2015a).*

Already during HABITAT III, the United Nations Conference on Housing and Sustainable Urban Development in Quito in October 2016, the New Urban Agenda (NUA) was adopted to illustrate a paradigm shift. Standards and principles were defined in the light of the SDGs for sustainable urban planning (UN-Habitat, 2020a), thus identifying and acknowledging the relevance of cities for the future challenges. Approved not only by HABITAT III but as well by the UN General Assembly in December 2016, the NUA constitutes a guideline for "national urban policies, urban legislation, urban planning and design, local economy and municipal finance and local implementation." (UN-Habitat, 2020a)

1.3. Urban Infrastructure Planning

Infrastructure planning can be the technical preparation of construction of infrastructural elements, the financial preparation for personnel and operating resources, and establishing the administrative and legal framework for the utilization of the infrastructure service (Beckmann, 1988).

Urban infrastructure planning aims at accessing areas for anthropogenic use, conducting spatial and functional differentiation, and directing anthropogenic use of natural and environmental resources. It also pursues ensuring spatial, economic and social participation (Moss, 2011). In the context of this presented thesis, the term of urban infrastructure planning aims at planning the technical supply and disposal infrastructure, for example for water, electricity and waste management. Further urban infrastructure, but not in direct focus of this thesis, are the transportation network, telecommunication and sanitation. Water and energy are an essential resource for urban population to ensure health and quality of life (Loske and Schaeffer, 2005). Accordingly, the access to water and energy is the precondition for the fight against poverty and economic progress (UN-DESA, 2014). Providing supply and disposal services through urban infrastructure is a basic requirement for economic development and in parallel is key to control the urban footprint on the ecosystem and for environmental protection (Loske and Schaeffer, 2005; Tietz, 2011).

Decision-making within the planning practices is characterized traditionally by optimizing existing structures due to seemingly lower costs, rather than system revolution (Malekpour et al., 2015; Tietz, 2011). Climate change and demands on financial and environmental require sustainability more and more to step off these insufficient pathways and to profit from synergetic effects in

infrastructure planning and service provision (Peterek et al., 2019). Good practice in urban infrastructure planning demands the development of a "genuinely compelling and clearly expressed place-based vision" (National Infrastructure Commission, 2020). Based on these visions, integrated strategies should be developed, including transport, energy, health, environment, and social issues. Good vision is ambitious but has realistic long-term goals and can be developed through scenario development and evaluation based on best knowledge of the city (National Infrastructure Commission, 2020). Traditionally, urban infrastructure planning was performed sector specific, but in order to reduce financial and environmental impacts, concepts of integrated planning approaches gain growing attention: Service should not be provided by a singular system, but through multiple systems. Reversely, one system optimally contributes to multiple purposes to profit from synergetic effects, intended by integrated planning approaches (Moss, 2011).

Considering the urban infrastructure as Urban Metabolism helps exemplifying the idea of integrated planning. The perspective of a city with all its flows and processes as an Urban Metabolism underlines the key role of integrated planning for supply and disposal infrastructure. Just like the blood system in the human body supplies with oxygen, removes carbon dioxide from the cells, and circulates warmth, waste incinerator plants can provide electricity and heat besides disposing solid waste. Through the circularity of the system, inefficient inputs and outputs are intended to be minimized (Kraas et al., 2016). This very placative example illustrates the benefits of the synergetic effects, which allow reducing operating costs and constructional effort and thus increase economic and ecological sustainability. To achieve an efficient urban metabolic system, precise planning based on scenarios developed under consideration of recent scientific knowledge, is required. Consequences of inadequate scenario development can lead to the failure of the planning process (Furlong et al., 2017).

Integrated urban infrastructure is key to increase resource productivity, which means economic growth with decreasing resource input. For developing countries, a factor 4 can be a realistic target to improve resource productivity through integrated urban infrastructure (Ness, 2008). Centralized and decentralized integrated urban infrastructure solutions can be established in order to increase sustainability especially of disposal solutions (Derrible, 2017). Examples for integrated water management (IWM) approaches can be approaches to relieve municipal water drainage

systems and wastewater treatment plants for capacity limitations, as well as concepts for rain water infiltration in urban green spaces and urban agriculture (Derrible, 2017; Furlong et al., 2017; Peterek et al., 2019). For example in case of flash flooding, Kuala Lumpur can close parts of the underground transport network in order to temporarily collect the rainwater (Derrible, 2017). These concepts are often referred to as the Sponge City Approach.

Improper urban waste management can cause severe health issues and environmental harm, as waste is often handled in a one-way approach, where it accumulates untreated in landfills. Through municipal solid waste management (MSWM) approaches, integrated infrastructure solutions can be circular systems of recycling, composting and reusing (Peterek et al., 2019; Seadon, 2006). Integrated approaches based on waste separation allow to separate waste into recyclable components, compostable biomass and a fraction to be used to generate heat and electricity in incineration plants or biogas reactors (Sadef et al., 2016). Through implementing such approaches, the environmental impact of waste management can be reduced, furthermore revenues can be generated from trading recyclable raw materials (Sadef et al., 2016). Through composting, a major part of the solid waste can be recovered, recycled and reintegrated into the natural nutrient cycle (Zurbrügg et al., 2012) thus reducing the amount of waste which ends on landfills and valorizing reusable fractions.

Besides keeping the urban metabolism running, providing urban infrastructure is key to reduce slum dwelling population. Differences in temporal and spatial access to urban infrastructure cause social disparities (Tietz, 2011). Urban infrastructure grants access to essential supply and disposal services for households, businesses and public institutions, with increasing demand to be area covering, consistent and affordable by the service recipients with increasing expectations on sustainability (Moss, 2011).

According to UN-Habitat, a slum building or household is not defined through the building condition or building material, but through the lack of one of the following: Durable housing, sufficient living space, easy access to safe water, access to adequate sanitation or security of tenure. If besides lacking one of these conditions the requirements on sufficient living areas are given, criteria for informal settlements are fulfilled (UN-Habitat, 2019). Therefore, slum issues cannot be solved by clearing slum areas but through the provision of basic urban infrastructure to enable

access to basic services. The reduction of the slum dwelling population was considered under goal 7 of the MDGs. Between 1990 and 2015, drinking water access was improved for 2.6 billion people and sanitation conditions were improved for 2.1 billion people. Moreover, living conditions of more than 300 million slum dwellers could be improved between 1990 and 2015 (United Nations, 2015b). As shown in Table *3*, the share of the population living in slums and informal settlements decreased from 43.3 % to 23.0 % in the same period. However, due to the growing global population, the total number of slum dwellers increased by 42.9 % between 1990 and 2018. The percentage of urban population living in slum condition even increased from 23 % to 28 % between 2000 and 2014 (UN-Habitat, 2019).

As already indicated through the conditions for the slum definition, infrastructure is one key to improve life of slum dwellers and inhibit slum formation. In order to achieve this or upgrading slums – after recognizing the need to improve slum areas and lives of slum dwellers – a major task besides forming a legal framework is the provision of affordable urban infrastructure under consideration of the population's needs and integrated processes.

Table 3: *Global and regional overview on the development of the total number of population the slum-dwelling population and the share of the population living in slums and informal settlements (UN-Habitat, 2020b).*

Region		1990	1995	2000	2005	2010	2014	2018
World	total (thous.)	**723,020**	**779,678**	**817,221**	**853,740**	**925,965**	**928,063**	**1,033,545**
	%	**43.3**	**40.4**	**28.0**	**25.9**	**24.4**	**23.0**	**24.0**
Australia & New Zealand	total (thous.)						7	8
	%						0.03	0.01
Europe & Northern America	total (thous.)			764	787	820	833	1,022
	%			0.1	0.1	0.1	0.1	0.1
Northern Africa & Western Asia	total (thous.)	44,194	44,701	46,335	45,217	52,061	63,814	83,052
	%	28.4	25.0	23.0	19.8	19.4	22.0	25.6
Latin America & the Caribbean	total (thous.)	106,118	112,253	115,148	111,311	113,942	104,652	114,207
	%	33.7	31.5	29.0	23.9	23.9	21.0	20.9
Eastern & South-Eastern Asia	total (thous.)	284,293	307,593	317,123	332,067	348,756	349,409	369967
	%	46.6	42.7	38.0	33.8	30.0	28.0	27.2
Central & Southern Asia	total (thous.)	193,216	201,838	205,661	206,888	212,024	206,704	226,780
	%	57.1	51.7	46.0	40.3	35.3	32.0	31.2
Oceania (excl. Australia & New Zealand)	total (thous.)	386	430	468	514	572	602	670
	%	24.1	24.1	24.0	24.1	24.1	24.0	23.7

1.4. Earth Observation Techniques to Support Urban Planning

Remote sensing is defined as a technique to capture information of the earth's surface contactless (Albertz, 2009), where sensors can exploit the complete electromagnetic spectrum and capture information from various distances to the considered objects. These opportunities of earth observation (EO) allow changing the spectator's perspective of view: From a very personal, familiar and spatially limited angle of view to observing from above with a wider angle of view. This challenges the observer to leave the familiar sphere to interpret the new perspective in an objective and comprehensive way. In the urban context, EO offers the possibility to expand the horizon of observation from an area, that usually is limited through the streetscape due to the surrounding building structure, to see whole quarters and cities in one objective, constant and recurring view. Spatial relationships difficult to identify so far can thus be identified more effectively.

In this section, a general overview is given on the recent scientific focus of remote sensing applications in the urban context. For more specific literature overviews in the contexts of the single studies of this thesis, please refer to the articles in section "Publication List for the Dissertation", page vii, where detailed literature overviews are presented.

Analyzing over 100 of the most relevant research articles related to "urban remote sensing" since 2018, as suggested by the Google Scholar search engine, reveals interesting characteristics: Deep Learning (DL) and Artificial Intelligence (AI), which recently are one of the publicly most present scientific topics, do not dominate the research articles with remote sensing context. Only 14 % of the articles address DL/AI topics, mainly using very high-resolution (VHR) satellite and aerial imagery. Main application of these methods is the building extraction and building segmentation (Xu et al., 2018; Yi et al., 2019), where U-Net segmentation approaches enable the best results for semantic object segmentation (Dong et al., 2019). Especially data fusion of optical and laser scan data improves accuracy for urban object detection (Audebert et al., 2018). Besides single object detection, DL proves to be an alternative approach for urban land use mapping (Huang et al., 2018; Yi et al., 2019).

The most relevant urban EO topic addresses detecting and characterizing urban heat islands (UHI) with a share of around 22 % of the relevant research articles. The discussed studies mainly base

on evaluating information in the thermal infrared spectrum from Landsat and MODIS data in the face of urbanization and climate change. The main research focus lies on the long term descriptive UHI analysis using the satellite image archives for metropolitan areas to describe dynamics in intensity and spatial distribution (Faria Peres et al., 2018; Shirani-bidabadi et al., 2019; Zhou et al., 2018). First applications are discussed to analyze the effect of urban 3D morphology on UHI (Huang and Wang, 2019).

17.1 % of the articles address mapping land use and land-cover (LULC) change in the context of urban expansion. Most studies report approaches for urban expansion mapping through multi-temporal change of the urbanized areas using Landsat data with 30 m spatial resolution (Magidi and Ahmed, 2019; Yang et al., 2019) or the land use mapping on the block level using VHR WorldView or Pléiades imagery (Grippa et al., 2018).

Further 15.2 % of the research articles address the monitoring of urban green spaces (UGS), urban vegetation and green infrastructure (GI) as a quality of life indicator in the urban environment. Spectral information from the near infrared bands of Landsat, Sentinel-2 and MODIS allow evaluating urban vegetation. Increase in population and built-up areas, cause a loss in UGS (Atasoy, 2018). Gaofen-2 data with 4 m spatial resolution is used for improved level of detail (Chen, W. et al., 2018). (Frick and Tervooren, 2019) and to show that the volume of urban vegetation can be analyzed by adding laser scanning information. Health status of urban vegetation can be assessed by using multispectral aerial imagery (Näsi et al., 2018)

Insights through EO techniques usually end at objects surface. Information on building use, functional connections, qualitative and sensual information are hardly measurable. In order to overcome this limitation, social media can deliver valuable reference. 7.6 % of the research article address the possibilities of social sensing data to increase functional information content of urban analyses. Points of interest from a web mapping platform to determine functional use of UGS (Chen, W. et al., 2018). Mobile phone data for residential land suitability analysis or land use mapping (Huang et al., 2019; Jia et al., 2018).

Another often noted topic is urban hydrology. Chen et al. (2018) apply DL algorithms on high-resolution on Gaofen-2, Ziyuan-3 data to assess urban water bodies. Shao et al. (2019) present

approaches to retrieve impervious surfaces in the urban environment. Landsat data is used to study cooling effects of water bodies on the UHI effect (Xue et al., 2019). Other research handles the topics of air pollution (Man Yuan et al., 2018; Zheng et al., 2018) and urban functional zoning (Song et al., 2018; Tu et al., 2018).

Earth observation techniques in the context of urban planning and urban infrastructure planning mostly aim at providing city covering data and information on the city level. UGS and GI as quality of life factors in combination with temperature estimations are studied to deliver data for approaches to work UHI effects with Landsat. Cai et al. (2019) put changes in urban temperature in context with change in urban land use. The spatial resolution can be increased by combining Landsat thermal infrared information with crowd sourcing temperature information and Sentinel-2 data in order to identify local UHI hotspots (Venter et al., 2020). Correlations between environmental quality and socioeconomic conditions have been identified for Bogota by Musse et al. (Musse et al., 2018). Using satellite imagery as a database, urban hydrological modelling for water supply was studied (Rausch et al., 2018) and surface runoff was modelled as a result of land use change for surface water management (Kandissounon et al., 2018; Li et al., 2018).

A special focus in urban remote sensing lies on the analysis of informal settlements and slums. The attention is therefore directed at mapping slum areas and generating an understanding of slums using VHR satellite imagery (Kuffer et al., 2016; Taubenböck, Kraff, Wurm, 2018; Wurm and Taubenböck, 2018). Besides the development of slum detection approaches, publications on qualitative slum studies based on EO techniques are discussed, i.e. to describe heat effects exposure in slums (Wang et al., 2019), to explain spatial separation of socioeconomic groups in cities with VHR remote sensing data and social media (Taubenböck, Staab et al., 2018) or to evaluate the potential of integrating EO techniques to map SDG indicators (Kuffer et al., 2018).

As presented, optical remote sensing data dominate in urban remote sensing applications, because they offer very high spatial resolution and multispectral information. Although radar data analysis is reported for urban studies, the comparably low spatial resolution and complex backscatter mechanisms in urban environments limit the usability of these data. Table 4 gives an overview on the urban remote sensing applications and the used EO systems presented in this section.

Table 4: *Operational earth observation platforms for urban remote sensing applications. Information based on literature overview in section 1.4.*

Urban Application	Spatial resolution	EO systems
Urban land use/ land cover	15 - 30m	Landsat, Sentinel-2, MODIS
UHI	30 - 100m	Landsat, MODIS
Urban Green Spaces	0.5 - 30m	Landsat, Sentinel-2, MODIS, Planet, WV-1-4, Pléiades
Object detection	0.3 - 0.5m	WorldView-1-4, Pléiades, aerial imagery
Urban Elevation	0.3 - 1m	Pléiades, WorldView, LiDAR
Urban Hydrology	1 - 20m	Gaofen-2, Ziyuan-3
Object identification	0.01 - 0.1m	UAV

1.5. Research Deficit

As presented in the previous section, applications in urban remote sensing are manifold, where "earth observation for urban planning" is a recurring term. Remote sensing, especially in combination with AI algorithms is presented as a technique to deliver the answers for most spatial issues. Numerous studies are designed to describe urban environments such as urban heat or green infrastructure: using these approaches, an understanding of the urban system can be generated. However, despite the long-known deficiency of sufficient data and information for appropriate urban planning (Taubenböck and Dech, 2010b), the availability of data generation to support local urban planning or urban infrastructure planning is lacking (Musse et al., 2018).

Successful urban planning requires a deep understanding of the system city (Taubenböck and Dech, 2010a) and the "analysis of numerous spatial scenarios is inevitable" for urban infrastructure planning, considering a variety of different scenarios (Mikovits et al., 2018). "Spatially explicit indicators [are required] to support urban planners and policy makers" (Artmann et al., 2019). Through this first approaches were presented for waste management supported by remote sensing techniques (Singh, 2019; Vetter-Gindele et al., 2019).

Still, "urban planning" and "urban infrastructure planning" are often used as buzzwords to attract attention in the scientific EO community. However, ways to integrate remote sensing-based information into the process of urban infrastructure planning are usually not presented. Instead, phrases such as "may assist […] urban planners", "provide better decision making capabilities" or

"can provide important guidance" are widely used (Anees et al., 2019; Li et al., 2018; Venter et al., 2020). Wellmann in this context underlines in his review article that the integration of remote sensing methods for urban planning is rarely developed and reported (Wellmann et al., 2020).

"To achieve [successful urban infrastructure planning], precise planning based on scenarios, developed under consideration of recent scientific knowledge, is required. Consequences of inadequate scenario development can be failure of the planning" (Furlong et al., 2017). On the way to prepare cities for their future challenges, the presented research and studies in this thesis aim to close the gap between the claims of remote sensing to provide planning-ready data and the present situation of lacking approaches for EO data integration into the process of urban infrastructure planning, in order to follow the call and demand from UN Secretary General Guterres "towards evidence-based planning" for sustainable cities (Furlong et al., 2017; Guterres, 2018b).

2. Objectives

Due to the increasing availability of earth observation (EO) information which results from growing orbital satellite systems and reduced revisit times, a main focus in urban remote sensing lies on the development of algorithms and applications to automatically process global data products from satellite data. Such products offer the advantage of consistent data availability on a global scale. Using the keyword "urban planning", numerous studies were published during the recent years, explaining approaches to describe the physical character of urban areas by means of impervious surfaces, urban greenness, road network, UHI and so forth.

For urban planning, such information is a valuable input to get an understanding on cities, but the success of urban planning and urban infrastructure planning is particularly dependent on the availability of precise a database for decision making. Scenario development under the premise of increased transparency in order to implement masterplans and planning goals for example, require high precision and high-quality data. Studies in this context hardly appear in the relevant publications. Therefore, deeper efforts have to be made to develop and to propose approaches to deliver planning relevant specific data and to meet the demands on evidence planning.

In order to encourage evidence-based planning (Guterres, 2018a) and a culture of evidence-based political decisions (Falk, 2021), reliable and precise data are essential for the planning process. So far high-quality material and energy flow data, especially on household level, is missing or difficult to access (Klopp and Petretta, 2017).

The motivation for the studies, presented in this work, is to improve existing EO approaches and to develop and to present approaches to meet demands on data for the process of urban planning and urban infrastructure planning. To avoid mistakes and misconceptions in the process of urban supply and disposal infrastructure planning, scenario development requires high-resolution information on the urban metabolism. Under consideration of empirical data integration, VHR remote sensing techniques can be expected to provide data on the single building level to support decision making and scenario development. Additionally, the developed approaches need to be obstacle-low to be process-implementable by local administration and planners with limited EO expertise.

In this context, the study designs were guided by the following research hypotheses:

1. The quality of planning relevant data products highly depends on the spatial resolution of remote sensing data.
2. Planning relevant data products profit from height data or building height information respectively.
3. Building-types (BT) information as a basis information increases data content and data quality for urban infrastructure planning.
4. Socioeconomic status and electricity consumption can be predicted on the base of BT.
5. VHR EO data processing can provide data for scenario development.
6. Globally generated EO products to describe urban processes cannot provide sufficient information for urban planning, therefore re-focusing from the global to the local scale is highly beneficial for urban planning.
7. Planning-ready information can be generated from remote sensing data by means of non-complex approaches and therefore, can be carried out by non-scientific users in administrative and private planners.

3. Results

3.1. Study Overview

The research was conducted in Da Nang, Vietnam (Figure 3) and Belmopan, the capital city of Belize. As shown in the following paragraphs in detail, both of the cities are facing rapid growth of population. Vietnam and Belize are classified as lower-middle income economies, for which continuously high urbanization rates are predicted (see section 1.1 and Figure 1). The World Bank states a gross national income (GNI) per capita for Belize of 4,700 US-Dollars (2019) and for Vietnam an GNI per capita of 2,590 US-Dollars (World Bank, 2021).

Da Nang is the 5th largest city in Vietnam and the largest and most important city in central Vietnam (Ostojic et al., 2013; UNESCAP, 2020). The central part of Da Nang around the Hàn River is historically grown, whereas the newer parts of city experienced a stronger planning influence. For 2019, the General Statistics Office of Vietnam reports a population of 1,141,100 inhabitants in Da

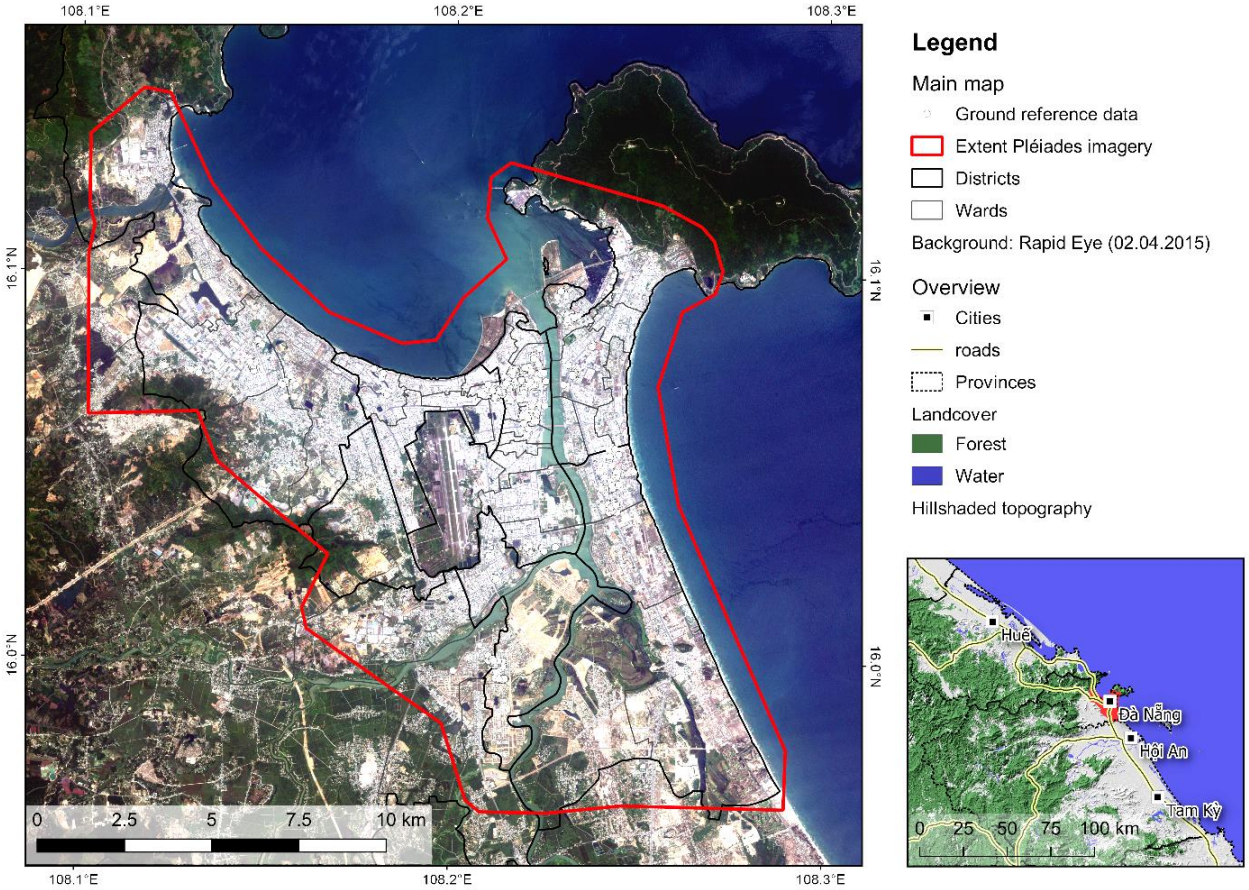

Figure 3: *Overview map of Danang (Warth et al., 2019)*

Nang (GSO, 2021). Da Nang is therefore categorized as medium-sized city, as defined by the UN in section 1.1. Own calculations show that according to the city definition of the New York University, 70.8 km² of the administrative of Da Nang are to be classified as 'Urban built-up', 60.0 km² as 'Suburban built-up', 362.8 km² as 'Rural built-up', and 484.5 km² are undeveloped (Figure 4). 88 % of the population lives in the urban regions and 12 % live in rural environments (UNESCAP, 2020).

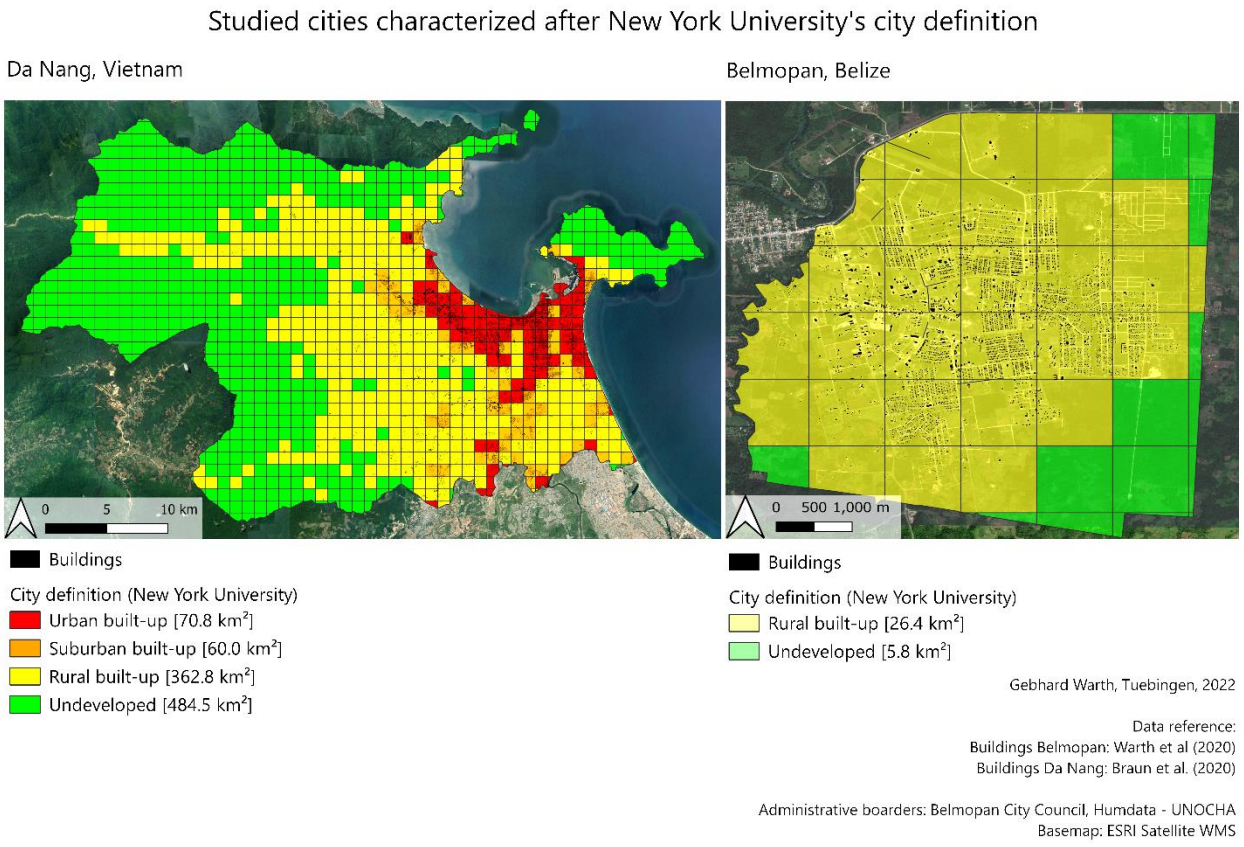

Figure 4: *City characterizations for Belmopan and Da Nang after the city definitions by the New York University (see section 1.1). Data reference: (UNOCHA, 2022)*

In Vietnam, the share of the urbanized population grew from 30.4 % to 36.6 % between 2010 and 2019, which is an increase of 17.0 % (UNdata, 2021). For Da Nang itself, the General Statistics Office of Vietnam reports a population increase from 946,000 inhabitants in 2011 to 1,141,100 inhabitants in 2019, which implies an increase of 20.6 % or 2.5 % per annum (GSO, 2021). This caused an increase of built-up areas and impervious surface of 17.7 % between 2010 and 2015 (Rau, 2016). Due to its location, international sea- and airport and economic incentives, Da Nang attracted very large sums of foreign investments (UNESCAP, 2020) and therefore, is very attractive

to population in search of economic prosperity and mobility. Urban planning in Vietnam is conducted municipally but managed by the central government (Bùi et al., 2021). The overall goal of the Da Nang masterplan by 2020 is the development towards an environment-friendly city by means of preventing pollution and soil degradation and awareness creation amongst all urban stakeholders (Bùi et al., 2021). In 2030, Da Nang expects 2.5 million inhabitants which made an adaption of the masterplan necessary. Accordingly, Da Nang plans to be developed to a modern national-level city with positive sustainable and socioeconomic synergies for the adjacent central and highland region. The spatial development is planned through residential areas in the central city, whereas touristic infrastructure, villas and recreation areas will be located at the eastern and northeastern beach-line (Bùi et al., 2021). As the western areas are already being characterized by industrial zones, high-tech and information industry is planned to be concentrated in these areas. The conservation of cultural and historical heritage is planned to be focused in the southern areas of Da Nang (Bùi et al., 2021).

Belmopan is the capital city of Belize, inaugurated in 1970 after hurricanes repeatedly hit the former capital Belize City as a planned city (Friesner, 1993; Kearns, 1973). In order to ensure governance, the capital was moved to the center of Belize and newly established (Kearns, 1973). As shown in Figure 5, the administrative area of Belmopan covers 32.25 km^2 (Warth et al., 2020).

After being constructed and administrated through a semi-public corporation, the first city council was elected in 2000. Belmopan with 25,583 residents in 2021 (Belmopan City Council, 2021) is categorized as small settlement (see section 1.1) and thus the second largest city in Belize after Belize City. 26.4 km^2 of Belmopan's administrative area are classified as rural built-up and 5.8 km^2 are undeveloped following the city definition by the New York University (Figure 4). Belmopan experienced a population growth rate of 6.4 % between 2014 and 2018 (Statistical Institute of Belize, 2020), which exceeds the urban growth rates of Belize (2.1 %), Central America (1.3 %) and worldwide (1.1 %) (United Nations, 2018). These numbers highlight the need for proper and precise urban planning and urban infrastructure planning, to conduct the urban development in sustainable paths.

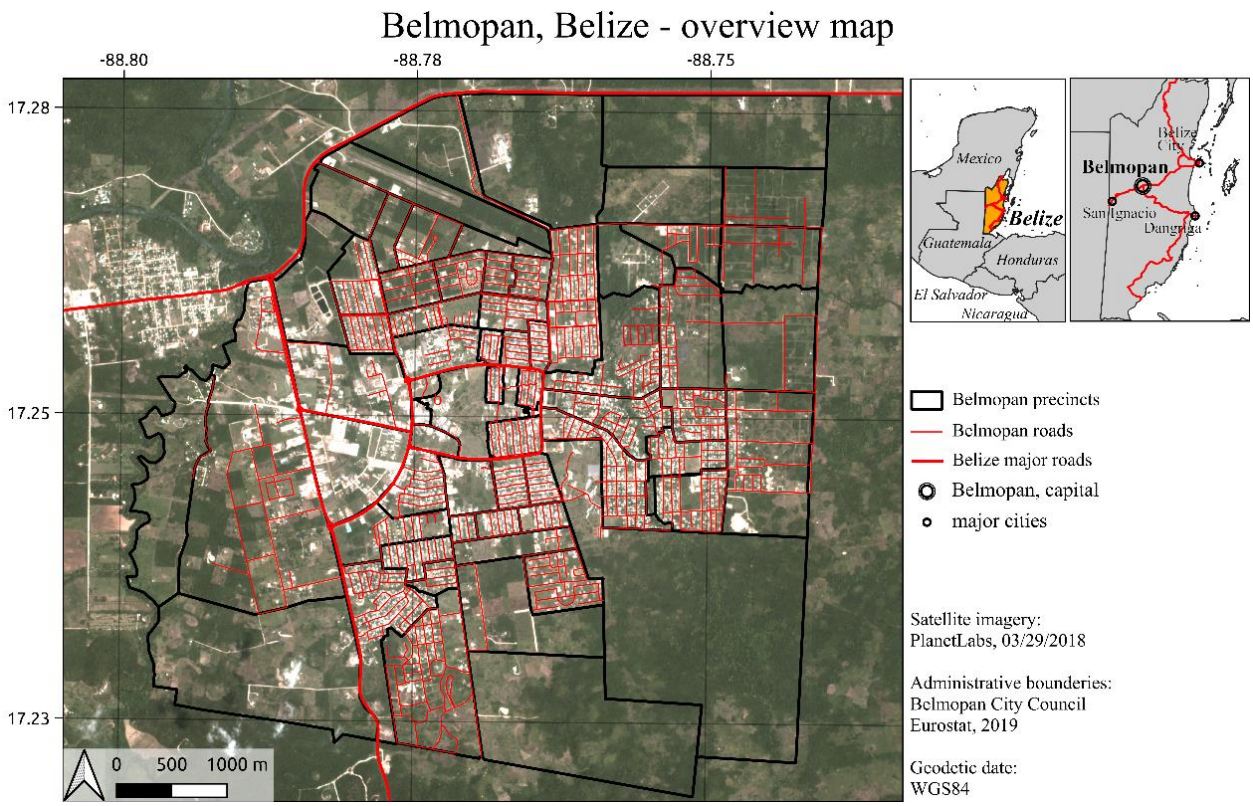

Figure 5: *Overview map of Belmopan/Belize (Warth et al., 2020)*

The urban area of Belmopan is dominated by sparsely built-up residential areas, where the initial development was concentrated within the central Ring Road (rectangle shaped in the map). The eastern wards of Belmopan are influenced by migrant groups and characterized by rudimentary building, whereas high class building expansion occurs in the north-western and south-eastern part. Industry and commerce are concentrated in the western areas.

In 2014, the Belmopan Municipal Development Plan (MDP) was published by the Belmopan City Council in a participative approach. The MDP formulates the following main planning goals: Creating a new down town, leveraging the University of Belize to attract the private sector, improving transportation infrastructure under consideration of appropriate solution for bike paths and pedestrian paths, and to develop Belmopan as the "Garden City" in order to preserve and expand green spaces for increased quality of life (Belmopan City Council, 2014). However, the MDP does not propose suggestions for spatial implementation. Thus, in a subsequent planning approach in collaboration with UN-HABITAT a city-wide spatial urban planning approach on green and blue

infrastructure was developed in 2017 to increase climate resilience and quality of life (Mayr et al., 2017; UN-Habitat, 2017).

Both selected cities Da Nang and Belmopan show high rates of urban population growth and therefore are challenged by urban dynamics and constant change in the urban environment and accordingly are suitable study sites to conduct and evaluate research to describe urban dynamics in more detail and to develop approaches in order to support urban supply and disposal infrastructure planning.

3.2. Da Nang: DSM Differencing for Change Monitoring using Pléiades Imagery

Research demand

Present studies on urban dynamic description with EO data are mostly based on post-classification approaches, which evaluate temporal pixel dynamics to determine constancy or change in classified land use or land cover (LULC) based on satellite imagery. Because LULC approaches build on a very non-complex structure, they can be implemented in fully automated and globally scaled applications. Therefore, the post-classification approach can convince through high grade of automatization and consistent quality and data content. However, the results basing on post-classification approaches only enable the description of areal changes of the building stock or urban class, as the change in LULC is being detected - but cannot help to describe dynamics within the building stock or urban classes. Areal changes of urban classes express only one facet of urban dynamics, internal change and dynamics through construction, demolition or upgrading activities however, cannot be described through post-classification approaches.

Therefore, we make up the hypothesis that adding the third dimension into urban analysis through differencing photogrammetrically derived digital surface models (DSM) enables detecting dynamics within the building stock to characterize areas of intra-urban change and transition. These areas are characterized through demolition, new construction and addition of storeys and therefore, can be detected through change of surface elevation. Thus, this approach contributes to gain a deeper understanding of dynamic processes within urban areas that not detected by conventional LULC methods.

Data

Table 5: *Data overview for the Da Nang study on urban dynamics*

Data	Information	Date
Two stereoscopic Pléiades imagery triplets	Panchromatic bands, spatial resolution: 0.5m	2015/10/20, 2017/08/13
Building mask	Classified from Pléiades imagery	2015/10/20
Ground truthing data	Reference point dataset on 975 buildings: GPS position, building height, number of floors	March 2015, March 2016, December 2017

Methodology

This section gives a brief overview on the methodology, for detailed information please refer to Warth et al. (2019) (Appendix A-1). The approach implies four steps to detect urban dynamics:

1. DSMs generation from two points in time (2015 and 2017) using photogrammetric methods on tri-stereoscopic Pléiades imagery (see Table 5).
2. DSM matching to remove vertical shifts and DSM differencing to detect surface elevation changes.
3. Threshold-based removal of false detections.
4. Context adding for change categorization and change assessment.

Figure 6 provides a schematic overview of the approach, the four steps are presented in the following paragraphs.

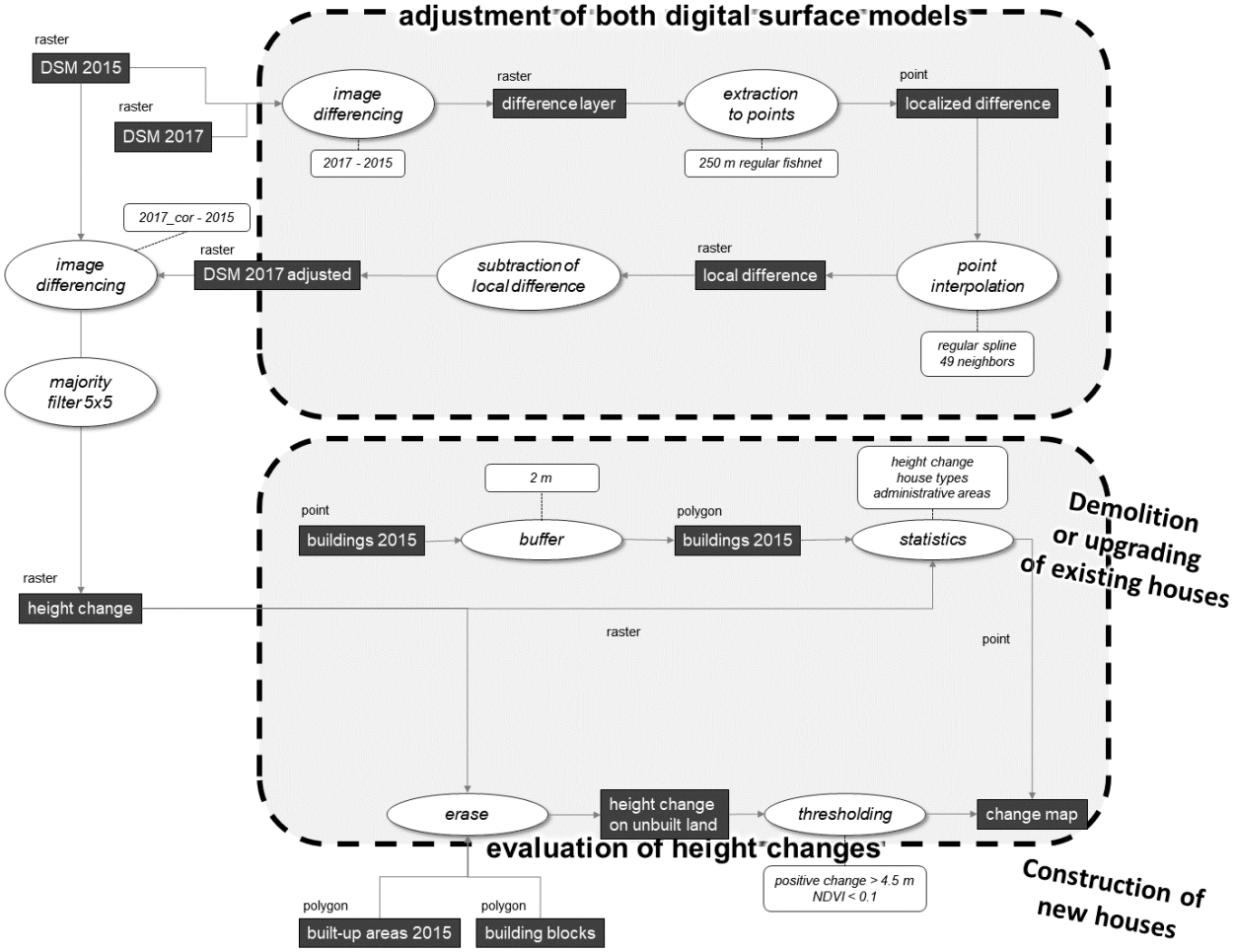

Figure 6: *Schematic description of the approach to detect urban dynamics by means of DSM differencing (Warth et al., 2019)*

1. DSM generation from stereoscopic Pléiades triplets (2015 and 2017)

Same as the human eye allows three-dimensional perception, EO data can be a means to three-dimensionally reconstruct the Earth's surface. Because the photogrammetric approach is implemented in all three presented studies, it is briefly presented in the following paragraphs.

Given at least two images covering the same area of interest from different positions, object parallaxes can be determined from panoramic distortions (see Figure 7). In relation to the camera height above the datum and the distance between the camera positions, object heights are calculated using the following formula (Hadjitheodorou, 1963):

$$P_\alpha = X_\alpha - X_\alpha' \quad (1)$$

$$h = H - \frac{B}{P} \quad (2)$$

Where *X* is the object positions in the line of flight, *P* is the absolute parallax of the object, *h* is the height of the object above the datum, *B* is the distance above ground of the camera positions.

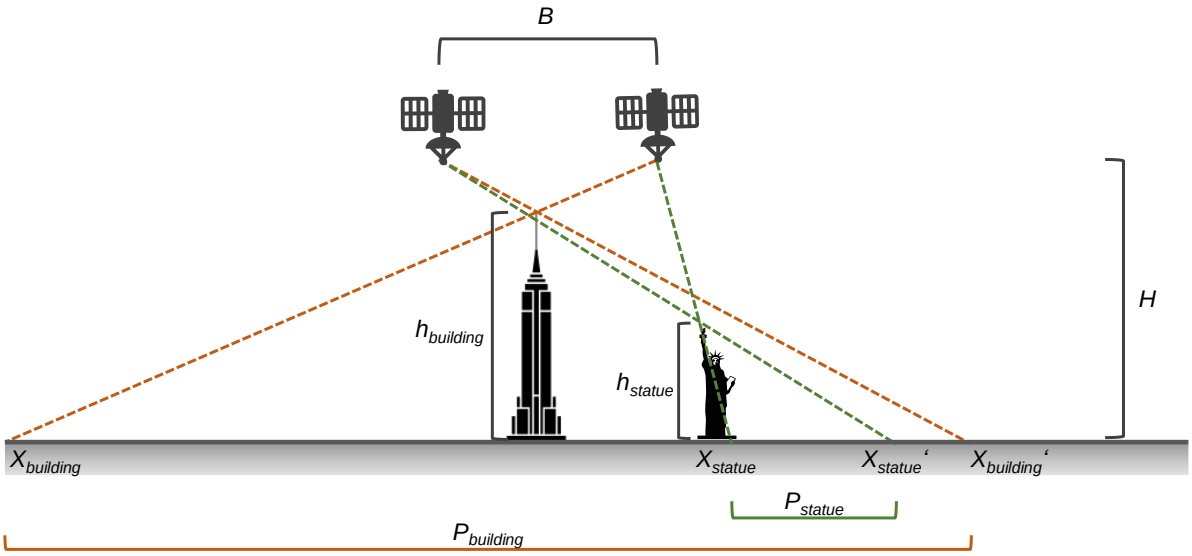

Figure 7: *Schematic illustration of the photogrammetric parallax formula. P is the photogrammetric parallax, h is the object height, H is the camera height above the datum, X is the object position in the line flight. For methodology details see section 3.2*

This approach is used to generate DSMs on the basis tri-stereoscopic Pléiades images from 2015 and 2017.

2. DSM matching and DSM differencing

Absolute vertical accuracies of the elevation data are not relevant for the DSM differencing process. Instead, the relative accuracy of both DSM to each other is rather important to detect elevation change. Therefore, in order of precise vertical matching of both DSMs to avoid vertical offsets due to temporal change, the initial vertical distance is detected in a 250m-grid on non-built and non-vegetated areas. Based on the detected differences, a spline interpolation approach is applied to generate an artificial rectification surface to correct the 2017 DSM. The matched DSMs can then be compared to obtain the changes in elevation.

3. Change identification and removal of false detections

No difference in the DSM difference dataset indicate no change, whereas positive or negative differences display a change in the urban surface. Polygons are formed from pixel groups with homogeneous change, from which incorrectly detected change objects are subsequently removed. Reasons of falsely detected change for these objects can be manifold: Error potential in photogrammetric approaches is given through movement in vegetation due to wind which causes misconception in height. Furthermore, too bright, too dark pixels or areas without contrast can cause mismatches during the photogrammetric processing. On the basis of the ground-truthing data, a mean floor height was estimated, which is used to serve as error threshold, below which detections in the DSM difference are interpreted as errors. The thresholds for DSM differences of 4.5 m for built-up areas and 6 m for unbuilt areas are applied to eliminate false detections.

4. Context adding for change categorization and change assessment

The results are masked with built-up area information to increase the information content of the results. Thus, changes located within the built-up mask indicate a change in the existing building stock, such as building demolitions, new construction, or addition of storeys. Positive changes outside of the building stock mask indicate extension of the built-up areas through new construction of former unbuilt areas.

Results

The photogrammetric processing of the stereoscopic Pléiades triplets resulted in DSMs that cover the whole city area of Da Nang with a ground sampling distance of 0.5m representing status quo conditions in 2015 and 2017 with a temporal baseline of 22 months.

After the DSM matching, a very small average vertical error of 0.044 m remained between both datasets. This vertical deviation is too low to have an effect on the detection of the building change, as the difference thresholds to exclude false detection is 4.5 or 6.0 m respectively.

The DSM difference, shown in Figure 8, confirms the quality of the DSM matching and of the results. The yellow areas, which are dominating in the map, represent a difference of 0 m without any spatial trends in the difference. Only forest and mining areas in the marginal parts of the study

area show differences unrelated to urban processes. Single changed objects can visually be detected, see Figure 8, such as industrial halls on formerly unbuilt area, touristic resorts next to cleared forest land, and changes within the building stock.

The change analysis resulted in 10,080 detected building changes within the study area in 22 months, of which 1,499 buildings show a decrease in height and therefore represent demolition, and 8,531 objects show an increase in height. Out of the 8,531 objects with increase in height, 4,714 changes were detected within the existing building stock and 3,867 objects were detected in initially unbuilt areas. To estimate a detection accuracy, we randomly selected 200 detected changes and visually inspected the change in the Pléiades imagery, which resulted in a very satisfying detection rate of 82 %.

According to the findings, the building stock increase about 1.5 %, 1.9 % of the building were under construction or extended and 0.6 % of the building stock has been demolished (see Table 6)

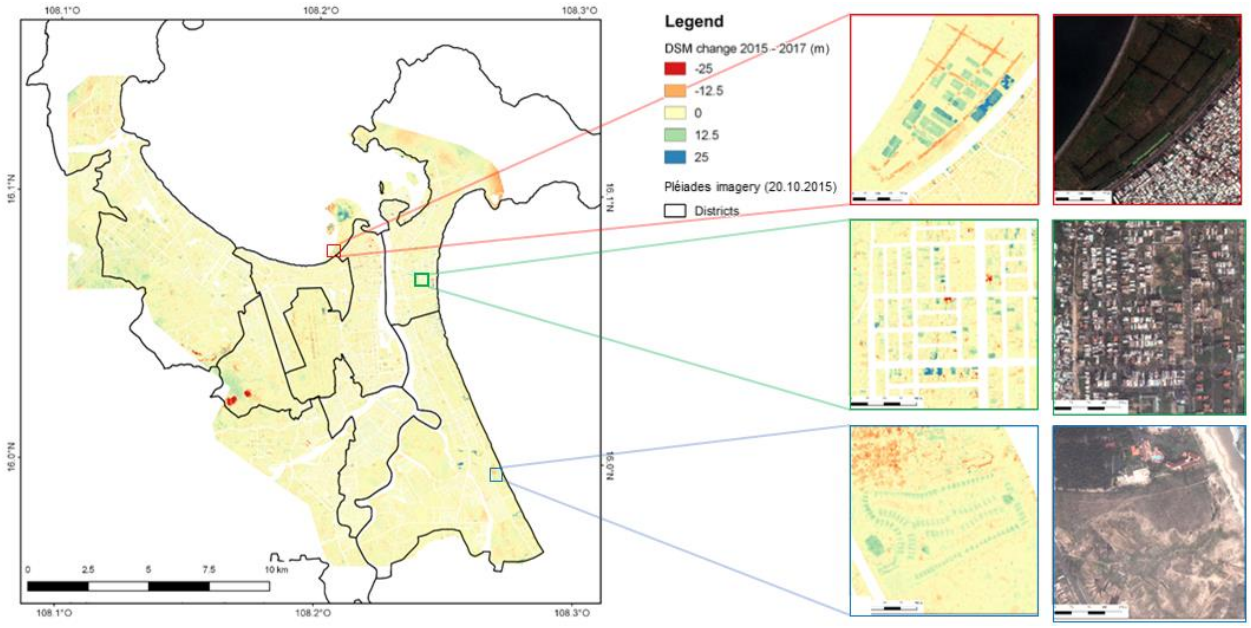

Figure 8: *Result of differenced DSMs from 2017 and 2015. Blue colors indicate increase of the surface elevation and therefore show newly built structures. Red colors indicate decrease of the surface elevation or demolished areas resprectively. Detailed views on the right side show a development site for a tourisic resort (upper row), a former maritime area filled for industrial project (middle row) and a residential area with demolishions and newly built structures (lower row) (Warth et al., 2019)*

Table 6: *Table on detected change in the building stock in Da Nang between 2015 and 2017 (Warth et al., 2019)*

Number of buildings 2015: 244,180	Absolute change 2015-17	Relative change 2015-17
New constructions	3,867	1.6 %
demolitions	1,499	0.6 %
Total change	10,080	4.1 %

The heatmap in Figure 9 illustrates the regional density of changed objects in a 1 km radius. This display allows identifying spatial patterns of change on a regional scale. It is apparent that three areas in Da Nang are characterized by intensive change: The beach-front at the eastern shoreline, where hotels and apartment buildings are concentrated and most touristic activities are located. Secondly, the neighboring area to the west between the Hàn River and the airport, where the historic city center is located. Furthermore, the Cẩm Lệ peninsula, which was under intense urban development in the studied period, is located in this area as well. Thirdly, a residential area at the western border of the study area, where the Hòa Kánh industrial park is under development in close distance (Gruschwitz, 2020).

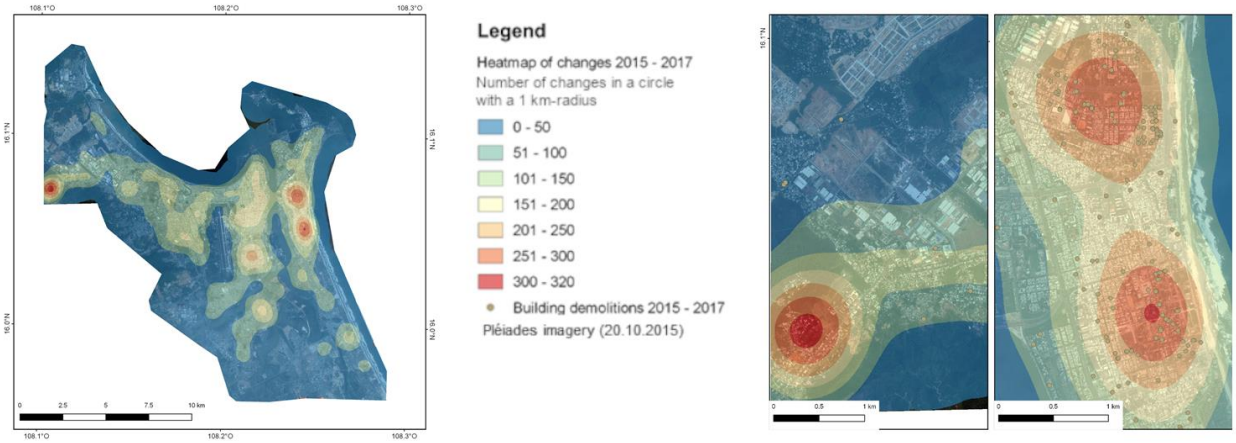

Figure 9*: Change heatmaps show spatial densities of detected changes in building stock in a 1-km radius. The detailed maps show changes in the heatmap symbology combined with demolishions as point information. The left detail map covers a newly established industrial area, the right detail map shows higher complexity at the beach front with detected building demolishions (Warth et al., 2019)*

When analyzing the results on a more local scale, Figure 10 gives an overview of accumulated detected changes in 250m hexagons. Here, the changes can be located more precisely. The figure indicates a few punctual areas, which stand out from the general trend in Da Nang (red hexagons), whereas the displayed detected demolitions seem to be spread more widely in the historic city center in Da Nang.

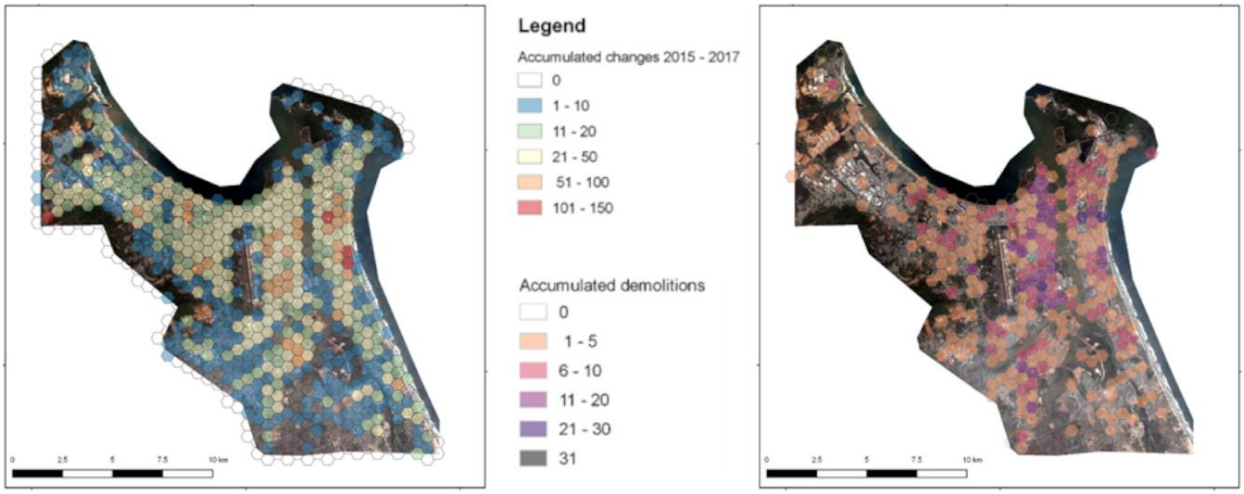

Figure 10: *Local changes represented through accumulated change detections between 2015 and 2017 in a 250 m hexagonal structure. The left map shows detected changes, the right map shows detected demolishions (Warth et al., 2019)*

Summary

- DSM differencing is a robust approach to detect change in dynamic urban environments.
- High accuracy of detected change: 82 %
- Evaluating 3rd dimension information reveals intra-urban change of namely new constructions, upgrades/reconstructions and demolitions. Therefore, the results increase the information content compared to post-classification results from LULC data sets.
- Highly dynamic built-up urban areas can be distinguished from constant areas.
- In comparison with findings from Braun et al. (2020) (see Figure 11), the presented approach is suitable to determine areas of urban dynamic. Due to difference in spatial aggregation, slight differences numbers of single changes.
- The approach is uncomplex and not limited to Pléiades imagery. Any kind of VHR DSM data be used. Other sources, such as WorldView imagery or LiDAR data can be combined with each other and therefore increase the flexibility of the DSM-based change detection approach.

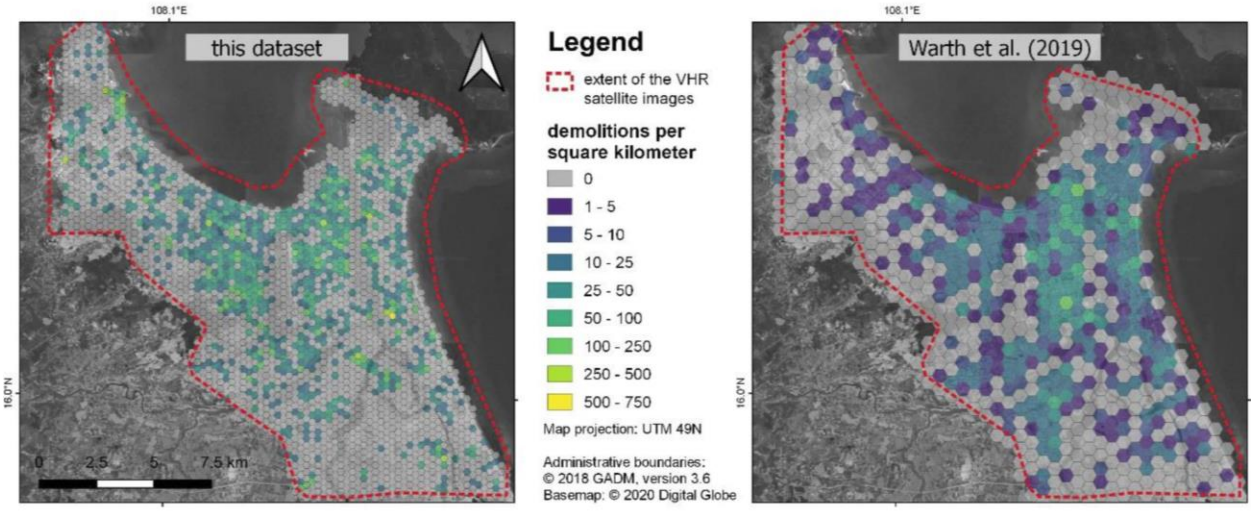

Figure 11: *Comparison of systematically and manually detected demolitions (left) and detected demolitions through DSM differencing (right) (Braun et al., 2020). Overall regional trends match in both studies, however slight differences in absolute numbers of change are noticeable, especially in the areas west of the airport.*

3.3. Belmopan: Prediction of Socioeconomic Information Using WordView-1 Data

Research demand

The demands for evidence-based planning and an evidence-based decision culture in order to increase sustainability and transparency of planning get declared more distinctly and frequently (Falk, 2021; Guterres, 2018b). Therefore, a solid data base for scenario development is required for the planning process.

In the recent research literature on remote sensing in the urban planning context, we usually come across approaches to describe the physical-morphological structure of the city: urban structure, UHI, greenness indicators, impervious surface analysis, and so forth. Such information can have relevance in urban planning for structural characterization of urban areas. However, urban infrastructure planning requires specific planning data that allow conclusions about material and energy flows. In order to define and develop accurate planning scenarios. For this reason, area covering and consistent data in high spatial resolution and rich in information is required to close the gap for urban planning application.

In order to provide specific data for the process of urban infrastructure planning, we hypothesize that VHR resolution EO data is suited to be a data source to close this gap and provide planning relevant data. Furthermore, we hypothesize that residential socioeconomic information is related to residential building-type (BT) and therefore, socioeconomic information can be predicted through BT classification for Belmopan based on EO data on a single building level.

Information on socioeconomic parameters has high relevance in urban infrastructure planning, because socioeconomic groups have different lifestyle habits and therefore cause different material flows are closely correlated to socioeconomic states of residents, such as consumption of electricity (Jones et al., 2015) and household solid waste production (Khan et al., 2016; Oribe-Garcia et al., 2015).

Data

Table 7: *Data overview on the Belmopan building-type study*

Data	Information	Date
Two WV-1 stereo pairs	Panchromatic band, spatial resolution: 0.5m	2018/03/16, 2018/03/29
PlanetLabs imagery	Blue, green, red, red-edge bands, spatial resolution: 0.5m	2019/03/29
Household survey	395 interviews: socioeconomic information	March – April 2018
Ground truthing data	405 samples: building-type, building height, number of floors	January 2019 March 2019
OpenStreetmap	Building footprints	

Methodology:

The following section outlines the methodological approach for the estimation of socioeconomic indicators in Belmopan. For detailed information of the single steps and literature refer to Warth et al. (2020) in the appendix. The whole approach consists of six general steps, which are presented in following paragraphs. Figure 12 provides a graphical description of the methodology.

1. Generation of a building footprint data set
2. Establishment of a residential building typology for Belmopan
3. BT classification
4. Generation of a socioeconomic scale for Belmopan
5. Adapting BT and socioeconomic scaling
6. Regionalizing socioeconomic information on the city scale

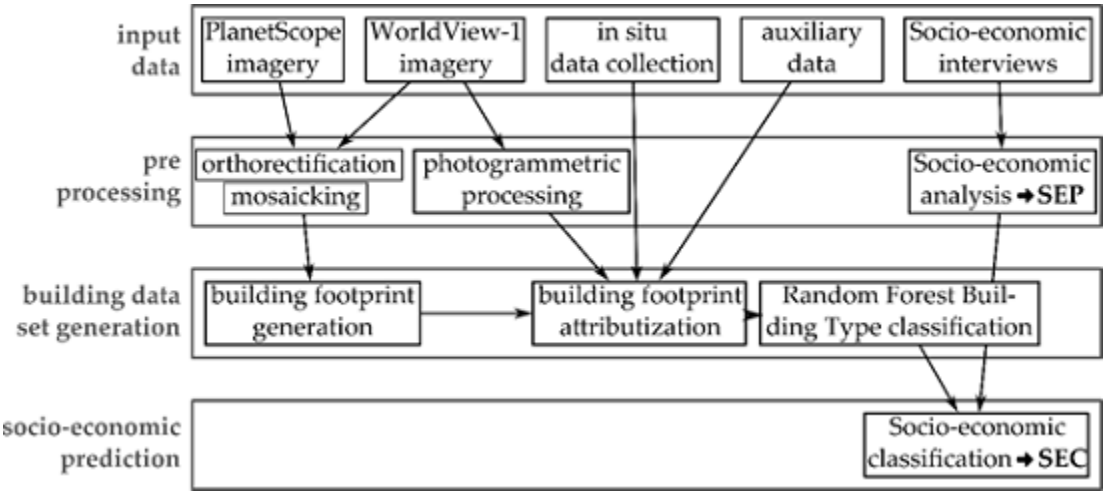

Figure 12: *Schematic methodology description to estimate socioeconomic indicators in Belmopan (Warth et al., 2020).*

1. Generation of a building footprint data set

In order to estimate socioeconomic indicators on a city covering scale, a complete building dataset was generated. Two WorldView-1 (WV-1) satellite image pairs from March 2018 (see Table 7) hereby served as spatial data basis for building delineation. For the reason of contributing the updated building footprint data set to the OpenStreetmap (OSM) database, we adapted the 1,500 pre-existing building footprints from the OSM database to the ortho-rectified WV-1 imagery and replenished the missing building footprint. For a small number of buildings, as expected in Belmopan, the manual approach to generate the building dataset is assumed to be more time efficient compared to automatic classification approaches. With regard to the BT classification accuracy, we prioritized the precision of the building footprints over scientific excellency. Therefore, the building footprints were defined manually.

2. Establishment of a residential building typology for Belmopan

Based on experiences of a field trip to Belmopan and the exchange with the Belmopan City Council, a building typology was defined for Belmopan, consisting of each four BT for single family buildings and multifamily buildings. The BT can be distinguished through the building footprint area, building footprint complexity, number of floors, roof complexity, construction materials and the number of dwelling units. Figure 13 illustrates the defined building typology for Belmopan.

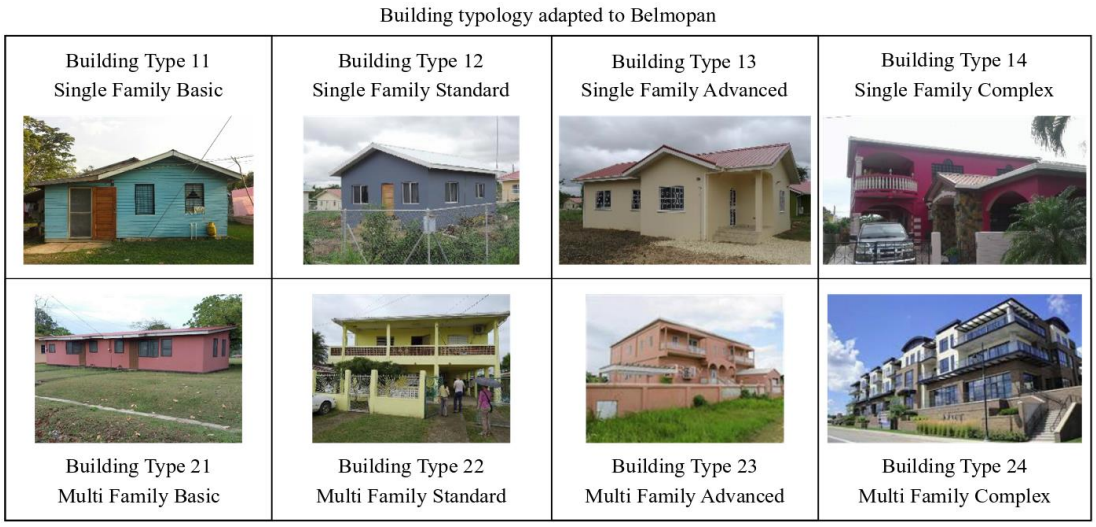

Figure 13: *Building typology adapted to Belmopan/Belize. Buildings in the upper row (BT11 - BT14) represent single family buildings, building-types in the lower row (BT21 - BT24) represent multifamily buildings (Warth et al., 2020)*

3. Building-type classification

Random Forest (RF) classifiers, which are categorized as machine learning classifiers, convince through accurate results when providing a large number of classification attributes (Breiman, 1999). In this regard, a set of 25 attributes was provided for each building, which contain information on the building footprint geometry, building height derived from photogrammetric processing of WV-1 stereo pairs, spectral information from PlanetScope imagery, spatial indices to describe Euclidean distances to places with urban functions, and quality of life indicators. From the reference dataset, collected in January and March 2019 in Belmopan, 363 samples were randomly selected to train the classifier. The initial RF classification reached an overall accuracy of 56.7 %, where especially BT 11/ BT 12 and BT 14/ BT 21 showed class overlaps. For this reason, a rule-based classification refinement was necessary. Hereby, we derived thresholds from the reference dataset for footprint area and building height to separate to better split overlapping BTs. Applying these thresholds increased overall classification accuracy to 86.3 %.

4. Generation of a socioeconomic scale for Belmopan

A household survey campaign was conducted in order to collect socioeconomic data in Belmopan in parallel to the building reference data collection campaign (see **Table** 7). Based on the "Social Class Index" applied in a German health survey (Winkler and Stolzenberg, 1998), a point scheme ranging from 3 to 18 was established to describe the socioeconomic status (SES) of the household,

considering information on household expenditures, educational level of the main household earner and household assets. For the establishment for the socioeconomic point (SEP) scheme, a sample size of 395 household interviews were available.

5. Adapting building-types and socioeconomic scaling

Predicting a 15-part SEP scheme spatially implies a level of data accuracy that cannot be provided by our methodology, which uses eight different BT for the spatial predictions. For this reason, five socioeconomic classes (SEC) were established, hereby statistics on the SEP scheme for the BT were the most relevant information to define class thresholds. The establishment of SECs based on the building typology allows assigning SECs to all residential buildings in Belmopan in accordance with its BT.

6. Regionalizing socioeconomic information on the city scale

After assigning SEC information to the respective BT, especially BT 12, BT 13 and BT 22 showed discrepancies between predicted SEC and the derived SEC data from the reference survey. In order to reduce this error and to compensate the prediction precision, BT subclasses were needed to be established. Considering land values in dependence of urban centrality (Bachofer et al., 2019; Kau and Sirmans, 1979; Rosengren et al., 2019), correlations between SEP and the distance to the market center, the distance to the US embassy (provides security patrols in the neighboring area) and the building density could be presented. These quality-of-life indicators were used to sub-classify the BTs into BT 12a/b, BT 13a/b and BT22a/b and to reduce the discrepancy of predictions and reference in SEC.

Results

The building dataset generation resulted in 6,627 identified residential buildings. Buildings with public, commercial or industrial use were excluded from an initial dataset by using information from the Belmopan City Council and the Google database. The subsequent refined classification of the building footprints resulted in the statistical BT distribution displayed in Table 8. Accordingly, single family BTs (SFBT) are dominating in Belmopan with a share of 84.6 % over multifamily BTs (MFBT), which have a share of around 4.0 %. Within the SFBTs, BT 12 and BT 13 dominate with

Table 8: *Building-type distribution in Belmopan (Warth et al., 2020)*

Building-type	Number of buildings	Share of total number
BT 11 – Single Family Basic	764	11.5 %
BT 12—Single Family Standard	3,060	46.2 %
BT 13—Single Family Advanced	1,211	18.3 %
BT 14—Single Family Complex	566	8.6 %
BT 21—Multi-Family Basic	33	0.5 %
BT 22—Multi-Family Standard	138	2.0 %
BT 23—Multi-Family Apartment	94	1.4 %
BT 24—Multi-Family Modern Apartment	1	<0.1 %
Public	166	2.5 %
Commercial	219	3.3 %
Industrial	6	<0.1 %
Uninhabited	369	5.5 %
Total	6,627	100 %

a share of 46.2 % and 18.3 % respectively and thus almost make up two thirds of the Belmopan building stock.

Figure 14 displays an overview map on all detected residential buildings in Belmopan including the respective BT. As the dominance of BT 12 and BT 13 indicates, these BTs are distributed all over the city area. For other BTs, local concentrations can be recognized. MFBTs are concentrated in the southern precincts of Belmopan, as indicated by the blue colors, BT 11 is concentrated in the eastern and south-western parts of the city. BT 14 is mainly concentrated in the northern-central part of Belmopan around the US embassy.

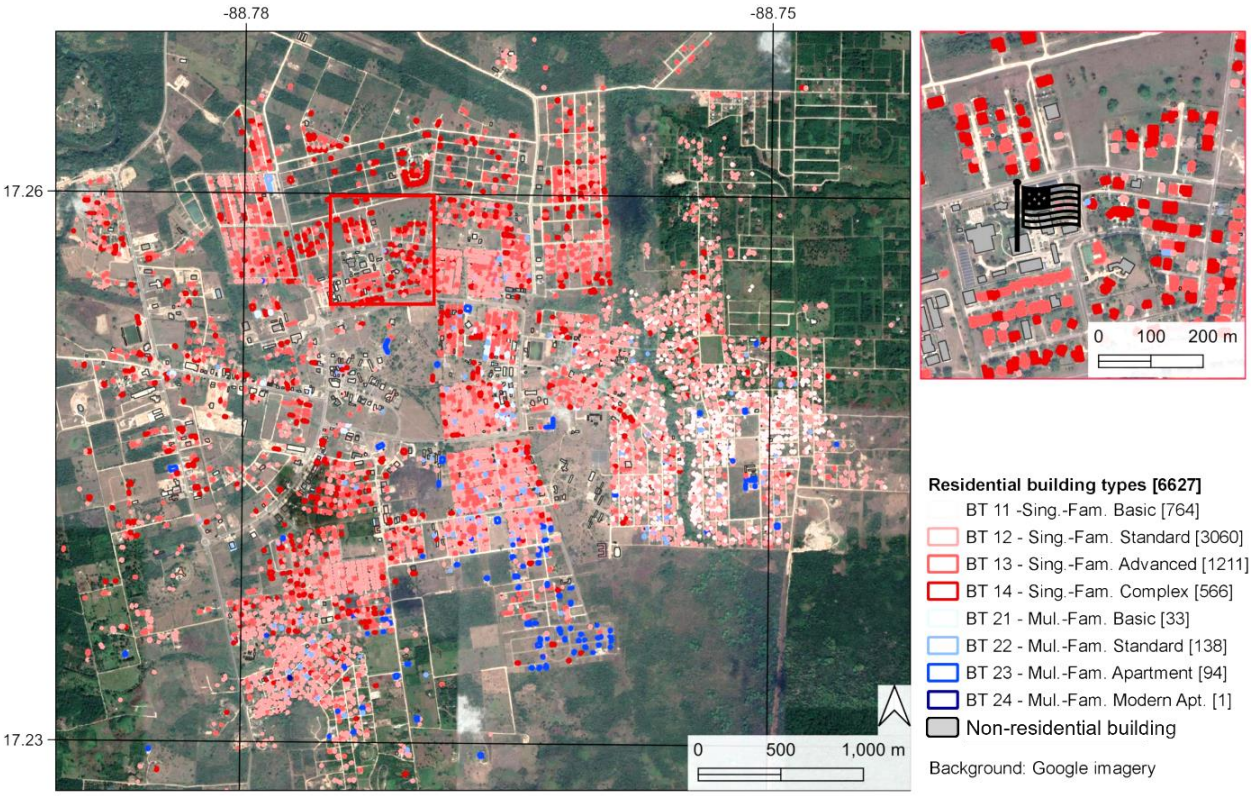

Figure 14: *Total view on Belmopan showing building-types on the single building level (Warth et al., 2020). BT 11 dominates in the eastern areas of Belmopan, BT 14 is concentrated in northern central part of Belmopan.*

Based on the household survey information, the socioeconomic point (SEP) scheme between 3 and 18 points was established. The SEPs describe a normal distribution, as shown in the histogram in Figure 15. The histogram breakdown into the BT confirms the hypothesis, that socioeconomically weaker groups inhabit BT with lower number and socioeconomically stronger groups inhabit BT with higher numbers.

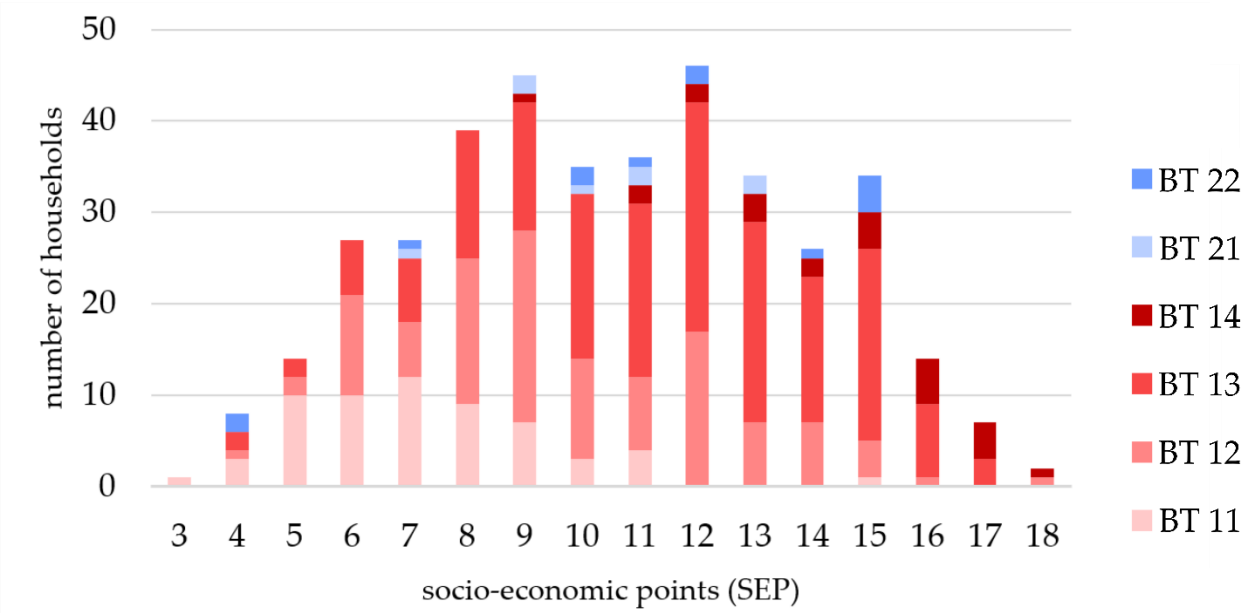

Figure 15: *Histogram on socioeconomic points distribution in Belmopan (Warth et al., 2020)*

This initial conclusion is supported by the statistical SEP analysis for the BTs, as shown in Figure 16. Clearly recognizable from the boxplots are the different mean socioeconomic points for the BTs. BT 12 and BT 13 have a relatively large range and variation in SEP statistics, as the boxplots indicate. This is most probably related to the dominating share of these two BTs of almost 66 % on the total residential building stock in Belmopan. This also illustrates the necessity of subdividing BT 11, BT 12, and BT 13 into subclasses. Still in this initial BT classification scheme, the SEP characterization for the residents is well differentiated.

Figure 16 as well shows the SEC characteristics for the subclassified building typology on the right part of the figure through the colored boxplot contours. The subclassified BTs are established based on the assumption of location dependent land value development. According to these, central urban areas have higher land values in comparison to peripheral locations. As a result, SEC I is assigned to both BT 11 and BT 12b, SEC II is assigned to BT 13b and BT 22a, SEC III is assigned to BT 12a and BT 21.

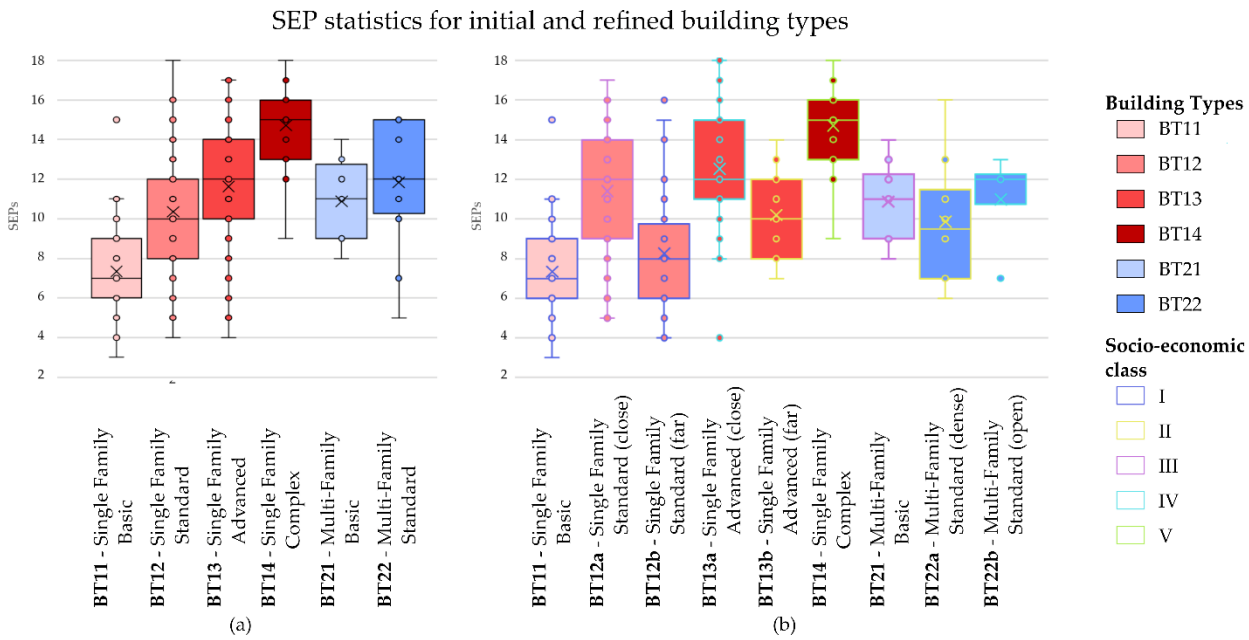

Figure 16: *Boxplots on SEP statistics for initial building-types (left) and adapted building-types with assigned socioeconomic class information (right) (Warth et al., 2020)*

SEC IV is only assigned to BT 13a and SEC V, which represents the highest socioeconomic indicator, is assigned to BT 14. For more detailed information, Table 9 provides socioeconomic statistics for the BT based on the household survey data.

Table 9: *Detailed socioeconomic statistics for building-types in Belmopan (Warth et al., 2020).*

Initial BT	**n**	**Mean SEP**	**Standard dev. SEP**	**SEC**
BT 12 – Single-family standard	108	10.4	2.79	
BT 13 – Single-family Advanced	172	11.6	2.94	
BT 22 – Multi-Family Standard	12	11.8	3.3	
Refined BT	**n**	**Mean SEP**	**Standard dev. SEP**	
BT 11 – Single-family Basic	55	7.3	2.2	I
BT 12a – Single-family Standard (close)	74	11.3	2.59	III
BT 12b – Single-family Standard (far)	34	8.3	1.99	I
BT 13a – Single-family Advanced (close)	69	12.8	2.6	IV
BT 13b – Single-family Advanced (far)	103	10.9	2.9	II
BT 14 – Single-family Complex	24	14.7	2.1	V
BT 22a – Multifamily Advanced (open)	6	9.8	3.1	II
BT 22b – Multifamily Advanced (close)	6	11.0	2.3	IV
BT 23 – Multi-family Apartment	1	15		

Thus, socioeconomic indicators can be predicted for all residential buildings in Belmopan by the availability of the SEC assignments to the refined BT. The maps in Figure 17 provide an overview on the BT information and SEC assignments for Belmopan. For reasons of resident's privacy protection, we decided to not provide more details on building location and therefore, removed local context information.

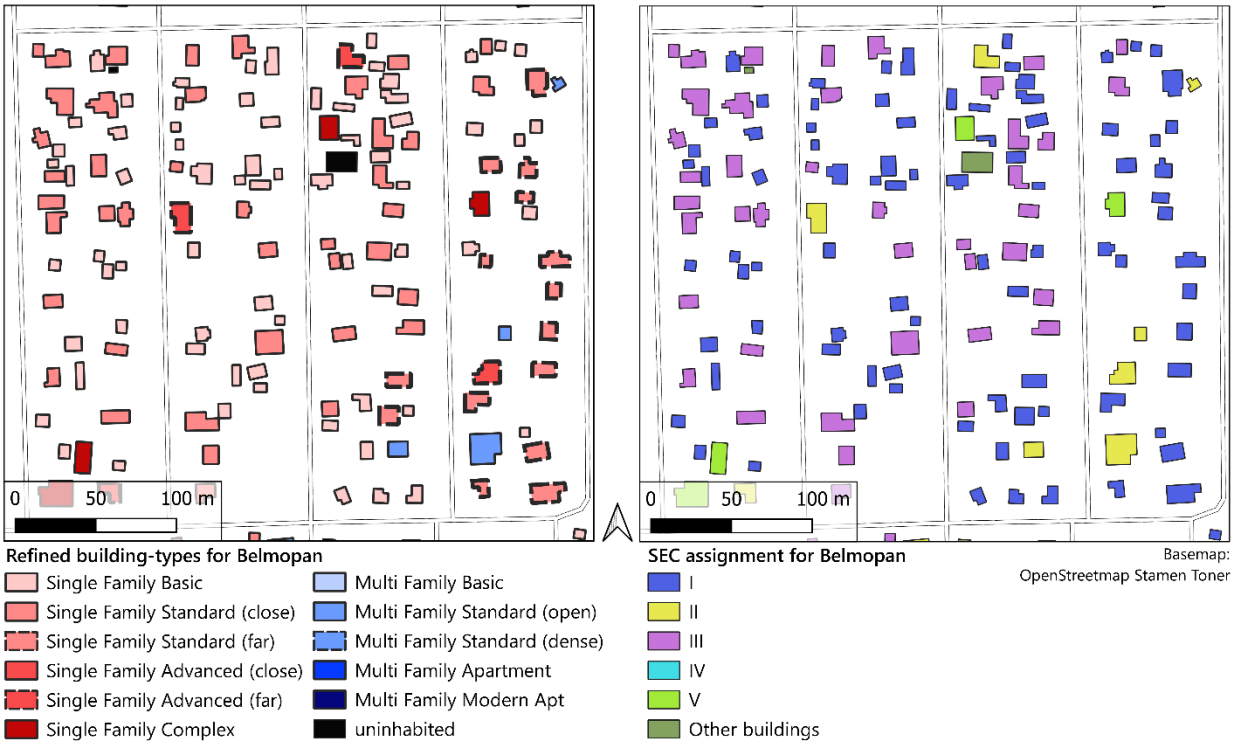

Figure 17: *Refined building-types (left) and socioeconomic class (right) for a selected subset in Belmopan (Warth et al., 2020)*

Additional analysis of the household survey data shows interesting patterns for residential water expenses for the building types presented in Figure 18. Residents in BT 11 with lowest SES, often ensure supply by water from informal wells in order to reduce water expenses. Fruits and vegetables are often cultivated on private properties, which could cause high water consumption in BT 12. Groups with high SES in BT 13 and BT 14 are not dependent on self-grown food, therefore, water demands could be reduced. Additionally, the low number of interviews in BT 14 can distort the statistical interpretation.

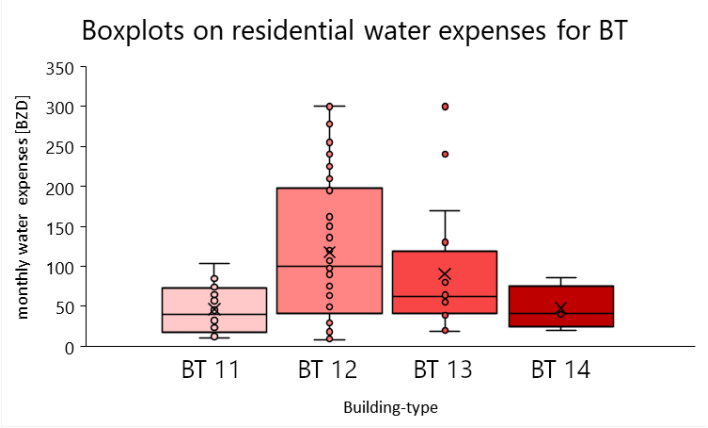

Figure 18: *Boxplots on residential water expenses for BTs in Belmopan.*

Summary

- VHR satellite imagery, in this study WV-1, is well suited to provide building footprints for the RF BT classification process.
- RF classification with subsequent rule-based classification provides very good overall classification accuracies.
- Socioeconomic information on a single building level can be provided as planning evidence
- In order to prevent misleading impressions of accuracy in the 15-part SEP scheme, a five-part socioeconomic classification is established.
- BTs can contain large SEP variation and therefore, need to be subclassified. Hereby, quality-of-life indicators and building distance to central urban institutions with influence on land values, enable good subclassification results.
- Local knowledge or expert knowledge is the key for successful BT classification in order to predict socioeconomic indicators. Without local understanding of the urban area, a representative building typology cannot be established. Furthermore, socioeconomic information in relation to BTs is difficult to be estimated without household survey information. The same applies for the parameters to subclassify the BTs. Without local expertise, the US embassy could hardly have been identified as relevant factor to influence land value.

3.4. Belmopan: PV Balancing on Single Building Level Using UAV Data

Research demand

Methodological research demands

Proper urban infrastructure planning aims at preparing urban spaces, functions, and structures for future urban demands, conditions and environments. Changes in population, climate, society, policies, mobility, trends and so forth, can influence the transformation process. In order to meet the future demands of cities, urban planning processes need to develop scenarios that include the relevant processes to be expected in future.

Poor planning can have severe economic and ecological consequences due to enormous financial expenses and mainly long-term investments in the sector of urban infrastructure planning. Planning processes and scenario development, therefore, require as detailed, large-scale, and consistent data as possible.

Local needs for attention

Although hydropower accounted for the majority for the produced electrical energy in Belize, the combined share of fossil sources increased during the last years in Belize's energy mix up to 62 % (Belize Energy Unit, 2020). Thus, Belize still relies on climate-harming energy sources on a large scale, even though Belize's capital city was relocated due to climatic effects. Furthermore, Belize is highly energy-dependent on neighboring countries, as 36 % of its energy demand is imported from partner countries to provide electricity security (Belize Energy Unit, 2020).

From a social point of view, the COVID pandemic had strong impacts. During the lockdown periods that came as a consequence of high infection incidences, residential energy consumption increased, which is very challenging economically especially for socioeconomically weaker households (Belmopan City Council)

We hypothesize that:

1. Belmopan is highly suited located for PV energy production.
2. Photovoltaic (PV) roof systems can be a central pillar in the energy mix for Belmopan.

3. Following the approach from Warth et al. (2020), a residential building typology can indicate electricity consumption.
4. EO data at highest spatial resolution from UAV imagery can deliver information valuable for urban planning and increase BT determination.
5. Using electricity consumption information and elevation data from UAV campaigns enables estimating PV energy balances on a single building level.
6. Therefore, this information can be used to plan future urban energy supply and to develop strategies to decarbonize future energy mix, to plan decentral energy grids, and to propose policies for socially-just approaches to promote PV as energy source to cover the basic baseload energy.

Data

Table 10: *Data overview on the Belmopan PV study*

Data	Information	Date
UAV aerial imagery	Total covered area: 201.2 ha 6 study areas, 15 flights, 2,866 images	2019/11
Building footprints	Warth et al. (2020)	
Household survey	190 interviews on annual electricity consumption and annual electricity expenses	2019/11
National Solar Radiation Database	Modeled solar radiation data (temporal resolution: 0.5h)	

Methodology

The approach for the PV balancing study bases on the ideas and findings Warth et al. (2020), which show the relation between the residential BT and socioeconomic indices. In order to balance roof-based PV energy generation on residential buildings and the electric energy consumption, two methodological processing paths have to be carried out. Firstly, an estimation of potential PV energy production on residential building roofs and secondly, a prediction of household electricity consumption based on BTs and household surveys. Thus, the approach consists of the following

steps, which are presented schematically in Figure 19 and described in more detail in the following paragraphs. For detailed information, refer to Warth et al. (2021) in the appendix.

1. Residential household survey on electricity consumption
2. UAV aerial image campaign and Structure-from-Motion data processing
3. BT classification
4. Electricity consumption analysis based on household survey
5. PV potential analysis
6. PV energy balance analysis

The methodology is presented in the subsections M-1 – M-6, results accordingly, are presented in subsection R-1 – R-6.

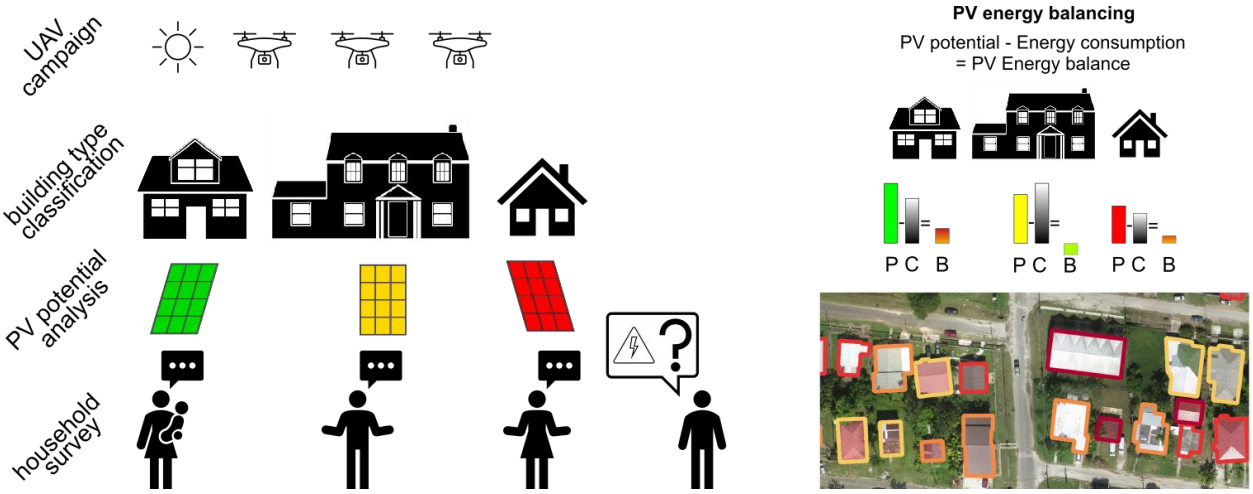

Figure 19: *Schematic description of the approach for PV energy balancing in Belmopan*

M-1 Residential household survey on electricity consumption

To estimate the residential electricity consumption, a household survey was conducted to collect empirical data in November and December 2019. Based on the outcomes of the socioeconomic study by Warth et al. (2020), a spatial interview sampling was designed in order consider all relevant BTs in Belmopan. Therefore, we defined six areas with dominance of specific BTs (see Figure 20). The questionnaire itself includes questions on habits in regards of electricity consumption that are relevant for this study. A total number of 190 household interviews could be achieved, from which 63 interviewees could provide bills to verify the statements.

Figure 20: *Overview on research areas, covered by the UAV imaging campaign (Warth et al., 2021)*

M-2. UAV aerial image campaign and Structure-from-Motion data processing

For precise estimation of PV energy potential, elevation data in very high spatial resolution are required to determine information on roof orientation and slope. These demands can be met through Structure-from-Motion (SfM) processing of overlapping VHR imagery. In order to fulfil these data requirements, an aerial campaign was conducted in November and December 2019, using an unmanned aerial vehicle (UAV) in the defined research areas in Belmopan. The payload for the custom UAV is a S110 Canon compact camera (CameraDecision, 2021), mounted in a nadir orientation. The UAV was navigated via auto pilot on pre-defined tracks.

The SfM methodology bases on photogrammetric principles (see section 3.2), however imagery can be provided from unstructured surveys and the amount of input imagery determines the image quality of the results (Ullman and Brenner, 1979). The SfM processing provides a digital surface model (DSM), which includes height information on the surface and objects, and an orthomosaic of the aerial imagery. The flight altitude in the 15 single flights was defined at 65m, which in combination with the image overlapping factor of 70 % resulted in spatial resolutions between

1.9 and 2.4 cm. All datasets were resampled to a ground sampling distance of 2.5 cm so as to define a consistent spatial resolution.

In order to derive building height statistics, a normalized DSM (nDSM) is produced based on the SfM processing results, in which the ground elevation is subtracted from the DSM. Thus, only object heights remain in the nDSM.

M-3. BT classification

For reasons of methodical comparability to the SEC study and to evaluate the effect of integrating UAV orthomosaics in highest spatial resolution, the RF classifier was selected for the BT classification again. Furthermore, the building footprint dataset from Warth et al. (2020) was used for the RF classification but was adapted to the higher level of detail in the UAV orthomosaic to increase the footprint precision. As mentioned in section 3.3, the roof complexity is a BT defining criterion, which in theory should improve BT classification accuracy. However, the WV-1 imagery could not serve as an information source to determine roof complexity due to insufficient spatial resolution. The UAV data, with a spatial resolution of 2.5 cm offer a 400-fold increase in the level of detail compared to WV-1 data. This enables capturing parameters to describe roof complexity. For this, a set of roof ridge parameters were derived for each building, namely the sum of roof ridge lengths, the roof ridge densities per roof or area and the variation of roof ridge orientation. Other attributes to train the classifier from the previous study were not changed, only updated to the increased spatial resolution of the UAV data products. 213 samples from ground-truthing data collection campaigns (Table 10) were used as reference data to train the RF BT classifier, which is 65 % of the complete ground-truthing dataset. Identically to the socioeconomic study, 35 % of data are used to validate the classification.

M-4. Electricity consumption analysis based on household survey

The household survey provided insights in residential electricity consumption based on 190 interviews. Both electric consumption (kWh/month) and electric expenses (Belize Dollar/month) were queried, though the data analysis revealed that the residents seem to have a better comprehensibility of electricity expenses than electric energy consumption. Due to this, BT-specific electric

energy consumption statistics were determined on the basis of electric expenses and an average electricity price.

M-5. PV potential analysis

A local PV potential can be estimated based on three main factors: Firstly, the local surface orientation and inclination. Secondly, the global horizontal irradiation, which defines the average available solar energy. And thirdly, the PV system performance, which describes the PV module efficiency and power losses within the system, and due to module pollution.

The National Solar Radiation Database (NSRDB) by the US National Renewable Energy Laboratory (NREL) provides data on GHI for the northern hemispheres of North and Latin America in a 0.5h temporal resolution and a 4 km spatial resolution with a mean error between 5 % and 10 % (Sengupta et al., 2018). This dataset allows the determination of the annual GHI. A local PV suitability factor for each pixel in the spatial raster dataset is calculated by performing a solar radiation model (Hofierka and Suri, 2002) on SfM DSM. This factor describes the expectable amount of solar irradiation in comparison to flat terrain (COF). To estimate the PV module performance in tropical regions, literature reports performance ratios between 0.7 and 0.89 (Kim et al., 2014; Romero-Fiances et al., 2019). Therefore, we decided to use a performance ratio value of 0.78 for our study. Recent analyses show that PV panel's efficiency can reach 23 % (pv magazine, 2021). We decided to apply standard sizes of 1,650 x 992mm (Doelling, 2017) as PV module area. The roof area available for PV panel installation, is the most important factor for the analysis of the PV potential. Based on calculated roof area orientations from the SfM DSM, the roof pixels are classified in eight roof orientation classes. When spatially aggregated, these eight classes result in single fields of roofs (FOR). Considering space for PV panel installation, a spatial buffer of 0.3 m is removed from each FOR. Because the number of possible PV panels on irregular FOR geometries can only be approximated with GIS techniques, we chose a conservative method to determine the maximum number of PV panels per FOR by calculating iteratively the maximum inner circle for each FOR. The maximum number of installable PV panels for each radius can be adopted from a lookup table. Further maximum inner circles are determined for the remaining areas not covered by the

initial maximum inner circle. Following this iterative approach allows to estimate a number of possible PV modules for each FOR, as shown in Figure 21.

The study aims at providing an approach that can be used to test different PV strategy scenarios. Therefore, two out of many possible scenarios are to be tested in this work. In scenario 1, the "optimal scenario", the best suited FOR per building is to be fully covered with PV panels. In scenario 2, the "realistic scenario", two PV panels are installed on the best suited FOR on each building. In this regard, for each FOR the PV suitability is determined by generating the product of the number of possible PV panels, the COF factor and the GHI. The FOR with the highest suitability product is selected for PV installation for each studied building. For the best suited FOR, the PV energy potential can thus be determined by multiplying the possible number of PV panels, the PV panel area, the GHI, the COF factor, the PV module efficiency, and the performance ratio.

M-6. PV energy balance analysis

By assigning BT-specific statistics on annual electricity consumption to the BT classified building footprints, the statistical electricity consumption is available for each. By differencing the PV energy potential of both scenarios and the statistical electricity consumption, the PV energy balance is determined. Positive differences indicate an PV energy surplus, negative differences indicate a PV energy deficit.

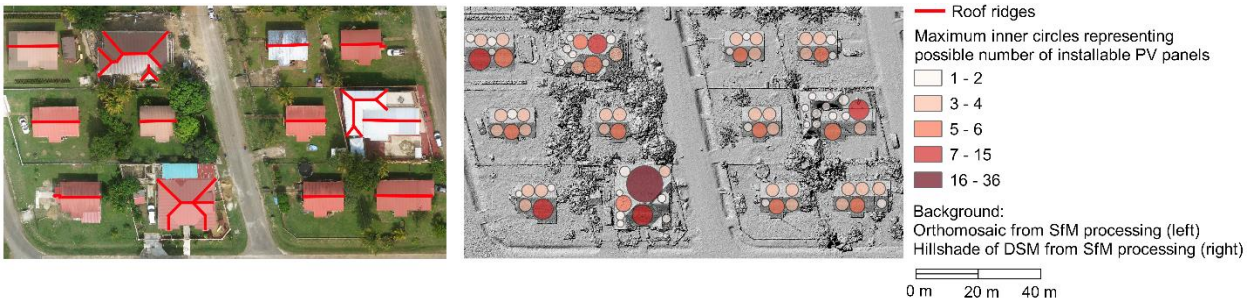

Figure 21: *Detailed view on roof ridges and maximum inner circles for the estimation of maximum number of possible PV panels*

Results

R-1. UAV aerial campaign

During 15 flights, a number of 2,866 aerial images were acquired. The covered research area is 201.2 ha, thus 14.2 images per ha were available for SfM processing.

R-2. SfM processing: VHR DSM and orthomosaic

The SfM processing of the UAV images resulted in each a DSM and an orthomosaic for the six study areas in Belmopan. All datasets resulting from the SfM processing were horizontally adapted to the WorldView-1 acquisition using a spline interpolation in order to maintain data integrity from the previous study. Figure 22 shows a detailed view on the SfM results in the 2.5 cm spatial resolution.

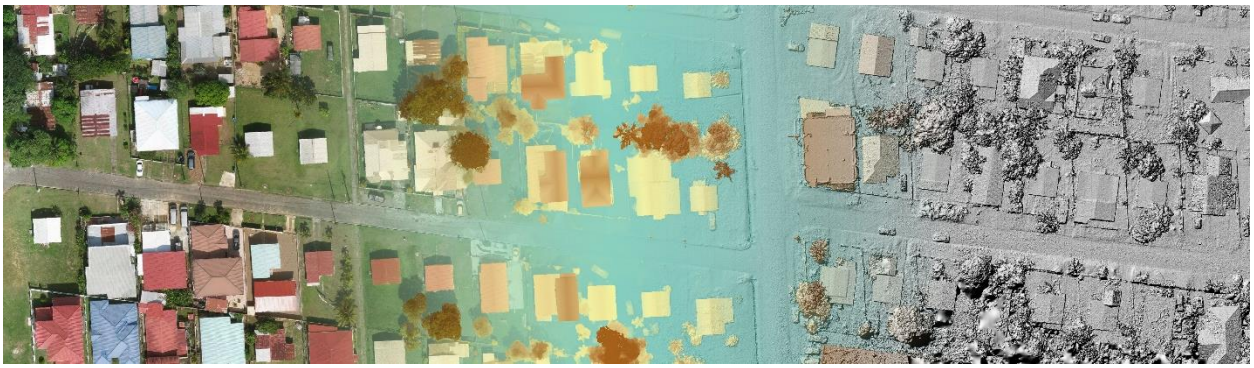

Figure 22: *Animated presentation of the SfM products showing level of details of the UAV data: Orthomosaic (left), DSM (center) and hillshade (right). All datasets are defined by a spatial resolution of 2.5 cm.*

R-3. Manual building footprint adaption

The defined study areas enabled covering residential 1,619 buildings with UAV data. In comparison to the previous study, 24.4 % of the residential buildings in Belmopan could be covered. All building footprints were adapted according to the higher level of detail from the orthomosaics. Using the DSM and the orthomosaic, roof ridges were manually detected for all buildings. Additionally, building height statistics were recalculated based on the UAV nDSM.

R-4. BT classification

The identical building typology as presented in section 3.3 was applied with the identical RF classification parametrization (see Warth et al. 2020 in appendix A-2) to classify the BTs.

The classification attributes were complemented by roof ridge characteristics in order to consider the roof complexity of the buildings for classification improvement.

The ranking of the building attributes for the RF classification in Table 11 shows very clearly, that the shape parameters of the building footprints and the roof ridge characteristics have the main importance for the classification. The first 16 ranked attributes are all assigned to the shape parameter category. Spatial parameters, which describe distances to central places or building densities, have a minor role in the classification process, as they are ranked between 20 and 33.

Table 11: *Ranking of RF classification attributes for the building-type classification in Belmopan using UAV imagery. The higher the Gini inequality index, the more relevant the attribute for the RF building-type classification.*

Shape parameters	Gini ineq. index/ Rank		Three-dimensional parameters	Gini ineq. index/ Rank		spatial/distance parameters	Gini ineq. index/ Rank	
Building footprint area (A)	0.152	#1	Building height (mean)	0.055	#14	Distance to bus line	0.031	#20
Roof ridge length [sum]	0.142	#2	Building height (median)	0.04	#17	Distance to paved roads	0.031	#21
Building footprint perimeter (P)	0.136	#3	Building height (standard dev.)	0.033	#18	Distance to industry	0.027	#23
Building D/A	0.134	#4	Building height (variance)	0.032	#19	Distance to ring road	0.024	#24
Building maximum distance (D)	0.124	#5	Roof slope (mean)	0.019	#26	Distance to education	0.022	#25
Roof ridge number	0.109	#6				Building density 100m	0.018	#27
Building P/A	0.102	#7				Distance to commercial center	0.014	#28
Roof ridge density [RR number/ A]	0.092	#8				Building density 250m	0.013	#29
Roof ridge length [standard deviation]	0.092	#9				Distance to public institution	0.012	#30
Building footprint corners	0.087	#10				Building density 150m	0.011	#31
rr_angle_stdev	0.081	#11				Building density 200m	0.011	#32
Roof ridge density [sum length/ A]	0.063	#12				Building density 50m	0.01	#33
Roof ridge length [mean]	0.058	#13						
Building shape index	0.044	#15						
shape_P/sqrt(A)	0.044	#16						
shape_D/sqrt(A)	0.03	#22						

This is in contrast to the findings of the previous study in section 3.3, where we assumed that they can improve the classification result.

Table 12 shows building characteristics on footprint area, building height and roof ridge numbers for the BT in Belmopan. Between the BTs, differences can be recognized. BT 11 shows lowest values in building footprint area, height and roof ridge numbers, whereas BT 14 shows highest numbers in all categories.

Table 12: *Building-type characteristics for buildings in Belmopan: Mean values on building footprint area, building height and number of roof ridges.*

building-type	Area [m^2]	Height [m]	rr_number
11 [204]	59.4	2.9	1.2
12 [767]	102.8	3.1	1.5
13 [481]	177.5	3.4	3.4
14 [129]	250.2	4.7	8.4
21 [22]	104.1	2.8	1.3
22 [12]	141.9	5.9	2.9
23 [3]	135.0	4.4	3.7

R-5. Electricity consumption analysis based on household survey

Although information on electric energy consumption (kWh/month) and monthly expenses for electric energy (BZD/month) was collected in the household survey, the monthly expenses were used to estimate electric energy consumption. Statistics on monthly energy consumption showed large variation, which could be caused by missing knowledge on this relatively abstract unit. Expenses for electricity, on the other hand, are a very concrete unit, which are very present in mind, especially in regions with high electricity prices. Provided bills during the household interviews and statistic evaluations indicate an electricity price of 0.42 BZD/kWh and confirm accuracy in statements on monthly electricity expenses. Statistical reports confirm the price for electricity (Belize Electricity Limited, 2021).

By multiplying the monthly expenses for electric energy by 12, the annual electricity expenses are determined, which are converted to annual electricity consumption by multiplying the price for the kWh of electric energy. As shown in Warth et al. (2021), the BT distribution in the household survey corresponds to the BT distribution of the entire city of Belmopan. Therefore, the statistical

analysis of the electricity consumption can be considered valid. Thus, the average annual electric consumption in Belmopan can be assumed 3,435.6 kWh/year, with a standard deviation of 2,011.8.

R-6. Linking electricity consumption to BT

In parallel to the distribution of socioeconomic indicators, electric consumption differs between the BT, as shown in Figure 23. Due to insufficient sample numbers for multifamily buildings, only SFBTs, which make up 95% of the successful interviews, are presented. BT 11 has the lowest mean annual electricity consumptions of 2,458.5 kWh/year with a standard deviation of 1,152.8. BT 12 has a mean annual electricity consumption of 3,220.7 kWh/year with a standard deviation of 1,765.2. BT 13 has the second-largest annual electricity consumption of 4,042.1 kWh/year with a standard deviation of 2,240.2. The annual electricity consumption BT 14 has the highest electricity consumption with clearly higher values of 6,276.2 kWh/year with a standard deviation of 2,766.6.

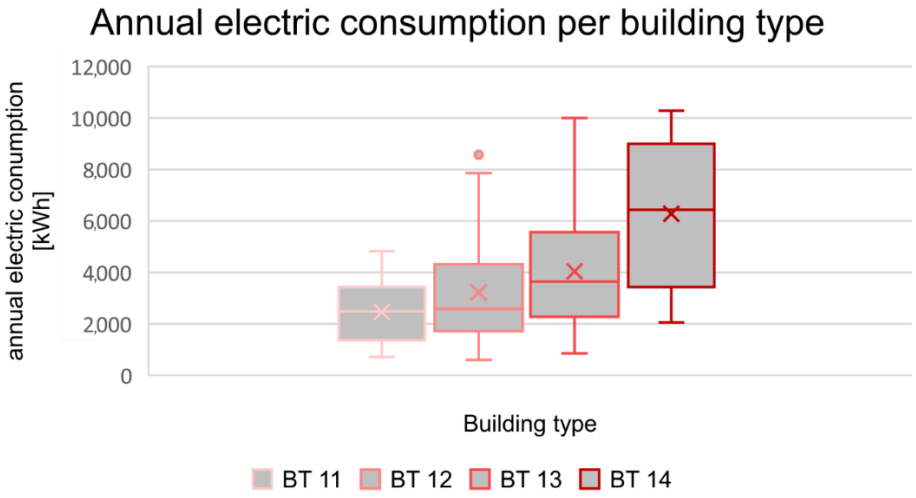

Figure 23: *Boxplots displaying annual energy consumption (kWh) for residential buildings in Belmopan.*

R-6.1. PV potential analysis based on DSM

On the 1,619 studied buildings in Belmopan, 4,546 FOR are suitable for PV panel installation through meeting the requirements of the required installation area and insolation free from vegetation cover. Figure 24 shows histograms on PV panels per FOR in Belmopan on the best suited FOR per building. 50.9 % of the FOR are suitable to install 1-4 PV panels, another 26.9 % of the FOR can take 5-9 PV panels.

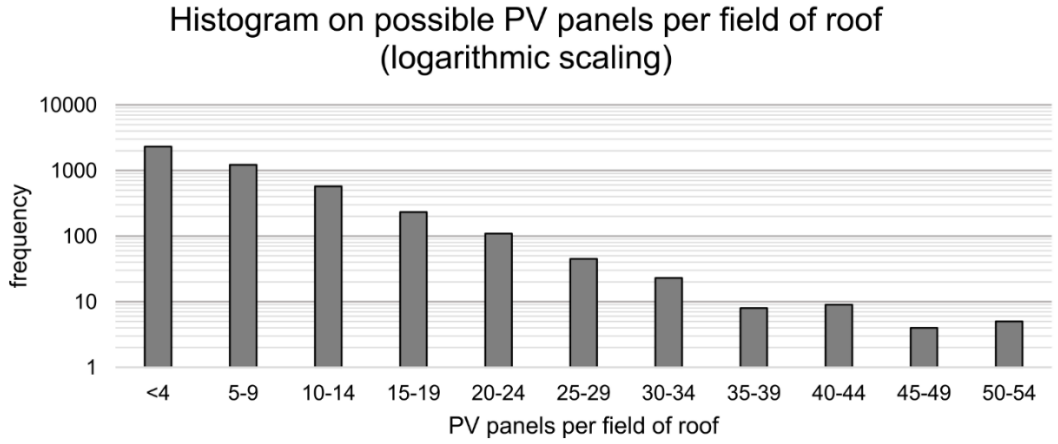

Figure 24: *Histogram on FOR capacity for PV panels in logarithmic scaling in Belmopan.*

To calculate the PV potential for each building, we assume the PV panel efficiency of 23 % and a performance ratio of 0.78 from the literature. The number of installable PV panels is calculated from maximum inner circles for the FOR, GHI is given from the NSRDB and ranges in Belmopan between 1,852 and 1,859 kWh/m^2/year. The PV suitability for the FOR is determined from the SfM DSM. One thousand five hundred eighty-five buildings are suitable for PV production, the others were excluded due to high vegetation foliage coverage or too small FOR areas. In scenario 1, the building with minimum PV energy yield can generate 979 kWh/year, the building with maximum PV energy yield can generate 127,780 kWh/year. The buildings with the best FOR can generate an average of 22,965 kWh/year with a standard deviation of 17,949.

The BT is not decisive for the PV energy generation, but rather the area of the FOR or roof fragmentation. Therefore, buildings with complex roofs have disadvantages, like for BT 14 buildings. BT 14 has very large building footprint areas, but the high number of roof ridges leads to a high roof fragmentation with smaller FOR.

R-6.2. PV energy balancing

In order to show the feasibility to calculate different scenarios for PV energy balancing, two scenarios were presented:

1. Optimal scenario: Best FOR per building fully equipped with PV panels
2. Realistic scenario: Best FOR per building equipped with two PV panels

The histograms in Figure 25 show the distribution of the potential PV energy yield for both scenarios and display wide range of potential PV yield for scenario 1. The histograms indicate as well that by considering a third or fourth PV panel for scenario 2, the peak in PV yield in the left histogram between 3,000 and 5,999 kWh/year can be approached in scenario 2, and more PV energy potential could be accessed.

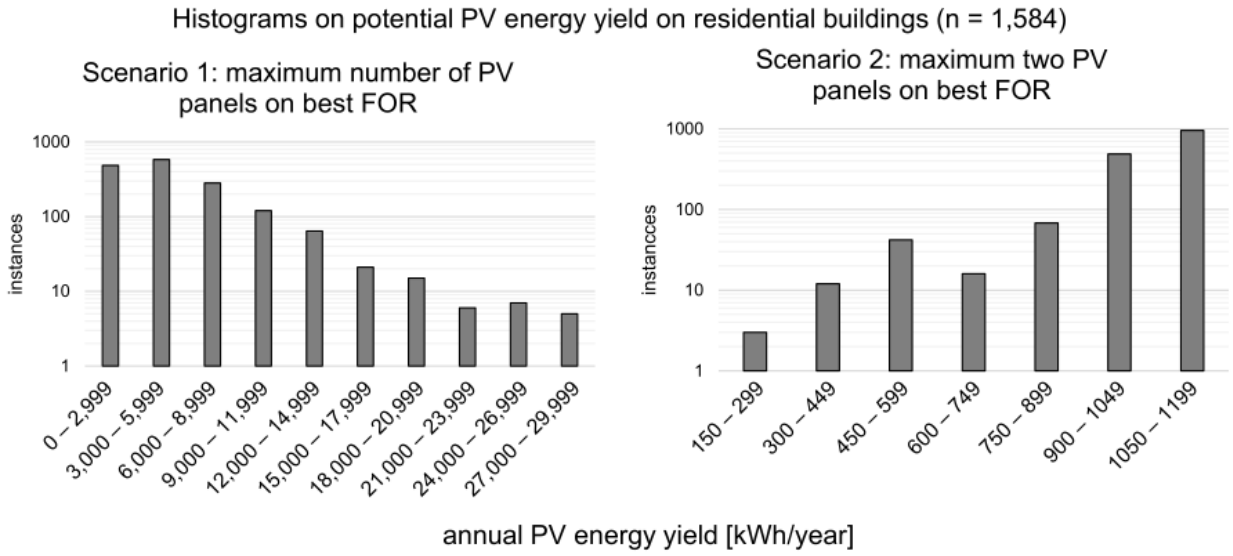

Figure 25: *Potential PV power yield on residential buildings in Belmopan for both tested scenarios.*

Extreme values for the PV energy yields in scenario 1 can be 2,500 % above the PV energy yields in scenario 2, which indicate the discrepancy of the PV energy balances for both scenarios, presented in the next paragraphs.

For detailed numbers for the PV energy balancing please see Table 13. Furthermore, only the major findings are discussed in this text, please refer to Warth et al. (2021) in the appendix for more details. In scenario 1, all BT except BT 11 have a positive energy balance and show an average PV energy balance of 1,847 kWh/year or a PV energy coverage ratio of 148 %. BT 11 has an energy balance of -337 kWh/year. Small roof areas inhibit higher PV energy yields. Despite the deficit, still 86 % of the energy demand can be covered by PV installations. Surprisingly, BT 13 and not BT 14 has the highest positive PV energy balance of 3,489 kWh/year or an energy coverage ratio of 186 %. The PV energy surplus for BT 14 is comparably low due to the very high energy consumption and the high roof fragmentation (see Table 12), which results in smaller FOR. BT 21 has large area

FOR due to its rectangular building footprint and simple roof structure and, therefore, achieves very high PV energy surpluses as well.

For scenario 2, the PV energy balance for all buildings in Belmopan in average is -2,607 kWh/year which enebles a PV energy coverage of 29.5 %. In detail, the results show almost inverted characteristics compared to scenario 1: As the numbers of PV panels are limited to maximum two panels, the electricity consumption mainly determines the PV energy balancing results. Therefore, BT 11 with the lowest electric energy consumption, can profit most from the scenario, as 36.0 % of its energy consumption can be covered with PV energy. BT 14, on the other hand, shows very high electric energy consumption patterns and thus, can only cover 17.1 % of its energy demand from PV energy. Socioeconomically weak groups therefore, can profit most from scenario 2, as large shares of energy can be provided by PV energy and therefore can financially relieve these groups from high energy expenses (financial investments are not considered but could be covered in federal programs).

Table 13: *PV energy balances for residential building-types in Belmopan.*

	Scenario 1: maximum number of PV panels on best FOR		**Scenario 2: maximum two PV panels on best FOR**	
	PV balance [kWh/year]	PV energy coverage [%]	PV balance [kWh/year]	PV energy coverage [%]
Total	1,847 (+/- 4,049)	148 % (+/- 108)	-2,607 (+/- 903)	29.5 % (+/- 6.5)
BT 11	-337 (+/- 1,930)	86 % (+/- 78)	-1,573 (+/- 227)	36.0 % (+/- 9.9)
BT 12	1,318 (+/- 3,420)	141 % (+/- 106)	-2,191 (+/- 118)	32.0 % (+/- 3.7)
BT 13	3,489 (+/- 4,443)	186 % (+/- 110)	-2,971 (+/- 74)	26.5 % (+/- 1.8)
BT 14	1,670 (+/- 5,528)	127 % (+/- 88)	-5,203 (+/- 63)	17.1 % (+/- 1.0)
BT 21	3,189 (+/- 2,625)	202 % (+/- 84)	-2,120 (+/- 104)	32.1 % (+/- 3.3)
BT 22	925 (+/- 2,779)	122 % (+/- 65)	-3,230 (+/- 87)	24.1 % (+/- 2.0)
BT 23	8,662	352 %	-2,324	33.0 %
Precinct I	2,353 (+/- 3,442)	161 % (+/- 84)	-3,006 (+/- 1,072)	27.8 % (+/- 6.3)
Precinct II	2,814 (+/- 4,443)	174 % (+/- 117)	-2,601 (+/- 685)	29.5 % (+/- 4.5)
Precinct III	2,125 (+/- 4,537)	158 % (+/- 128)	-2,664 (+/- 1,011)	29.0 % (+/- 6.9)
Precinct IV	837 (+/- 3,385)	117 % (+/- 85)	-2,326 (+/- 807)	31.5 % (+/- 7.1)
Precinct V	734 (+/- 2,624)	117 % (+/- 83)	-2,171 (+/- 863)	32.3 % (+/- 9.1)
Precinct VI	1,676 (+/- 3,926)	146 % (+/- 99)	-2,712 (+/- 726)	28.9 % (+/- 4.7)

R-6.3. BT specific analysis and spatial analysis

Table 13 as well presents spatial characteristics for PV energy balances. For scenario 1, areas with the highest frequencies of BT 12 and BT 13 (Precinct I and Precinct II) show the highest averages for the PV energy balances. In the contrast, the areas with highest frequencies of BT 11 (Precinct IV and Precinct V) have the lowest PV energy balances. In scenario 2, the areas with highest frequencies of BT 11 have the highest PV energy coverage ratios, whereas areas with high frequencies of BT 12 and BT 13 have the lowest PV energy coverage ratios. Figure 26 illustrates these findings: On the overview maps on the right side, the colors represent the PV energy coverage ratios or the PV energy balance, respectively. As the PV energy analysis in consideration of the BT can characterize whole precincts and thus, indicate the efficiency or expected effect of planning measures, these scenarios can be used for spatial urban infrastructure planning.

Additional analysis, visualized in the diagrams in Figure 27, reveal that information on residential electricity expenses and water expenses cannot be directly put into discernible relation with the

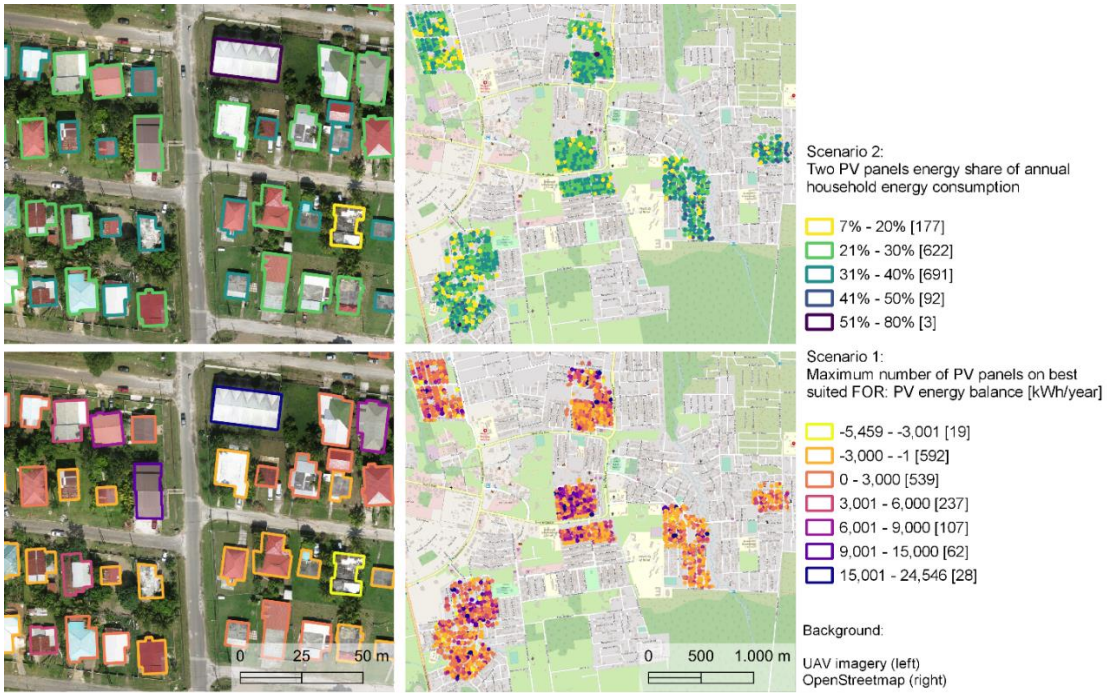

Figure 26: *PV energy balance on single building level for Belmopan. The upper views display the results of the "maximum two panels" scenario, whereas the lower row displays the results of the "optimum" scenario. Single buildings are displayed on the left column, the right column gives an overview on the city scale. For scenario 2, highest energy coverage rates are located in the eastern areas of Belmopan as indicated by blue colors, where low SES households dominate. Highest energy balances for scenario 1 are located in central areas of Belmopan where BT 12 and BT 13 dominate, as indicated by purple and blue colors as well.*

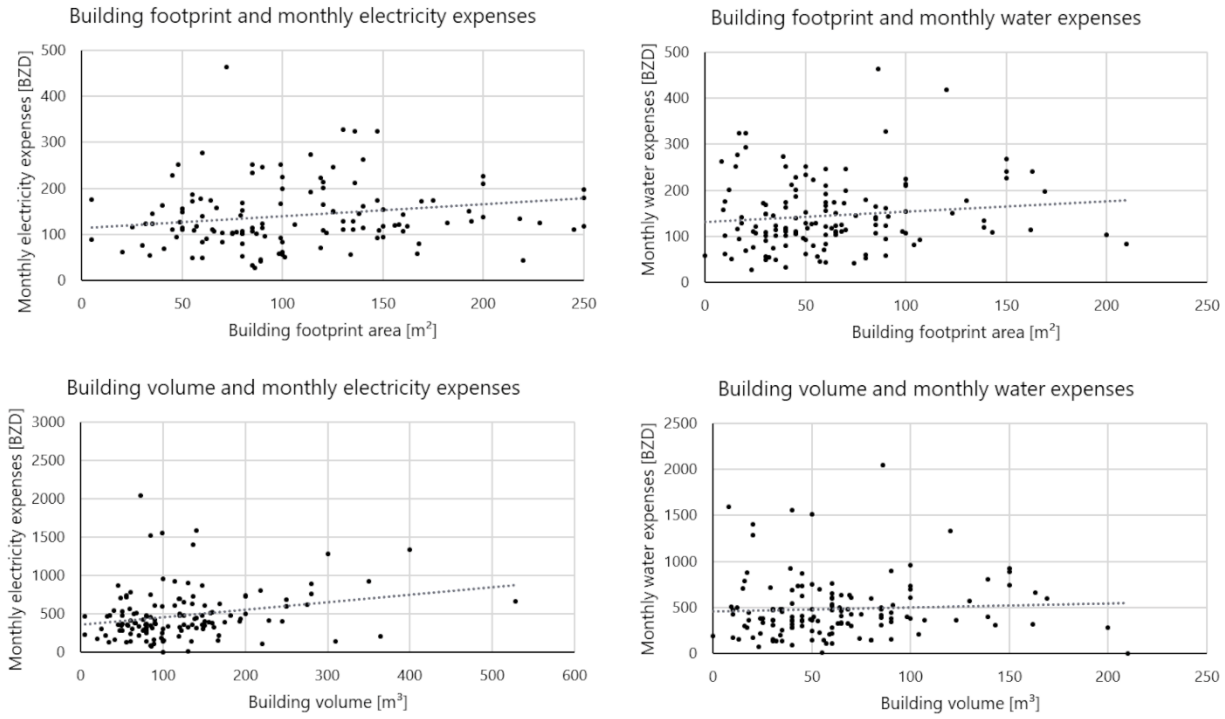

Figure 27: *Diagrams on water and electricity expenses in dependency with building footprint area and building volume for Belmopan. Missing dependencies underline the necessity of the building type classification in order to predict electricity and water consumption.*

physical attributes building footprint and building. Therefore, the classified BT cannot be substituted by simple morphological building attributes.

The statistical analysis of the household surveys shows distinct consumption patterns for electricity and water in relation to SEC, as shown by the boxplots in Figure 28. Whereas a trend of increasing electricity expenses with increasing SEC can be identified, highest water expenses are seen for SEC III. Because habits on water consumption were not focused on in the household surveys. Reasons for highest water consumption could be the water use for irrigation purposes in self-sufficient food supply. This is usually not necessary for socioeconomically higher groups. Migrants in the eastern parts of Belmopan often ensure supply through wells (Belmopan City Council, 2021).

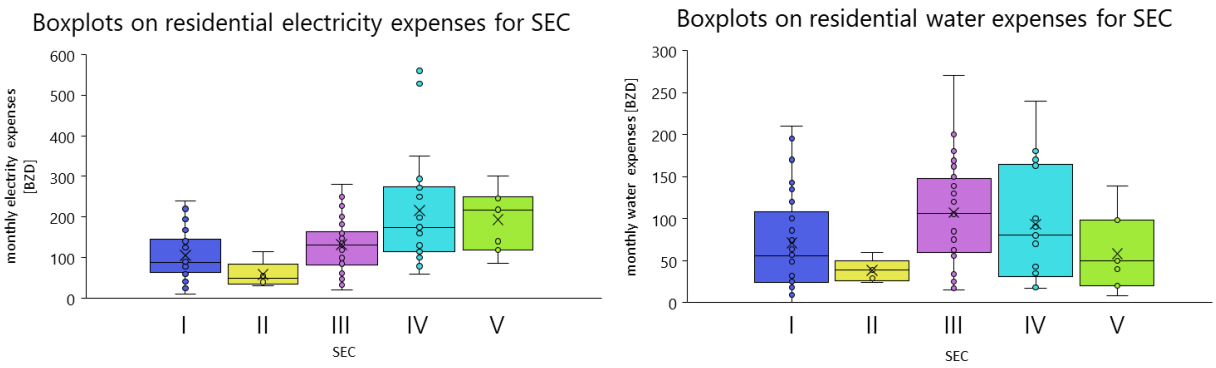

Figure 28: *Boxplot illustrating statistical characteristics of electricity expenses and water expenses in relation to SEC in Belmopan.*

Summary

- UAV aerial data enables SfM processing for very high spatial resolution orthomosaics and DSM data.
- UAV aerial imagery is a valuable data source to analyze smaller urban areas.
- UAV SfM data products increase RF BT classification, as building footprints area and building height can be estimated more precisely in comparison to estimations based on VHR satellite imagery, such as Pléiades or WorldView-1.
- Based on UAV data, most important building attributes for RF BT classification are building footprint characteristics, building height information and information on roof complexity.
- Unlike from VHR satellite imagery, UAV aerial imagery can provide roof complexity information for RF BT classification, which is essential for classification accuracy. Based on UAV orthomosaics and DSM information, roof ridges can be captured.
- Residential household energy consumption is in relation to the defined BTs for Belmopan.
- Estimations on roof-based PV energy yields based on UAV DSMs in combination with BT specific energy consumption enables PV energy balancing on a single building level.
- For the optimal scenario with the best fitted roof per building fully covered with PV panels, 148 % of the residential energy can be covered, whereas BT 12 and BT 13 have the highest coverage ratios.

- For the realistic scenario with two PV panels on the best suited roof, 29.5 % of the residential energy demand can be covered in average. Due to the low energy consumption, BT 11 can cover 36 % of its energy demand from PV energy.
- Residential buildings in Belmopan can cover significant shares of the energy consumption from roof-based PV energy.
- The presented approach allows scenario development for urban infrastructure planning and building PV strategies and policies.
- Socially weak groups, dwelling in BT 11, can be relieved from high energy prices through adapted solar policies and funding strategies.
- Local knowledge, for example through household interviews, is essential for precise estimations of energy consumption.

3.5. Summary

In both studied cities, Da Nang and Belmopan, the presented studied revealed their benefits and contribution to the process of urban planning and urban infrastructure planning. Both earth observation techniques showed their opportunities to provide data for planning decision making. For Da Nang, the Pléiades imagery allowed covering the whole city, but through photogrammetric processing, the ground sampling distance of 0.5m gets slightly blurred, so that the full level of detail is not available in the elevation data sets. In Belmopan, the UAV aerial imagery products prove their capabilities in regard of the extreme high spatial resolution of around 2 cm, which allows capturing building details in the highest precision. However, the spatial coverage is very limited with this technique.

The Da Nang study (section 3.2) proves to provide information on urban dynamics using satellite imagery going beyond areal changes of LULC classes in order to provide data on building stock dynamics. Elevation or DSM data, respectively, from photogrammetrically processed Pléiades imagery built the data base for change detection in the building stock. Through differencing DSM of two points in time, change within this time interval is being delineated. The 0.5m GSD of the Pléiades imagery is sufficient to detect changes on a single building level, although determining single building footprints from the spectral imagery in Da Nang would be very challenging due to the high building density. By adding local and spatial context information, in this study a built-up

mask and a change threshold, change was classified in new built, upgraded or into demolished buildings. The high accuracies of the detected changes of 82 % confirm the potential of the methodology to characterize city parts through building stock internal dynamics into highly dynamic or constant areas.

With the main finding of the initial Belmopan study (section 3.3), the representation of a socioeconomic indicator through the residential BT could be demonstrated. Socioeconomic measures cannot directly be implemented into the process of urban planning or urban infrastructure planning, but consumption of electricity and water or production of solid waste and waste-water are correlated to socioeconomic states of residents. For Belmopan a building typology was defined, containing four SFBT and four MFBT. A residential five-part socioeconomic classification was established on the basis of a SEP scale, which covers information on educational degree, monthly household expenses and household assets. The reference information hereby was collected through extensive household surveys. WV-1 imagery enabled the capture of all building footprints in Belmopan. On this basis, the residential buildings were classified using a RF classification. After threshold-based classification refinement, using quality of life indicators, such as the distance of the building to the US embassy, a classification accuracy of 86.3 % could be achieved. The statistical analysis of the socioeconomic scaling in relation to the BTs showed distinct socioeconomic differences between the BT. With this approach, the described socioeconomic indicator was predicted for all 6,627 residential buildings in Belmopan.

Building on the findings of the initial Belmopan study, the motivation arose to analyze residential PV energy balances in Belmopan using BT, presented in section 3.4. A UAV campaign was carried out, thus meeting necessary data demands for precise solar potential estimation with aerial imagery and elevation information in the highest spatial resolution. Thus, 1,619 buildings or 24.4 % of the Belmopan building stock could be covered. In order to highlight the relevance of spatial resolution for the BT classification process, the RF classifier was used as well to determine BTs in Belmopan. The analysis of the classifying process showed that building features, describing the shape of the building footprints, building height and the roof complexity are ranked highest for a successful classification result. Data from a household survey in Belmopan revealed BT specific electricity consumption patterns. Using SfM techniques, DSM can be processed on the basis of

overlapping aerial imagery. These DSM data are used to estimate PV yields on residential building roofs. Differencing BT specific electricity consumption and roof-based PV energy generation, results in the PV energy balance. In the presented study, two scenarios were shown: Firstly, the best suited roof per building fully covered with PV panels ("optimal scenario") and secondly, two PV panels installed on the best suited roof per building ("realistic scenario"). In Belmopan, an optimal energy coverage ratio of 148 % can be achieved through PV energy, ranging between 86 % for BT 11 and 202 % for BT 21. The realistic scenario showed contrary results: BT 11 could achieve the highest coverage rates with 36 %, whereas BT 14 could only cover 17.1% of its energy demand through PV. The study's main outcomes underline the enormous potential of PV being a main pillar in the energy mix of Belmopan or Belize. Furthermore, the study showed the capability of the methodology to model scenarios for urban infrastructure planning and energy policy development, in order to establish a decentral energy source or to support financially weak groups to reduce energy expenses.

4. Discussion

Improvement of EO based approaches for urban planning

Remote sensing techniques are unrivaled in their ability to monitor highly dynamic areas, especially urban areas (Taubenböck and Dech, 2010b). When he stated his observations, Taubenböck surely expected progress in the EO sector, but can only have guessed the massive developments in growing number operational satellites and the revolutions in data handling and data processing during the last decade. Methods such as machine learning and deep learning evolved and were established, innovations in processor and graphic unit hardware and cloud architecture enabled processing of inconceivable data quantities. However, urban dynamics, of course on smaller scales, are still determined through post-classification approaches by multi-temporal comparison of urban areas. Single building detection is a persistent challenge that causes most attraction - only that nowadays deep learning methods are applied instead of object-based image analysis (OBIA) approaches. The literature overview in section 1.4 very well underlines these developments.

The studies presented in this thesis illustrate how remote sensing applications provide information in the urban context that allows a deeper understanding of urban dynamics than the area change of urban land use classes or the number of buildings in a certain area can indicate.

The Da Nang study proves that adding a third dimension increases the information content in the detection of urban dynamics. Within the urban areas of Da Nang, conventional approaches would only detect change of urban land use class. As shown in section 3.2, the change in urban surface heights detected from 3D EO data products helps to increase the information content on intra-urban change dynamics and indicates very heterogenous structural dynamics within the building stock. Both of these cannot be derived from conventional EO approaches.

Solely knowing the number of buildings or their physical structure in cities is not sufficient to describe urban material flows and to build an understanding on the urban metabolism. Urban infrastructure planning demands directly integrable data on to develop planning scenarios. Both Belmopan studies showed that remote sensing techniques and data classification approaches can provide important part in valuable or otherwise unattainable data contribution to such planning procedures by generating information on locally adapted BT on a single building level. The BT as

proxy for socioeconomic indicators or lifestyle classes on a and electricity demand can therefore deliver planning-ready data for scenario development and substantiated decision making.

In order to classify building footprints in BT, choosing the RF classifier has proven to provide convincing results. Figure 29 shows that BTs cannot be distinguished by applying thresholds on morphological building attributes, because class boundaries for the BTs are seemingly fuzzy and non-linear. Classifying BTs, therefore, increase the data content for the buildings in comparison to characterize buildings through a morphological description.

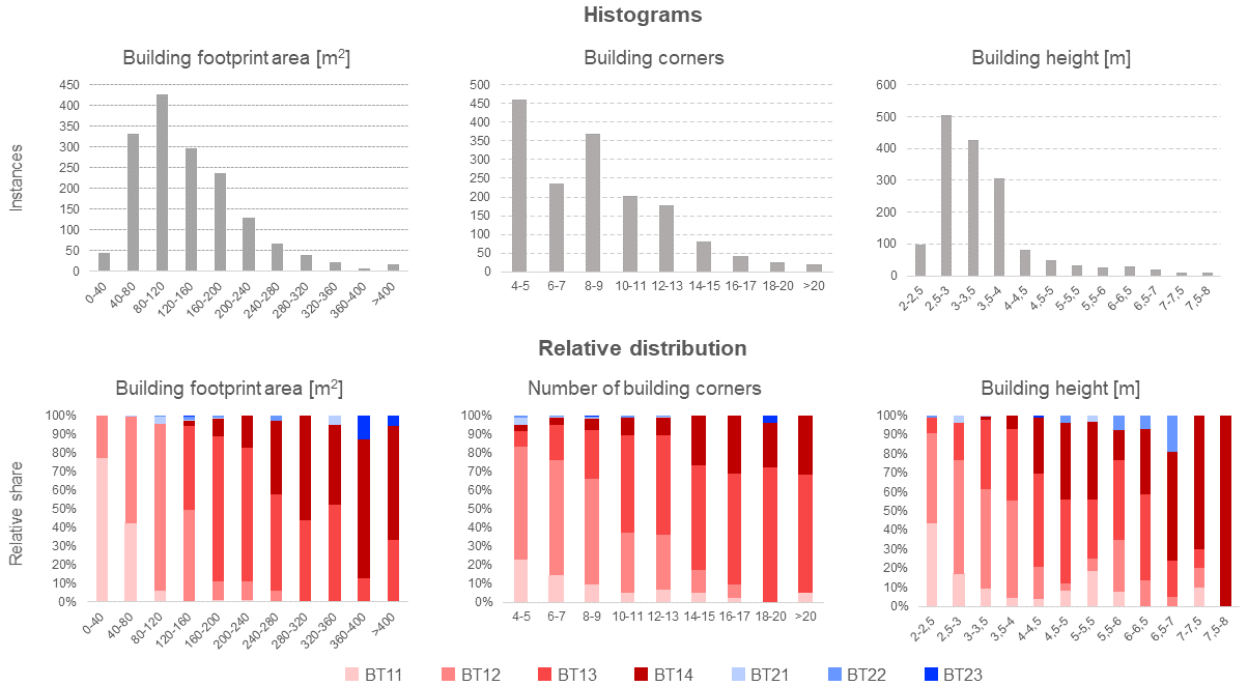

Figure 29: *Upper row: Histograms on building footprint, building corners and building height statistics. Lower row: relative share of the building-types in the statistical distributions. Multi-criteria approaches are required to classify building-types.*

Benefits from the high spatial resolution of EO data

The comparison of the BT classification accuracies in both Belmopan studies presented in sections 3.3 and 3.4 reveals the benefit and advantage from using UAV data over WV-1 imagery and elevation information. The initial OA for BT through the UAV-based approach is 70 % compared to 56.7 % from the WV-1-based approach. This accuracy divergence can be directly explained through the difference in spatial resolution. With a spatial resolution of 2 cm, the UAV imagery can illustrate 625-times more information than the 50 cm spatial resolution of the WV-1 data.

Consequently, UAV data better approximate the actual shape of spatial entities and can reproduce buildings information in more detail, for example height gradients in roofs or the number of building corners. The histograms in Figure 30 illustrate the difference in key building attributes as detected from both WV-1 and UAV imagery for the same buildings and underline the advantages of UAV data in the urban context.

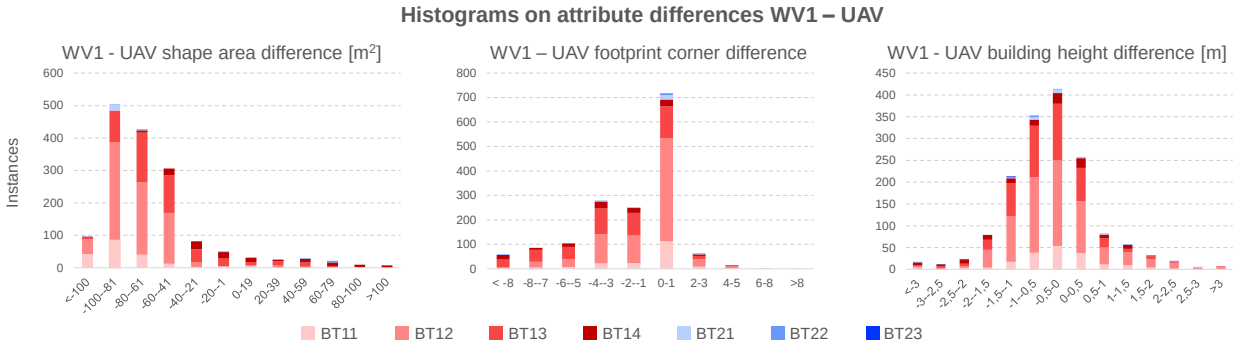

Figure 30: *Histograms displaying differences of selected building attributes derived from WV1 and UAV data.*

All three histograms presented in Figure 30 show a certain left skew which indicates an underestimation of the building attributes with WV-1 data in comparison to UAV data, represented by negative differences. The measured differences in shape area or building footprint corners respectively are very distinct: The majority of the buildings show a footprint area difference between -100 m^2 and -41 m^2. Similarly, the number of building corners to describe building complexities are also underestimated through the use of WV-1 imagery, though not as distinct as the footprint area. The interpretation of differences in building height confirms that UAV data deliver different estimations in comparison with the satellite imagery. As the BT shown in the histograms are equally distributed over all histogram bins, these findings do not apply to specific BT and are therefore, most probably caused by differences in the spatial resolution of the used imagery. Other very relevant building attributes, such as the roof ridge statistics to describe roof complexity (presented in section 3.4), cannot be detected in WV-1 imagery or elevation data due to insufficient spatial resolution and therefore, require increased ground sample distances, such as for example from UAV imagery. Figure 31 displays the difference in information content in WV-1 and UAV data.

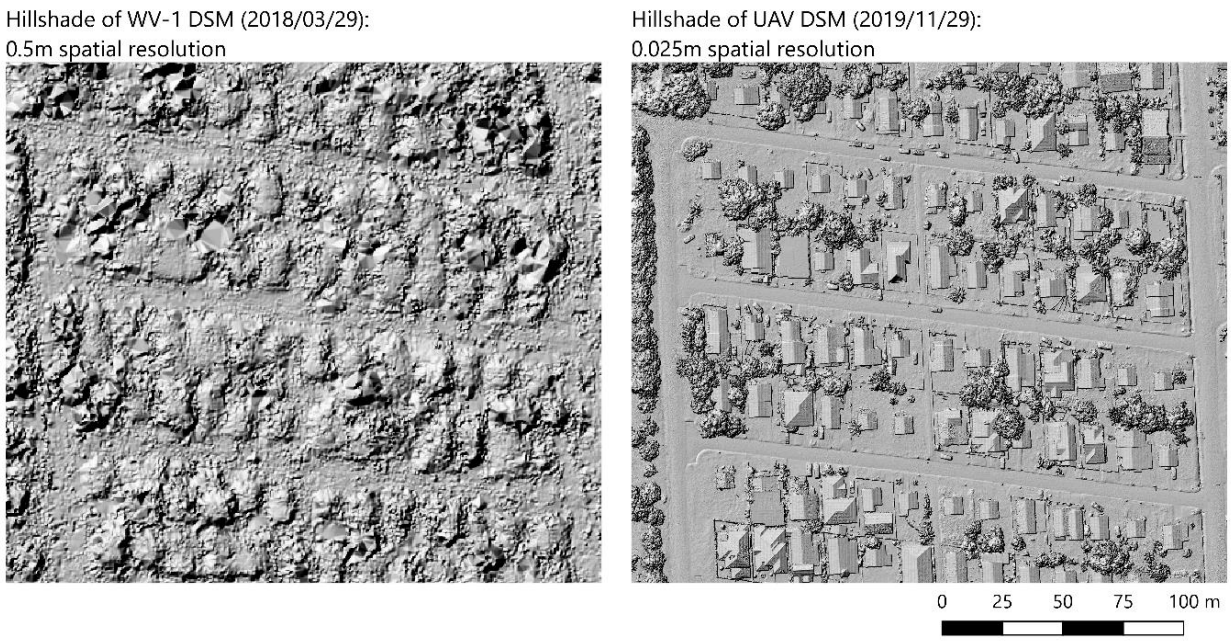

Figure 31: *Comparison of details in WorldView-1 and UAV DSMs as displayed by hillshade.*

The shown gain in spatial resolution from using UAV data accordingly results in more accurate information and opens the opportunity to deliver additional information to improve the accuracy of the BT classification. The study in section 3.3 proved that quality of life indicators can be estimated through EO techniques, thus increasing the accuracy of BT classification without the availability of UAV data. For Belmopan, the proximity of the residential building to the US embassy, which conducts security patrols, and the proximity to the central ring road are relevant indicators in this context and lead to increased BT classification accuracies.

In the given thematic and spatial context, UAV based approaches offer major advantages to provide data relevant for planning: First, UAV based data capturing campaigns can be planned and conducted flexibly, as opposed to satellite-based approaches which are limited by the defined orbit for each satellite. In addition, data generation intervals for building detection and BT classification can be defined flexibly according to the urban dynamics in the respective periods. Furthermore, UAVs operate independently from atmospheric conditions. While cloud coverage prevents the usability of satellite and aerial imagery, UAV are operated below the cloud line. Cloud coverage is even beneficial for SfM processing quality, as indirect insolation prevents high contrasts in images, direct reflections on smooth surfaces and large shaded areas. Last but not least, operating UAV is a low-obstacle technique because it only requires extensive practical training

and legal introduction. Meanwhile, all processes can be fully automated, including vessel launch, navigation according to defined tracks, image acquisition and landing.

From the local to the global scale?

Remote sensing techniques, especially satellite imagery, allows data acquisition of almost every place on our planet in short temporal intervals. Commercial satellite corporations usually operate VHR imaging satellite systems, whereas federal space agencies such as the National Aeronautics and Space Administration (NASA) and the European Space Agency (ESA) operate spatially high-resolution imaging satellite systems. This seeming disadvantage is compensated through large area image coverage and reliable continuation of the satellite missions, backed by federal institutions.

This spatial and temporal data abundance allows developing algorithms and approaches to automatically process satellite imagery and to provide global data products, as for example the Global Urban Footprint (GUF dataset) (Esch et al., 2017), a global water mask (Pekel et al., 2016) or a global forest masks (Hansen et al., 2013). Such datasets and approaches deliver information in unprecedented temporal intervals, spatial resolution and data consistency on the global scale. Initiatives such as the International Panel on Climate Change (IPCC) to monitor and model climate change scenarios or the UNDESA particularly rely on information derived from consistent data and methodologies in order to monitor SDGs, as well as target achievement, and to ensure comparability of information. Thus, federal programs like the Landsat and Copernicus are essential for global mapping and monitoring tasks.

However, urban planning or urban infrastructure planning requires different levels of information and data for the planning processes. The planning success depends on the understanding of the urban metabolism which is affected through urban material flows and inputs as well as output of the urban system. Too many factors that cannot be estimated from remote sensing data influence patterns of consumption and production of waste materials. Accordingly, as both of the Belmopan studies demonstrated, auxiliary information through empirical data collection and processing is needed to gain a deep understanding of processes in the respective planning area that take place in spheres hidden from EO sensors.

The BT approach, which includes four BT each for single and multi-family buildings, should be transferable to most places on the global scale. To provide precise and reliable results, the building typology needs to be adapted to specific countries and regions according to *in situ* knowledge. The same applies to the specification of socioeconomic scales and classes, as well as the interpretation of quality of life in different urban environments. Last but not least, planning processes are not standardized and differ from region to region. Consequently, data needs to be provided according to the local needs. Therefore, information capture on the local urban metabolism from household survey or census data are essential to ensure the success of planning efforts despite all the expectations to VHR satellite imagery, high return intervals of the satellites and deep learning capabilities.

Benefits for urban (infrastructure) planning from presented approaches

As underlined in sections 1.2 and 1.3, the success of urban planning and urban infrastructure planning heavily depends on evidence-based decision making, for which good planning practice demands scenario simulation on the basis of accurate and valid data.

Both presented studies in Belmopan (sections 3.3 and 3.4) showed that data analysis based on remote sensing data is capable of providing relevant data for the process of urban infrastructure planning. Satellite images are snapshots which cover events and conditions at particular moments. In addition, data capturing capabilities of commercial satellite systems end at the roof top and everything beneath this shielding layer remains private and covert. As the work in Da Nang during the RapidPlanning project has proven, urban morphological structure can be mapped with appropriate methods. Remote sensing approaches, however, are limited in mapping and detecting functional information in the urban context. EO approaches to overcome this limitation therefore need to find and identify entities which can be related to relevant information, such as socioeconomic status, electricity consumption, or water consumption. We were able to show that the BT for this need can be a suitable measure.

As presented in section 1.3, the term "urban metabolism" describes the arteries that keep the urban system running through providing transportation capabilities, necessary supply and disposal of waste products, but it can also comprise descriptions of quality of life indicators and

characterizations of urban dynamics. Monitoring urban dynamics, as presented in section 1.4 'Earth Observation Techniques to Support Urban Planning' mainly analyzes areal change of urban land use classes through high resolution Landsat or Sentinel-2 data. The Da Nang study proves that intra-urban dynamics of the building stock can be detected by using stereoscopic VHR imagery. Through very sophisticated and user-friendly photogrammetric data processing implementations and simple arithmetic raster processing, dynamics within the building stock can determined as changes in surface elevation (see section 3.2). Especially in large cities with lacking capabilities in city administrations, this approach can help identifying and monitoring areas in transition and therefore can provide valuable information to generate deeper knowledge and understanding of the urban metabolism. With presently available satellite systems, stereoscopic EO imagery can be provided for any city in this globe annually and thus, high interval monitoring can be provided. 3D data processing is and will be dependent on commercial satellite data and commercial software. However, data processing is very user-friendly and prices are reasonable, especially as the advantages of area-efficiency EO data processing are obvious.

According to the general consensus amongst the stakeholders in urban infrastructure planning and the demands of the scientific sector, as shown in the introduction section, integrated scenario development must be a standard component in the planning process. A reliable and consistent data basis is critical for the success of the planning process. Both studies performed in Belmopan proved the ability of RS-based methods to provide relevant information and data for the development of planning scenarios. Furthermore, demands on low obstacle methods for the integration of remote sensing techniques in the planning process can be met. The three studies contain in part commercial data or software, but data processing is very user-friendly and relevant

The BT can serve as valuable proxy, as it is shown to be able to represent socioeconomic measures, electric energy consumption, and water consumption. Moreover, using the BT as a proxy for the named information makes it possible to increase the spatial level of information up to the single building level, which in turn allows drawing a very precise picture of the urban metabolism. A major requirement for using the BT as a proxy is the integration of VHR EO imagery, but the approach itself is independent from specific sensors. Using UAV data optimizes the accuracy of the BT classification, whereas VHR satellite can cover even megacities such as Lagos or Lima to

over 90 % with one satellite acquisition, since the satellite captures swath widths of 13.1 km as for WorldView-3 and WorldView-4 at a GSD of 0.31 m (Satellite Imaging Corporation, n.d.) and even a swath width of 20 km for Pléiades satellites at a GSD of 0.5 m (Airbus Defence and Space, n.d.). With the planned launch of the next generation of VHR optical satellite systems, such as the 4 identical Pléiades Neo satellites (Airbus Defence and Space, n.d.) and the six satellites of the WorldView Legion (Maxar, 2020), image availability will be improved significantly, making EO based data products operationally integrable in the planning process. Additionally, with large number of satellites, the system of optical VHR resolution is resilient to the failure of single satellites. With largest shares of urbanization being expected in smaller urban settlements (see section 1.1), coverage issues through limited satellite imagery footprint should not be relevant in these cities.

Especially through the PV study in Belmopan (see section 3.4, p. 44) we were able to show the potential of the EO based BT approach for urban infrastructure planning in multiple aspects. First, and most importantly, the BT can be used to estimate residential electricity consumption as studied with empirical data from 190 household interviews. This relation between BT and electricity consumption alone is very valuable, as the BT, which can be derived from EO data and therefore, allows estimating electricity consumption on a city-wide scale. As this approach provides information on electricity consumption in the physical unit of kWh/year, the generated information is planning-ready data that can directly be used to develop scenarios for urban infrastructure planning. Secondly, the BT in combination with the PV energy potential, determined from UAV elevation data, enables generating PV energy balances on a single building level. Such information on PV energy balances is important to evaluate the energy potential of rooftop PV solutions and to make decisions towards the development of solar energy strategies. Thirdly, balancing PV energy production and energy consumption on a single building level allows PV energy balancing on multiple spatial levels. Thus, the approach is suitable to test bottom-up scenarios on different scales, starting from analyzing a single building, then proceeding to local neighborhoods and city district to the city level. As a result, spatially adapted strategies can be developed to achieve ideal results in accordance with the local preconditions. Fourthly, with the presented approach, developed planning scenarios can be tested, as the methodology allows to flexibly vary and evaluate

the number of PV panels. In our study, this was shown in two scenarios: the realistic scenario, in which a maximum of two PV panels per building were used, and the optimal scenario with the best suited field of roof fully equipped with PV panels. The chosen number of two PV panels for the realistic scenario hereby can be adapted, as histograms indicate that the optimum PV energy yield for all buildings in Belmopan can be approaches with few more than two PV panels. Last but not least, approach can be a decision base for policy development and thus can be used to develop PV policies on both the local planning level, as well as the national level. The optimal scenario predicts an energy coverage ratio through PV energy of 148 %, which allows generating large energy surpluses with the possibility to be fed into the national energy grid, thus massively reducing the national carbon dioxide emissions from electricity generation. Financial aspects and benefits for the residents are not evaluated within this study, but positive effects on the private households can be assumed. The evaluation of the realistic scenario opened the view on social effects of policy development. As socioeconomically weaker groups with 36 % can cover the largest share of consumed electricity from PV energy, strategies to relieve the socioeconomically weakest groups from high energy expenses, especially in times of the Covid-19 pandemic in which the residential electricity consumption is reported to be strongly increased during lock down periods (Belmopan City Council).

Integrated planning demands not only the planning and establishment of power line networks and power plants, but also requires the development of a political framework according through the approach "governing through enabling and/or provision" (Bulkeley and Kern, 2006), i.e. through a national or local solar energy policy or strategies to establish grant and loan programs for PV energy upgrades on residential buildings. Adapted legal framework can significantly increase the share of renewable energies (Peters and Schweiger, 2011). The presented BT based approaches can provide a basis of information to develop grant and loan programs for the decarbonization of the energy supply of the residential sector, as the effects of PV implementation on carbon dioxide reduction, the deficit of national electricity balance, and economic effects for socioeconomically weaker groups can be estimated and evaluated. Tools within a PV policy can be feed-in-tariffs or tax free and interest free loans.

A main criticism, formulated as research deficit, is the missing presentation of approaches to include EO data in urban planning. Instead the buzzword “urban planning” to gain attraction. As shown by our studies, the approaches are a progress in this context, because our derived and provided data are possible to be integrated into multiple direct applications in planning of urban supply and disposal infrastructure.

5. Outlook

The visual inspection of the UAV orthomosaics revealed the existence of only one installed PV module on the rooftops of 1,619 buildings in the six studies areas in Belmopan. This, on the one hand, underlines the necessity to consider PV energy but, on the other hand, prevents from validating the estimations on potential PV energy generation. A next effort should concentrate on the realization of a pilot study to evaluate the predicted PV yield.

The research ideas and approaches were developed within the context of the RapidPlanning project. Therefore, a major focus was put on the implementation of the results within an interdisciplinary approach, in which the best quality of results needed to be achieve within a limited time frame. Accordingly, building footprints in Belmopan were manually adapted and complemented on the basis of pre-existing building footprints from the city council for reasons of time efficiency. In this regard, deep learning approaches to detect and outline buildings should be considered in the methodological approach of the work, as studies prove the very high building detection rates. Besides their special suitability to detect single objects or buildings respectively, DL algorithms prove their abilities in object classification. Therefore, DL classifiers should as well be evaluated to classify BT in subsequent studies. In order to improve the separability between BT11 and BT12, the roof condition could be a building attribute that can be described by the share of rusty areas on the roof. In this context, multi- or hyperspectral cameras for UAV can deliver relevant insights through the ability to characterize materials and material composition.

The results of the BT classification in Belmopan (section 3.3) showed the dominance single-family buildings with a share of 84.6 % of the complete building stock which leads to a very good understanding of these BT. However, the very little portion of MFBT in contrast caused a suboptimal characterization of these BTs. This situation is aggravated by the difficult access to the buildings for household interviews, because entrances are often locked and inaccessible, and residents did not react to the doorbells as in the single-family buildings. Still an increase of knowledge on MFBTs is necessary to understand the typical number of dwelling units in these buildings, the number of dwellers per unit/building and to relate MFBTs with socioeconomic information and specific consumption information. For Belmopan, the lack of knowledge may not be decisive for overall the results, however in larger cities in Belmopan, MFBT can have a more dominant share.

In the presented stage, the research is limited to the residential sector. Extending the approach to business and industrial building use holds new challenges, because the determination of the functional use of buildings at this point requires additional information and non-EO data. Evaluating possibilities to integrate census data and data from statistics departments in the process of estimating SEP and electricity consumption as alternative data source to household interview data needs special attention. The process planning integration should as well focus on the consideration of collecting, processing and provision of planning relevant information by the bureaus of statistic.

For two reasons, the study designs were not designed based on the latest techniques. Firstly, the work was conducted within the RapidPlanning project, for which the development of time-efficient and low-obstacle approaches were preferred, and secondly, the studies were performed using robust and sophisticated methods to prove the value of the BT for urban (infrastructure) planning capabilities and the capabilities of EO derived three-dimensional information to generate insight into urban dynamics.

An important topic which needs further investigation is the spatial resolution of the EO data. UAV imagery and elevation or height data respectively was proven to be very beneficial for the purpose of providing planning-ready data, whereas the limitations of the 0.5 m spatial resolution of the WV-1 data could be shown. But which spatial resolution is really necessary for the purpose? In between both of the presented modes, several options exist which should be evaluated. Many satellites with spatial resolutions of 0.3 m are already operational (WorldView-3, WorldView-4), just recently were launched (Pléiades Neo) or will be launched in near future (WorldView Legion, expected in 2022) (Erwin, 2021). Additionally, aerial image collection approaches by airplane can generate data with 10 cm to 20 cm spatial resolution. These options should be evaluated in the context of demands on spatial resolution under consideration of aspects of financial efforts and of data availability and accessibility.

Last but not least, the process of integrating planning-ready data from EO approaches into processes of urban infrastructure planning and scenario development needs to be evaluated. Insights gained therefrom, have to be considered and EO data processing has to be adjusted accordingly so that such approaches won’t remain scientific studies but become usable in urban planning.

References

Airbus Defence and Space (n.d.) *Pléiades* [Online]. Available at https://www.intelligence-airbusds.com/en/8692-pleiades (Accessed 5 December 2021).

Albers, G. (1988) *Stadtplanung: eine praxisorientierte Einführung*, Darmstadt, Wissenschaftliche Buchgesellschaft.

Albertz, J. (2009) *Grundlagen der Interpretation von Luft- und Satellitenbildern*, Darmstadt, WBG Academic.

Anees, M. M., Sajjad, S. and Joshi, P. K. (2019) 'Characterizing urban area dynamics in historic city of Kurukshetra, India, using remote sensing and spatial metric tools', *Geocarto International*, vol. 34, no. 14, pp. 1584–1607.

Artmann, M., Inostroza, L. and Fan, P. (2019) 'Urban sprawl, compact urban development and green cities. How much do we know, how much do we agree?', *Ecological Indicators*, vol. 96, pp. 3–9.

Atasoy, M. (2018) 'Monitoring the urban green spaces and landscape fragmentation using remote sensing: a case study in Osmaniye, Turkey', *Environmental Monitoring and Assessment*, vol. 190, no. 12, pp. 1–8.

Audebert, N., Le Saux, B. and Lefèvre, S. (2018) 'Beyond RGB: Very high resolution urban remote sensing with multimodal deep networks', *ISPRS journal of photogrammetry and remote sensing*, vol. 140, pp. 20–32.

Bachofer, F., Bower, J., Braun, A., Brimble, P. and MacSharry, P. (2019) *Using machine learning to value property in Kigali, Rwanda*, Washington.

Baker, E. H. (2014) 'Socioeconomic Status, Definition', in Cockerham, W. C., Dingwall, R. and Quah, S. (eds) *The Wiley Blackwell Encyclopedia of Health, Illness, Behavior, and Society,* Chichester, UK, John Wiley & Sons, Ltd, pp. 2210–2214.

Beckmann, K. J. (1988) *Vom Umgang mit dem Alltäglichen–Aufgaben und Probleme der Infrastrukturplanung–Antrittsvorlesung. Karlsruhe*, Schriftenzeihe des Instituts für Städtebau und Landesplanung, Karlsruhe, Universität Fridericana zu Karlsruhe.

Belize Electricity Limited (2021) *Current Rate Schedule (2021)* [Online]. Available at https://www.bel.com.bz/Rate_Schedule.aspx (Accessed 3 November 2021).

Belize Energy Unit (2020) *Belize - Annual Energy Statistics Report - 2018*, Belmopan, Belize Ministry of Public Service, Energy and Public Utilities.

Belmopan City Council *Financial effects of the COVID-pademic on households (Personal communication, 15 April 2021)*, Belmopan, Belmopan City Council.

Belmopan City Council (2014) *Belmopan Municipal Development Plan*, Belmopan, Belmopan City Council.

Belmopan City Council (2021) *Belmopan City Council* [Online]. Available at https://belmopancitycouncil.org/welcome/ (Accessed 18 May 2021).

BMUB (2007) *LEIPZIG CHARTER on Sustainable European Cities* [Online], BMUB. Available at https://www.bmu.de/fileadmin/Daten_BMU/Download_PDF/Nationale_Stadtentwicklung/leipzig_charta_en_bf.pdf (Accessed 10 September 2021).

Braun, A., Warth, G., Bachofer, F., Quynh Bui, T. T., Tran, H. and Hochschild, V. (2020) 'Changes in the Building Stock of Da Nang between 2015 and 2017', *Data*, vol. 5, no. 2, p. 42.

Breiman, L. (1999) 'Random forests', *UC Berkeley TR567*.

Bronger, D. (2004) *Metropolen, Megastädte, Global Cities: Die Metropolisierung der Erde*, Darmstadt, WBG.

Bùi, T., Mai, H. and Vo, L. (2021) *General Analysis of Urban Development Plannings, Strategies & Programs in Da Nang City for the Period of 2010-2020 (Documentation within the Emplement project)*, Da Nang, DISED.

Bulkeley, H. and Kern, K. (2006) 'Local Government and the Governing of Climate Change in Germany and the UK', *Urban Studies*, vol. 43, no. 12, pp. 2237–2259.

Cai, Y., Chen, Y. and Tong, C. (2019) 'Spatiotemporal evolution of urban green space and its impact on the urban thermal environment based on remote sensing data: A case study of Fuzhou City, China', *Urban Forestry & Urban Greening*, vol. 41, pp. 333–343.

CameraDecision (2021) *Canon S110 Review* [Online]. Available at https://cameradecision.com/review/Canon-PowerShot-S110 (Accessed 15 February 2021).

Chen, W., Huang, H., Dong, J., Zhang, Y., Tian, Y. and Yang, Z. (2018) 'Social functional mapping of urban green space using remote sensing and social sensing data', *ISPRS journal of photogrammetry and remote sensing*, vol. 146, pp. 436–452.

Chen, Y., Fan, R., Yang, X., Wang, J. and Latif, A. (2018) 'Extraction of urban water bodies from high-resolution remote-sensing imagery using deep learning', *Water*, vol. 10, no. 5, p. 585.

Derrible, S. (2017) 'Urban infrastructure is not a tree: Integrating and decentralizing urban infrastructure systems', *Environment and Planning B: Urban Analytics and City Science*, vol. 44, no. 3, pp. 553–569.

Doelling, R. J. (2017) *PV Modul-Größen im Überblick* [Online]. Available at https://www.energie-experten.org/erneuerbare-energien/photovoltaik/solarmodule/groesse (Accessed 28 April 2021).

Dong, R., Pan, X. and Li, F. (2019) 'DenseU-net-based semantic segmentation of small objects in urban remote sensing images', *IEEE Access*, vol. 7, pp. 65347–65356.

Elmqvist, T., Redman, C. L., Barthel, S. and Costanza, R. (2013) 'History of Urbanization and the Missing Ecology', in Elmqvist, T., Fragkias, M., Goodness, J., Güneralp, B., Marcotullio, P. J., McDonald, R. I., Parnell, S., Schewenius, M., Sendstad, M., Seto, K. C. and Wilkinson, C. (eds) *Urbanization, Biodiversity and Ecosystem Services: Challenges and Opportunities,* Dordrecht, Springer Netherlands, pp. 13–30.

Erwin, S. (2021) *Maxar still confident Legion constellation will be in orbit in 2022* [Online], Spacenews. Available at https://spacenews.com/maxar-still-confident-legion-constellation-will-be-in-orbit-in-2022/ (Accessed 11 December 2021).

Esch, T., Heldens, W., Hirner, A., Keil, M., Marconcini, M., Roth, A., Zeidler, J., Dech, S. and Strano, E. (2017) 'Breaking new ground in mapping human settlements from space–The Global Urban Footprint', *ISPRS journal of photogrammetry and remote sensing*, vol. 134, pp. 30–42.

European Commission (2020) *Applying the Degree of Urbanization: A methodological manual to define cities, towns and rural areas for international comparisons* [Online], European Commission. Available at https://ec.europa.eu/eurostat/documents/10186/11395216/DEGURBA-manual.pdf/3a6bab6a-3fb1-4261-ad5b-e604cb67dc0d (Accessed 19 August 2021).

Falk, A. (2021) 'Evidenz in der Politik: Im Land der Kleinmütigen', *DIE ZEIT*, 4 July [Online]. Available at https://www.zeit.de/2021/27/evidenz-politik-deutschland-bauchgefuehl-corona-massnahmen (Accessed 28 August 2021).

Faria Peres, L. de, Lucena, A. J. de, Rotunno Filho, O. C. and Almeida França, J. R. de (2018) 'The urban heat island in Rio de Janeiro, Brazil, in the last 30 years using remote sensing data', *International journal of applied earth observation and geoinformation*, vol. 64, pp. 104–116.

Fragkias, M., Güneralp, B., Seto, K. C. and Goodness, J. (2013) 'A Synthesis of Global Urbanization Projections', in Elmqvist, T., Fragkias, M., Goodness, J., Güneralp, B., Marcotullio, P. J., McDonald, R. I., Parnell, S., Schewenius, M., Sendstad, M., Seto, K. C. and Wilkinson, C. (eds) *Urbanization, Biodiversity and Ecosystem Services: Challenges and Opportunities,* Dordrecht, Springer Netherlands, pp. 409–435.

Frick, A. and Tervooren, S. (2019) 'A framework for the long-term monitoring of urban green volume based on multi-temporal and multi-sensoral remote sensing data', *Journal of geovisualization and spatial analysis*, vol. 3, no. 1, pp. 1–11.

Friesner, J. (1993) *Hurricanes and the Forests of Belize,* Forest Department.

Furlong, C., Brotchie, R., Considine, R., Finlayson, G. and Guthrie, L. (2017) 'Key concepts for Integrated Urban Water Management infrastructure planning: Lessons from Melbourne', *Utilities Policy*, vol. 45, pp. 84–96 [Online]. DOI: 10.1016/j.jup.2017.02.004.

Grippa, T., Georganos, S., Zarougui, S., Bognounou, P., Diboulo, E., Forget, Y., Lennert, M., Vanhuysse, S., Mboga, N. and Wolff, E. (2018) 'Mapping urban land use at street block level using openstreetmap, remote sensing data, and spatial metrics', *ISPRS International Journal of Geo-Information*, vol. 7, no. 7, p. 246.

Gruschwitz, D. (2020) *Fernerkundungsgestützte Veränderungsanalyse der Industriezonen in der zentralvietnamesischen Stadt Da Nang und Provinz Quang Nam* (Bachelor Thesis), Tübingen.

GSO (2021) *PX Web - General Statistics of Vietnam* [Online]. Available at https://www.gso.gov.vn/en/px-web/?pxid=E0201&theme=Population%20and%20Employment (Accessed 8 August 2021).

Guterres, A. (2018a) *Actions for the further implementation of the Programme of Action of the International Conference on Population and Development: monitoring of population programmes,*

focusing on sustainable cities, human mobility and international migration, United Nations Economic and Social Council.

Guterres, A. (2018b) *Sustainable cities, human mobility and international migration,* United Nations Economic and Social Council.

Hadjitheodorou, C. (1963) 'Elevations from parallax measurements', *Photogrammetric Engineering*, vol. 29, no. 5, pp. 840–849.

Hansen, M. C., Potapov, P. V., Moore, R., Hancher, M., Turubanova, S. A., Tyukavina, A., Thau, D., Stehman, S. V., Goetz, S. J., Loveland, T. R., Kommareddy, A., Egorov, A., Chini, L., Justice, C. O. and Townshend, J. R. G. (2013) 'High-Resolution Global Maps of 21st-Century Forest Cover Change', *Science*, vol. 342, no. 6160, pp. 850–853.

Hofierka, J. and Suri, M. (2002) 'The solar radiation model for Open source GIS: implementation and applications', vol. 2002.

Huang, B., Zhao, B. and Song, Y. (2018) 'Urban land-use mapping using a deep convolutional neural network with high spatial resolution multispectral remote sensing imagery', *Remote sensing of Environment*, vol. 214, pp. 73–86.

Huang, H., Li, Q. and Zhang, Y. (2019) 'Urban residential land suitability analysis combining remote sensing and social sensing data: A case study in Beijing, China', *Sustainability*, vol. 11, no. 8, p. 2255.

Huang, X. and Wang, Y. (2019) 'Investigating the effects of 3D urban morphology on the surface urban heat island effect in urban functional zones by using high-resolution remote sensing data: A case study of Wuhan, Central China', *ISPRS journal of photogrammetry and remote sensing*, vol. 152, pp. 119–131.

Jia, Y., Ge, Y., Ling, F., Guo, X., Wang, J., Le Wang, Chen, Y. and Li, X. (2018) 'Urban land use mapping by combining remote sensing imagery and mobile phone positioning data', *Remote Sensing*, vol. 10, no. 3, p. 446.

Jöchner, C. (2011) 'Stadt', in Jaeger, F. (ed) *Enzyklopädie der Neuzeit. Subsistenzwirtschaft - Vasall,* Stuttgart, Weimar, Metzler.

Jones, R. V., Fuertes, A. and Lomas, K. J. (2015) 'The socio-economic, dwelling and appliance related factors affecting electricity consumption in domestic buildings', *Renewable and Sustainable Energy Reviews*, vol. 43, pp. 901–917.

Kandissounon, G. A., Karla, A. and Ahmad, S. (2018) 'Integrating system dynamics and remote sensing to estimate future water usage and average surface runoff in Lagos, Nigeria', *Civil Engineering Journal*, vol. 4, no. 2, p. 378.

Kau, J. B. and Sirmans, C. F. (1979) 'Urban land value functions and the price elasticity of demand for housing', *Journal of Urban Economics*, vol. 6, no. 1, pp. 112–121.

Kearns, K. C. (1973) 'Belmopan: perspective on a new capital', *Geographical Review*, pp. 147–169.

Khan, D., Kumar, A. and Samadder, S. R. (2016) 'Impact of socioeconomic status on municipal solid waste generation rate', *Waste Management*, vol. 49, pp. 15–25.

Kim, S., Koh, B., Park, J. and Cheon, D. (2014) 'Comparative Study on Performance of Grid-Connected Photovoltaic Modules in Tropical Monsoon Climate under Thailand condition', *Journal of the Korean society for New and Renewable Energy*, vol. 10, pp. 39–46.

Klopp, J. M. and Petretta, D. L. (2017) 'The urban sustainable development goal: Indicators, complexity and the politics of measuring cities', *Cities*, vol. 63, pp. 92–97.

Knie, A. and Marz, L. (1997) *Die Stadtmaschine: zu einer Raumlast der organisierten Moderne,* WZB Discussion Paper.

Kraas, F., Leggewie, C., Lemke, P., Matthies, E., Messner, D., Nakicenovic, N., Schellnhuber, H., Schlacke, S., Schneidewind, U., Brandi, C., Butsch, C., Busch, S., Hanusch, F., Haum, R., Jaeger-Erben, M., Köster, M., Mareike, K., Loose, C., Ley, A. and Wanner, M. (2016) *WBGU – Wissenschaftlicher Beirat der Bundesregierung Globale Umweltveränderungen (2016): Der Umzug der Menschheit: Die transformative Kraft der Städte. Berlin. 544 S*, Berlin.

Kuffer, M., Pfeffer, K., Sliuzas, R. and Baud, I. (2016) 'Extraction of Slum Areas From VHR Imagery Using GLCM Variance', *IEEE Journal of Selected Topics in Applied Earth Observations and Remote Sensing*, vol. 9, no. 5, pp. 1830–1840.

Kuffer, M., Wang, J., Nagenborg, M., Pfeffer, K., Kohli, D., Sliuzas, R. and Persello, C. (2018) 'The Scope of Earth-Observation to Improve the Consistency of the SDG Slum Indicator', *ISPRS International Journal of Geo-Information*, vol. 7, no. 11, p. 428.

Levin-Keitel, M., Othengrafen, F. and Behrend, L. (2019) 'Stadtplanung als Disziplin. Alltag und Selbstverständnis von Planerinnen und Planern', *Raumforschung und Raumordnung Spatial Research and Planning*, vol. 77, no. 2, pp. 115–130.

Li, C., Liu, M., Hu, Y., Shi, T., Zong, M. and Walter, M. T. (2018) 'Assessing the Impact of Urbanization on Direct Runoff Using Improved Composite CN Method in a Large Urban Area', *International journal of environmental research and public health*, vol. 15, no. 4.

Loske, R. and Schaeffer, R. (eds) (2005) *Die Zukunft der Infrastrukturen: Intelligente Netzwerke für eine nachhaltige Entwicklung*, Marburg, Metropolis-Verlag für Ökonomie, Gesellschaft und Politik GmbH.

Magidi, J. and Ahmed, F. (2019) 'Assessing urban sprawl using remote sensing and landscape metrics: A case study of City of Tshwane, South Africa (1984–2015)', *The Egyptian Journal of Remote Sensing and Space Science*, vol. 22, no. 3, pp. 335–346.

Malekpour, S., Brown, R. R. and Haan, F. J. de (2015) 'Strategic planning of urban infrastructure for environmental sustainability: Understanding the past to intervene for the future', *Cities*, vol. 46, pp. 67–75.

Man Yuan, Yaping Huang, Huanfeng Shen and Tongwen Li (2018) 'Effects of urban form on haze pollution in China: Spatial regression analysis based on PM2.5 remote sensing data', *Applied Geography*, vol. 98, pp. 215–223 [Online]. DOI: 10.1016/j.apgeog.2018.07.018.

Maxar (2020) *WorldView Legion. Our next-generation constellation* [Online]. Available at https://www.maxar.com/splash/worldview-legion (Accessed 12 February 2020).

Mayr, M., Alonso, C. and Rouse, C. (eds) (2017) *Blue-green network planning as a spatial development and climate-resilient strategy - the case of Belmopan, Belize*, Belize City.

McDonald, R. I., Kareiva, P. and Forman, R. T. (2008) 'The implications of current and future urbanization for global protected areas and biodiversity conservation', *Biological Conservation*, vol. 141, no. 6, pp. 1695–1703.

McNeill, J. R. and Engelke, P. (2013) 'Mensch und Umwelt im Zeitalter des Anthropozän', in Iriye, A. and Osterhammel, J. (eds) *Geschichte der Welt; 1945 bis heute: Die globalisierte Welt,* München, Verlag C.H.BECK Literatur - Sachbuch - Wissenschaft, pp. 357–534.

Mikovits, C., Rauch, W. and Kleidorfer, M. (2018) 'Importance of scenario analysis in urban development for urban water infrastructure planning and management', *Computers, Environment and Urban Systems*, vol. 68, pp. 9–16.

Moss, T. (2011) 'Planung technischer Infrastruktur für die Raumentwicklung: Ansprüche und Herausforderungen in Deutschland', in Tietz, H.-P. and Hühner, T. (eds) *Zukunftsfähige Infrastruktur und Raumentwicklung: Handlungserfordernisse für Ver- und Entsorgungssysteme,* Hannover, Verl. d. ARL.

Mumford, E. P. (2002) *The CIAM discourse on urbanism, 1928-1960*, MIT press.

Mumford, L. (1956) 'The natural history of urbanization', *Man's Role in Changing the Face of the Earth*, vol. 1, pp. 382–398.

Musse, M. A., Barona, D. A. and Rodriguez, L. M. S. (2018) 'Urban environmental quality assessment using remote sensing and census data', *International journal of applied earth observation and geoinformation*, vol. 71, pp. 95–108.

Näsi, R., Honkavaara, E., Blomqvist, M., Lyytikäinen-Saarenmaa, P., Hakala, T., Viljanen, N., Kantola, T. and Holopainen, M. (2018) 'Remote sensing of bark beetle damage in urban forests at individual tree level using a novel hyperspectral camera from UAV and aircraft', *Urban Forestry & Urban Greening*, vol. 30, pp. 72–83.

National Infrastructure Commission (2020) *Principles for effective urban infrastructure: Lessons learned from the Next Steps for Cities programme* [Online]. Available at https://nic.org.uk/app/uploads/Principles-for-Effective-Urban-Infrastructure.pdf (Accessed 2 September 2021).

Ness, D. (2008) 'Sustainable urban infrastructure in China: Towards a Factor 10 improvement in resource productivity through integrated infrastructure systems', *The International Journal of Sustainable Development & World Ecology*, vol. 15, no. 4, pp. 288–301.

Oribe-Garcia, I., Kamara-Esteban, O., Martin, C., Macarulla-Arenaza, A. M. and Alonso-Vicario, A. (2015) 'Identification of influencing municipal characteristics regarding household waste generation and their forecasting ability in Biscay', *Waste Management*, vol. 39, pp. 26–34.

Ostojic, D. R., Bose, R. K., Krambeck, H., Lim, J. and Zhang, Y. (2013) 'Da Nang, Vietnam', in Ostojic, D. R., Bose, R. K., Krambeck, H., Lim, J. and Zhang, Y. (eds) *Energizing Green Cities in Southeast Asia,* The World Bank, pp. 157–176.

Pahl-Weber, E. and Schwartze, F. (2018) *Stadtplanung*, Hannover, ARL - Akademie für Raumforschung und Landesplanung.

Pekel, J.-F., Cottam, A., Gorelick, N. and Belward, A. S. (2016) 'High-resolution mapping of global surface water and its long-term changes', *Nature*, vol. 540, no. 7633, pp. 418–422.

Peterek, M., Restrepo Rico, S., Hebbo, Y. and Reichhardt, U. (2019) 'Collaborative Planning for Sustainable Urban Infrastructure in Frankfurt am Main', *Czasopismo Techniczne*, pp. 31–50.

Peters, I. and Schweiger, A. (2011) 'Konsequenzen technologischer Entwicklungen von Ver- und Entsorgungssystemen', in Tietz, H.-P. and Hühner, T. (eds) *Zukunftsfähige Infrastruktur und Raumentwicklung: Handlungserfordernisse für Ver- und Entsorgungssysteme,* Hannover, Verl. d. ARL.

pv magazine (2021) *JinkoSolar announces 23.01% efficiency for n-type monocrystalline panel* [Online]. Available at https://www.pv-magazine.com/2021/01/12/jinkosolar-announces-23-01-efficiency-for-n-type-monocrystalline-panel/ (Accessed 15 February 2021).

Rau, H. (2016) *Change Detection zur Analyse von Landnutzungsänderungen in Da Nang, Vietnam* (Master Thesis), Tübingen.

Rausch, L., Friesen, J., Altherr, L., Meck, M. and Pelz, P. (2018) 'A Holistic Concept to Design Optimal Water Supply Infrastructures for Informal Settlements Using Remote Sensing Data', *Remote Sensing*, vol. 10, no. 2, p. 216.

Ritchie, H. and Roser, M. (2018) *Urbanization* [Online] (Our world in data). Available at https://ourworldindata.org/urbanization (Accessed 12 August 2021).

Romero-Fiances, I., Muñoz-Cerón, E., Espinoza-Paredes, R., Nofuentes, G. and La Casa, J. de (2019) 'Analysis of the Performance of Various PV Module Technologies in Peru', *Energies*, vol. 12, no. 1, p. 186.

Rosengren, A., Smyth, A., Rangarajan, S., Ramasundarahettige, C., Bangdiwala, S. I., AlHabib, K. F., Avezum, A., Bengtsson Boström, K., Chifamba, J., Gulec, S., Gupta, R., Igumbor, E. U., Iqbal, R.,

Ismail, N., Joseph, P., Kaur, M., Khatib, R., Kruger, I. M., Lamelas, P., Lanas, F., Lear, S. A., Li, W., Wang, C., Quiang, D., Wang, Y., Lopez-Jaramillo, P., Mohammadifard, N., Mohan, V., Mony, P. K., Poirier, P., Srilatha, S., Szuba, A., Teo, K., Wielgosz, A., Yeates, K. E., Yusoff, K., Yusuf, R., Yusufali, A. H., Attaei, M. W., McKee, M. and Yusuf, S. (2019) 'Socioeconomic status and risk of cardiovascular disease in 20 low-income, middle-income, and high-income countries: the Prospective Urban Rural Epidemiologic (PURE) study', *The Lancet Global Health*, vol. 7, no. 6, e748-e760.

Sadef, Y., Nizami, A. S., Batool, S. A., Chaudary, M. N., Ouda, O. K. M., Asam, Z. Z., Habib, K., Rehan, M. and Demirbas, A. (2016) 'Waste-to-energy and recycling value for developing integrated solid waste management plan in Lahore', *Energy Sources, Part B: Economics, Planning, and Policy*, vol. 11, no. 7, pp. 569–579.

Satellite Imaging Corporation (n.d.) *WorldView-4 Satellite Sensor* [Online], Satellite Imaging Corporation. Available at https://www.satimagingcorp.com/satellite-sensors/geoeye-2/ (Accessed 5 December 2021).

Schell, L. M. and Denham, M. (2003) 'Environmental Pollution in Urban Environments and Human Biology', *Annual Review of Anthropology*, vol. 32, no. 1, pp. 111–134.

Seadon, J. K. (2006) 'Integrated waste management – Looking beyond the solid waste horizon', *Waste Management*, vol. 26, no. 12, pp. 1327–1336 [Online]. DOI: 10.1016/j.wasman.2006.04.009.

Sengupta, M., Xie, Y., Lopez, A., Habte, A., Maclaurin, G. and Shelby, J. (2018) 'The National Solar Radiation Data Base (NSRDB)', *Renewable and Sustainable Energy Reviews*, vol. 89, pp. 51–60.

Seto, K. C., Parnell, S. and Elmqvist, T. (2013) 'A Global Outlook on Urbanization', in Elmqvist, T., Fragkias, M., Goodness, J., Güneralp, B., Marcotullio, P. J., McDonald, R. I., Parnell, S., Schewenius, M., Sendstad, M., Seto, K. C. and Wilkinson, C. (eds) *Urbanization, Biodiversity and Ecosystem Services: Challenges and Opportunities,* Dordrecht, Springer Netherlands, pp. 1–12.

Shao, Z., Fu, H., Li, D., Altan, O. and Cheng, T. (2019) 'Remote sensing monitoring of multi-scale watersheds impermeability for urban hydrological evaluation', *Remote sensing of Environment*, vol. 232, p. 111338.

Shirani-bidabadi, N., Nasrabadi, T., Faryadi, S., Larijani, A. and Shadman Roodposhti, M. (2019) 'Evaluating the spatial distribution and the intensity of urban heat island using remote sensing, case study of Isfahan city in Iran', *Sustainable Cities and Society*, vol. 45, pp. 686–692 [Online]. DOI: 10.1016/j.scs.2018.12.005.

Singh, A. (2019) 'Remote sensing and GIS applications for municipal waste management', *Journal of environmental management*, vol. 243, pp. 22–29.

Song, J., Lin, T., Li, X. and Prishchepov, A. V. (2018) 'Mapping urban functional zones by integrating very high spatial resolution remote sensing imagery and points of interest: A case study of Xiamen, China', *Remote Sensing*, vol. 10, no. 11, p. 1737.

Statistical Institute of Belize (2020) *Annual Report 2018-19*, Belmopan, Statistical Institute of Belize.

Streich, B. (2011) *Stadtplanung in der Wissensgesellschaft*, Wiesbaden, VS Verlag für Sozialwissenschaften.

Taubenböck, H. and Dech, S. (2010a) 'Die Stadt im Blick - eine Annäherung', in Taubenböck, H. and Dech, S. (eds) *Fernerkundung im Urbanen Raum-Erdbeobachtung auf dem Weg zur Planungspraxis,* Wissenschaftliche Buchgesellschaft (WBG), pp. 11–14.

Taubenböck, H. and Dech, S. (2010b) 'Stadtplanung und Fernerkundung: eine gemeinsame Zukunft?', in Taubenböck, H. and Dech, S. (eds) *Fernerkundung im Urbanen Raum-Erdbeobachtung auf dem Weg zur Planungspraxis,* Wissenschaftliche Buchgesellschaft (WBG), pp. 185–186.

Taubenböck, H., Kraff, N. J. and Wurm, M. (2018) 'The morphology of the Arrival City - A global categorization based on literature surveys and remotely sensed data', *Applied Geography*, vol. 92, pp. 150–167.

Taubenböck, H., Staab, J., Zhu, X., Geiß, C., Dech, S. and Wurm, M. (2018) 'Are the Poor Digitally Left Behind? Indications of Urban Divides Based on Remote Sensing and Twitter Data', *ISPRS International Journal of Geo-Information*, vol. 7, no. 8, p. 304.

Teuteberg, H. J. (1987) *Zum Problemfeld Urbanisierung und Ernährung im 19. Jahrhundert*, Universitäts-und Landesbibliothek Münster.

Tietz, H.-P. (2011) 'Funktion und Struktur von Ver- und Entsorgungssystemen im Wandel', in Tietz, H.-P. and Hühner, T. (eds) *Zukunftsfähige Infrastruktur und Raumentwicklung: Handlungserfordernisse für Ver- und Entsorgungssysteme,* Hannover, Verl. d. ARL.

Tu, W., Hu, Z., Li, L., Cao, J., Jiang, J., Li, Q. and Li, Q. (2018) 'Portraying urban functional zones by coupling remote sensing imagery and human sensing data', *Remote Sensing*, vol. 10, no. 1, p. 141.

Ullman, S. and Brenner, S. (1979) 'The interpretation of structure from motion', *Proceedings of the Royal Society of London. Series B. Biological Sciences*, vol. 203, no. 1153, pp. 405–426.

UNdata (2021) *UNdata - A world of information* [Online]. Available at http://data.un.org/Default.aspx (Accessed 8 August 2021).

UNDESA (2014) *Securing Acess to Water and Energy: Information Brief,* United Nations Department of Economic and Social Affairs [Online]. Available at https://www.un.org/waterforlifedecade/pdf/01_2014_securing_access_eng.pdf (Accessed 9 August 2021).

UNDESA (2015) *World Urbanization Prospects: 2014 Revision,* United Nations, Department of Economic and Social Affairs, Population Division [Online]. Available at https://population.un.org/wup/Publications/Files/WUP2014-Report.pdf (Accessed 4 June 2021).

UNDESA (2019) *World Urbanization Prospects: The 2018 revision,* United Nations, Department of Economic and Social Affairs, Population Division [Online]. Available at https://population.un.org/wup/Publications/Files/WUP2018-Report.pdf (Accessed 4 June 2021).

UNESCAP (2020) *Da Nang City, Viet Nam,* United Nations Economic and Social Commission for Asia and the Pacific [Online]. Available at https://www.unescap.org/sites/default/d8files/2020-08/DaNangCity_0.pdf (Accessed 15 October 2021).

UN-Habitat (2006) *State of the World's Cities: Urbanization: A Turning Point in History* [Online]. Available at https://mirror.unhabitat.org/documents/media_centre/sowcr2006/SOWCR%201.pdf (Accessed 12 August 2021).

UN-Habitat (2017) *Belmopan Urban Development: Towards a Sustainable Garden City*, Nairobi, Kenya.

UN-Habitat (2019) *The Urban SDG Monitoring Series: Global monitoring of slums remains a key concern for achieving the right to adequate housing,* UN-Habitat [Online]. Available at https://unhabitat.org/sites/default/files/2020/06/the_urban_sdg_monitoring_series_monitoring_sdg_indicator_11.1.1.pdf (Accessed 10 September 2021).

UN-Habitat (2020a) *The New Urban Agenda Handbook* [Online], Nairobi, Kenya. Available at https://unhabitat.org/sites/default/files/2020/12/nua_handbook_14dec2020_2.pdf (Accessed 28 November 2021).

UN-Habitat (2020b) *UN-Habitat Urban Indicators Database* [Online]. Available at https://data.un-habitat.org/pages/housing-slums-and-informal-settlements (Accessed 29 September 2021).

UN-Habitat (2020c) *What is a City?* [Online], UN-Habitat. Available at https://unhabitat.org/sites/default/files/2020/06/city_definition_what_is_a_city.pdf (Accessed 19 August 2021).

United Nations (2015a) *Transforming our World: The 2030 Agenda for Sustainable Development*.

United Nations (2015b) *United Nations Millenium Development Goals* [Online]. Available at https://www.un.org/millenniumgoals/environ.shtml.

United Nations (2018) *World Urbanization Prospects: The 2018 Revision,* United Nations.

UNOCHA (2022) *Viet Nam - Subnational Administrative Boarders* [Online], United Nations Office for the Coordination of Humanitarians Affairs. Available at https://data.humdata.org/dataset/viet-nam-administrative-boundaries-polygon-polyline (Accessed 2 January 2022).

Venter, Z. S., Brousse, O., Esau, I. and Meier, F. (2020) 'Hyperlocal mapping of urban air temperature using remote sensing and crowdsourced weather data', *Remote sensing of Environment*, vol. 242, p. 111791.

Vetter-Gindele, J., Braun, A., Warth, G., Bui, T. T., Bachofer, F. and Eltrop, L. (2019) 'Assessment of Household Solid Waste Generation and Composition by Building Type in Da Nang, Vietnam', *Resources*, vol. 8, no. 4.

Wang, J., Kuffer, M., Sliuzas, R. and Kohli, D. (2019) 'The exposure of slums to high temperature: Morphology-based local scale thermal patterns', *The Science of the total environment*, vol. 650, Pt 2, pp. 1805–1817.

Warth, G., Assmann, O., Fleckenstein, K., Braun, A. and Hochschild, V. (2021) 'Photovoltaic energy balancing in Belmopan based on building types, UAV aerial imagery and household data', *Geography and Sustainability*.

Warth, G., Braun, A., Assmann, O., Fleckenstein, K. and Hochschild, V. (2020) 'Prediction of socio-economic indicators for urban planning using VHR satellite imagery and spatial analysis', *Remote Sensing*, vol. 12, no. 11, p. 1730.

Warth, G., Braun, A., Bödinger, C., Hochschild, V. and Bachofer, F. (2019) 'DSM-based identification of changes in highly dynamic urban agglomerations', *European Journal of Remote Sensing*, vol. 52, no. 1, pp. 322–334.

Wellmann, T., Lausch, A., Andersson, E., Knapp, S., Cortinovis, C., Jache, J., Scheuer, S., Kremer, P., Mascarenhas, A., Kraemer, R., Haase, A., Schug, F. and Haase, D. (2020) 'Remote sensing in urban planning: Contributions towards ecologically sound policies?', *Landscape and Urban Planning*, vol. 204, p. 103921.

Winkler, J. and Stolzenberg, H. (1998) 'Der Sozialschichtindex im Bundes- Gesundheitssurvey', *Gesundheitswesen*, vol. 61.

World Bank (2021) *World Development Indicators* [Online]. Available at https://data.worldbank.org/?locations=BZ-VN (Accessed 25 July 2021).

Wurm, M. and Taubenböck, H. (2018) 'Detecting social groups from space – Assessment of remote sensing-based mapped morphological slums using income data', *Remote Sensing Letters*, vol. 9, no. 1, pp. 41–50.

Xu, Y., Wu, L., Xie, Z. and Chen, Z. (2018) 'Building extraction in very high resolution remote sensing imagery using deep learning and guided filters', *Remote Sensing*, vol. 10, no. 1, p. 144.

Xue, Z., Hou, G., Zhang, Z., Lyu, X., Jiang, M., Zou, Y., Shen, X., Wang, J. and Liu, X. (2019) 'Quantifying the cooling-effects of urban and peri-urban wetlands using remote sensing data: Case study of cities of Northeast China', *Landscape and Urban Planning*, vol. 182, pp. 92–100.

Yang, C., Li, Q., Hu, Z., Chen, J., Shi, T., Ding, K. and Wu, G. (2019) 'Spatiotemporal evolution of urban agglomerations in four major bay areas of US, China and Japan from 1987 to 2017: Evidence from remote sensing images', *Science of the Total Environment*, vol. 671, pp. 232–247.

Yi, Y., Zhang, Z., Zhang, W., Zhang, C., Li, W. and Zhao, T. (2019) 'Semantic segmentation of urban buildings from VHR remote sensing imagery using a deep convolutional neural network', *Remote Sensing*, vol. 11, no. 15, p. 1774.

Zheng, C., Zhao, C., Li, Y., Wu, X., Zhang, K., Gao, J., Qiao, Q., Ren, Y., Zhang, X. and Chai, F. (2018) 'Spatial and temporal distribution of NO2 and SO2 in Inner Mongolia urban agglomeration obtained from satellite remote sensing and ground observations', *Atmospheric environment*, vol. 188, pp. 50–59.

Zhou, D., Bonafoni, S., Zhang, L. and Wang, R. (2018) 'Remote sensing of the urban heat island effect in a highly populated urban agglomeration area in East China', *Science of the Total Environment*, vol. 628, pp. 415–429.

Zurbrügg, C., Gfrerer, M., Ashadi, H., Brenner, W. and Küper, D. (2012) 'Determinants of sustainability in solid waste management – The Gianyar Waste Recovery Project in Indonesia', *Waste Management*, vol. 32, no. 11, pp. 2126–2133 [Online]. DOI: 10.1016/j.wasman.2012.01.011.

Appendix

a) Accepted publications as first author:

Appendix A-1:

Warth, G., Braun, A., Bödinger, C., Hochschild, V. and Bachofer, F. (2019) 'DSM-based identification of changes in highly dynamic urban agglomerations', *European Journal of Remote Sensing*, vol. 52, no. 1, pp. 322–334.

Appedix A-2:

Warth, G., Braun, A., Assmann, O., Fleckenstein, K. and Hochschild, V. (2020) 'Prediction of socio-economic indicators for urban planning using VHR satellite imagery and spatial analysis', *Remote Sensing*, vol. 12, no. 11, p. 1730.

b) b) Submitted manuscripts as first author:

Appendix A-3:

Warth, G., Assmann, O., Fleckenstein, K., Braun, A. and Hochschild, V. (2021) 'Photovoltaic energy balancing in Belmopan based on building-types, UAV aerial imagery and household data', *Geography and Sustainability (under review)*.

Appendix A-1

Taylor & Francis
Taylor & Francis Group

European Journal of Remote Sensing

ISSN: (Print) (Online) Journal homepage: https://www.tandfonline.com/loi/tejr20

DSM-based identification of changes in highly dynamic urban agglomerations

Gebhard Warth, Andreas Braun, Christian Bödinger, Volker Hochschild & Felix Bachofer

To cite this article: Gebhard Warth, Andreas Braun, Christian Bödinger, Volker Hochschild & Felix Bachofer (2019) DSM-based identification of changes in highly dynamic urban agglomerations, European Journal of Remote Sensing, 52:1, 322-334, DOI: 10.1080/22797254.2019.1604083

To link to this article: https://doi.org/10.1080/22797254.2019.1604083

Published online: 22 Apr 2019.

EUROPEAN JOURNAL OF REMOTE SENSING
2019, VOL. 52, NO. 1, 322–334
https://doi.org/10.1080/22797254.2019.1604083

DSM-based identification of changes in highly dynamic urban agglomerations

Gebhard Warth[a], Andreas Braun[a], Christian Bödinger[a], Volker Hochschild[a] and Felix Bachofer[b]

[a]Department of Geography, University of Tübingen, Tübingen, Germany; [b]German Remote Sensing Data Center (DFD), German Aerospace Center (DLR), Oberpfaffenhofen, Germany

ABSTRACT

Rapidly urbanizing areas are challenged by a lack of information on urban growth in many parts of the earth. As the speed of building construction often exceeds traditional surveying methods, remote sensing can serve as a valuable input for the monitoring of urbanization processes. This study investigates changes in DaNang, Vietnam, between 2015 and 2017 identified based on photogrammetric analysis of surface elevations retrieved from Pléiades very high-resolution imagery. In contrast to traditional post-classification change detection approaches, we propose a time-efficient method solely based on digital surface model differencing to identify newly constructed buildings as well as demolitions. It is therefore easy to apply and suitable for the continuation of outdated base data available to local authorities. High importance is addressed to the vertical matching of both surface models to avoid misdetections. After differencing these surface elevations, thresholds based on field measurements are applied to identify areas of change. A total of 10,800 changes were detected between 2015 and 2017, of which 8,531 were to newly constructed buildings. The study proves that changes in rapidly urbanizing agglomerations can be reliably identified by a simple and transparent approach by using elevation changes and expert-based knowledge on floor numbers and building heights.

ARTICLE HISTORY
Received 15 July 2018
Revised 19 February 2019
Accepted 2 April 2019

KEYWORDS
Change detection; urban areas; photogrammetry; digital surface models; normalized DSM; Da Nang

Introduction

Urban agglomerations are facing several serious challenges, especially in countries of the Global South (Cohen, 2006). Driven by a rapid growth of the urban population, environmental and socio-economic problems arise, amongst others pollution of the air and urban environment (Schell & Denham, 2003), poverty and crime (Satterthwaite & Mitlin, 2012) supply and mobility of the population (Vasconcellos, 2014), leading to uncontrolled growth and limited regulation measures by local authorities (Bhatta, 2010; Goodfellow, 2013).

Municipalities require reliable and up-to-date information for land-use and infrastructure planning, for creation and continuation of development plans and overall monitoring of changes. Remote sensing can serve as a valuable input for the characterization of urban structures and the identification of dynamics (Jensen & Cowen, 1999; Patino & Duque, 2013; Rashed & Jürgens, 2010; Weng, Quattrochi, & Gamba, 2018).

However, the application of geospatial techniques in authorities is constrained in many countries of the global south, especially in many developing and newly industrializing countries due to several reasons: Lack of technical support for a sustainable establishment and continuation of public geospatial infrastructures (Hastings & Clark, 1991; Leiser, 2011), inefficient collaboration between authorities of different sectors and levels (de Vries & Lance, 2011), budgetary constraints (George, 2000) or technical and educational impediments (Jha & Chowdary, 2007). Consequently, applications for the use in urban agglomerations of non-industrial nations must be efficient, affordable, user-friendly, independent of ancillary base data and of appropriate complexity.

Our study focuses on the development of the city of Da Nang, Vietnam, for which Linh, Erasmi, and Kappas (2009) used Landsat and ASTER satellite images to identify the land use and land cover changes between 1979 and 2009 and found a significant decrease in forest and shrub land while urban areas increased by over 10,000 ha. Like in various other studies using high resolution (HR) satellites, such as Landsat or Sentinel-2, their results are based on post-classification change detection methods, requiring two or more classified image pairs, which together form a difference layer that is interpreted quantitatively and qualitatively (Alphan & Güvensoy, 2016; Hegazy & Kaloop, 2015; Mundia & Aniya, 2005; Shalaby & Tateishi, 2007; Yuan, Sawaya, Loeffelholz, & Bauer, 2005). However, images from very high resolution (VHR) satellites, such as

CONTACT Gebhard Warth gebhard.warth@uni-tuebingen.de Rümelinstraße19-23, Tübingen 72070, Germany

Quickbird, Pléiades or WorldView, need other techniques to cope with the degree of information. One of the most popular methods is object-based image analysis (OBIA), which aggregates several pixels into objects that can be characterized by several features, such as mean spectral values, but also texture or neighbourhood characteristics (Blaschke, 2010; Blaschke, Lang, & Hay, 2008). OBIA is applied in particular in various studies focusing on urban environments (De Pinho, Fonseca, Korting, de Almeida, & Kux, 2012; Moskal, Styers, & Halabisky, 2011; Zhou & Troy, 2008), monitoring of construction activities (Durieux, Lagabrielle, & Nelson, 2008; Im, Jensen, & Tullis, 2008; Wickramasinghe, Vu, & Maul, 2018) or building recognition and classification (Belgiu & Drăguţ, 2014; Salehi, Zhang, Zhong, & Dey, 2012; Tsai, Stow, & Weeks, 2011).

While change detection in VHR imagery is widely used for damage assessments (Dell'Acqua & Gamba, 2012; Lu, Guo, & Corbane, 2013; Olsen, Chen, Hutchinson, & Kuester, 2013), only a few approaches exist to identify gradual changes in large cities through uncontrolled building activities, urbanization and densification (Kopecká & Rosina, 2014; Shahtahmassebi, Song, Zheng et al., 2016).

We regard the information of surface elevation change in urban areas as an indicator for change in building stock, which in very high resolution describes change on the single building level. Therefore, in this paper, we present a method applicable for rapidly growing cities to assess changes in building infrastructure based on measures of elevation change. Because of its robust approach, it brings several advantages to local authorities: a) it can be adapted by non-experts, b) it can be used for the continuation of already existing data, and c) it is, compared to most urban studies using VHR imagery, cost-effective regarding input data and software packages.

The retrieval of height information of buildings can be achieved with various datasets and methods: The presumably most reliable approach is the use of airborne LiDAR measurements (Rottensteiner & Briese, 2002; Yu, Liu, Wu, Hu, & Zhang, 2010), due to its high vertical accuracy and high point density. However, due to the individual mission conception for each flight campaign, these campaigns are comparably expensive and require extensive preparation and post-processing. Studies based on Synthetic Aperture Radar (SAR) are presented by Brunner, Lemoine, Bruzzone, and Greidanus (2010), Soergel, Michaelsen, Thiele, Cadario, and Thoennessen (2009) or Colin-Koeniguer and Trouve (2014). The advantage of interferometric SAR approaches is the relative independency from atmospheric conditions, which offers high flexibility regarding the time and date of acquisition. Yet, many of the SAR-related approaches struggle with very dense build-up patterns because of the side-looking geometry of the system, which causes shadow and overlay effects in urban areas (Hill, Moate, & Blacknell, 2006). Photogrammetric methods provide an ideal trade-off between applicability and quality in urban areas (Baltsavias, 1999). Their use was demonstrated in numerous studies (Haala & Kada, 2010; Kadhim & Mourshed, 2018; Liu, Huang, Wen et al., 2017; Peng, Gong, Le Wang, & Yang, 2016; Poli & Caravaggi, 2012). The Pléiades mission is of special value because of its tri-stereoscopic acquisition mode. It is composed of three nearly simultaneously acquired images, one backward looking, one forward looking, plus a third near-nadir image (Gleyzes, Perret, & Kubik, 2012; Perko, Raggam, Gutjahr, & Schardt, 2014). Pléiades image triplets have proven their ability in deriving submeter scale elevation and elevation changes (Bagnardi, González, & Hooper, 2016; Zhou, Parsons, Elliott et al., 2015). The tri-stereoscopic configuration allows to retrieve more detailed Digital Surface Models (DSM) in rough terrain or urban areas (Panagiotakis, Chrysoulakis, Charalampopoulou, & Poursanidis, 2018). Poli, Remondino, Angiuli, and Agugiaro (2015) and Perko et al. (2014) evaluated the DSM processing of Pléidades imagery in the urban context of Trento and Innsbruck. The two studies achieved RMSEz of 0.75 and 2.4 m, respectively. Panagiotakis et al. (2018) achieved an RMSEz of 1.17 m compared to differential GPS measurements in Athens. Bachofer (2017) used the height information derived from a Pléiades triplet to extract building volume information for the Central Business district of Kigali, Rwanda. Lefebvre, Nabucet, Corpetti, Courty, and Hubert-Moy (2016) used a Pléiades derived DSM to extract urban vegetation.

Recent developments include the use of unmanned aerial vehicles (UAVs) for building height estimation (Gal & Doytsher, 2014; Kelbe, White, Hardin, Moehl, & Phillips, 2016; Rebelo, Rodrigues, Tenedório, Goncalves, & Marnoto, 2015; Unger, Reich, & Heipke, 2014), or multi-sensor approaches (Geiß et al., 2015; Sportouche, Tupin, & Denise, 2011; Xu, Ma, Ng, & Lin, 2015). UAV data provide obviously higher spatial resolutions, yet can usually cover only small study areas and need enormous processing capabilities.

Data and methods

Study area and data

Extent of the study

The study area is located in Da Nang province in Central Vietnam and covers large parts of Da Nang city. Due to constraints regarding the acquired area, an area of interest (AOI) has been defined for the tasked VHR imagery (Figure 1, red outline). It covers approximately 225 km^2 of the urban area and includes the districts Cẩm Lệ, Hải Châu, Liên

Chiểu, Ngũ Hành Sơn, Sơn Trà and Thanh Khê. Since its classification as a Class I city in 1997, Da Nang underwent rapid socio-economic and environmental changes (JICA, 2010). As a consequence, large shrubland and forest areas were logged down for urban extension areas in many parts of the city (Linh et al., 2009).

Satellite imagery

The two satellites of the Pléiades constellation (1A and 1B) for VHR earth surface observation were launched in 2011 and 2012 respectively. The panchromatic sensor provides images with a resolution of 70 cm and 2.8 m for the 4 multispectral bands. The physical resolution is resampled to 50 cm, respectively, 2 m, ground sampling distance, and the stereo angle can vary from ~6° to ~28° (GSD) (De Lussy et al., 2012; Gleyzes et al., 2012). Compared to other VHR stereo satellite missions, such as the WorldViews, Pléiades tri-stereo mode offers a third stereoscopic image acquired at an off-nadir angle of 1.6°. Through that, ground areas between high-rise buildings can be captured with a higher probability. Pléiades stereoscopic triplets were acquired of the urban region of Da Nang at 20.10.2015 and 13.08.2017 (Tables 1 and 2).

Field reference data

To validate the results, reference information of buildings and the buildings structure was collected for 975 buildings in March 2015, March 2016 and December 2017. Amongst other things, the reference data includes information on the location (retrieved by GPS), building type, height and number of floors. For 405 of these reference buildings, the building height was measured with a handheld laser measure device and the floor number was collected additionally.

Table 1. Characteristics of Pléiades-1B panchromatic triplet – 20.10.2015.

	Image 1	Image 2	Image 3
Global incidence	13.69	7.08	13.00
Along-track (°)	−10.19	2.36	12.21
Across-track (°)	9.34	6.68	4.59
Acquisition time	03:24:32	03:24:52	03:25:09
Solar Azimuth (°)	146.09	146.09	146.50
Solar Elevation (°)	58.89	58.89	59.02

Table 2. Characteristics of Pléiades-1B panchromatic triplet – 13.08.2017.

	Image 1	Image 2	Image 3
Global incidence	16.12	11.62	7.76
Along-track (°)	−12.26	−7.64	−1.65
Across-track (°)	10.78	8.85	7.59
Acquisition time	03:24:36	03:24:44	03:24:54
Solar Azimuth (°)	90.69	90.58	90.58
Solar Elevation (°)	68.67	68.73	68.73

Administrative data

Land-use information of the General Construction Plan of Da Nang City 2030 was used to differentiate between building blocks and other land-use such as natural areas, agriculture, transport infrastructure. By using the geometries of the building plots, the results of this study can be integrated into the planning and development processes of the local administration (Urban Planning Institute (UPI); Department of Construction (DoC)). Additional cadastral data

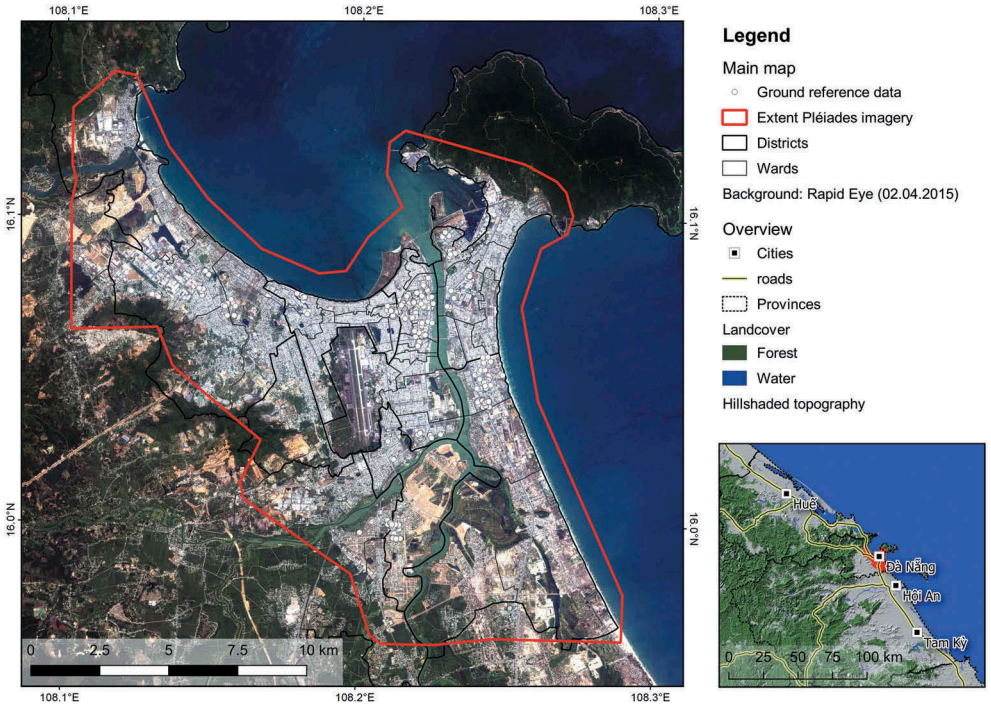

Figure 1. Study area and extent of Pléiades acquisition.

delineating building parcels was provided for large parts of the districts of Cẩm Lệ, Hải Châu, Liên Chiểu, Ngũ Hành Sơn, Sơn Trà and Thanh Khê, as well as a selection of LIDAR ground elevation points. In some cases, the building blocks were incomplete and had to be extended and attributed manually.

Administrative boundaries of the city districts and wards were retrieved from the GADM database of Global Administrative Areas (GADM, 2012).

Derivation of surface heights and built-up areas

Based on the 2015 and 2017 Pléiades acquisitions, the two DSMs were photogrammetrically processed by means of the panchromatic band (0.5-m resolution) in Erdas IMAGINE© using the Rational Polynomial Coefficients (RPCs) to describe the exterior and interior orientation of each panchromatic image of the Pléiades triplets (Hu, Gao, Li & Li, 2016; Topan, Taskanat, & Cam, 2013). Tie points were automatically generated and visually checked for their consistency. The total image RMSE of the triangulation was 0.211 for 2015 and 0.017 for 2017. Enhanced Automatic Terrain Extraction (eATE) was applied, using dense point matching and Normalized Cross-Correlation (NCC) to match images and extract elevation (Mikhail, Bethel, & McGlone, 2001; Straub, Stepper, Seitz, & Waser, 2013). The resulting point cloud was interpolated to a raster surface in CloudCompare (Girardeau-Montaut, 2015). The resulting DSM represents surface elevation information for the displayed areas including all anthropogenic structures and vegetation. To assess the accuracy of the DSM, the point cloud of 2015 was clipped with a ground mask and a digital elevation model (DEM) was derived from the extracted ground surface point information. The DEM contains ground elevation information, artificial structures and vegetation are excluded. A normalized surface model (nDSM) was differentiated from DSM and DEM. Positive differences in the nDSM represent vegetation and artificial structures, such as buildings. To validate the nDSM, its values were compared to the reference information on building heights. Figure 2 shows the elevations of the nDSM related to the available LIDAR points (see chapter "administrative data"), resulting in an R^2 of 0.87.

For the initial delineation of build-up structures, the panchromatic and multispectral bands of the 2015 Pléiades scene were pansharpened and an object-based image analysis (OBIA) approach was chosen (Blaschke, 2010; Blaschke et al., 2014). The OBIA approach groups neighbouring pixels with similar spectral or thematic values into image segments with spectral, geometric and thematic properties (Benz, Hofmann, Willhauck, Lingenfelder, & Heynen, 2004). To improve the segmentation result for build-up structures, a Canny edge operator was applied to the Pléiades scene and included

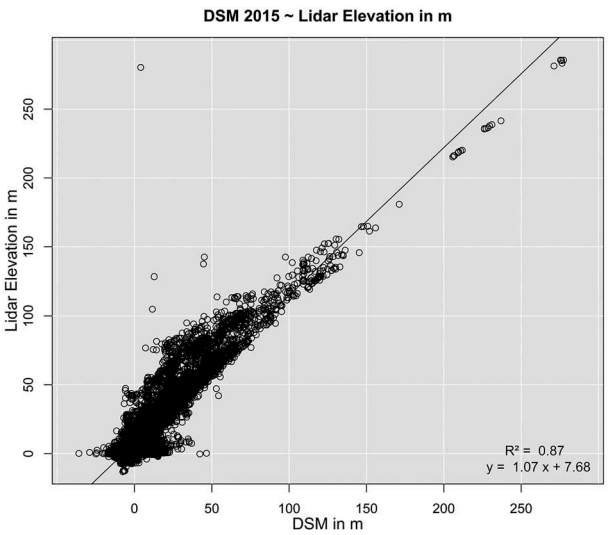

Figure 2. Relationship between DSM and LIDAR reference point data.

in the segmentation process (Bachofer, Quénéhervé, Zwiener et al., 2016; Canny, 1986). For the resulting segments, a complex ruleset was developed, which is based on spectral and height values, geometrical features, as well as spatial relationships between image objects. The properties of the object features were enriched by computing additional raster layers, such as the first three components of a Principal Component Analysis (PCA), the Normalized Differential Vegetation Index (NDVI) (Rouse, Haas, Schell, & Deering, 1973) and the Topographic Position Index (TPI) (Bachofer, 2017; De Reu et al., 2013; Guisan, Weiss, & Weiss, 1999; Weiss, 2001). The latter index was computed with the DSM to support the differentiation between elevated objects and ground surface. Remaining artefacts were edited manually. Due to the dense building structure of the city, identification of single buildings was not automatable. Build-up areas were then intersected with parcel boundaries, where available (see section "administrative data"), and centroids representing single buildings were derived. For areas without parcel data, visual identification of buildings was conducted by digitizing single points.

Identification of changes

As shown in Figure 3, the identification of changes in built-up structures between 2015 and 2017 was conducted in a two-step approach. In order to overcome the need for absolute building heights, both DSMs were horizontally adjusted in a first step and a difference image describing the absolute height change between both dates was generated. In the second step, the derived changes were classified on a threshold-based approach to delineate building or demolition activities. This is described at more detail in the following.

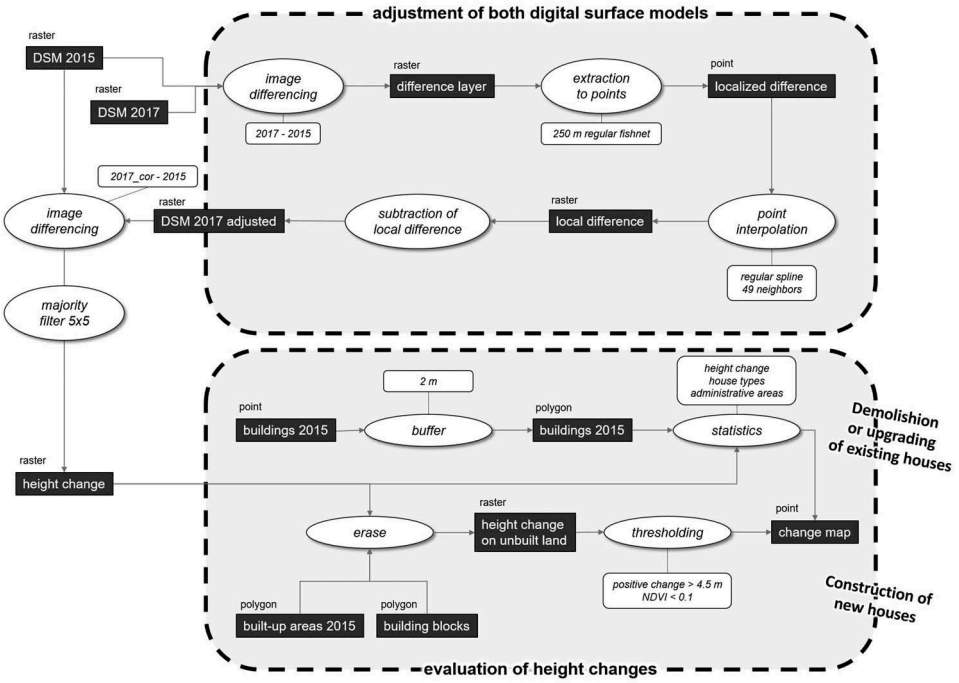

Figure 3. Workflow to identify building changes.

Vertical adjustment of both images

In order to differentiate the DSMs, both of the surface models have to be finely registered at the vertical dimension. Inaccuracies in vertical registration lead to misclassifications and therefore cause over- or underestimation of change.

To derive a surface that represents regional adapted differences between both DSMs, a first stratified random point sampling was implemented to generate 76,085 points representing ground elevation. For that, classified built-up areas were used to exclude buildings from the point sampling. To exclude vegetation-caused elevation deviations, areas with NDVI values greater 0.1 were excluded from the sampling as well. The masked-out areas were buffered with a 2.5-m distance to eliminate the influence of buildings and vegetation on the ground elevation. The heights from 2015 and 2017 were extracted at the 76,085 points and differenced in order to get information about regional differences of both models. To minimize the influence of potential outliers and to avoid overfitting of the differential surface, the points were averaged at a regular 250-m sampling grid (see Figure 4). Based on this regular point grid a spline interpolation was implemented to generate a smooth and steady differential rectification surface (Franke, 1981).

As systematically induced errors are expected to occur in the difference between the 2015 and 2017 models, an approach based on 49 points in a 7 × 7 neighbourhood is chosen to conduct the interpolation. Thereby the influence of single values can be reduced to enable a steady interpolation result. To apply the vertical correction, the interpolated differential rectification surface was applied to the 2017 DSM by subtracting its values. After the vertical adjustment, both elevation models show a very good correlation (R^2 = 0.99, see Figure 5).

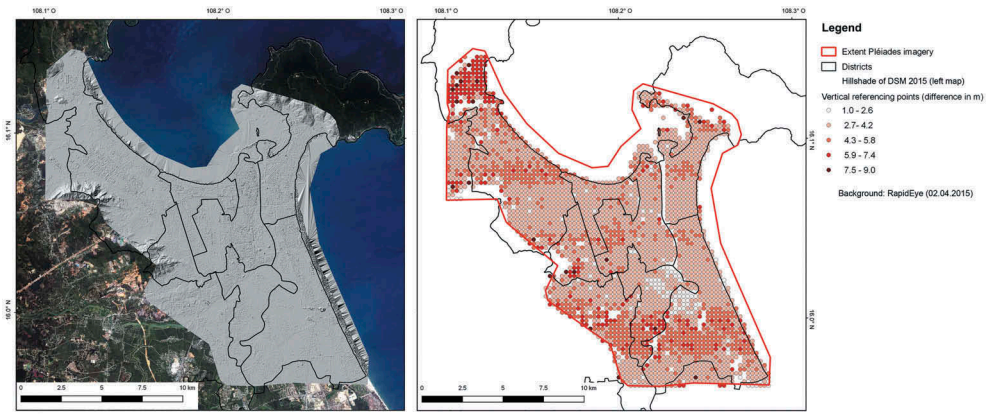

Figure 4. Hillshade of 2015 DSM (left) and differences at ground points for vertical fine registration of DSMs (right).

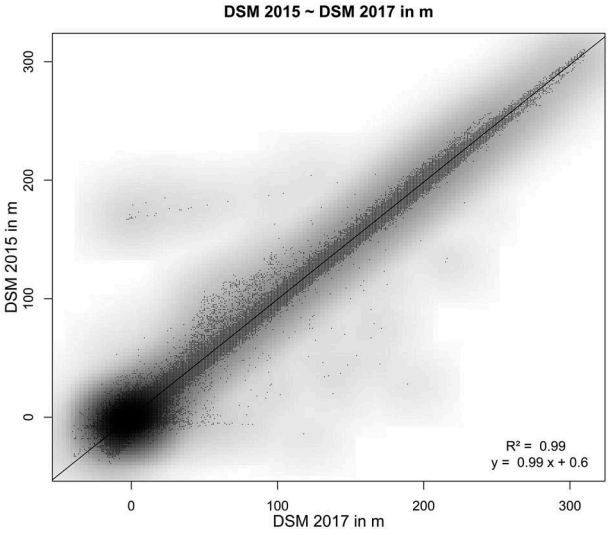

Figure 5. Fine vertical registration of DSMs 2015 and 2017.

Changes of existing buildings and in newly constructed areas

On the base of two finely registered DSMs, the differencing can be conducted with simple subtraction of the corresponding elevation values.

$$Change\ surface = DSM2017 - DSM2015 \quad (1)$$

The result shows positive differences representing an increase of elevation, whereas negative differences represent a decrease of elevation during the 2-year period. A 5 × 5 majority filter reduces outliers in the DSM difference to avoid misclassifications in the following procedure.

In a first approach, the change surface is masked by built-up areas to retrieve a raster representing only changes in 2015 built-up areas. To derive changes in build-up areas, each house is considered based on building centroids (see chapter "Derivation of surface heights and built-up areas"). A 2-m buffer is applied on the building centroid to construct a representative building area without knowledge of its exact orientation. Based on the coverage of the building buffers, the change surface is averaged to derive a statistical and filtered change value for each building. Our field measurements show that the majority of the buildings in DaNang have two or more floors (Table 3) and consist of narrow local-type houses (67% of our reference data). As demonstrated by Downes, Storch, Schmidt, van Nguyen, and Tran (2016), these local-type buildings make up the majority of the building stock (approximately 90% of all buildings in DaNang), are typically constructed with two or more floors and are preferably used in construction areas. Based on these observations, we defined thresholds given in Table 3 to classify changes.

To determine the changes on 2015 unbuilt-areas, previously mentioned building footprints are used to remove buildings from the change surface,

Table 3. Thresholds for the identification of changes.

	Positive changes		Negative changes	
	moderate	severe	moderate	severe
Built-up areas	4.5 to 10 m	> 10 m	−6.5 to −10 m	> −10 m
Unbuilt areas	6 to 10 m	> 10 m	-	-

Table 4. Building change detection 2015–2017.

	Number of detected change		Newly built		Demolished	
Category	n	%	n	%	n	%
Built-up	6,213	*61.6*	4,714	*54.9*	1,499	*100*
Unbuilt	3,867	*38.4*	3,867	*45.1*	-	-
Overall detections	**10,080**	*100*	**8,581**	*100*	**1,499**	*100*

additionally, areas with NDVI values greater than 0.1 are excluded to avoid vegetation related changes. In this second approach, only positive changes are considered representing the increased building. Negative changes are not expected to be caused by building dynamics. Applying the thresholds given in Table 4, the area representing the change surface on the unbuilt ground is classified to moderate and severe change. Polygonising the classified patches allows for the application geometrically based refinement. Classified change patches below 35 m^2 are removed from the polygon areas.

Small area water bodies, mining areas (in the Liên Chiểu and Cẩm Lệ districts), filling zones, container yards close to ports (in Sơn Trà) and planes at the prefield of the airport which show constant elevation changes are hard to be identified by means of automatic classification. For this reason, the mentioned areas were visually identified and manually removed from the classified result. Remaining detections represent recent building activities between 2015 and 2017.

Results

Accuracy of the DSM

The DSMs were generated with a 0.5-m resolution. Since there is no focus on absolute heights in this approach, but on correct heights, the quality of the derived heights was estimated by comparing the 405 building height measurements with the described nDSM. The coefficient of determination shows with r^2 = 0.6 a good conformity of the derived heights with true building heights (see Figure 6).

Accuracy of the DSM difference

The vertical referencing, which is crucial for correct interpretation of detected changes, resulted in very high accuracies. The validation was performed on the 76,085 ground points, on which the differencing values

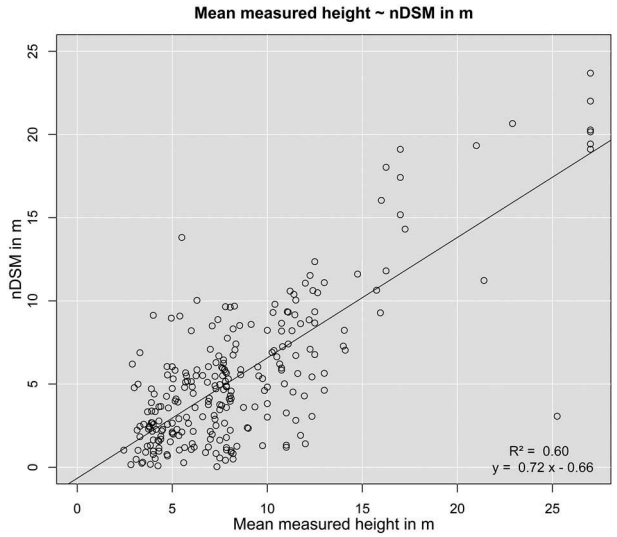

Figure 6. Relationship between measured building height and nDSM.

were extracted. Statistical analysis on the points produced an average discrepancy of 0.044 m for the 2015 and the 2017 DSM with a standard deviation of 2.02 m. The low standard deviation symbolizes a very fine vertical registration, especially as it lies below the classification threshold to detect building and demolition activities (Table 4). Consequently, the differences can be used with the given thresholds as indicators to detect building changes.

Considering a small scale, the difference image shows a generally very homogenous distribution of values around the zero value, which represents no change in elevation between both acquisition dates. At the north eastern part of the study area, slight deviations are identifiable (varying between +6.5 m and −11 m) and are to be interpreted as effects of misregistration, as these patches cover steep and densely wooded terrain. Again, no ground points for vertical referencing could be generated in these areas. As a consequence of the locally concentrated mining activities at the western part of the study area and the transition of the terrain into wooded and mountainous terrain, the area is under-represented by valid ground points for the vertical registration process as well. The strong differences in the eastern part of the Da Nang bay are caused by land filling activities to expand development ground.

Regarding the difference raster in more detail reveals spatially high resoluted changes over the given period. On unbuilt areas in 2015, the changes appear very explicitly. In these cases, the shape of the changed building is very accentuated. Especially large-area commercially and industrially used buildings are distinguishable due to the shapes of the changes. Also, apartment and hotel complexes close to the shoreline, which were constructed in the investigated period, are identifiable by the shape of the single detected changes and moreover by their mutual spatial arrangements.

The change raster allows identifying a change in the city centre, where the city initially was already densely built-up in 2015. Changes are characterized by homogeneous values over an entire building footprint. High-rise buildings can cause false change marks because photogrammetric approaches can struggle with exactly modelling surface and shape characteristics at the same time. This can cause a "bagel effect" in the difference raster when the shape of buildings is estimated slightly different in both DSMs. Homogeneous surfaces such as streets, lawns, water bodies and runways at the airports induce high positive or high negative values in the difference raster, due to the disability of photogrammetric processing to set valid cross-correlations between image sections without sufficient contrast.

Figure 7 gives an overview of the changes in the study area and some selected examples at higher detail.

Changes in the city

Overall changes

The classification of building stock changes resulted in 10,080 detected building changes between 2015 and 2017 in the area covered by both Pléiades acquisitions (see Tables 1 and 2). This total number is split into 8,531 buildings showing an increase in heights above given thresholds and 1,499 buildings have been demolished at the acquisition time in 2017 compared to 2015. In formerly unbuilt areas, building change detections represent newly built houses. Spatial intersection of detected changes and unbuilt areas shows 3,867 newly constructed buildings in the two-year period. The spatial intersection of detected height increase and built-up areas reveal 4,714 changes in the existing building stock. The numbers can not indicate rebuilding or upgrading of buildings. Based on an assumed total building number of 244,180 buildings in 2015 (based on spectral based building detection – see chapter "Derivation of surface heights and built-up areas") and 7,082 differenced newly buildings, the building stock in the image covered agglomeration area increased about 1.5% in two years through buildings on the newly built ground. 1.9% of the buildings in the existing building stock in 2015 were extended or rebuilt in the two-year period and 0.6% of the existing building stock has been demolished at the time of the second acquisition compared to the 2015 acquisition.

Regional examination of building changes

The heatmap (see Figure 8) shows the density of changed buildings in a 1 km radius. It visualizes a general regional trend in the building stock dynamics. It reveals two major areas with high change dynamics. The areas east of the airport, which include parts of the districts of Hải Châu,

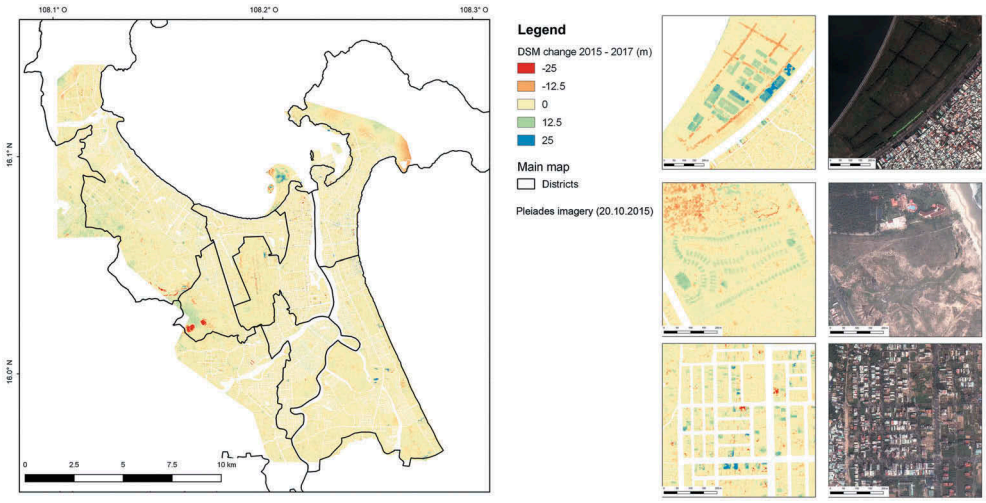

Figure 7. Change maps of Da Nang. Overview (left) and detailed view on building complexes (upper right), industrial areas (middle right) and city centre (lower right).

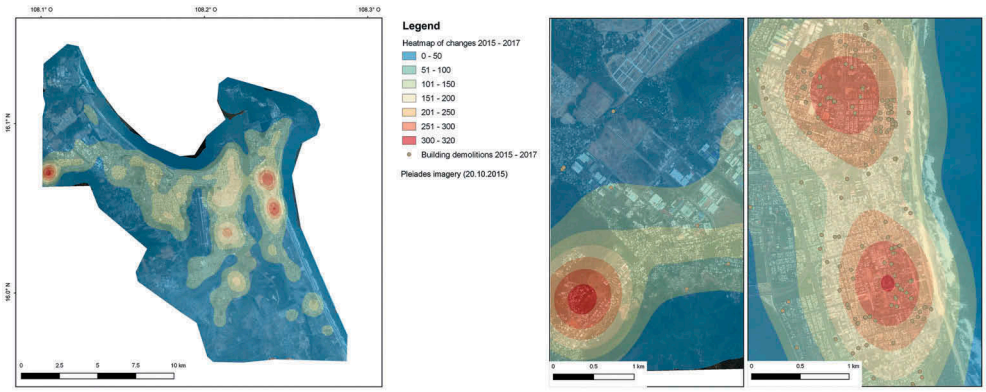

Figure 8. Heatmap shows regional trends of building changes over the Da Nang area. Subsets showing dynamic zones without detected demolitions and with detected demolitions.

Sơn Trà and Ngũ Hành Sơn, show the highest change densities. These areas contain the traditional city centre of Da Nang, which undergoes a steady process of change and renewal. In densely built-up areas, building renovation generally involves demolition of building stock, which is detected by the applied thresholds on the change surface as well. Overlaying detections of demolition verifies the active process of ongoing renewal in the building stock.

In the western part of the Da Nang agglomeration, west of Liên Chiểu, changes are detected in spatially high concentrations. Considering missing detections of building demolitions, these peripheral areas are recently developed areas to extend the Da Nang settlement area. These areas were formerly agriculturally used land converted from cropland to development areas. The Cẩm Lệ peninsula shows comparably high change activities, though the change densities do not reach the values of the Liên Chiểu development area. The tip of the peninsula likewise is a transformation area from cropland to development area; however, the development was initialized prior to the first acquisition in 2015, which is why the change densities do not stand out compared to similar areas. As well, building activities on the Cẩm Lệ peninsula seem to be spread more extensively over the development area, which causes a comparatively lighter change density.

Local examination of building changes

The spatial aggregation of changes by means of regular hexagons with 500-m diameter supplements the change heatmap by enabling assignments of change to smaller scale units. Red colours symbolize highest change dynamics with 100 detected changes or more, whereas blue hexagons are assigned the lowest changes with 1 to 10 detected changes (Figure 9, left). Hexagons without detected changes remain transparent. Hexagons with highest change rate exist 3 times in the city centre, one according to hexagon is located at the western development area near Liên Chiểu. The highest concentration of orange coloured (20–50 changes) and yellow coloured hexagons (10–20 changes) lies between the airport and the east shoreline. With increasing distance to the city centre the existence of blue coloured hexagons grow,

indicating the lowest numbers of detection. Except from the western development areas near Liên Chiểu, the blue hexagons form a ring structure, which surrounds the city centre and forms a transition to the outskirts of Da Nang.

Regarding the hexagons representing demolitions, a value range between 1 and 31 demolitions per polygon is displayed (Figure 9, right). Similar to the total detected changes, the concentration of demolitions is located in the city centre, where red, violet and black colours are plotted, representing demolition ranges between 11 and 31 changes. Especially along the western riverbank, the highest demolition numbers are located. These findings indicate starting and ongoing renewal processes in these areas. In peripheral areas environing the city centre, detected demolitions range on a comparably low level.

Accuracy assessment

We tested 200 randomly selected change points in regards to correct detection. As the results consist of detected changes only, we had no possibility to calculate a true-negative accuracy. 162 out of 200 test points were detected correctly, which is a true-positive rate of 81%.

Discussions

The validation results of the DSM generation, on information content regarding building heights and vertical DSM registration, approve the usage of relative elevation information. Knowledge of existing buildings is the main prerequisite for this approach, as detecting change in initially present building stock is based on the spatial information of single buildings. The examination of the change raster revealed slight misregistrations on mountainous and wooded terrain because valid ground points to enhance the surface for precise DSM registration cannot be set on the covered ground. This limitation can occur in very densely built-up areas, wherein addition only very narrow streets and tracks separate building block. Given such cases, it is hardly possible to define valid ground points for ground elevation sampling. Therefore, in such areas, the vertical referencing surface can possibly contain raised uncertainties. In our study, the fine registration surface showed a mean difference of 0.04 m and a standard deviation of 2.02 m.

Photogrammetry derived elevation information must be interpreted differently compared spectral remote sensing approaches, as photogrammetric processes do not exactly reproduce sharp edges or ridges as they occur between houses and streets or between houses with large height differences. This characteristic of photogrammetric processing can cause a "bagel effect", when building extends got derived more extensive in one DSM, which must not be interpreted as detected change.

By using thresholds on elevation information and on horizontal changed areas, the approach is though very robust and comparably incomplex to implement, as a simple reclassification of elevation difference is applied instead of spectral building classification. Bi- and tri stereoscopic Pléiades data are beneficial in pricing compared to other sources and, after the photogrammetric processing, the differencing has to be referred to present information.

In the case study, the results show a concentration of change at the city centre. Highest rates of change and demolition are detected between the airport and the eastern coastline. Comparing to studies, reporting a strong expansion of the Da Nang urban area (Linh et al. (2009)), our results show the concentration of building changes on the city centre of Da Nang, which are caused by redensification tendencies and renewal of existing building stock. Nevertheless, near Liên Chiểu and on the Cẩm Lệ peninsula, developing areas are under construction. Detected patterns on the southern regions of the eastern shoreline show building activities with complexes of buildings or

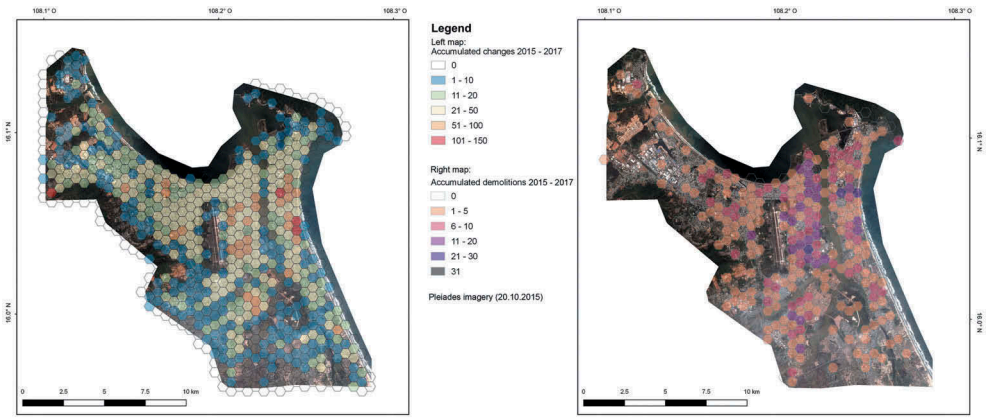

Figure 9. Locally detected changes (left) and detected demolitions (right).

hotel areas. These detections confirm perceptions from field campaigns in the study area, where upmarket building projects are realized close to the shore line.

To distinguish between redensification areas and building development areas, demolitions can be used as a valuable indicator. The detected demolitions can only show demolitions in 2017 respectively at the second acquisition time and therefore must not be interpreted as a total demolition number of the period under consideration.

Conclusion and outlook

The presented results show that the approach on differencing relative DSMs provides a practical tool to monitor change in building stock of urban areas. A true positive rate of 81% of our findings confirms our assumptions.

VHR remote sensing imagery has proven to be a benefit of this study, as not only the dynamic of city growth was detected, but also the type of change in already built-up areas. To detect change at the building level, imagery with spatial resolution below the smallest objects to be detected is necessary. So besides the advantages of medium resolution remote sensing imagery, which allow monitoring areal urban changes (Wei, Blaschke, Kazakopoulos, Taubenböck, and Tiede (2017)), our results show that VHR remote sensing imagery enables the identification of local and small-scale urban processes, such as building construction, upgrading and demolition on single building level.

The 2017 image has been acquired in a very active phase with construction in progress, as many areas show spectral characteristics of open ground. A continuous implementation of this approach can reconstruct the steady change of activities. Besides the spatially high-resolution change information, the implementation of satellite imagery in the approach offers the advantage of the availability of imagery and thus can provide temporally high-resolution change information as well for long-term change monitoring. In the continuation, the approach can be adapted more precisely to the local building characteristics, by implementing local knowledge to improve threshold definition for height changes and building footprint area. The improvement of detecting ground areas, so far implemented by NDVI thresholding and buffering of building structures, would benefit in increasing the accuracy of the vertical registration of both input DSMs. This leads to more precise change detection in densely built-up areas.

Disclosure statement

No potential conflict of interest was reported by the authors.

Funding

This study was funded by the German Federal Ministry of Education and Research (BMBF) under the project "RapidPlanning" (grant identifier 01LG1301K).

ORCID

Andreas Braun http://orcid.org/0000-0001-8630-1389
Felix Bachofer http://orcid.org/0000-0001-6181-0187

References

Alphan, H., & Güvensoy, L. (2016). Detecting coastal urbanization and land use change in Southern Turkey. *Journal of Environmental Engineering and Landscape Management*, *24*(2), 97–107. doi:10.3846/16486897.2015.1113976

Bachofer, F. (2017). Assessment of building heights from pléiades satellite imagery for the Nyarugenge sector, Kigali, Rwanda. *Rwanda Journal*, *1*(DI). doi:10.4314/rj.v1i2s.6d

Bachofer, F., Quénéhervé, G., Zwiener, T., Maerker, M., & Hochschild, V. (2016). Comparative analysis of edge detection techniques for SAR images. *European Journal of Remote Sensing*, *49*(1), 205–224. doi:10.5721/EuJRS20164912

Bagnardi, M., González, P.J., & Hooper, A. (2016). High-resolution digital elevation model from tri-stereo Pleiades-1 satellite imagery for lava flow volume estimates at Fogo Volcano. *Geophysical Research Letters*, *43*(12), 6267–6275. doi:10.1002/2016GL069457

Baltsavias, E.P. (1999). A comparison between photogrammetry and laser scanning. *ISPRS Journal of Photogrammetry and Remote Sensing*, *54*(2–3), 83–94. doi:10.1016/S0924-2716(99)00014-3

Belgiu, M., & Drăguţ, L. (2014). Comparing supervised and unsupervised multiresolution segmentation approaches for extracting buildings from very high resolution imagery. *ISPRS Journal of Photogrammetry and Remote Sensing*, *96*, 67–75. doi:10.1016/j.isprsjprs.2014.07.002

Benz, U.C., Hofmann, P., Willhauck, G., Lingenfelder, I., & Heynen, M. (2004). Multi-resolution, object-oriented fuzzy analysis of remote sensing data for GIS-ready information. *ISPRS Journal of Photogrammetry and Remote Sensing*, *58*(3–4), 239–258. doi:10.1016/j.isprsjprs.2003.10.002

Bhatta, B. (2010). Causes and consequences of urban growth and sprawl. In *Analysis of urban growth and sprawl from remote sensing data* (pp. 17–36). Springer. Berlin, Heidelberg.

Blaschke, T. (2010). Object based image analysis for remote sensing. *ISPRS Journal of Photogrammetry and Remote Sensing*, *65*(1), 2–16. doi:10.1016/j.isprsjprs.2009.06.004

Blaschke, T., Hay, G.J., Kelly, M., Lang, S., Hofmann, P., Addink, E., … van Coillie, F. (2014). Geographic object-based image analysis–Towards a new paradigm. *ISPRS Journal of Photogrammetry and Remote Sensing*, *87*, 180–191. doi:10.1016/j.isprsjprs.2013.09.014

Blaschke, T., Lang, S., & Hay, G. (2008). *Object-based image analysis: Spatial concepts for knowledge-driven remote sensing applications*. Springer Science & Business Media. Berlin, Heidelberg.

Brunner, D., Lemoine, G., Bruzzone, L., & Greidanus, H. (2010). Building height retrieval from VHR SAR imagery based on an iterative simulation and matching technique.

IEEE Transactions on Geoscience and Remote Sensing, *48* (3), 1487–1504. doi:10.1109/TGRS.2009.2031910

Canny, J. (1986). A computational approach to edge detection. *IEEE Transactions on Pattern Analysis & Machine Intelligence*, (6), 679–698. doi:10.1109/TPAMI.1986.4767851

Cohen, B. (2006). Urbanization in developing countries: Current trends, future projections, and key challenges for sustainability. *Technology in Society*, *28*(1–2), 63–80. doi:10.1016/j.techsoc.2005.10.005

Colin-Koeniguer, E., & Trouve, N. (2014). Performance of building height estimation using high-resolution PolInSAR images. *IEEE Transactions on Geoscience and Remote Sensing*, *52*(9), 5870–5879. doi:10.1109/TGRS.2013.2293605

De Lussy, F., Greslou, D., Dechoz, C., Amberg, V., Delvit, J. M., Lebegue, L., … Fourest, S. (2012). Pleiades HR in flight geometrical calibration: Location and mapping of the focal plane. *Int. Arch. Photogramm. Remote Sens. Spat. Inf. Sci*, *39*, 519–523. doi:10.5194/isprsarchives-XXXIX-B1-519-2012

De Pinho, C.M.D., Fonseca, L.M.G., Korting, T.S., de Almeida, C.M., & Kux, H.J.H. (2012). Land-cover classification of an intra-urban environment using high-resolution images and object-based image analysis. *International Journal of Remote Sensing*, *33* (19), 5973–5995. doi:10.1080/01431161.2012.675451

De Reu, J., Bourgeois, J., Bats, M., Zwertvaegher, A., Gelorini, V., de Smed, P., … Finke, P. (2013). Application of the topographic position index to heterogeneous landscapes. *Geomorphology*, *186*, 39–49. doi:10.1016/j.geomorph.2012.12.015

de Vries, W., & Lance, K. (2011). SDI reality in Uganda: Coordinating between redundancy and efficiency. In Z. Nedovic-Budic, J. Crompvoets, & Y. Georgiadou (Eds.), *Spatial data infrastructures in context: North and South* (pp. 103–119). CRC press. Boca Raton.

Dell'Acqua, F., & Gamba, P.E. (2012). Remote sensing and earthquake damage assessment: Experiences, limits, and perspectives. *Proceedings of the IEEE*, *100*(10), 2876–2890. doi:10.1109/JPROC.2012.2196404

Downes, N.K., Storch, H., Schmidt, M., van Nguyen, T.C., & Tran, T.N. (2016). Understanding Ho Chi Minh City's urban structures for urban land-use monitoring and risk-adapted land-use planning. In *Sustainable Ho Chi Minh City: Climate policies for emerging mega cities* (pp. 89–116). Springer. Berlin, Heidelberg.

Durieux, L., Lagabrielle, E., & Nelson, A. (2008). A method for monitoring building construction in urban sprawl areas using object-based analysis of Spot 5 images and existing GIS data. *ISPRS Journal of Photogrammetry and Remote Sensing*, *63*(4), 399–408. doi:10.1016/j.isprsjprs.2008.01.005

Franke, R. (1981). Smooth interpolation of scattered data by local thin plate splines. *Computers & Mathematics with Applications, 8*(4), 273-281. doi:10.1016/0898-1221(82)90009-8

GADM. (2012). *GADM database of global administrative areas: Version 2.0*. University of California Berkeley. Retrieved from https://gadm.org

Gal, O., & Doytsher, Y. (2014). Fast and efficient visible trajectories planning for the Dubins UAV model in 3D built-up environments. *Robotica*, *32*(1), 143–163. doi:10.1017/S0263574713000787

Geiß, C., Pelizari, P.A., Marconcini, M., Sengara, W., Edwards, M., Lakes, T., & Taubenböck, H. (2015). Estimation of seismic building structural types using multi-sensor remote sensing and machine learning techniques. *ISPRS Journal of Photogrammetry and Remote Sensing*, *104*, 175–188. doi:10.1016/j.isprsjprs.2014.07.016

George, H. (2000). Developing countries and remote sensing: How intergovernmental factors impede progress. *Space Policy*, *16*(4), 267–273. doi:10.1016/S0265-9646(00)00042-4

Girardeau-Montaut, D. (2015). CloudCompare version 2.6. 1 user manual. Grenoble

Gleyzes, M.A., Perret, L., & Kubik, P. (2012). Pleiades system architecture and main performances. *International Archives of the Photogrammetry, Remote Sensing and Spatial Information Sciences*, *39*(1), 537–542. doi:10.5194/isprsarchives-XXXIX-B1-537-2012

Goodfellow, T. (2013). Planning and development regulation amid rapid urban growth: Explaining divergent trajectories in Africa. *Geoforum*, *48*, 83–93. doi:10.1016/j.geoforum.2013.04.007

Guisan, A., Weiss, S.B., & Weiss, A.D. (1999). GLM versus CCA spatial modeling of plant species distribution. *Plant Ecology*, *143*(1), 107–122. doi:10.1023/A:1009841519580

Haala, N., & Kada, M. (2010). An update on automatic 3D building reconstruction. *ISPRS Journal of Photogrammetry and Remote Sensing*, *65*(6), 570–580. doi:10.1016/j.isprsjprs.2010.09.006

Hastings, D.A., & Clark, D.M. (1991). GIS in Africa: Problems, challenges and opportunities for co-operation. *International Journal of Geographical Information System*, *5*(1), 29–39. doi:10.1080/02693799108927829

Hegazy, I.R., & Kaloop, M.R. (2015). Monitoring urban growth and land use change detection with GIS and remote sensing techniques in Daqahlia governorate Egypt. *International Journal of Sustainable Built Environment*, *4*(1), 117–124. doi:10.1016/j.ijsbe.2015.02.005

Hill, R.D., Moate, C.P., & Blacknell, D. (2006). Urban scene analysis from SAR image sequences. In E.G. Zelnio & F. D. Garber (Eds..), *SPIE proceedings, algorithms for synthetic aperture radar imagery XIII, Orlando* (Vol. 6237, pp. 623702). SPIE. doi:10.1117/12.664418

Hu, F., Gao, X.M., Li, G.Y., & Li, M. (2016). DEM extraction from WorldView-3 stereo images and accuracy evaluation. *International Archives of Photogrammetry Remote Sensing and Spatial Information Sciences*, *41*. 327-332.

Im, J., Jensen, J.R., & Tullis, J.A. (2008). Object-based change detection using correlation image analysis and image segmentation. *International Journal of Remote Sensing*, *29*(2), 399–423. doi:10.1080/01431160601075582

Jensen, J.R., & Cowen, D.C. (1999). Remote sensing of urban/suburban infrastructure and socio-economic attributes. *Photogrammetric Engineering and Remote Sensing*, *65*, 611–622.

Jha, M.K., & Chowdary, V.M. (2007). Challenges of using remote sensing and GIS in developing nations. *Hydrogeology Journal*, *15*(1), 197–200. doi:10.1007/s10040-006-0117-1

JICA. (2010). *The study on integrated development strategy for da nang city and its neighboring area in the socialist republic of vietnam (DaCRISS): Final Report*. December 2010. Tokyo. Retrieved from http://open_jicareport.jica.go.jp/pdf/12014924.pdf

Kadhim, N., & Mourshed, M. (2018). A shadow-overlapping algorithm for estimating building heights from VHR satellite images. *IEEE Geoscience*

and Remote Sensing Letters, *15*(1), 8–12. doi:10.1109/LGRS.2017.2762424

Kelbe, D., White, D., Hardin, A., Moehl, J., & Phillips, M. (2016). Sensor-agnostic photogrammetric image registration with applications to population modeling. In *2016 IEEE International Geoscience & Remote Sensing Symposium: Proceedings: July 10-15, 2016, Beijing, China* (pp. 1831–1834). Piscataway, NJ: IEEE. doi:10.1109/IGARSS.2016.7729470

Kopecká, M., & Rosina, K. (2014). Identification of changes in urbanized landscape based on VHR satellite data: Study area of Trnava. *Geografický Časopis*. 66. 247-267.

Lefebvre, A., Nabucet, J., Corpetti, T., Courty, N., & Hubert-Moy, L. (2016). Extraction of urban vegetation with Pleiades multiangular images. In T. Erbertseder, T. Esch, & N. Chrysoulakis (Eds.), *SPIE proceedings, remote sensing technologies and applications in urban environments*. Vol. 10008, pp. 100080H-1. SPIE Remote Sensing, Edinburgh. doi:10.1117/12.2241162

Leiser, S. (2011). Institutionalization does not occur by decree: Institutional obstacles in implementing a land administration system in a developing country. In Z. Nedovic-Budic, J. Crompvoets, & Y. Georgiadou (Eds.), *Spatial data infrastructures in context: North and South* (pp. 21–48). CRC press. Boca Raton.

Linh, N.H.K., Erasmi, S., & Kappas, M. (2009). Quantifying land use/cover change and landscape fragmentation in Danang City, Vietnam: 1979-2009. *Aster*, *2*, 4.

Liu, C., Huang, X., Wen, D., Chen, H., & Gong, J. (2017). Assessing the quality of building height extraction from ZiYuan-3 multi-view imagery. *Remote Sensing Letters*, *8*(9), 907–916. doi:10.1080/2150704X.2017.1335904

Lu, L., Guo, H., & Corbane, C. (2013). Building damage assessment with VHR images and comparative analysis for Yushu Earthquake, China. *Disaster Adv*, *6*, 37–44.

Mikhail, E.M., Bethel, J.S., & McGlone, J.C. (2001). Introduction to modern photogrammetry. New York.

Moskal, L.M., Styers, D.M., & Halabisky, M. (2011). Monitoring urban tree cover using object-based image analysis and public domain remotely sensed data. *Remote Sensing*, *3*(10), 2243–2262. doi:10.3390/rs3102243

Mundia, C.N., & Aniya, M. (2005). Analysis of land use/cover changes and urban expansion of Nairobi city using remote sensing and GIS. *International Journal of Remote Sensing*, *26*(13), 2831–2849. doi:10.1080/01431160500117865

Olsen, M.J., Chen, Z., Hutchinson, T., & Kuester, F. (2013). Optical techniques for multiscale damage assessment. *Geomatics, Natural Hazards and Risk*, *4*(1), 49–70. doi:10.1080/19475705.2012.670668

Panagiotakis, E., Chrysoulakis, N., Charalampopoulou, V., & Poursanidis, D. (2018). Validation of Pleiades Tri-Stereo DSM in urban areas. *ISPRS International Journal of Geo-Information*, *7*(3), 118. doi:10.3390/ijgi7030118

Patino, J.E., & Duque, J.C. (2013). A review of regional science applications of satellite remote sensing in urban settings. *Computers, Environment and Urban Systems*, *37*, 1–17. doi:10.1016/j.compenvurbsys.2012.06.003

Peng, F., Gong, J., Le Wang, W.H., & Yang, J. (2016). Impact of building heights on 3D urban density estimation from spaceborne stereo imagery. *International Archives of Photogrammetry Remote Sensing and Spatial Information Sciences*, *41*, 677. doi:10.5194/isprsarchives-XLI-B3-677-2016

Perko, R., Raggam, H., Gutjahr, K., & Schardt, M. (2014). Assessment of the mapping potential of Pléiades stereo and triplet data. *ISPRS Annals of the Photogrammetry, Remote Sensing and Spatial Information Sciences*, *2*(3), 103. doi:10.5194/isprsannals-II-3-103-2014

Poli, D., & Caravaggi, I. (2012). Digital surface modelling and 3D information extraction from spaceborne very high resolution stereo pairs. *JRC Scientific and Technical Reports, Ispra*. doi:10.1094/PDIS-11-11-0999-PDN

Poli, D., Remondino, F., Angiuli, E., & Agugiaro, G. (2015). Radiometric and geometric evaluation of GeoEye-1, WorldView-2 and Pléiades-1A stereo images for 3D information extraction. *ISPRS Journal of Photogrammetry and Remote Sensing*, *100*, 35–47. doi:10.1016/j.isprsjprs.2014.04.007

Rashed, T., & Jürgens, C. (2010). *Remote sensing of urban and suburban areas*. Springer Science & Business Media. Berlin, Heidelberg.

Rebelo, C., Rodrigues, A.M., Tenedório, J.A., Goncalves, J. A., & Marnoto, J. (2015). Building 3D city models: Testing and comparing Laser scanning and low-cost UAV data using FOSS technologies. In *International Conference on Computational Science and Its Applications, Girona* (pp. 367–379).

Rottensteiner, F., & Briese, C. (2002). International archives of photogrammetry remote sensing and spatial information sciences. *A New Method for Building Extraction in Urban Areas from High-Resolution LIDAR Data*, *34*(3/A), 295–301.

Rouse, J.W., Haas, R.H., Schell, J.A., & Deering, D.W. (1973). Monitoring the vernal advancement and retrogradation (green wave effect) of natural vegetation.

Salehi, B., Zhang, Y., Zhong, M., & Dey, V. (2012). Object-based classification of urban areas using VHR imagery and height points ancillary data. *Remote Sensing*, *4*(8), 2256–2276. doi:10.3390/rs4082256

Satterthwaite, D., & Mitlin, D. (2012). *Urban poverty in the global south: Scale and nature*. Routledge. London.

Schell, L.M., & Denham, M. (2003). Environmental pollution in urban environments and human biology. *Annual Review of Anthropology*, *32*(1), 111–134. doi:10.1146/annurev.anthro.32.061002.093218

Shahtahmassebi, A.R., Song, J., Zheng, Q., Blackburn, G.A., Wang, K., Huang, L.Y., … Haghighi, R.S. (2016). Remote sensing of impervious surface growth: A framework for quantifying urban expansion and re-densification mechanisms. *International Journal of Applied Earth Observation and Geoinformation*, *46*, 94–112. doi:10.1016/j.jag.2015.11.007

Shalaby, A., & Tateishi, R. (2007). Remote sensing and GIS for mapping and monitoring land cover and land-use changes in the Northwestern coastal zone of Egypt. *Applied Geography*, *27*(1), 28–41. doi:10.1016/j.apgeog.2006.09.004

Soergel, U., Michaelsen, E., Thiele, A., Cadario, E., & Thoennessen, U. (2009). Stereo analysis of high-resolution SAR images for building height estimation in cases of orthogonal aspect directions. *ISPRS Journal of Photogrammetry and Remote Sensing*, *64*(5), 490–500. doi:10.1016/j.isprsjprs.2008.10.007

Sportouche, H., Tupin, F., & Denise, L. (2011). Extraction and three-dimensional reconstruction of isolated buildings in urban scenes from high-resolution optical and SAR spaceborne images. *IEEE Transactions on Geoscience and Remote Sensing*, *49*(10), 3932–3946. doi:10.1109/TGRS.2011.2132727

Straub, C., Stepper, C., Seitz, R., & Waser, L.T. (2013). Potential of UltraCamX stereo images for estimating timber volume and basal area at the plot level in mixed

European forests. *Canadian Journal of Forest Research*, *43*(8), 731–741. doi:10.1139/cjfr-2013-0125

Topan, H., Taskanat, T., & Cam, A. (2013). Georeferencing accuracy assessment of Pléiades 1A images using rational function model. *International Archives of the Photogrammetry, Remote Sensing and Spatial Information Sciences*, *7*, W2.

Tsai, Y.H., Stow, D., & Weeks, J. (2011). Comparison of object-based image analysis approaches to mapping new buildings in Accra, Ghana using multi-temporal QuickBird satellite imagery. *Remote Sensing*, *3*(12), 2707–2726. doi:10.3390/rs3122707

Unger, J., Reich, M., & Heipke, C. (2014). UAV-based photogrammetry: Monitoring of a building zone. *International Archives of Photogrammetry Remote Sensing and Spatial Information Sciences*, *40*(5), 601. doi:10.5194/isprsarchives-XL-5-601-2014

Vasconcellos, E.A. (2014). *Urban transport environment and equity: The case for developing countries*. Routledge. London.

Wei, C., Blaschke, T., Kazakopoulos, P., Taubenböck, H., & Tiede, D. (2017). Is spatial resolution critical in urbanization velocity analysis? Investigations in the pearl river delta. *Remote Sensing*, *9*(1), 80. doi:10.3390/rs9010080

Weiss, A.D. (2001). *Topographic position and landforms analysis: Poster presentation*. ESRI User Converence, San Diego, CA.

Weng, Q., Quattrochi, D., & Gamba, P.E. (2018). *Urban remote sensing*. CRC press. Boca Raton.

Wickramasinghe, D.C., Vu, T.T., & Maul, T. (2018). Satellite remote-sensing monitoring of a railway construction project. *International Journal of Remote Sensing*, *39*(6), 1754–1769. doi:10.1080/01431161.2017.1415481

Xu, Y., Ma, P., Ng, E., & Lin, H. (2015). Fusion of worldView-2 stereo and multitemporal TerraSAR-X images for building height extraction in urban areas. *IEEE Geoscience and Remote Sensing Letters*, *12*(8), 1795–1799. doi:10.1109/LGRS.2015.2427738

Yu, B., Liu, H., Wu, J., Hu, Y., & Zhang, L. (2010). Automated derivation of urban building density information using airborne LiDAR data and object-based method. *Landscape and Urban Planning*, *98*(3–4), 210–219. doi:10.1016/j.landurbplan.2010.08.004

Yuan, F., Sawaya, K.E., Loeffelholz, B.C., & Bauer, M.E. (2005). Land cover classification and change analysis of the twin cities (Minnesota) metropolitan area by multitemporal Landsat remote sensing. *Remote Sensing of Environment*, *98*(2–3), 317–328. doi:10.1016/j.rse.2005.08.006

Zhou, W., & Troy, A. (2008). An object-oriented approach for analysing and characterizing urban landscape at the parcel level. *International Journal of Remote Sensing*, *29*(11), 3119–3135. doi:10.1080/01431160701469065

Zhou, Y., Parsons, B., Elliott, J.R., Barisin, I., & Walker, R. T. (2015). Assessing the ability of Pleiades stereo imagery to determine height changes in earthquakes: A case study for the El Mayor-Cucapah epicentral area. *Journal of Geophysical Research: Solid Earth*, *120*(12), 8793–8808.

Appendix A-2

remote sensing

MDPI

Article

Prediction of Socio-Economic Indicators for Urban Planning Using VHR Satellite Imagery and Spatial Analysis

Gebhard Warth [1,*], Andreas Braun [1], Oliver Assmann [2], Kevin Fleckenstein [2] and Volker Hochschild [1]

[1] Institute of Geography, University of Tübingen, Ruemelinstrasse 19-23, 72070 Tübingen, Germany; an.braun@uni-tuebingen.de (A.B.); volker.hochschild@uni-tuebingen.de (V.H.)

[2] AT-Association, Waldburgstrasse 96, 70563 Stuttgart, Germany; oliver.assmann@at-verband.de (O.A.); k.fleckenstein@stud.uni-heidelberg.de (K.F.)

* Correspondence: gebhard.warth@uni-tuebingen.de

Received: 22 April 2020; Accepted: 25 May 2020; Published: 28 May 2020

Abstract: Ongoing urbanization leads to steady growth of urban areas. In the case of highly dynamic change of municipalities, due to the rates of change, responsible administrations often are challenged or struggle with capturing present states of urban sites or accurately planning future urban development. An interest for urban planning lies on socio-economic conditions, as consumption and production of disposable goods are related to economic possibilities. Therefore, we developed an approach to generate relevant parameters for infrastructure planning by means of remote sensing and spatial analysis. In this study, the single building defines the spatial unit for the parameters. In the case city Belmopan (Belize), based on WorldView-1 data we manually define a city covering building dataset. Residential buildings are classified to eight building types which are locally adapted to Belmopan. A random forest (RF) classifier is trained with locally collected training data. Through household interviews focusing on household assets, income and educational level, a socio-economic point (SEP) scaling is defined, which correlates very well with the defined building typology. In order to assign socio-economic parameters to the single building, five socio-economic classes (SEC) are established based on SEP statistics for the building types. The RF building type classification resulted in high accuracies. Focusing on the three categories to describe residential socio-economic states allowed high correlations between the defined building and socio-economic points. Based on the SEP we projected a citywide residential socio-economic building classification to support supply and disposal infrastructure planning.

Keywords: VHR imagery; WorldView-1; PlanetScope; urban remote sensing; socio-economic information; urban planning indicators; Belmopan/Belize; spatial analysis

1. Introduction

During the present century urbanization will be one of the major challenges for society, politicians, and planners. Urbanization as a complex socio-economic process that transforms the built environment, converting formerly rural into urban settlements [1], has—besides all well-known challenging tasks—positive effects for society, such as economic growth, poverty reduction, and human development of urbanization [2]. "Urban areas also serve as hubs for development, where the proximity of commerce, government and transportation provide the infrastructure necessary for sharing knowledge and information. Urban dwellers are often younger, more literate and more highly educated, are more likely to have access to decent work, adequate housing and social services, and can

enjoy enhanced opportunities for cultural and political participation as well as gender equality" [2]. When urbanization progresses unguided, effects of inadequate planning are evident: unsustainable production and consumption patterns and impaired sustainability resulting from urban sprawl, pollution, and environmental degradation [1].

A basic challenge is the lack of capacity within public institutions to manage urbanization [1]. To guide and direct urbanization in order to achieve its potential positive effects and to enable implementing the sustainable development goals (SDG) proclaimed by the United Nations [3], paradigms for urban planning, therefore, need to be shifted towards transparent approaches of evidence-based planning [4]. Infrastructure planning should be considered as a core element in strategic spatial planning, based on the understanding of the underlying forces, which includes knowledge of the economic base amongst other things [5].

Socio-economic parameters can serve as indicators for both urban supply and disposal infrastructure planning. Knowledge of education and economic situations have importance relevant to household waste production in various regions [6–8], more precisely household income and household expenditures correlate accurately with household solid waste generation [9]. Jones (2015) shows in a review article [10] the influence of socio-economic criteria on the consumption of electricity with the household income as the main factor.

We see a growing potential regarding the use of remote sensing techniques to supply socio-economic information for planning urban supply and disposal infrastructure—a potential which has not been considered in present research as the following paragraphs show.

To characterize urbanization, first global datasets of urban expansion were established based on Landsat data [11] and optical nighttime imagery data [12]. The global urban footprint dataset was fully generated automatically based on TanDEM-X synthetic aperture radar (SAR) data [13,14]. Most recently, the world settlement footprint for the years 2012 and 2015 were generated by combining Sentinel-1 radar data and optical Landsat-8 data [15]. To increase the spatial resolution of the information and to retrieve qualitative information on the change that occurred between different acquisitions, Warth et al. proposed a method to retrieve information on dynamics in building stock on a single building scale by differencing urban digital surface models (DSM) [16]. Braun et al. [17] refined these results publishing a refined urban change dataset on single building scale for Da Nang, VN.

With the increasing availability of VHR remote sensing imagery, there is a need for techniques to detect objects as a spatial and radiometric product of multiple pixels. Object based image analysis (OBIA) techniques [18] have been used to detect single buildings [19,20]. Recent studies show the implementation of OBIA techniques for measuring urban ecosystem functionality [21,22] and indication of quality of life factors [23,24]. Foci on approaches for image-based object detection approaches have been shifted most recently towards machine learning (ML) methods [25]. The approaches were successfully implemented using VHR remote sensing imagery [25,26]. Regarding context based VHR image analysis in the urban context, a focus lies on mapping slums and informal settlements using ML techniques [27–29]. Zhu [30] gives an overview on the key developments regarding ML approaches in urban remote sensing. As a recent example, morphological descriptions of neighborhoods retrieved by VHR images and spatial distance measures have been successfully applied to predict property values in other cases [31].

Three-dimensional data derived by photogrammetric approaches [32] supports the physical description of building stock analysis and detecting changes in building stock [16,33]. Light Detection and Ranging (LiDAR) approaches using the propagation of light [34] in the urban context have advantages in vegetation related studies and therefore are applied for tree species detection [35], urban forest mapping [36], volume estimation [37], and urban ecosystem service (ESs) modelling [38].

Besides the application of SAR data for generating global settlement data and mapping of impervious surfaces [39], radar technology the ability to detect changes in elevation offered by processing of the phase information [40]. The increased availability of Sentinel-1 time series data [41] enables implementing Persistent Scatterer Interferometry (PSI) to precisely monitor surface deformation

processes [42]. Besides analyzing subsidence as an effect of ground water extraction [43–45], subsidence could be correlated to construction projects [46–48] by PSI technique. SAR tomography approaches [49] are performed in the urban context with Sentinel-1 [50,51] and TanDEM-X data [52]. Interferometric SAR products have been proven to enable the detection of urban flood extension [53].

To support urban planning on a city level, information related to function and context is required. In this regard, Kuffer worked on the mapping of slum areas [54,55], ML based approaches have been performed as well [27–29]. Socio-economic parameters as planning relevant indicators have been derived by Jensen [56], where population and quality-of-life-indices were estimated by means of VHR imagery. Approaches using Landsat-5 TM data were described by Lo [57]. Urban vegetation is an indicator for socio-economic rating [58]. In this context, urban mapping and planning can benefit from ESs mapping that helps indicating urban quality factors and urban climate [59,60].

Socio-economic data gathering and analyzing methods that use socio-economic indices to determine the relative socio-economic status of individuals or households in a sample group have been applied with different purposes in various scientific fields. Important areas of research include medical and epidemiological studies [61,62], educational studies [63], or the measuring of inequality in living standards [64] or health [65]. The research focus in these studies lies in the evaluation of the correlation between the socio-economic status and health conditions [66–68]. With the help of criteria like educational level, occupation, and income the influence of the socio-economic status on health and life expectancy of an individual is examined [69].

The goals of urban planning must be to guide and to manage the dynamics of municipalities which are caused by many factors, such as persistent urbanization amongst other things. Successfully implemented urban planning enables citizens to obtain benefit from the advantages of urbanization, like "access to education, health care and housing, to increase their productivity and to expand opportunity" [70] and enables the realization of the SDGs [3]. Therefore, decision makers need to adopt strategies towards planning future urban growth [70]. Knowledge on present states and dynamics of the urban complex is decisive to plan the future development of a city and its surroundings. In the case of rapidly growing urban agglomerations, it is challenging to capture current dynamics because of the rate of change and the inertia of many data gathering methods.

With this study we follow up previous work of designing a development plan for green and blue infrastructure for Belmopan [71]. Belmopan is a small capital city with 23,038 inhabitants [72] and can be used as a practical example considering, as Cohen and Barney predict, a majority of urban dwellers will be living in small cities (<100,000 inhabitants) [2]. Special focus needs to be applied on such cities, because these municipalities often lack basic services such as piped water, flush toilets, and electricity [2]. In Latin America and Caribbean region, where the study area of this research is located, waste production is expected to increase by one third by 2050 as compared to 2016 and 58% of waste ends up in landfills and open dump sites [73], which causes negative environmental effects.

To establish methods of evidence-based planning and therefore to reduce the gap of data and knowledge, we propose an approach to support planning of residential supply and disposal infrastructure by predicting socio-economic information at the scale of residential buildings using very high-resolution (VHR) remote sensing imagery. VHR optical remote sensing systems, such as the WorldView or Pléiades satellites, deliver imagery at sub-meter resolution, which allows the precise detection of buildings with high temporal flexibility. The access to VHR imagery is improved and the constant data availability is being established [74,75]. A lot of research has been carried out to describe and prove the relationships between consumption of energy and waste production via socio-economic indicators. The influence of the socio-economic status (SES) on the urban metabolism—in terms of material and energy flows generated by households—at the level of individual buildings has not yet been researched in this way. As a new scientific issue, the correlation of different socio-economic states—along with potentially differing consumption and generation patterns—to varying building types is researched within this study. The purpose being to derive relevant values for a well-founded planning of supply and disposal infrastructure. In the context of planning appropriate supply and

disposal infrastructure in dynamic environments this correlation might be very important and should be considered with respect to the building of a reliable database.

To put these findings in effect when planning, remote sensing data sources should be implemented to support planning processes, in addition to reasons of objectivity and time efficiency, qualitative and quantitative information relevant for planning can be gathered region-wide.

2. Materials and Methods

2.1. Study Area and Data

2.1.1. Study Area

While still a British Colony known as British Honduras, the study city of Belmopan was inaugurated in 1970 as the new capital city [76]. The maps in Figure 1 give an overview on Belmopan's location. Due to its geographical location, the former capital Belize City was repeatedly threatened by hurricanes, the last major hurricane named Hattie hit Belize city and the Belize district in 1961 destroying approximately 80% of the city [76,77].

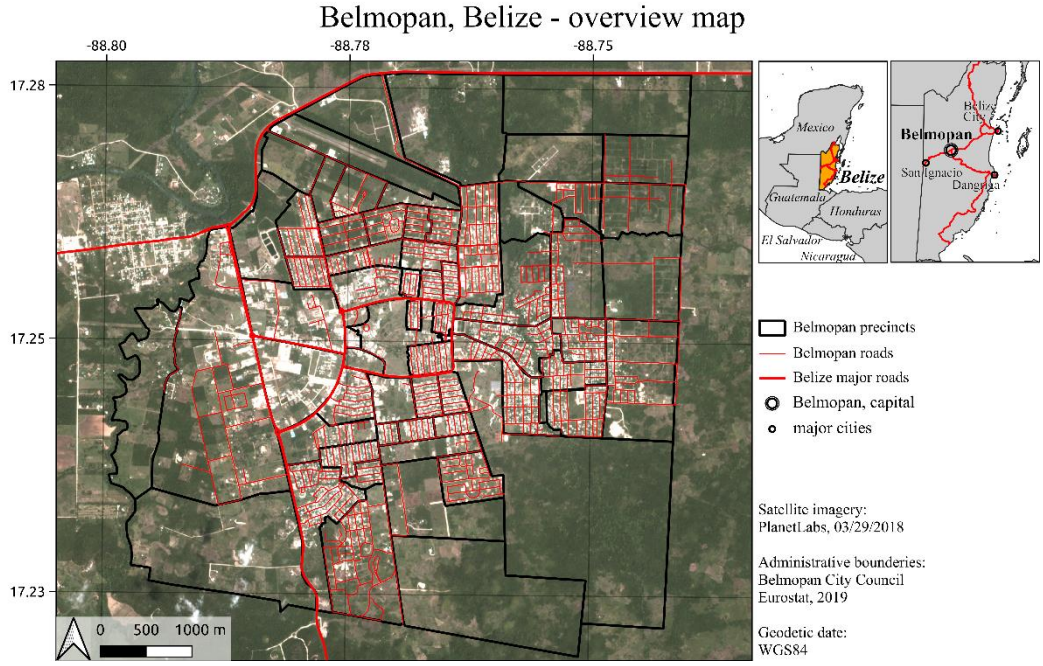

Figure 1. General map of Belmopan and its regional geographical situation.

Besides causing human losses and physical damage, the hurricanes interrupted governmental work and destroyed governmental documents, as well [76]. In addition to reduction of risk of natural hazards, which was the main reason for the relocation of the capital, the dominant and authoritative position of Belize City in the country was reduced by the inauguration of the new capital city of Belmopan [76]. The decision on the location for the new capital was based on the following main criteria: (1) a potable water supply, (2) safety from flooding, (3) its location at the hub of national transportation network and (4) equidistance from the two largest coastal centers of Belize City and Stann Creek [76]. The city name of Belmopan was inspired by the confluence of the Belize river and Mopan river. Administrative data indicate an area of 32.25 km^2 covered by the Belmopan administrative boundaries.

In 2018 Belize had a population of 398,050 inhabitants, whereas 23,038 people lived in Belmopan [72]. In comparison to global and regional urbanization rate, Belize is estimated to be experiencing above-average urbanization [1], as it is shown in a global and regional comparison in Figure 2.

The Belmopan annual population growth rate is estimated at 5.7% [78]. These dynamics underline the necessity for standardized urban mapping at regular intervals.

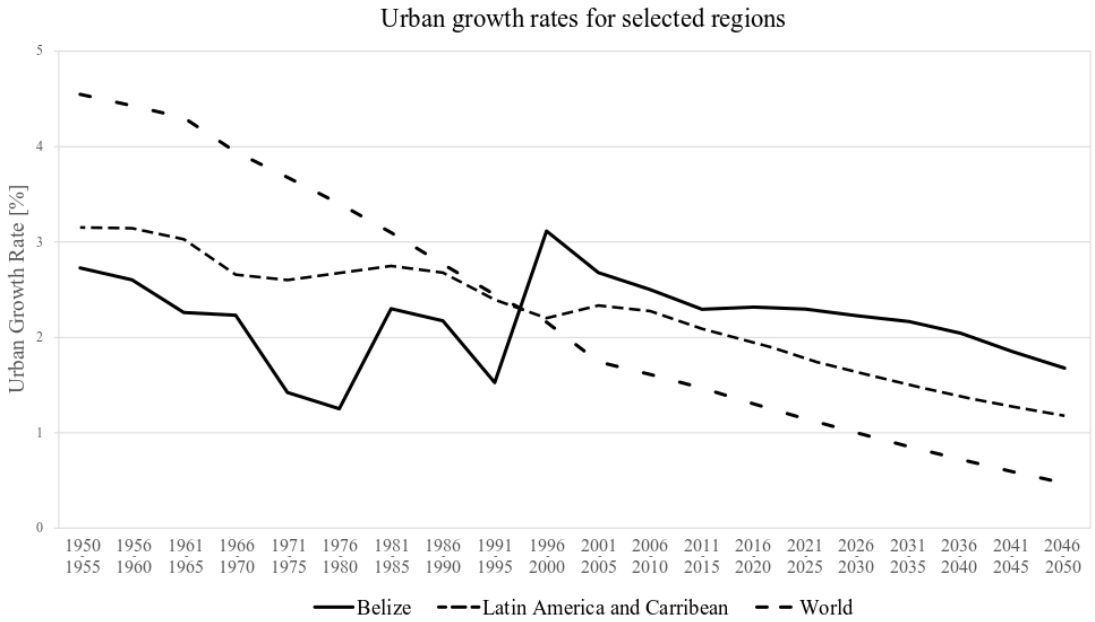

Figure 2. Comparison of measured and prospected urban growth rates for Belize, the Latin America and Caribbean region and the World as based on UN data [1].

2.1.2. VHR Imagery

The WorldView-1 (WV-1) satellite, launched in 2007, offers stereo imagery, which is achieved by a single pass bi-directional acquisition mode. At nadir, the panchromatic band has a ground sampling distance of 0.5 m [79]. In this research two stereo image scenes were used acquired on 2018/03/16 and on 2018/03/29, respectively, as shown in Table 1, in order to achieve high quality results the datasets cover 28.04 km^2 of the Belmopan administrative area. A total of 13.1% of the administrative area not covered by the WV-1 imagery is undeveloped. For the imagery data radial polynomial coefficients (RPC) are delivered by the imagery provider. The first scene has a share of cloud-covered areas of 6.3%, affected areas lie partly above built-up zones. For details on WV-1 imagery and acquisition please refer to Table 1.

Table 1. Overview on WorldView-1 acquisitions used.

	WorldView-1 Stereo Pair 1	**WorldView-1 Stereo Pair 2**	**PlanetScope Two Frames**
Acquisition date	2018/03/16	2018/03/29	2018/03/29
Ground sampling distance	0.5 m	0.5 m	3.0 m
In track view angles	−24.3°, 15.3°	−9.4°, 29.9°	0.1°, 0.12°
Cloud coverage	6.3%	0.2%	0%

2.1.3. HR Imagery

PlanetScope data were chosen to get access to multispectral imagery [80]. Images acquired on 2018/03/29 were selected to achieve minimum cloud coverage and identical image contents in comparison with the WV-1 imagery described in Section 2.1.1. PlanetScope operates in a sun synchronous orbit with a four-band frame imager. The visual spectrum is captured by the blue (455–515 nm), green (500–590 nm), and red (590–670 nm) channels at a ground sampling distance of 3 m. The near infrared spectrum is captured at 780–860 nm [81]. The PlanetScope imagery is delivered radiometrically preprocessed in surface reflectance values. In the imaging mode as used,

a PlanetScope scene covers 180 km^2, but the entire urban area of Belmopan was not covered in a single scene. Therefore, two scenes were used for the analyses. Figure 3 gives an overview on the used satellite imagery.

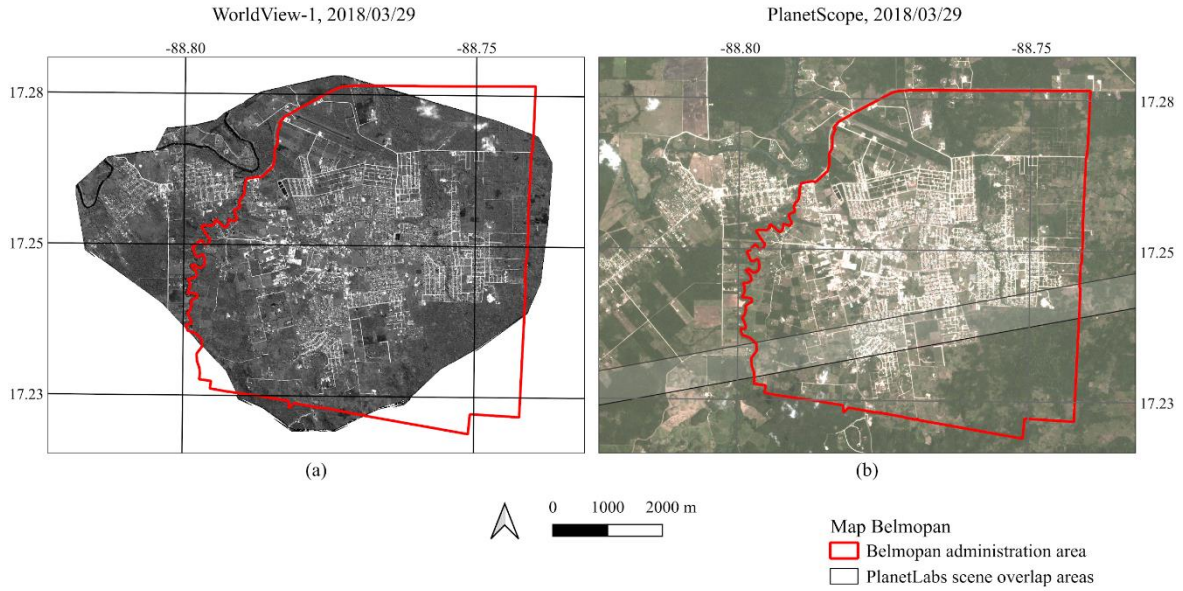

Figure 3. Overview of satellite imagery used for the study. The red polygon shows the Belmopan city boundary. (**a**) WorldView-1 image covering the developed areas of Belmopan. (**b**) PlanetScope images fully covering Belmopan.

2.1.4. Ground Truthing Data

A questionnaire-based survey using the mobile KoboCollect tool [82] was performed to collect ground truthing data for the building type classification. During two field campaigns in January and March 2019 datasets with a total sample size of 405 building were collected. Each building was assigned to the building types defined in Section 2.2.4. Additionally, information on the number of stories, mean roof height, roof type, and parcel-related information describing accessibility and vegetation share were collected. Building height information was measured with a *Bosch GLM 50C* handheld laser measurement device. Locations of the buildings surveyed were recorded with handheld GPS devices and manually location corrected-based on the WorldView-1 imagery in a geographical information system (GIS) (see Section 2.1.2.).

2.1.5. Auxiliary Data

Auxiliary data on non-residential building use was collected during the field campaigns. Non-residential building use was sub-classified into business, public sector, and industry. The non-residential buildings were collected by GPS measurements as point information and position corrected based on the WorldView-1 image. The collected building-use information was added with information on business, public sector (administration, education, health institutions), and industry based on OpenStreetmap (OSM) [83] and Google registrations. Data on the official plan of land use, administrative boundaries (sectors, precincts, and parcels), as well as on the road network and public transportation infrastructure were provided by the city council of Belmopan as vector geometries.

2.1.6. Socio-Economic Interviews

For gathering socio-economic data and information on household level in Belmopan an interview-based survey was designed and carried out in March and April 2019. KoboCollect was used as described in Section 2.1.4. According to the six main representative building types

determined for Belmopan and their detected shares/spatial concentration in the city (Section 2.2.5), test areas were defined for the implementation of the socio-economic survey. Building types 23 and 24 (see Section 2.2.4) do not occur in statistically sufficient numbers in Belmopan. Within the test areas a total of 425 households were surveyed by means of digital questionnaires with about 210 questions on the main subject areas:

- housing and infrastructure (type and devices of the house);
- specific information on the household (size, age structure, occupation, education, etc.);
- items, features and devices (assets) owned by the household;
- expenditures (on housing, food, health, etc.) of the household;
- food and buying habits of the household;
- income (amount, sources) of the household.

2.2. Methods

Our proposed methodology predicts socio-economic measures on a single building scale, Figure 4 schematically shows the single steps of the approach. Basing on VHR remote sensing imagery, single buildings are detected. Supported by local ground truthing information, building types are classified. Through statistical analysis of resident's interviews, a relationship between building types and socio-economic groups can be established. Detailed information on the methodology is given in the following sections.

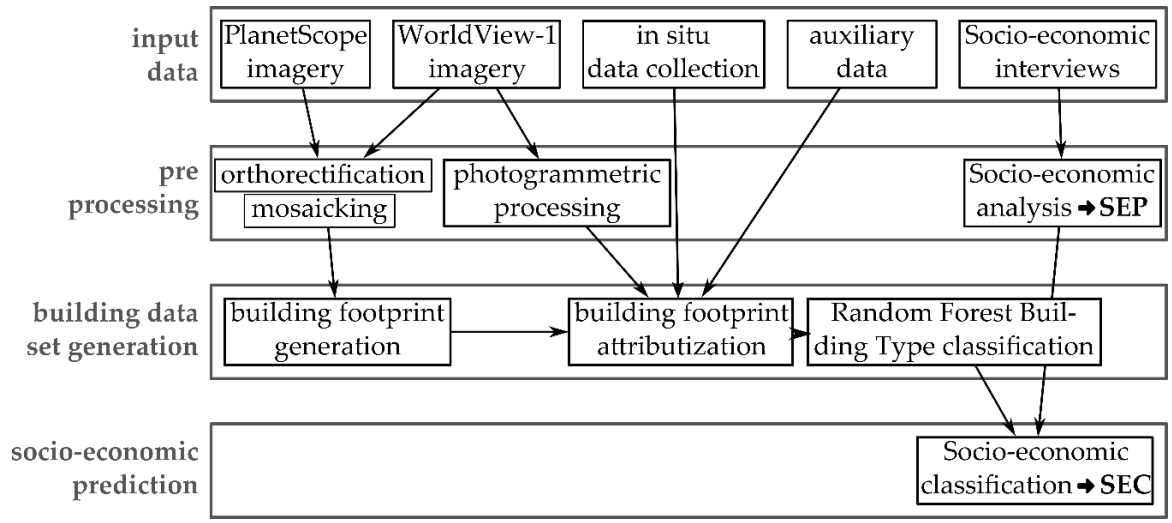

Figure 4. Schematic overview of the approach. Socio-economic analysis leads to the "socio-economic points" (SEP) ranking (see Section 2.2.6. and Section 3.3.). The prediction of socio-economic status bases on building types via socio-economic classes (SEC) (see Section 2.2.7. and Section 3.4.).

2.2.1. VHR Image Processing

In order to orthorectify WV-1 imagery for generating the building dataset and to derive building heights, the WV-1 data described in Section 2.1.1, were processed photogrammetrically. To increase the quality in urban areas, two stereo pairs were chosen to achieve a fourfold coverage. The off-nadir angles are clearly differentiated, as shown in Table 1, and therefore the usage of four input images increase the quality of the resulting elevation dataset.

For the photogrammetric processing, the EATE approach in ERDAS Imagine [84] was chosen, as already implemented by Bachofer and Warth [16,33].

The main elevation dataset was calculated with all four WV-1 images. To replace cloud affected pixels, a substitute elevation dataset was calculated based on the cloud free image pair.

For cloud-covered pixels, elevation information of the main dataset was substituted with elevation data from the alternative elevation dataset. In addition to this, the fourfold coverage reduces the impact of the cloud coverage on small parts.

In order to determine building heights from WV-1 height information, a normalized DSM (nDSM) was calculated. A digital terrain model (DTM) was generated based on the WV-1 DSM. Therefore, building heights were removed by means of building footprints (see Section 2.2.2) and heights affected by tree or forest were removed as well via threshold based NDVI (see Section 2.2.3) masking using PlanetScope imagery. The resulting gaps in the DSM were closed by applying spline interpolation. Differencing DSM and DTM gives the nDSM, which contains height information on buildings, trees, and other non-ground objects.

2.2.2. Delineation of Building Footprints

On the base of the orthorectified WV-1 scene from 2019/03/29, the building dataset was generated. With an HPF multi-resolution approach the orthorectified PlanetScope scene was pansharpened using the panchromatic WV-1 scene to combine the very high spatial resolution of the panchromatic channel with the multispectral information delivered in the PlanetScope scene. The orthorectified scene is the correctly positioned main basis for the manually observed building detection. In cases of indistinct building outline, the unrectified WV-1 scene without distortions caused by the orthorectification was used as reference. To digitize building footprints the Java-OpenStreetMap-Editor (JOSM) [85] was used for reasons of simple digitization and attributization routines and the intended publishing of the building dataset on the OpenStreetmap server.

2.2.3. HR Image Processing

As two acquisitions are necessary for full coverage of the Belmopan city, both PlanetScope scenes were mosaicked. No preprocessing before the mosaicking was necessary due to the data delivery already being surface reflectance. The orthorectification process for multispectral PlanetScope imagery was performed by an RPC based approach implemented in ERDAS Imagine. Data on RPC for the PlanetScope imagery was delivered by the data provider. The WV-1 DSM, described in Section 2.2.1, was used as very high-resolution elevation data input.

Based on the orthorectified multispectral imagery, the normalized difference vegetation index (NDVI) was calculated to delineate vegetated areas. Studies [60,86] have proven that NDVI based tree detection approaches deliver practicable results in urban environments. Applied to PlanetScope imagery, the NDVI is derived as follows:

$$\mathrm{NDVI}_{\mathrm{PlanetScope}} = \frac{\mathit{PlanetScope\ Band\ 4} - \mathit{PlanetScope\ Band\ 3}}{\mathit{PlanetScope\ Band\ 4} + \mathit{PlanetScope\ Band\ 3}}, \quad (1)$$

For the generation of the normalized DSM which represents object heights, a tree mask must be calculated to distinguish between trees and ground level areas. Observations during the field campaigns have shown, that grass is very low in Belmopan and therefore can be interpreted as ground elevation in the DSM. To separate between ground and tree covered areas, a histogram-based threshold-based approach was chosen. In the histogram a local minimum value between the NDVI values of tree covered areas and non-tree covered areas represents the threshold to create the tree mask. Based on the PlanetScope scene acquired on 2018/03/29, the NDVI threshold is 0.21.

2.2.4. Definition of Building Typology

The prediction of socio-economic status bases on building type information. Therefore, the method aims to propose a global definition for residential building types. This study focusses on the prediction of socio-economic indicators on residential buildings, as other building functions cannot be derived solely based on remote sensing information. In this regard, we defined eight residential building types

(BT), which are denominated by numbers and neutral designations, in order to avoid preconceptions of its residents and surrounding neighborhoods. Buildings types 11–14 represent single family buildings, whereas building types 21–24 represent multifamily buildings. We define the term "Multi-Family Building" as a building with two or more residential units, as already suggested by Vetter-Gindele et al. [87]. The proposed building types are defined by construction materials used and the physical structure of the buildings and have no significance over the building condition or building maintenance. For building type nominations see Table 2.

Table 2. Building types with respective nomination.

Building Type	Nomination	Building Type	Nomination
BT 11	Single Family Basic	BT 21	Multi-Family Basic
BT 12	Single Family Standard	BT 22	Multi-Family Standard
BT 13	Single Family Advanced	BT 23	Multi-Family Apartment
BT 14	Single Family Complex	BT 24	Multi-Family Modern Apartment

Due to cultural and historical influence, building types differ worldwide and therefore must be adapted to local building structures. For Belmopan we assigned the buildings to the building typology as follows.

Buildings with one dwelling unit were assigned from BT 11 to BT 14. The main criteria for the assignment of BT 11 is the use of natural construction materials. BT 12 is characterized by four corners, rectangular building footprint and gabled or shed roof types. BT 13 can be similar to BT 12, but shows deviations from the rectangular footprint. Additional stories can also exist, but not full stories. Buildings with multiple full stories are assigned to BT 14, as well as buildings with complex footprints and complex roof structures.

BT 21 is the only Multi-Family Building type with two dwelling units at a single floor building structure. It is usually characterized by gabled or shed roofs and, therefore, can only be structurally differentiated from BT 12/13 by increased footprint area. In Belmopan, BT 22 is characterized by a simple rectangular footprint. Usually these buildings enclose two dwelling units on two stories. BT 23 contains multiple apartments; the increased footprint area allows multiple apartments per story. The number of stories can exceed two. BT 24 is a modern multifamily apartment, which is constructed by modern materials and highly equipped with modern technical devices. It shows complex footprints and roof structures. Table 3 and Figure 5 give an overview on the building typology for Belmopan.

Table 3. Building typology for Belmopan, criteria to visual on-site differentiation.

Criteria	BT 11	BT 12	BT 13	BT 14
Denomination	Single Family Basic	Single Family Standard	Single Family Advanced	Single Family Complex
Building footprint characteristics	Any	Rectangular	Rectangular with extensions	Complex
Roof characteristics	Any	Rectangular/gabled roof	Cross gabled roof	Complex roof
Construction material	Natural	Concrete	Concrete	Concrete
Number of stories	1	1	>1	>1.5
Criteria	**BT 21**	**BT 22**	**BT 23**	**BT 24**
Denomination	Multi-Family Basic	Multi-Family Standard	Multi-Family Apartment	Multi-Family Modern
Building footprint complexity	Rectangular	Rectangular	Rectangular	Complex
Roof complexity	Rectangular, gabled/shed roof	Flat, rectangular	Flat, rectangular	Complex
Construction material	Concrete	Concrete	Concrete	Concrete
Number of stories	1	2	>2	>2

Figure 5. The proposed building typology adapted to the case city Belmopan, Belize. Upper row representing single family buildings, lower representing multi-family buildings. Image sources Building Type 23: [88].

2.2.5. Classification of Building Types

The classification of building types was conducted in two steps. First a supervised classification was conducted based on the reference classes collected during the field survey (Section 2.1.4.). Of the 405 collected buildings, 363 were identified as residential and used for the training. A variety of attributes were computed per building polygon that served as explanatory features for the prediction:

- Geometry features (n = 6): area; perimeter; number of corners; shape ratio (area/perimeter); shape index [89]; average height (Section 2.2.1.).
- Distance features (Euclidean, n = 8): roads; paved roads; bus lines; parcels of land use commercial; parcels of land use education; parcels of land use green spaces; parcels of land use industry; parcels of land use public.
- Density features (n = 5): average building density within a radius of 150 and 250 m; absolute number of buildings within 50, 100, and 200 m.
- Land use features (according to the official plan provided by the city council, n = 2). 10 parcel classes: agriculture, commercial, education, green space, industrial, mixed use, public/institutional, residential, utilities, vacant. Four sector classes: built-up, developing, vacant/agriculture/forest, university.
- Spectral features (average per polygon, n = 4): HR red; HR green; HR blue; HR infrared.

These 25 features were used for the training of a random forest classifier, an algorithm originating from machine learning, which repeatedly uses subsets of the training data and explanatory features to calculate classification trees based on variable thresholding [90]. In our case, 1500 trees were computed based on five randomly selected features and 236 randomly selected building types for training (subset of 65%). In the end, a final classification is retrieved for each building based on the majority class of all 1500 iterations.

This resulted in a classification of all buildings in the city. Of course, buildings which were attributed as public, commercial, industrial, or uninhabited based on the field survey or data from OpenStreetMap and Google Maps were not assigned a residential building type.

2.2.6. Processing of Socio-Economic Data

The key assumption underlying our approach of gathering relevant data for supply and disposal infrastructure planning is that different socio-economic groups of households living in different

building types have different habits and lifestyles, which in turn result in different material and energy flows. In order to prove this correlation, the different socio-economic states of the households in Belmopan had to be determined and classified before assigning them to different building types.

All 425 interviews were checked for plausibility. In the case of unrealistic replies and insufficient numbers of replies for statistical categorization, such related questionnaires were not considered. A total of 395 out of the 425 socio-economic datasets surveyed in Belmopan proved to be statistically reliable after initial analyses. In order to determine the socio-economic status of the surveyed households as relative position in the sample groups, a multidimensional approach was developed. Similar to the "Social Class Index" applied in a German health survey [91], the socio-economic index developed within this current study is based on three categories of questions and their respective answers. On the basis of the socio-economic data gathered in Belmopan the categories which proved to be appropriate for creating the relevant index were:

1. Expenditures.
2. Educational level.
3. Household assets (owned items).

Expenditures was chosen as the first category because answers involving questions on expenditures in an interview-based survey are usually more reliable than those on income [92]. The OECD equivalence square root scale was used to take differences in household sizes and nonlinearities with respect to growing household sizes and related expenditures into account [93]. The educational level was integrated in the index with six different characteristics. Following the "Udai Pareek Scale" developed to examine the socio-economic status of rural population in India by Singh (2017) [92], the third category focusses on the different assets (owned items) of the household. This allows contemplating the financial situation of a household in a long-term perspective.

The six different educational levels ascertained for Belmopan, ranging between "no graduation (category 1)" and "Master/or higher (category 6)", determined the main structure of the six classes in each category of the socio-economic index which was developed via this context. Following this structure, the total expenditures of the households were grouped into six classes of equal size. Likewise, the household assets (owned items) queried with binary questions were divided into six classes to fit into this structure.

In order to determine the socio-economic status of a surveyed household, and so to make it comparable, points were assigned to the six classes in the three primary categories, thus forming a point scheme ranging from 3 to 18 socio-economic points. As a result, a generated proxy variable within this scheme with a value of 3 determines the lowest and with a value of 18 the highest socio-economic status (SES) of a household.

2.2.7. Classification and Prediction of Socio-Economic Data

Related to the building types, socio-economic projections can be assigned to the single buildings, as described in the previous section. To avoid the impression of precision of the 15-point scale (3–18), and a source of errors in the prediction of socio-economy, socio-economic points are aggregated into socio-economic classes (SEC). Besides reducing errors in predicting socio-economic information, it can be critical to publish detailed sensitive information regarding resident's socio-economic status at a single building level. Creating classes helps avoid the possibility of instrumentalizing the results so to marginalize and expose residents of single buildings. Therefore, because different building types can host dwellers of similar socio-economic status, there is no reason to define an identical number of SEC as building types. The determining criterion for the number of SEC must be the statistical similarity of SEP.

Furthermore, as land value varies depending on the location and distance from places of urban activity, the necessity to subdivide building types based on spatial and location-based information may be identified. Studies have shown that the highest land values are to be expected in the city

centers and central business districts [31,94]. Without local expertise it is hardly possible to define a city center, to which the land value development is related and to access the key influences on value generation. Therefore, for this purpose, besides interviewing local experts [95] we created a set of quality of life indicators [56,57] by means of geo-spatial attributes to test the process of building types subdivision. The distance US Embassy located in Belmopan hereby was considered as quality of life indicator because the security service regularly patrols the surrounding neighborhood, which leads to higher security and due to this causes higher land values. Our selection results in the following quality of life indicators:

- distance to main roads (ring road)
- distance to administrative center (city administration);
- distance to places of education;
- distance to market center (market square);
- distance to US Embassy;
- building density;
- vegetation density.

Correlating the above geo-spatial attributes to building types with high variation in socio-economical description enables determining a threshold to divide a building type in the subclasses "near" and "far", e.g., building type "12 near" and building type "12 far". The subdivision "near" represents spatial proximity to city center, "far" represents buildings relatively distant to the city center.

3. Results

3.1. Building Detection

Following the goal to give free access to the building footprints via the OSM database, the already existing buildings had to be adjusted to the 2018/03/29 WV-1 acquisition. The standard base image on OSM was acquired between 2008 and 2010. This could be verified via the water treatment plant being under construction in the base image, which was under construction in the stated period. Therefore approximately 1500 pre-existing buildings were adjusted to their correct location by means of the orthorectified WV-1 scene and their building footprints updated accordingly. Buildings which were generated on the previous scene, which are no longer present in the recent acquisition, were removed for the present state of the database.

Based on this initial building footprint adaption the remaining buildings were digitized. At the time the WV-1 image was acquired on 2019/03/29 we detected a total number of 6627 buildings.

3.2. Building Type Classification

The initial trainings accuracy of the random forest classifier was comparably low: 56.7%. This is because there was considerable class overlap between the building types Single Family Basic, Standard, and advanced, as well as between Single Family Standard and Multi-Family Standard as shown in Table 4. Accordingly, user's and producer's accuracies are largely below 60%. To reduce this overlap, the created building type classifications were refined through logical expressions based on the criteria presented in Table 3 and statistical evaluation of critical thresholds. For instance, any building which was classified as Single Family (BT1x) but has a size below 30 m^2 will be reclassified to "uninhabited". Hereby to reclassify building types, the building height is an important building attribute. A set of 249 building measurements was measured in situ to verify the building heights derived by the WV-1 nDSM. The accuracy analysis revealed a root mean square error (RSME) of 1.23 (measurement unit: meters), which indicates good quality of the determined building heights. A chart containing information in this respect is shown in Appendix A. The full list of the applied rules is shown in Appendix B.

Table 4. Error matrix of building types after the random forest classification.

		Classified								∑	PA
		BT11	BT12	BT13	BT14	BT21	BT22	BT23	BT24		
real	BT11	**18**	20	1	0	0	0	0	0	39	46.2
	BT12	4	105	21	0	2	1	0	0	133	78.9
	BT13	0	33	48	3	1	1	1	0	87	55.2
	BT14	1	2	15	18	2	3	2	0	43	41.9
	BT21	1	6	6	2	4	1	0	0	20	20.0
	BT22	0	9	3	7	0	5	2	0	26	19.2
	BT23	0	0	2	3	0	1	8	0	15	57.1
	BT24	0	1	0	0	0	0	0	0	1	0.0
∑		24	176	96	33	9	12	13	0	363	
UA		75.0	59.7	50.0	54.5	44.4	41.7	61.5	0.0		**56.7**

BT = building type (Figure 2), PA = producer's accuracy in %, UA = user's accuracy in %.

After the application of the refinement rules, the overall classification accuracy increased to 86.8% with user's and producer's accuracies over 75% for most of the classes (Table 5). However, even with a manual refinement of the classes, a small class overlap could not be eliminated, especially between Single Family Standard (BT12) and Multi-Family Basic (BT21), as they are both characterized by one story and small to medium size. The table also shows that the Multi-Family Standard (BT22) has the lowest of all accuracies and is therefore probably underestimated in the prediction (only 43.8% producer's accuracy). However, based on its comparably low occurrence in Belmopan, this error is tolerable at the cost of high accuracies in the single family buildings. The same applies for Multi-Family Modern Apartment (BT24) which was not predicted by the classifier at all because of its low frequency in the training data (n = 1).

Table 5. Classification matrix of building types after the random forest classification.

		Classified								∑	PA
		BT11	BT12	BT13	BT14	BT21	BT22	BT23	BT24		
real	BT11	**32**	20	1	0	0	0	0	0	35	91.4
	BT12	4	**147**	3	0	0	1	0	0	155	94.8
	BT13	0	2	**84**	3	0	1	1	0	91	92.3
	BT14	1	2	2	**25**	1	1	0	0	32	78.1
	BT21	1	4	1	2	**10**	1	0	0	19	52.6
	BT22	0	2	3	2	0	**7**	2	0	16	43.8
	BT23	0	0	2	2	0	1	**10**	0	14	71.4
	BT24	0	1	0	0	0	0	0	0	1	0.0
∑		38	160	96	33	9	12	13	0	363	
UA		84.2	91.9	87.5	75.8	88.9	58.3	76.9	0.0		**86.8**

BT = building type (Figure 2), PA = producer's accuracy in %, UA = user's accuracy in %.

After the assignment of new classes all 6627 building footprints were classified as demonstrated in Table 6, with Single Family Standard as the most frequent class (46%). A total of 760 buildings were assigned to a primary non-residential use (public, commercial, industrial, uninhabited) based on the field survey and data from OpenStreetMap and Google Maps. It is however likely that there are even more non-residential buildings within the city which can be excluded from the socio-economic analyses. Building type 24 is present in Belmopan with minimal numbers. Therefore, it is challenging to characterize this building type in the training dataset with one sample. During data collection campaigns, the focus has solely been laid on residential building information. This leads especially to an underrepresentation of industrial used buildings, but as well other uses such as commerce, as a complete database for non-residential building use is not publicly available. Generally, single family buildings are classified more accurately than multi-family buildings. As dwelling numbers cannot be determined by remote sensing imagery, proxies such as building height must be applied. Even with a

very high spatial resolution of 0.5 m, the building heights derived by WV-1 can contain variations due to roof-covering vegetation, and other influences and therefore can lead to misclassification. The map in Figure 6 gives an overview on the building type classification in Belmopan.

Table 6. Building type information in Belmopan.

Building Type	Number of Buildings	Share of Total Number
11—Single Family Basic	764	11.5%
12—Single Family Standard	3060	46.2%
13—Single Family Advanced	1211	18.3%
14—Single Family Complex	566	8.6%
21—Multi-Family Basic	33	0.5%
22—Multi-Family Standard	138	2.0%
23—Multi-Family Apartment	94	1.4%
24—Multi-Family Modern Apartment	1	<0.1%
Public	166	2.5%
Commercial	219	3.3%
Industrial	6	<0.1%
Uninhabited	369	5.5%
Total	6627	100%

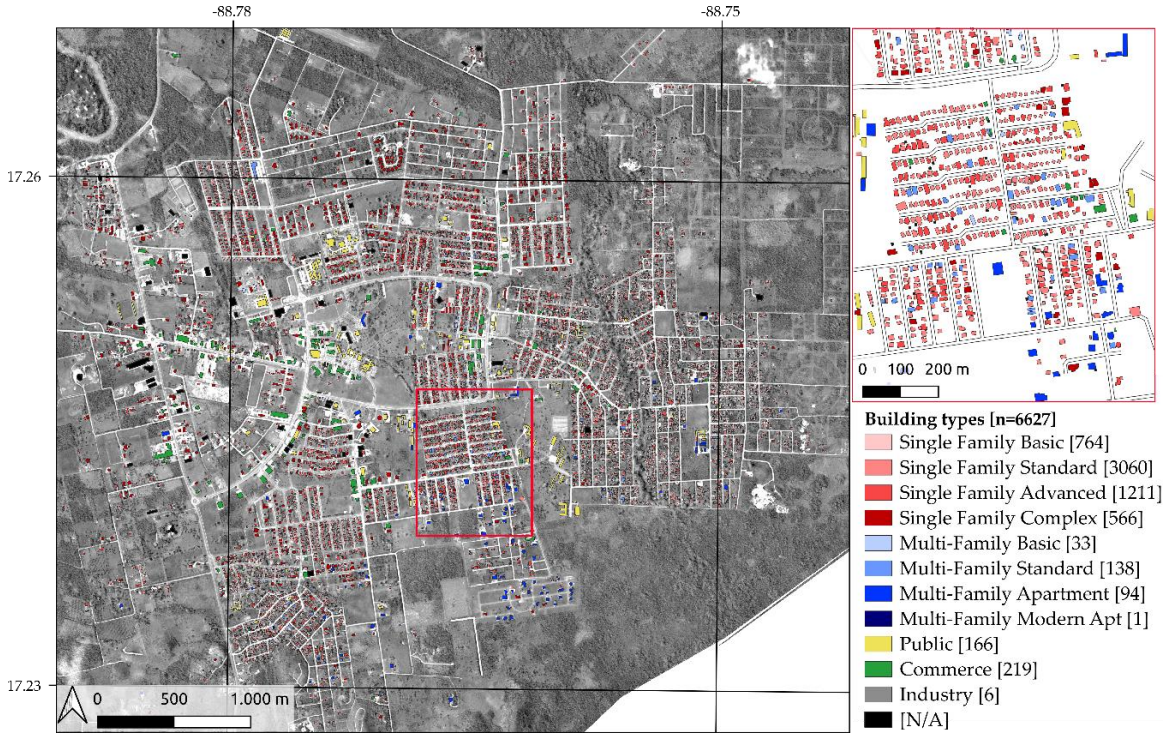

Figure 6. Map of detected buildings and classified building types in Belmopan (date: 2019/03/18). Total number of detected buildings: 6627. Manual assignment "Public", "Commerce", "Industry" on best knowledge. Background: PlanetLabs, 2018/03/18.; Stamen Design, Data by OpenStreetMap.

3.3. Socio-Economic Points Determination

The mean expenditures—normalized by the square root of the household size (corresponding to OECD recommendation [93])—of the investigated households amount to 1320 BZD per month ranging from less than 600 BZD for the lower 25% of households to more than 1450 BZD per month for the upper 25%. The median expenditures were 930 BZD per month. As can be seen in Figure 5, roughly half of the monthly expenditures are on food (27%) and housing including additional costs

(22%). Other major spending factors are medical care (16%) which include medicine, doctor's visits and health insurance, and mobility (15%).

As a second category of the socio-economic index, items owned by the households (assets) were considered. Within this category various items and features were queried, of which 24 selected assets were determined to be included into the index. Figure 7b shows these 24 main assets and the percentage of households that own them. As one can see, there are some assets that the majority of the surveyed households own like a stove (98%) or an electric fan (95%) but also assets that are relatively rare like a dishwasher (13%) or a generator (5%).

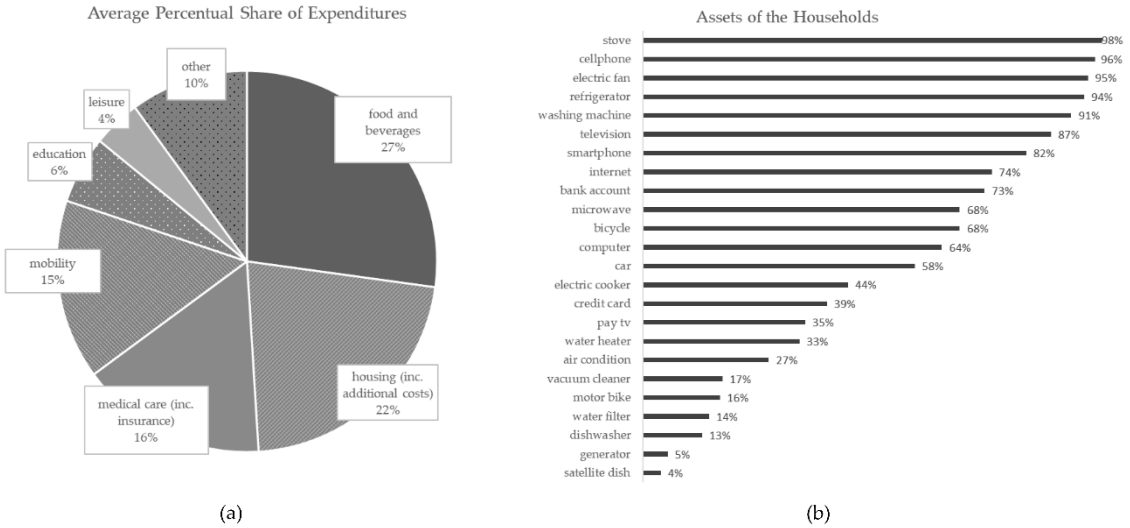

Figure 7. Percentage share of household expenditures (**a**) and household assets (**b**) in Belmopan (n = 395 interviews).

The third category considers educational degrees. With the "associate's degree" as the first university degree in Belize, six different educational levels were identified for Belmopan ranging from no school graduation (educational class 1) to master's degree or higher (educational class 6). Figure 8 shows the shares of the educational levels of the main income earners of the households in the surveyed areas. About a quarter of the main income earners in the interviewed households have only primary school graduation (17%) or no school graduation at all (10%), in contrast to the 45% that hold a university degree (associate's degree 17%, 18% bachelor's degree, 10% master's degree or higher). Figure 8 gives an overview on the educational degrees of the main income earners in Belmopan.

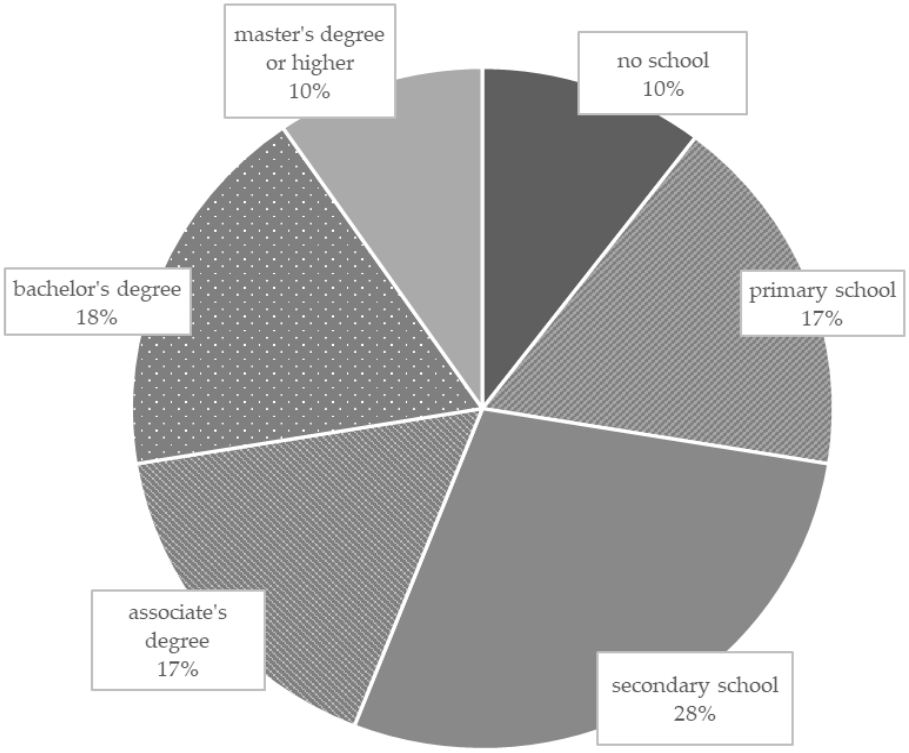

Figure 8. Educational degree for main income earner in Belmopan (n = 395 interviews).

Based on the developed socio-economic index (see Section 2.2.6.) the socio-economic points (SEP) were derived by the results of the three categories. The average socio-economic points of the 395 investigated households is 10.5. The distribution of the SEPs is shown in Figure 9. Appendix C provides a summary of the composition of SEP based on the three used components per building type.

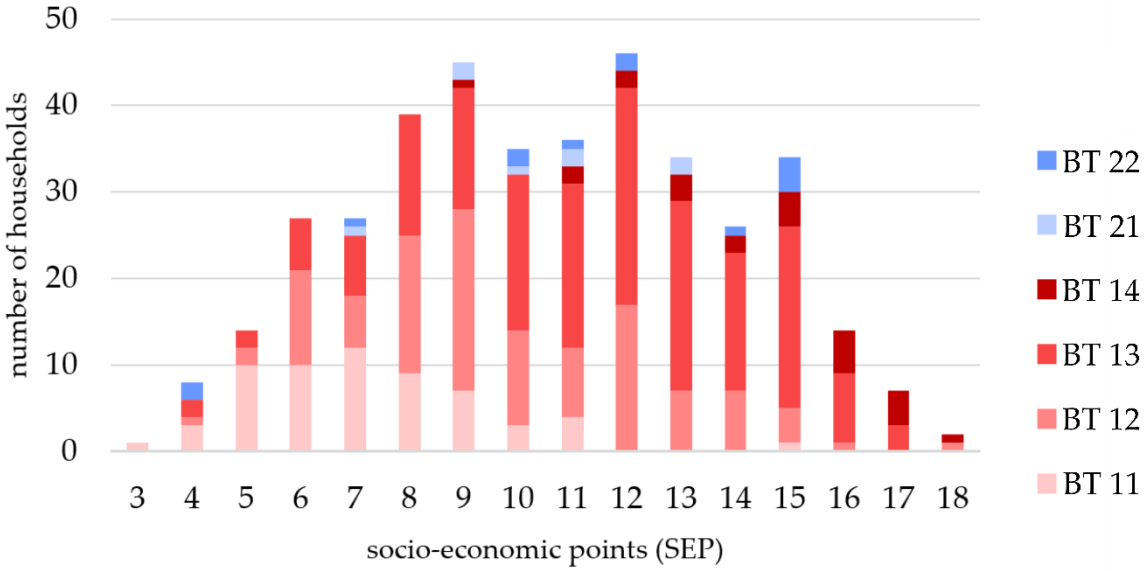

Figure 9. Histogram showing the statistical distribution of residential socio-economic points on household level in Belmopan. Data based on interviews.

3.4. Class Generation and Extrapolation

As Figure 10a shows, building types can be described by SEP. However, building types 12, 13, and 22 show high variations of socio-economic points. This leads to imprecise socio-economic

predictions. To reduce this variation, building types 12, 13, and 22 needed to be disaggregated in subclasses 12a/12b, 13a/13b, and 22a/22b. A set of best fitting spatial indicators were tested to serve as parameters for splitting the building types. Table A1 in Appendix D shows the relationships between intra-building type socio-economic measures and spatial indicators. Distance to market center, distance between the ring road and building, the share of buildings within a 250-m hexagon, delivered the best results. For building type 13, the distance to the US Embassy showed with an r = −0.33 the highest correlation coefficient to the decline of socio-economic measures compared to the other quality of life indicators tested with a $p = 0.00001$ showing high significance (Figure 11b). The correlation analysis between the SEP (BT22) and share of built-up area parameter revealed an r = 0.44, but a relatively high $p = 0.15$. This is due to the small sample size, but the obvious trend can be seen. Figure 11 shows the correlations between the spatial indicators and socio-economic measures within building types 12, 13, and 22. An overview on thresholds for building type separation and socio-economic statistics for the building types is given in Appendix E.

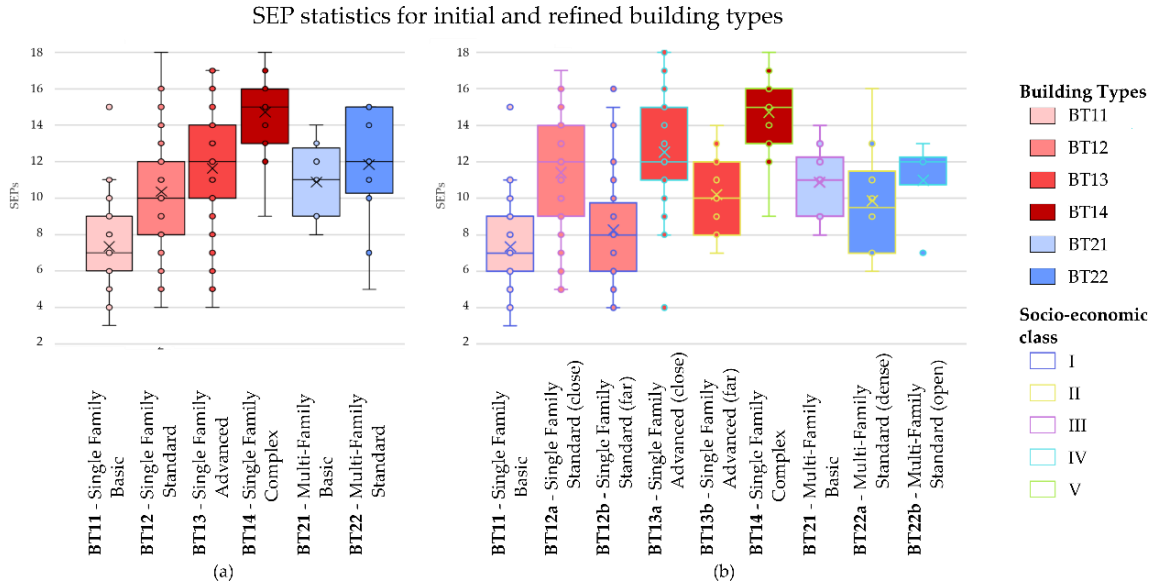

Figure 10. Boxplot chart showing statistical distribution of SEPs over building types. (**a**) Initial building typology with high SEP variation in building type classes 12, 13, and 22. (**b**) The statistical distribution of SEP on refined building typology with effect of reduced variation of SEP for the building type classes 12a/b, 12a/b, and 22a/b. In (**b**), socio-economic class (SEC) assignment is indicated by colored contours (SEC I: blue, SEC II: yellow, SEC III: pink, SEC IV turquoise, SEC V: green). For detailed statistics see Appendix E.

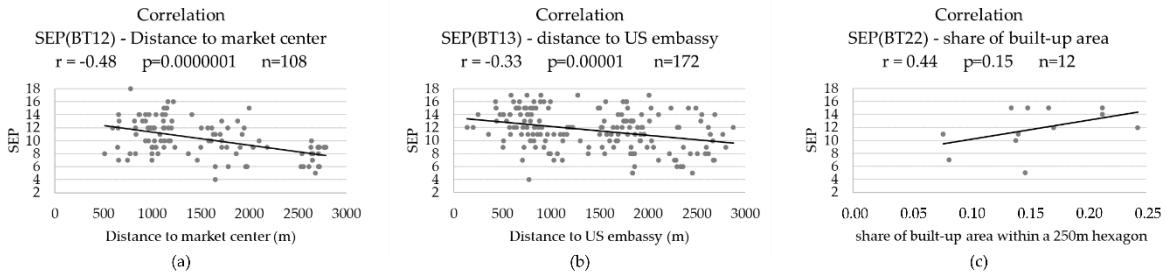

Figure 11. Identified effects of distance on SEP within building types to be disaggregated in Belmopan. For each relation (**a**–**c**) the correlation coefficient r is given, as well as statistical significance p and sample size n.

As described in Section 2.2.7, there is a necessity to create socio-economic classes for three reasons:

1. To predict socio-economic relevant planning values on a single building scale based on building type;
2. To avoid a false impression of precision;
3. Not to publish detailed sensitive information on resident's socio-economic status at a single building level.

The classes were chosen considering the SEP statistics of the building types. On this basis, the classes were assigned manually. We chose to establish five socio-economic classes, with the effect that not every building type represents a single socio-economic class, for which there is no need. Main decision criteria are the highest possible homogeneity in SEP. By comparing mean socio-economic points and standard deviations of SEP within the building types, we set up the class assignment shown in Table 7, which meets the stated criteria for homogeneity in SEPs.

Table 7. Table on assignment of socio-economic classes to building types and number of buildings to corresponding building type classes and socio-economic classes.

Socio-Economic Class	Building Types	Number of Buildings
I	11 12 far	764 2573
II	13 far 22 dense	792 80
III	12 close 21	487 33
IV	13 close 22 open	419 58
V	14	566
Total number of residential buildings		5772

Based on these assignment rules, the socio-economic class was predicted for residential buildings. Figure 12 gives an graphical example for building types and the referring SEC in Belmopan.

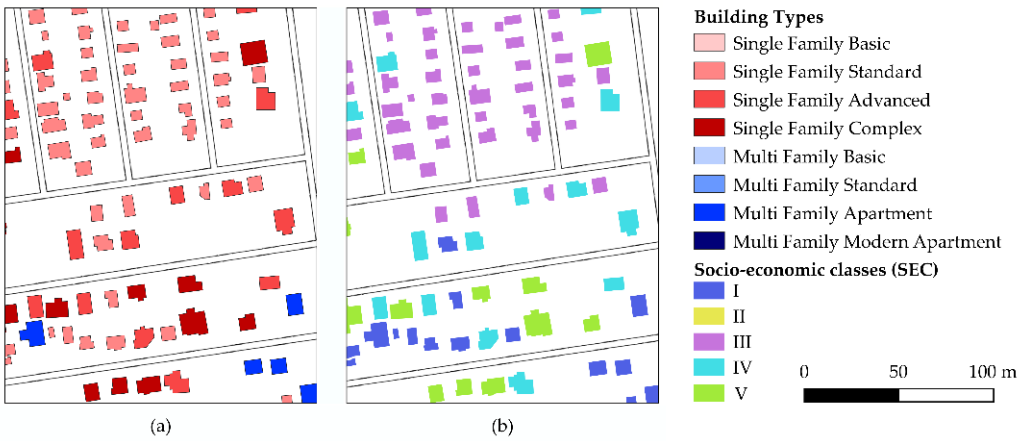

Figure 12. SEC prediction based on building types. (**a**) Building types, (**b**) SEC assignment based on rules shown in Table 7. Upper part in the legend showing building types referring to (**a**), lower part of the legend showing SEC referring to (**b**).

4. Discussion

Basing on building footprints, building types can be classified with random forest in high accuracy. Besides footprint area, a database of ancillary data for three-dimensional building description, spatial information, and rule-based adaptions are essential for successful classification results, as shown in Appendix B.

The intended and applied interview design based on a spatial sampling method that defines areas for interviews using areas of major building type abundances enables the socio-economic characterization for Belmopan. The establishment of the SEP as index to describe residential socio-economic backgrounds delivers good results by combining information on expenditure, educational level, assets, and household income. Correlations between building types and socio-economic information could be proven in this study. For predicting socio-economic attributes, we think it is necessary to create socio-economic classes. Predicting a socio-economic 15-part scale generates too much room for decreased accuracy, therefore a socio-economic classification containing five classes represents socio-economic information in relation to building types with sufficient information content.

The success of the work is directly linked to the collaboration with local authorities and in situ interviews. Our study showed that the implementation of local knowledge is essential to the result for multiple reasons:

1. The establishment of the building typology needs to be adapted for individual case cities. High variations in building types can even exist within countries;
2. The generation of socio-economic information and a socio-economic scaling, SEP in our study, must be based on local information and current surveys;
3. This work indirectly confirms findings of previous studies on location-dependent land value [31,94] through high variation of SEP within single building types. By applying spatial measures, building types can be disaggregated to achieve building types homogenous in SEPs. To identify reference points of urban function, local knowledge is needed as well.

As the relation between building types and socio-economic categorization is shown, it is possible to characterize municipalities for supply and infrastructure planning. Socio-economic information is not directly utilizable as planning value, but the relation between consumption/waste production and socio-economy has been shown [6–10]. Furthermore, the interview design allows conclusion on household assets—on which energy demands can be estimated. Knowledge on building types can support describing and predicting socio-economic attributes. As the socio-economic classification is an a-posteriori measure, a focus should be put on validating the socio-economic measures.

The presented methodology is not limited to WV-1 data. Other VHR imaging satellites can be implemented for building detection and building type classification, which offer a high flexibility for data generation, especially for upcoming satellites missions such as Pléiades Neo [74] and the WorldView Legion [75]. A higher number of VHR imaging satellites leads to increased data availability and higher data reliability. As a result of this, our presented approach is able to continue in operation for long-term urban mapping and planning.

Nonetheless, an awareness must be created that with using VHR imaging technology, data producers and data users are moving on both sides of the borderline of personal privacy and space. The presented methodology produces sensitive information, which can in incautious motivations help expose certain groups of inhabitants or, respectively, induce or increase social conflicts. Discussions must be conducted on how to handle this level of information in general.

5. Conclusions

Our presented methodology proved to be able to provide valuable relevant socio-economic indicators for planning. VHR remote sensing data and in-situ household interviews are essential for high accuracy results. For larger municipalities, other building detection approaches must be used to reduce processing time and manual corrections. Regarding this, techniques basing on machine learning have shown their potential for fast processing of large amounts of satellite imagery [26,30].

Considering Zhu's demand for future strategic directions in urban remote sensing to contribute to the use remote sensing techniques for the "characterization of urban heterogeneity, characterization of urban form and structure in two and three dimensions, and linking remote sensing with emerging urban data" [96], this study works in this manner and shows a way to implement VHR remote sensing data for urban infrastructure planning and delivers information to support evidence based planning [4]. As previously shown, the availability of satellite imagery will increase and therefore a constant data availability will be established. Furthermore, the potential of unmanned aerial vehicles (UAVs) for the quick and cost-effective mapping of urban areas can be exploited even more [97]. The findings of this study, to predict socio-economic information by using VHR images, have shown the potential to support urban planning. Subsequently, we see a necessity to do further investigation on the suitability of such data to derive relevant information for direct planning from similar databases. With knowledge regarding building parameters, such as building height and roof information, and having access to building type and socio-economic information on residents, further attempts should be made to predict specific consumption and production patterns, such as energy demands, waste water production, and solid waste production as Vetter-Gindele [87] has shown for waste production.

Author Contributions: Conceptualization, G.W.; methodology, G.W., A.B., O.A.; validation, A.B., G.W., V.H., O.A., K.F.; formal analysis, G.W., A.B., O.A., K.F.; investigation, G.W.; data curation, G.W., A.B., K.F.; writing—original draft preparation, G.W.; writing—review and editing, G.W., A.B., O.A.; visualization, G.W., A.B., K.F.; supervision, V.H., O.A.; project administration, V.H., O.A.; funding acquisition, V.H., O.A. All authors have read and agreed to the published version of the manuscript.

Funding: This research was funded by the German Federal Ministry of Education and Research (BMBF) under the project "RapidPlanning" (grant identifier 01LG1301K). We acknowledge support by Deutsche Forschungsgemeinschaft and Open Access Publishing Fund of University of Tübingen.

Acknowledgments: We thank Dieter Steinbach and Andrea Schultheis from AT-Association for developing and bringing up the idea of deriving planning relevant information with relevance of building types. Many thanks to the Belmopan City Council for their hospitality, as well as for the fruitful and professional collaboration which made this work possible, including the provision of data and the tireless support during our field work. Special thanks to Paul Wehrle, who organized, supervised, and conducted the interview campaign in 2019. We are very grateful for the language advising provided by Edward III Cahill. PlanetScope data was kindly provided by Planet with the Education and Research program.

Conflicts of Interest: The authors declare no conflict of interest.

Appendix A. Building Heights Validation

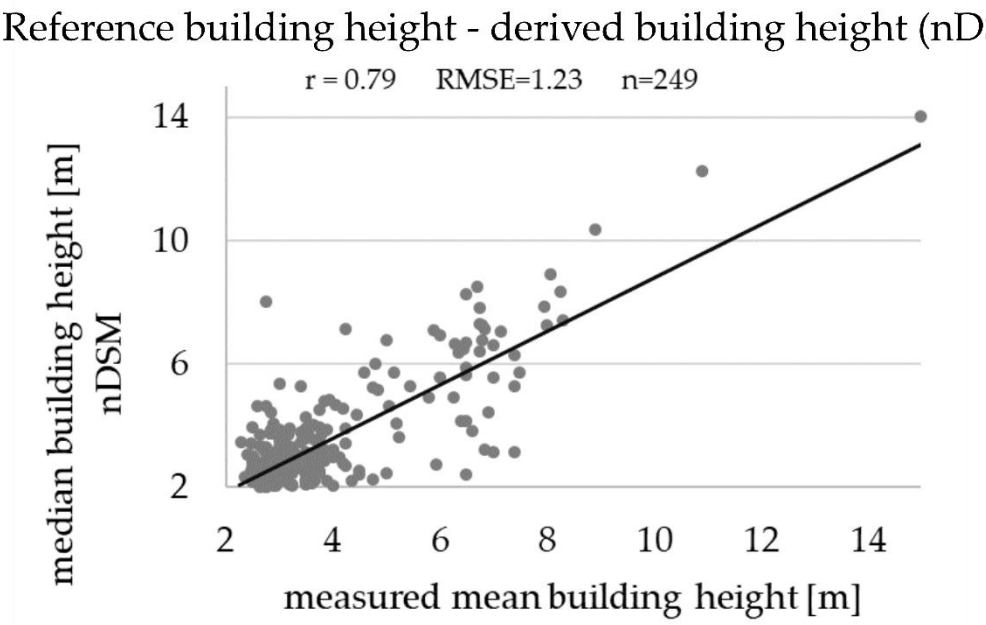

Figure A1. Validation for determined building heights from WV-1 nDSM. The reference dataset was generated by 249 measured buildings. The mean building represents the mean height from wall height and rooftop height.

Appendix B. Manual Refinement of Building Type Classifications

IF BT12 *AND* area < 125 *THEN* BT11
IF BT13 *AND* corners > 7 *THEN* BT12
IF BT12 *AND* area > 150 *AND* height > 4 *THEN* BT13
IF BT13 *AND* area < 140 *AND* height < 3.15 *THEN* BT12
IF BT13 *AND* shape_ratio > 3.05 *THEN* BT14
IF BT21 *AND* corners > 4 *AND* area < 220 *THEN* BT13
IF BT22 *AND* corners < 6 *AND* height < 3.9 *THEN* BT12
IF BT22 *AND* corners > 6 *AND* area < 350 *THEN* BT14
IF BT23 *AND* height > 5.25 *THEN* BT14
IF BT1x *AND* area > 150 *AND* height > 3.05 *THEN* BT21
IF BT14 *AND* corners < 7 *AND* area > 145 *THEN* BT22
IF BT14 *AND* height > 5.15 *ABD* AREA > 190 *THEN* BT23
IF BT11 *AND* ('Elysium' *OR* 'Florida' *OR* 'Maya Ketchi' *OR* 'Maya Mopan' *OR* 'Maya Yucatec' *OR* 'Utopian' *OR* 'Salvapan' *OR* 'North Salvapan' *OR* 'San Martin') *THEN* BT12
IF BT1x *AND* perimeter > 47 AND height > 3.7 AND corners > 7 AND shape_ratio > 3.4 AND area > 230 *THEN* BT14
IF BT1x *AND* area < 30 THEN uninhabited
IF BT1x *AND* area > 510 *AND* corners ≤ 5 THEN uninhabited

uninhabited
"btype_complete" like '%Single%' and "shp_area" > 510 and "shp_corners" <= 5
"shp_area" < 30

Single Family Advanced
"btype_complete" = 'Single Family Standard' and "hgt_building" > 4 and "shp_area" > 150

Appendix C. Figure Showing Socio-Economic Points Composition per Building Type

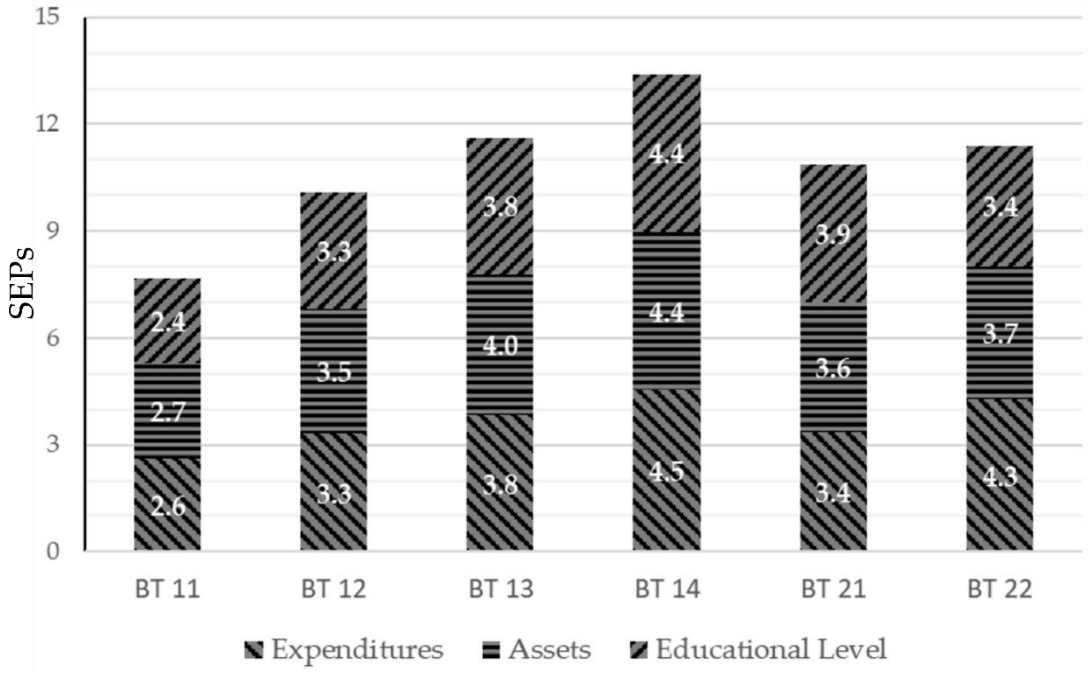

Figure A2. SEPs per building type. As described in Section 2.2.6, total SEP are composed of household expenditures, household assets, and educational level of household main earner.

Appendix D. Table Showing Correlation between SEP and Distances from Urban Points of Centrality

Table A1. Relation between distance from buildings to point urban centrality to socio-economy on building type level.

SEP (Building Type Level)	r Ringroad	r Center	r US Embassy	r Built-Up 250 m
12—Single Family Standard	−0.47 ($p = 1.8 * 10^{-7}$)	**−0.48** ($p = 1.1 * 10^{-7}$)	−0.44 ($p = 1.4 * 10^{-6}$)	0.29 ($p = 0.002$)
13—Single Family Advanced	−0.19 ($p = 0.01$)	−0.27 ($p = 0.0004$)	**−0.33** ($p = 1.2 * 10^{-5}$)	0.05 ($p = 0.5$)
22—Multi-Family Standard	−0.30 ($p = 0.33$)	−0.43 ($p = 0.15$)	−0.19 ($p = 0.55$)	**0.44** ($p = 0.15$)

r = correlation coefficient, p = p-value.

Appendix E. Overview on Parameters for Disaggregating Building Types 12, 13, and 22

Table A2. Overview on thresholds for building type disaggregation and socio-economic statistics on refined building types. Thresholds for building type disaggregation apply to BT12: distance to market center, BT13: distance to US embassy, BT22: share of built-up area within a 250 m hexagon.

Initial Building Types	*n*	Mean SEP	Standard Deviation SEP	Threshold
12—Single Family Standard	108	10.4	2.79	988 m
13—Single Family Advanced	172	11.6	2.94	1018 m
22—Multi-Family Standard	12	11.8	3.30	0.125
Refined Building types	***n***	**Mean SEP**	**Standard Deviation SEP**	
11—Single Family basic	55	7.3	2.2	
12a—Single Family Standard close	74	11.3	2.59	
12b—Single Family Standard far	34	8.3	1.99	
13a—Single Family Advanced close	69	12.8	2.6	
13b—Single Family Advanced far	103	10.9	2.9	
14—Single Family complex	24	14.7	2.1	
22a—Multi-Family Advanced open	6	13.8	1.47	
22b—Multi-Family Advanced dense	6	9.8	3.48	
23—Multi-Family Apartment	1	15	-	

Thresholds applied to following parameters: Building type 12: "distance to ring road (in meters)", building type 12: "distance to market center (in meters)", building type 22: "shared built-up area within a 250 m hexagon".

References

1. United Nations Department of Economic Social Affairs. *World Urbanization Prospects: The 2018 Revision*; United Nations: New York, NY, USA, 2018.
2. Cohen, B. Urbanization in developing countries: Current trends, future projections, and key challenges for sustainability. *Technol. Soc.* **2006**, *28*, 63–80. [CrossRef]
3. UN General Assembly. *Transforming Our World: The 2030 Agenda for Sustainable Development*; United Nations: New York, NY, USA, 2015.
4. Guterres, A. *Actions for the Further Implementation of the Programme of Action of the International Conference on Population and Development: Monitoring of Population Programmes, Focusing on Sustainable Cities, Human Mobility and International Migration*; United Nations Economic and Social Council: New York, NY, USA, 2018.
5. United Nations Human Settlements Programme. *Planning Sustainable Cities: Global Report on Human Settlements 2009*; Earthscan: London, UK, 2009.
6. Oribe-Garcia, I.; Kamara-Esteban, O.; Martin, C.; Macarulla-Arenaza, A.M.; Alonso-Vicario, A. Identification of influencing municipal characteristics regarding household waste generation and their forecasting ability in Biscay. *Waste Manag.* **2015**, *39*, 26–34. [CrossRef] [PubMed]
7. Khan, D.; Kumar, A.; Samadder, S.R. Impact of socioeconomic status on municipal solid waste generation rate. *Waste Manag.* **2016**, *49*, 15–25. [CrossRef] [PubMed]
8. Xu, L.; Lin, T.; Xu, Y.; Xiao, L.; Ye, Z.; Cui, S. Path analysis of factors influencing household solid waste generation: A case study of Xiamen Island, China. *J. Mater. Cycles Waste Manag.* **2016**, *18*, 377–384. [CrossRef]
9. Bosire, E.; Oindo, B.; Atieno, J.V. *Modeling Household Solid Waste Generation in Urban Estates Using SocioEconomic and Demographic Data*; Maseno University: Kisumu City, Kenya, 2017.
10. Jones, R.V.; Fuertes, A.; Lomas, K.J. The socio-economic, dwelling and appliance related factors affecting electricity consumption in domestic buildings. *Renew. Sustain. Energy Rev.* **2015**, *43*, 901–917. [CrossRef]
11. Brown de Colstoun, E.C.; Huang, C.; Wang, P.; Tilton, J.C.; Tan, B.; Phillips, J.; Niemczura, S.; Ling, P.-Y.; Wolfe, R.E. *Global Man-made Impervious Surface (GMIS) Dataset from Landsat*; NASA Socioeconomic Data and Applications Center (SEDAC): Palisades, NY, USA, 2017.
12. Zhou, Y.; Smith, S.J.; Zhao, K.; Imhoff, M.; Thomson, A.; Bond-Lamberty, B.; Asrar, G.R.; Zhang, X.; He, C.; Elvidge, C.D. A global map of urban extent from nightlights. *Environ. Res. Lett.* **2015**, *10*, 054011. [CrossRef]

13. Esch, T.; Marconcini, M.; Felbier, A.; Roth, A.; Heldens, W.; Huber, M.; Schwinger, M.; Taubenböck, H.; Müller, A.; Dech, S. Urban Footprint Processor—Fully Automated Processing Chain Generating Settlement Masks From Global Data of the TanDEM-X Mission. *IEEE Geosci. Remote Sens. Lett.* **2013**, *10*, 1617–1621. [CrossRef]
14. Esch, T.; Heldens, W.; Hirner, A.; Keil, M.; Marconcini, M.; Roth, A.; Zeidler, J.; Dech, S.; Strano, E. Breaking new ground in mapping human settlements from space–The Global Urban Footprint. *ISPRS J. Photogramm. Remote Sens.* **2017**, *134*, 30–42. [CrossRef]
15. Marconcini, M.; Metz-Marconcini, A.; Uereyen, S.; Palacios Lopez, D.; Hanke, W.; Bachofer, F.; Zeidler, J.; Esch, T.; Gorelick, N.; Kakarla, A.; et al. Outlining Where Humans Live—The World Settlement Footprint 2015. Available online: https://arxiv.org/abs/1910.12707 (accessed on 11 November 2019).
16. Warth, G.; Braun, A.; Bödinger, C.; Hochschild, V.; Bachofer, F. DSM-based identification of changes in highly dynamic urban agglomerations. *Eur. J. Remote Sens.* **2019**, *52*, 322–334. [CrossRef]
17. Braun, A.; Warth, G.; Bachofer, F.; Bui, T.; Tran, H.; Hochschild, V. Changes in the building stock of DaNang between 2015 and 2017. *Data* **2020**, *5*, 42. [CrossRef]
18. Blaschke, T. Object based image analysis for remote sensing. *ISPRS J. Photogramm. Remote Sens.* **2010**, *65*, 2–16. [CrossRef]
19. Dey, V.; Zhang, Y.; Zhong, M. Building detection from pan-sharpened GeoEye-1 satellite imagery using context based multi-level image segmentation. In Proceedings of the 2011 International Symposium on Image and Data Fusion, Tengchong, China, 9 August 2011; pp. 1–4.
20. Grippa, T.; Lennert, M.; Beaumont, B.; Vanhuysse, S.; Stephenne, N.; Wolff, E. An Open-Source Semi-Automated Processing Chain for Urban Object-Based Classification. *Remote Sens.* **2017**, *9*, 358. [CrossRef]
21. Banzhaf, E.; Kollai, H.; Kindler, A. Mapping urban grey and green structures for liveable cities using a 3D enhanced OBIA approach and vital statistics. *Geocarto Int.* **2018**, *35*, 1–18. [CrossRef]
22. Sari, N.M.; Kushardono, D. Quality Analysis of Single Tree Object with OBIA and Vegetation Index from LAPAN Surveillance Aircraft Multispectral Data in Urban Area. *Geoplanning J. Geomat. Plan.* **2016**, *3*, 93–106. [CrossRef]
23. Labib, S.M.; Harris, A. The potentials of Sentinel-2 and LandSat-8 data in green infrastructure extraction, using object based image analysis (OBIA) method. *Eur. J. Remote Sens.* **2018**, *51*, 231–240. [CrossRef]
24. Banzhaf, E.; de la Barrera, F. Evaluating public green spaces for the quality of life in cities by integrating RS mapping tools and social science techniques. In Proceedings of the 2017 Joint Urban Remote Sensing Event (JURSE), Dubai, UAE, 6–8 March 2017; pp. 1–4.
25. LeCun, Y.; Huang, F.J.; Bottou, L. Learning methods for generic object recognition with invariance to pose and lighting. In Proceedings of the 2004 IEEE Computer Society Conference on Computer Vision and Pattern Recognition, 2004. CVPR 2004, Washington, DC, USA, 27 June–2 July 2004; pp. II–104.
26. Vakalopoulou, M.; Karantzalos, K.; Komodakis, N.; Paragios, N. Building detection in very high resolution multispectral data with deep learning features. In Proceedings of the 2015 IEEE International Geoscience and Remote Sensing Symposium (IGARSS), Milan, Italy, 26–31 July 2015; pp. 1873–1876.
27. Persello, C.; Stein, A. Deep Fully Convolutional Networks for the Detection of Informal Settlements in VHR Images. *IEEE Geosci. Remote Sens. Lett.* **2017**, *14*, 2325–2329. [CrossRef]
28. Liu, R.; Kuffer, M.; Persello, C. The Temporal Dynamics of Slums Employing a CNN-Based Change Detection Approach. *Remote Sens.* **2019**, *11*, 2844. [CrossRef]
29. Xia, X.; Persello, C.; Koeva, M. Deep Fully Convolutional Networks for Cadastral Boundary Detection from UAV Images. *Remote Sens.* **2019**, *11*, 1725. [CrossRef]
30. Zhu, X.X.; Tuia, D.; Mou, L.; Xia, G.; Zhang, L.; Xu, F.; Fraundorfer, F. Deep Learning in Remote Sensing: A Comprehensive Review and List of Resources. *IEEE Geosci. Remote Sens. Mag.* **2017**, *5*, 8–36. [CrossRef]
31. Brimble, P.; McSharry, P.; Bachofer, F.; Bower, J.; Braun, A. *Using Machine Learning and Remote Sensing to Value Property in Kigali*; The International Growth Centre: London, UK, 2020.
32. Mikhail, E.M.; Bethel, J.S.; McGlone, J.C. *Introduction to Modern Photogrammetry*; Wiley: New York, NY, USA, 2001.
33. Bachofer, F. Assessment of building heights from pléiades satellite imagery for the Nyarugenge sector, Kigali, Rwanda. *Rwanda J.* **2017**, *1*. [CrossRef]
34. Dong, P.; Chen, Q. *LiDAR Remote Sensing and Applications*; CRC Press: Boca Raton, FL, USA, 2017.

35. Liu, L.; Coops, N.C.; Aven, N.W.; Pang, Y. Mapping urban tree species using integrated airborne hyperspectral and LiDAR remote sensing data. *Remote Sens. Environ.* **2017**, *200*, 170–182. [CrossRef]
36. Alonzo, M.; McFadden, J.P.; Nowak, D.J.; Roberts, D.A. Mapping urban forest structure and function using hyperspectral imagery and lidar data. *Urban For. Urban Green.* **2016**, *17*, 135–147. [CrossRef]
37. Giannico, V.; Lafortezza, R.; John, R.; Sanesi, G.; Pesola, L.; Chen, J. Estimating Stand Volume and Above-Ground Biomass of Urban Forests Using LiDAR. *Remote Sens.* **2016**, *8*, 339. [CrossRef]
38. Lafortezza, R.; Giannico, V. Combining high-resolution images and LiDAR data to model ecosystem services perception in compact urban systems. *Ecol. Indic.* **2019**, *96*, 87–98. [CrossRef]
39. Zhang, H.; Lin, H.; Wang, Y. A new scheme for urban impervious surface classification from SAR images. *ISPRS J. Photogramm. Remote Sens.* **2018**, *139*, 103–118. [CrossRef]
40. Crosetto, M.; Castillo, M.; Arbiol, R. Urban subsidence monitoring using radar interferometry. *Photogramm. Eng. Remote Sens.* **2003**, *69*, 775–783. [CrossRef]
41. Potin, P.; Rosich, B.; Miranda, N.; Grimont, P.; Shurmer, I.; O'Connell, A.; Krassenburg, M.; Gratadour, J.-B. Copernicus Sentinel-1 Constellation Mission Operations Status. In Proceedings of the IGARSS-2019 IEEE International Geoscience and Remote Sensing Symposium, Yokohama, Japan, 28 July–2 August 2019; pp. 5385–5388.
42. Gabriel, A.K.; Goldstein, R.M.; Zebker, H.A. Mapping small elevation changes over large areas: Differential radar interferometry. *J. Geophys. Res. Solid Earth* **1989**, *94*, 9183–9191. [CrossRef]
43. Notti, D.; Mateos, R.M.; Monserrat, O.; Devanthéry, N.; Peinado, T.; Roldán, F.J.; Fernández-Chacón, F.; Galve, J.P.; Lamas, F.; Azañón, J.M. Lithological control of land subsidence induced by groundwater withdrawal in new urban areas (Granada Basin, SE Spain). Multiband DInSAR monitoring. *Hydrol. Process.* **2016**, *30*, 2317–2331. [CrossRef]
44. Cascini, L.; Ferlisi, S.; Fornaro, G.; Lanari, R.; Peduto, D.; Zeni, G. Subsidence monitoring in Sarno urban area via multi-temporal DInSAR technique. *Int. J. Remote Sens.* **2006**, *27*, 1709–1716. [CrossRef]
45. Chaussard, E.; Amelung, F.; Abidin, H.; Hong, S.-H. Sinking cities in Indonesia: ALOS PALSAR detects rapid subsidence due to groundwater and gas extraction. *Remote Sens. Environ.* **2013**, *128*, 150–161. [CrossRef]
46. Tesauro, M.; Berardino, P.; Lanari, R.; Sansosti, E.; Fornaro, G.; Franceschetti, G. Urban subsidence inside the city of Napoli (Italy) Observed by satellite radar interferometry. *Geophys. Res. Lett.* **2000**, *27*, 1961–1964. [CrossRef]
47. Delgado Blasco, J.M.; Foumelis, M.; Stewart, C.; Hooper, A. Measuring Urban Subsidence in the Rome Metropolitan Area (Italy) with Sentinel-1 SNAP-StaMPS Persistent Scatterer Interferometry. *Remote Sens.* **2019**, *11*, 129. [CrossRef]
48. Wang, H.; Feng, G.; Xu, B.; Yu, Y.; Li, Z.; Du, Y.; Zhu, J. Deriving spatio-temporal development of ground subsidence due to subway construction and operation in delta regions with PS-InSAR data: A case study in Guangzhou, China. *Remote Sens.* **2017**, *9*, 1004. [CrossRef]
49. Fornaro, G.; Lombardini, F.; Pauciullo, A.; Reale, D.; Viviani, F. Tomographic Processing of Interferometric SAR Data: Developments, applications, and future research perspectives. *IEEE Signal Process. Mag.* **2014**, *31*, 41–50. [CrossRef]
50. Budillon, A.; Crosetto, M.; Johnsy, A.C.; Monserrat, O.; Krishnakumar, V.; Schirinzi, G. Comparison of Persistent Scatterer Interferometry and SAR Tomography Using Sentinel-1 in Urban Environment. *Remote Sens.* **2018**, *10*, 1986. [CrossRef]
51. Crosetto, M.; Budillon, A.; Monserrat, O. *Urban Deformation Monitoring using Persistent Scatterer Interferometry and SAR tomography*; MDPI: Basel, Switzerland, 2019.
52. Shi, Y.; Wang, Y.; Zhu, X.X.; Bamler, R. Non-Local SAR Tomography for Large-Scale Urban Mapping. In Proceedings of the IGARSS 2019–2019 IEEE International Geoscience and Remote Sensing Symposium, Yokohama, Japan, 28 July–2 August 2019; pp. 5197–5200.
53. Li, Y.; Martinis, S.; Wieland, M.; Schlaffer, S.; Natsuaki, R. Urban Flood Mapping Using SAR Intensity and Interferometric Coherence via Bayesian Network Fusion. *Remote Sens.* **2019**, *11*, 2231. [CrossRef]
54. Kuffer, M.; Pfeffer, K.; Sliuzas, R. Slums from space—15 years of slum mapping using remote sensing. *Remote Sens.* **2016**, *8*, 455. [CrossRef]
55. Kuffer, M.; Pfeffer, K.; Sliuzas, R.; Baud, I. Extraction of slum areas from VHR imagery using GLCM variance. *IEEE J. Sel. Top. Appl. Earth Obs. Remote Sens.* **2016**, *9*, 1830–1840. [CrossRef]

56. Jensen, J.R.; Cowen, D.C. Remote sensing of urban/suburban infrastructure and socio-economic attributes. *Photogramm. Eng. Remote Sens.* **1999**, *65*, 611–622.
57. Lo, C.P.; Faber, B.J. Integration of Landsat Thematic Mapper and census data for quality of life assessment. *Remote Sens. Environ.* **1997**, *62*, 143–157. [CrossRef]
58. Martinuzzi, S.; Ramos-González, O.M.; Muñoz-Erickson, T.A.; Locke, D.H.; Lugo, A.E.; Radeloff, V.C. Vegetation cover in relation to socioeconomic factors in a tropical city assessed from sub-meter resolution imagery. *Ecol. Appl.* **2018**, *28*, 681–693. [CrossRef] [PubMed]
59. Haas, J.; Ban, Y. Sentinel-1A SAR and sentinel-2A MSI data fusion for urban ecosystem service mapping. *Remote Sens. Appl. Soc. Environ.* **2017**, *8*, 41–53. [CrossRef]
60. Yang, Y.; Wu, T.; Wang, S.; Li, J.; Muhanmmad, F. The NDVI-CV Method for Mapping Evergreen Trees in Complex Urban Areas Using Reconstructed Landsat 8 Time-Series Data. *Forests* **2019**, *10*, 139. [CrossRef]
61. Lin, D.; Gold, H.T.; Schreiber, D.; Leichman, L.P.; Sherman, S.E.; Becker, D.J. Impact of socioeconomic status on survival for patients with anal cancer. *Cancer* **2018**, *124*, 1791–1797. [CrossRef]
62. Rosengren, A.; Smyth, A.; Rangarajan, S.; Ramasundarahettige, C.; Bangdiwala, S.I.; AlHabib, K.F.; Avezum, A.; Bengtsson Boström, K.; Chifamba, J.; Gulec, S.; et al. Socioeconomic status and risk of cardiovascular disease in 20 low-income, middle-income, and high-income countries: The Prospective Urban Rural Epidemiologic (PURE) study. *Lancet Glob. Health* **2019**, *7*, e748–e760. [CrossRef]
63. Kim, S.w.; Kim, E.J.; Wagaman, A.; Fong, V.L. A longitudinal mixed methods study of parents' socioeconomic status and children's educational attainment in Dalian City, China. *Int. J. Educ. Dev.* **2017**, *52*, 111–121. [CrossRef]
64. McKenzie, D.J. Measuring inequality with asset indicators. *J. Popul. Econ.* **2005**, *18*, 229–260. [CrossRef]
65. Renard, F.; Devleesschauwer, B.; Speybroeck, N.; Deboosere, P. Monitoring health inequalities when the socio-economic composition changes: Are the slope and relative indices of inequality appropriate? Results of a simulation study. *BMC Public Health* **2019**, *19*, 662. [CrossRef]
66. Hoffmann, R.; Kröger, H.; Pakpahan, E. Pathways between socioeconomic status and health: Does health selection or social causation dominate in Europe? *Adv. Life Course Res.* **2018**, *36*, 23–36. [CrossRef]
67. Tighe, L.; Webster, N.J. The Influence of Socioeconomic Status on health and Well-Being: Comparing Diverse Trajectories. *Innov. Aging* **2017**, *1*, 983–984. [CrossRef]
68. Kivimäki, M.; Batty, G.D.; Pentti, J.; Shipley, M.J.; Sipilä, P.N.; Nyberg, S.T.; Suominen, S.B.; Oksanen, T.; Stenholm, S.; Virtanen, M. Association between socioeconomic status and the development of mental and physical health conditions in adulthood: A multi-cohort study. *Lancet Public Health* **2020**, *5*, e140–e149. [CrossRef]
69. Lampert, T.; Kroll, L.E.; Kuntz, B.; Hoebel, J. *Gesundheitliche Ungleichheit in Deutschland und im Internationalen Vergleich: Zeitliche Entwicklungen und Trends*; Robert-Koch-Institut: Berlin, Germany, 2018.
70. Guterres, A. *Sustainable Cities, Human Mobility and Internationalmigration*; United Nations Economic and Social Council: New York, NY, USA, 2018.
71. United Nations Human Settlements Programme. *Belmopan Urban Development. Towards a Sustainable Garden City*; Earthscan: London, UK, 2017.
72. Statistical Institute of Belize. *Annual Report 2018–19*; Statistical Institute of Belize: Belmopan, Belize, 2019.
73. Kaza, S.; Yao, L.; Bhada-Tata, P.; Van Woerden, F. *What a Waste 2.0: A Global Snapshot of Solid Waste Management to 2050*; The World Bank: Washington, DC, USA, 2018.
74. Airbus Defence and Space. Pléiades Neo. Trusted Intelligence. Available online: https://www.intelligence-airbusds.com/en/8671-pleiades-neo-trusted-intelligence (accessed on 11 November 2019).
75. Maxar. WorldView Legion. Our Next-generation Constellation. Available online: https://www.maxar.com/splash/worldview-legion (accessed on 12 February 2020).
76. Kearns, K.C. Belmopan: Perspective on a new capital. *Geogr. Rev.* **1973**, *63*, 147–169. [CrossRef]
77. Friesner, J. *Hurricanes and the Forests of Belize*; Forest Planning and Management Project; Ministry of Natural Resources: Belmopan, Belize, 1993.
78. Statistical Institute of Belize. *Annual Report 2017-18*; Statistical Institute of Belize: Belmopan, Belize, 2018.
79. DigitalGlobe. WorldView-1. Available online: https://www.euspaceimaging.com/wp-content/uploads/2018/08/WorldView1-DS-WV1_V02.pdf (accessed on 3 December 2019).
80. Planet Team. Planet Application Program Interface: In Space for Life on Earth; San Francisco. 2017. Available online: https://api.planet.com (accessed on 2 February 2019).

81. Planet. Planet Imagery Product Specification: Planetscope & Rapideye. Available online: https://www.planet.com/products/satellite-imagery/files/1610.06_Spec%20Sheet_Combined_Imagery_Product_Letter_ENGv1.pdf (accessed on 1 September 2019).
82. Pham, P. KoBo Toolbox. In Proceedings of the Measure GIS Working Group Meeting, Rosslyn, VA, USA, 26 June 2012.
83. Haklay, M.; Weber, P. Openstreetmap: User-generated street maps. *IEEE Pervasive Comput.* **2008**, *7*, 12–18. [CrossRef]
84. Hexagon. *Erdas Imagine 2018*. Available online: https://download.hexagongeospatial.com/en/downloads/imagine/erdas-imagine-2018 (accessed on 11 January 2019).
85. Legner, S. JOSM-Java OpenStreetMap Editor. In Proceedings of the FOSSGIS 2012, Dessau, Germany, 20–22 March 2012.
86. Hashim, H.; Abd Latif, Z.; Adnan, N.A. Urban Vegetation Classifiction With NDVI Threshold Value Method with Very High Resolution (VHR) Pleiades Imagery. *Int. Arch. Photogramm. Remote Sens. Spat. Inf. Sci.* **2019**, *XLII-4/W16*, 237–240. [CrossRef]
87. Vetter-Gindele, J.; Braun, A.; Warth, G.; Bui, T.T.; Bachofer, F.; Eltrop, L. Assessment of Household Solid Waste Generation and Composition by Building Type in Da Nang, Vietnam. *Resources* **2019**, *8*, 171. [CrossRef]
88. Point2homes. 2-Storey House. Available online: https://www.point2homes.com (accessed on 13 December 2019).
89. Lang, S.; Blaschke, T. *Landschaftsanalyse mit GIS*; Ulmer: Stuttgart, Germany, 2007; p. 405.
90. Breiman, L. Random Forests. *Mach. Learn.* **2001**, *45*, 5–32. [CrossRef]
91. Winkler, J.; Stolzenberg, H. Der Sozialschichtindex im Bundes-Gesundheitssurvey. *Gesundheitswesen* **1998**, *61*, 178–183.
92. Singh, T.; Sharma, S.; Nagesh, S. Socio-economic status scales updated for 2017. *Int. J. Res. Med. Sci.* **2017**, *5*, 3264–3267. [CrossRef]
93. Biewen, M.; Juhasz, A. Direct Estimation of Equivalence Scales and More Evidence on Independence of Base. *Oxf. Bull. Econ. Stat.* **2017**, *79*, 875–905. [CrossRef]
94. Kau, J.B.; Sirmans, C.F. Urban land value functions and the price elasticity of demand for housing. *J. Urban Econ.* **1979**, *6*, 112–121. [CrossRef]
95. Pascascio, K.; (Belmopan City Council, Belmopan, Belize). Personal communication, 2019.
96. Zhu, Z.; Zhou, Y.; Seto, K.C.; Stokes, E.C.; Deng, C.; Pickett, S.T.A.; Taubenböck, H. Understanding an urbanizing planet: Strategic directions for remote sensing. *Remote Sens. Environ.* **2019**, *228*, 164–182. [CrossRef]
97. Nex, F.; Remondino, F. UAV for 3D mapping applications: A review. *Appl. Geomat.* **2014**, *6*, 1–15. [CrossRef]

Appendix A-3

Photovoltaic energy balancing in Belmopan based on building types, UAV aerial imagery and household data

Gebhard Warth[a]*, Oliver Assmann[b], Kevin Fleckenstein[c], Andreas Braun[a], Volker Hochschild[a]

[a]*Research Group Geography, Faculty of Sciene, University of Tuebingen, Ruemelinstrasse 19-23, 72070 Tübingen, Germany*

[b] *AT Association, Waldburgstraße 96, 70563 Stuttgart, Germany*

[c]*Research Area Landscape Ecology and Vegetation Science, University of Hohenheim, August-von Hartmann-Str. 3, 70599 Stuttgart, Germany*

*Corresponding author

E-mail address :gebhard.warth@uni-tuebingen.de (G. Warth)

Abstract:

Photovoltaic (PV) energy plays an important role in order to reduce the share of carbon fuels as energy source and increase energy independence due to its decentral potential as energy source. Therefore, PV electricity generation can serve as a piece of the puzzle in national energy strategies to reduce the carbon footprint but as well as an opportunity for households to reduce energy dependence and thus to reduce energy expenses. In this given context and to point out methods to support urban infrastructure planning, this study analyzes the feasibility of estimating electric consumption related to the building type and to perform PV energy balancing based on height information retrieved imagery from unmanned aerial vehicles (UAV). The overall approach bases on the determination of residential building types through a Random Forest classification, using spatially very high-resolution aerial imagery from UAV data collections. In this regard, the results show very satisfying overall accuracies of 0.73. Statistics on data from residential interviews show deviating energy consumption patterns within different building types, therefore, we show that building types can be indicators for electric consumption. Using Structure-from-Motion (SfM) based height information and recent PV panel characteristics, roof-based PV electricity generation can be predicted. Applying this approach, we can relate energy consumption with potential PV energy production to determine a PV energy balance. Out of 1,619 analyzed buildings in Belmopan, we found that 97.9% of the buildings are suitable for PV panel installation. We calculated two scenarios with firstly installing maximum number of PV panels on the best-suited field of roof of each building to show the overall PV potential in Belmopan and secondly, installing maximum two PV panels on the best-suited field of roof of each building to evaluate a more realistic and easier implementable scenario. For scenario 1, an average PV energy surplus per building of 148% can be achieved and for scenario 2, only one building shows a slightly negative energy PV energy balance. An average energy surplus per building of 29.5% can be achieved using only two PV panels. On the one hand the outcomes of this study in general show the enormous potential of PV electricity generation in Belmopan, but as well that this approach is able to deliver a data basis for decision making in urban planning and renewable energy policy development.

Keywords: building types, photovoltaic energy balancing, unmanned aerial vehicles, structure-from-motion, household survey, urban planning

1. Introduction

In 2018, 55.7% of the global city-dwelling population consumed 75% of global energy (United Nations, 2018; World Bank, 2018). This number elucidates the demand on energy supply and urban infrastructure, especially in the face of ongoing urbanization. The residential sector hereby has a significant share in electricity consumption, in the European Union the residential sector consumes 28.6% (Eurostat, 2021) and in Belize the residential sector covers 39.5% of the national electric energy consumption (Belize Energy Unit, 2020b). Moreover, the relation between urbanization rate and energy consumption underlines the necessity of proper urban infrastructure planning to meet future energy demands and to ensure stable energy supply and consumption. To minimize the environmental impact of energy production and energy supply, approaches for sustainable infrastructure planning have to be developed and implemented (Malekpour et al., 2015). The sustainable development goals (SDG), proclaimed by the United Nations in 2015 (United Nations, 2015), hereby set targets that have distinct relevance for urban infrastructure planning: SDG 7 affordable and clean energy and SDG 13 climate action (United Nations, 2015). Since the majority of the global population lives in urban areas, cities are a central place to implement SDGs, because municipal organizations can act as local coordinators to implement SDGs (Fenton and Gustafsson, 2017). To not increase inequalities in urban areas through climate change impacts, most vulnerable groups have to be kept in focus to develop adaptation and mitigation policies (Reckien et al., 2017). Photovoltaic (PV) electric energy production strategies can significantly contribute to SDG 7: affordable and clean energy production, SDG 10: reduce inequality and SDG 13: climate action (United Nations, 2015). Proper PV policies and feed-in-tariff strategies have positive short- and long-term effects (Poruschi and Ambrey, 2019), from which economically weak groups could benefit, as in general PV implementation is correlated to economic variables such as gross domestic product and social variables such as highest academic grade (Lin et al., 2018).

So far, planning decisions and strategies tend to ad hoc problem-oriented approaches, SDGs can help break out of these habits and draw attention to wider approaches (Sanchez-Rodriguez et al., 2018), which is why a strategy change towards evidence-based planning is demanded (Guterres, 2018). However, to meet the aims of SDGs through appropriate urban planning, high-quality data is missing for the planning processes, especially data based on household surveys (Klopp and Petretta, 2017) to gain an understanding of urban dynamics, especially as urban planning was criticized for only focusing physical adaptions and its lacking capacities to face economic, political and socio-cultural conflicts (Blair, 1973). Therefore, sustainable urban infrastructure planning requires social understanding of cities (Romero Rodríguez et al., 2017) going beyond highest classification accuracies of remote sensing (RS) analyses and a team effort of scientists and practitioners (Malekpour et al., 2015) to enable implementable planning on a solid data foundation, for which scientists have to develop appropriate approaches.

Our study city Belmopan in Belize undergoes an annual urban population growth rate of 6.4% between 2014 and 2018 (Statistical Institute of Belize, 2019), which underlines the need for an urban planning strategy. As later shown in the following sections, although Belize has a geographically favorable location for PV electricity production, it only has a minor share in the national energy mix. Considering Belmopan's location and relatively high prices for energy in Belize (see section 3.2), decentralized PV energy generation has the potential to be both a pillar in the national energy mix and to provide more affordable energy given an adequate solar policy, thus benefiting both the overall economy and minimizing economic disparities.

In this context, we see a potential for approaches based on RS techniques to support urban infrastructure planning by providing relevant data on building-specific energy consumption and modelled PV energy production. Such information is needed to plan energy supply infrastructure on a communal, regional and national level, but additionally, to develop socially fair policies for PV implementation.

In urban RS, a recent research focus lies on the determination of socio-economic indicators which is very relevant, as energy consumption correlates with higher GDP and HDI values (Martínez, 2015) and as urban quality is in relation to socio-economic factors (Musse et al., 2018). Using medium resolution data, urban structure has recently been determined through Landsat nighttime light (NTL) data (Liu et al., 2017), socio-economic information is explained by multi-temporal data analysis (Sapena et al., 2020).

Very high-resolution (VHR) RS data is used for tree detection and green space classification by aerial optical and LiDAR data using neural networks (Chen et al., 2021).

A building type-based approach was chosen for change detection in the building stock bach (Bachofer et al., 2019) and socio-economic assumptions on a single building level (Warth et al., 2020), residential waste production on a city level was estimated using urban structure information (Vetter-Gindele et al., 2019).

In order to estimate energy consumption, settlement classes were generated based on Landsat NTL data (Chowdhury et al., 2019) and energy consumption was correlated with thermal measurements through Landsat 8 (Jazizadeh and Taleghani, 2016). On a building-specific scale, approaches base on grouping buildings into similar thermo-physical characteristics and assigning building age classes (Wan and Yik, 2004; Ballarini et al., 2014). Deep learning approaches in the urban context have a main focus, because these approaches promise to achieve very high detection accuracies (Li et al., 2019). Using VHR RS data, deep learning approaches are adapted for building detection (Audebert et al; Yi et al., 2019), slum mapping (Stark et al., 2020), object detection (Dong et al., 2019), and land-use mapping (Huang et al., 2018).
Determination of functional urban zones is difficult using only RS data. Therefore, high-resolution imagery and mobile phone positioning data are combined (Tu et al., 2018) and urban land use estimations are improved with social-media data (Liu et al., 2017).

PV simulations have proven to provide high precision predictions for PV energy production (Compagnon, 2004; Brito et al., 2012; Romero Rodríguez et al., 2017). Therefore, to support cities in their transformation process towards a post-carbon city and to follow the hypothesis that knowledge on residential building type allows estimating electric energy consumption, we present an approach based on the single building level to determine electric energy demands and possible PV electric energy yield based on building types. This bottom-up approach allows energy balancing on different urban scales and provides valuable information for urban supply infrastructure planning and policy development. Cost effects are not considered in this study, but the results show the relevance of PV in this study to achieve SDG goals 7: affordable and clean energy and goal 13: climate action (United Nations, 2015).

2. Materials and Methods

This paper aims to present an approach for balancing photovoltaic energy production and residential energy consumption on a single building level to provide specific data for urban infrastructure planning purposes. The approach bases on building types, to which energy consumption can be related. UAV data enable predicting photovoltaic potential on a single building level. Through differencing energy consumption and energy production, an energy balance can be derived. The methodology consists of the following steps, which are presented in the following sections in detail:

- UAV imaging campaign and Structure-from-Motion processing
- Random Forest building type classification
- Household survey to estimate electricity expenditures and building type specific residential energy consumption patterns
- Scenario-based determination of roof-based photovoltaic energy production on single building level
- Photovoltaic energy balancing on single building level

2.1. Study area

This study focuses on study areas in Belmopan (I-VI), hereafter referred to as districts

because they are oriented to precincts. Belmopan is the capital city of Belize with a population of 25,583 inhabitants in 2021 (Belmopan City Council, 2021a). After a series of hurricanes, the former capital function was moved from Belize City to Belmopan (Friesner, 1993), which was inaugurated for this purpose in 1970 (Kearns, 1973) and was initially developed as a planned city (Everitt, 1984). The city is located in the center of Belize and covers an area of 32.25 km² (Warth et al., 2020). Despite its location in the tropical am climate zone after Köppen-Geiger (Kottek et al., 2006), Belmopan experiences in general very good conditions for photovoltaic energy generation, as will be shown in section 3.5.

Due to limitations from battery capacities to cover the whole city of Belmopan with aerial campaigns, six city areas were defined to perform aerial imagery collection campaigns, as it is shown in figure 1. These areas were chosen on the basis of the preceding study by Warth et al. (2020), where building types were determined using WorldView-1 data, to cover as many different building types as possible.

The total electric energy consumption in Belize in 2018 was 554,433 MWh, whereas 39.5% are accounted for the residential sector and 52.3% are accounted for the commercial sector (Belize Energy Unit, 2020b). The commercial sector increased its share in electric energy consumption by 0.8%, whereas the residential sector increased its share by 2.6% (Belize Energy Unit, 2020a). Hydropower comprises a 45.0% share of the energy mix in Belize, followed by fossil fuels (29.9%) and biomass (16.9%). PV electricity production accounts for 0.1%. From 2016, the use of hydropower decreased by 7.8% and the use of fossil fuels increased by 29.8%, the amount of produced PV electricity increased by 1,443.6 % (Belize Energy Unit, 2020a). To meet the energy demand in Belize, import from Mexico amount to 235,100 MWh, which is an increase of 2.2% compared to 2016 (Belize Energy Unit, 2020b). This means that Belize imports 42.4% of its energy demand and therefore, depends greatly from imported electricity.

Fig. 1. Overview map of Belmopan and selected city districts as study areas.

2.2. Structure-from-Motion analysis of Unmanned Aerial Vehicle campaign data

To achieve a spatial overlap between aerial data and interview data, both data collection campaigns cover the same city districts. In order to cover all building types occurring in Belmopan, six areas within the city were defined based on the results of the previous study by Warth et al. (2020).

Aerial image acquisition is performed by using an S110 Canon compact camera with a CMOS sensor, which can capture images up to a 4000x3000-pixel resolution (CameraDecision, 2021). The camera is mounted on a custom quad-copter in a nadir-view installation. During operation, the flight controller records the image location in geographical coordinates by using the GPS signal. The Android app QGroundControl (Dronecode, 2019) is used on a tablet device to calculate flight paths based on desired spatial resolution, flying height, and image overlapping. An image overlapping factor in front and side direction of 70% is defined to enable Structure-from-Motion (SfM) processing.

The aerial images are processed by applying SfM techniques (Ullman and Brenner, 1979), which is a very user-friendly and robust approach (Westoby et al., 2012) to

generate very high-resolution ortho-imagery and Digital Elevation Models (DEM) based on overlapping imagery. For SfM processing, the Metashape software by Agisoft is used (Agisoft LLC, 2021). Metashape allows the generation of elevation-related spatial raster products, such as the digital surface model (DSM), which describes surface heights, including all objects, and the normalized DSM (nDSM). It is normalized using the digital terrain model (DTM), which represents ground heights. The nDSM therefore only contains information on object heights. Additionally, optical orthomosaics are generated by using aerial imagery and height information.

2.3. Electric energy consumption analysis through a resident survey

To generate a data basis to estimate residential electricity consumption, a household survey in Belmopan was conducted in November 2019. The spatial sampling design for the interviews is generated based on the previous study on building types in Belmopan (Warth et al., 2020), for each residential building type, areas with dominating building type occurrence were identified and selected. After previous announcements using public communication channels, households were and asked to participate. The main focus of the household survey is on electricity consumption. Electric consumption is queried on the one hand by means of the yearly energy turnover (kWh) and on the other hand through the yearly paid electricity price. In both cases, residents were asked to provide bills in order to validate the resident's statements on energy consumption.

Based on the survey, specific energy consumption patterns are being determined for the residential building types, using standard statistical analyses such as mean annual energy consumption per building type.

2.4. Building footprints adaption and parametrization

For this study, the building footprints from a previous study conducted by Warth et al. (2020) are used in order to keep access to spatial, geometrical, and attribute information. Warth et al. (2020) integrated the building footprints into the

OpenStreetMap database (Haklay and Weber, 2008), where they can be downloaded.

The building data are manually adapted to the orthomosaic to benefit from the very high spatial resolution. Therefore, horizontal displacement is compensated and the footprints are corrected by adapting polygon vertices in accordance with building corners. In case buildings are covered by vegetation, such as trees or rampant shrubbery, these areas are mapped and excluded for solar analysis.

In order to provide building-describing parameters for training the building type classifier, several physical information is derived. Both building typology (see Fig. 2) and the attribute selection is strongly based on the previous study (Warth et al., 2020). To describe the geometry of the building footprints, the shape indices were found to be very useful (Lang and Blaschke, 2007). NDSM data provide information on building height and building volume. Classical DSM-based terrain describing products such as aspect and slope (Travis, 1975) provide information on roof slope and roof exposition. The information is processed using the SAGA GIS software (Conrad et al., 2015). Roof types can be described by the roof ridge occurrence, therefore roof ridges (RR) are manually captured using aspect and hillshade information. Besides the RR number and the total RR length per roof, RR densities related to total length and RR per area are calculated. Additionally, urban indices such as multi-scale building densities and distance parameters to places of urban functions are calculated: city center, places of education, central ring road, industry, US embassy, and distance to paved roads.

Fig. 2. Defined building types for Belmopan (Warth et al. 2020).

2.5. Building type classification: Random Forest

A Random Forest (RF) classifier (Breiman et al., 1984) was chosen to classify the building footprints. This machine learning approach generates a defined number of classification and regression trees (Breiman et al., 1984) with changing input attributes. Other than pixel-based RF approaches (Pal, 2005), spatial and geometric building footprint attributes serve as classification features. The RF classification parameters were adopted from Warth et al. (2020) in order to enable the comparison of classification results, namely to directly compare the influence of different spatial resolutions on classification accuracy (see **Error! Reference source not found.**).

A set of 33 parameters is provided for the RF classifier containing shape information of the building footprint, three-dimensional building information basing on the nDSM and spatial information such as density and distance information. During the training process, the RF evaluates the relevance of the parameters for the best classification results. An overview of the RF classification parameters is given in section 3.4.

For being able to evaluate and to compare the effect of the implementation of VHR UAV data instead of WorldView-1 imagery, the same parameters to train the RF classifier were chosen as in the previous study by Warth et al. (2020). Therefore, the Random Forest is defined by computing the majority building type classes of 1500

trees using five randomly selected features.

During the data collection campaign in November and December 2019, an in-situ dataset, containing 328 building samples, was generated. Besides interview-based information on electric power consumption, the dataset contains information on building type and GPS-based location information. In order to train the classifier and to evaluate the classification results, for each building type class the data set 65% of the data are randomly selected to train the RF classifier (213 samples) and the remaining 35% of the data (115 samples) to be used for accuracy assessment.

2.6. Single building photovoltaic potential approximation

The photovoltaic (PV) potential approximation was performed by relating estimated roof-based PV power production and predicted household electric consumption by building type.

2.6.1. Calculating annual PV electricity generation

The annual total electricity from a PV system can be calculated the following formula:

$E = P_k \times PR \times G$ (Šúri et al., 2007)

Where:

E is the annually produced PV energy and

P_k is the unit peak power, which is defined through the PV module efficiency and PV module area. Recent PV panel developer state realistic module efficiencies of 23% (pv magazine, 2021). In our study, we assume a standard PV module area for a 60 cell module of 1,650 x 992 mm (Doelling, 2017).

G is the annual global horizontal irradiation (GHI) (kWh/m2/year).

Data from the National Solar Radiation Data Base (NSRDB), provided by the

National Renewable Energy Library (NREL) (Sengupta et al., 2019), is used to calculate the climatological average annual GHI. The NSRDB offers GHI data on a 4x4km raster in a 0.5-hour spatial resolution with "mean percentage biases between 5% and 10%" (Sengupta et al., 2018). To predict the local insolation that accounts for inclination, exposition and shading effects, a local adaptation factor is calculated based on the DSM derived through the SfM-processing (see section 2.1) using SAGA GIS (Hofierka and Suri, 2002). This pixel-specific value quantifies the expected irradiation compared to flat terrain (COF), which is defined by the GHI. PR is the performance ratio, which describes the remaining part of PV energy after technical losses in the technical system. In tropical regions, the PR can vary between 0.70 – 0.85 in Peru (Romero-Fiances et al., 2019) and in Thailand between 0.89 for amorphous silicon modules and 0.815 for mono-crystalline silicon modules (Kim et al., 2014). Therefore, in this study, we decided to calculate with a conservative PR of 0.78.

2.6.2. Determination of maximum PV panel number per building

One scenario in this study is that only one field of roof (FOR) is maximally equipped with PV panels. To determine the best FOR, we reclassified each roof into eight classes using the local roof orientation, derived by the 0.02m-DSM (see section 2.1). For Belmopan, eight classes were chosen to avoid fragmentation of FOR but to not loose FOR due to generalization effects. Through visual building inspection, only one building with a gazebo-like extension showed FOR with more than eight field orientations. Aspect/surface orientation is linearly defined in degrees from 0° (north) to 359° (north). In order to avoid errors in the eight-class reclassification for northern oriented parts caused by the linearity of the, in fact, circular orientation, a constant value of 22.5° is added to the orientation to push northern orientations (337.5° - 22.5°) above 360°. The corrected orientation angles are then divided by 45 to achieve the eight-class reclassification with the orientation classes north, north-east, east, south-east, south, south-west, west, and north-west. Reclassified orientations larger than 8 due to larger values than 360° after adding the constants are then reclassified to

class north.

The eight-class raster dataset is subsequently converted into polygons, which allows the application of topological measures. Incorrect island polygons representing false orientations within FOR, caused by inaccuracies in the DSM, can be improved by deleting island polygons followed by closing the holes by the neighboring polygon.

Applying a negative spatial buffer of 0.3 meters, each FOR is reduced to consider the assembly area. To specify the maximum number of PV modules per area, GIS does not offer direct tools and approaches, as this is a geometrical issue and not a spatial issue. Therefore, to retrieve a maximum number of PV modules per roof, an iterative determination of the largest inner circles within is performed using the FME software (Safe Software Inc., 2021). For each circle radius, the number of installable PV modules can be determined. For the parts of the FOR not covered by the first maximum inner circle, the process of generating the maximum inner circle is repeated until four circles are generated. For this study, we chose a standard PV module size of 1,650 x 992 mm, or 1,637 m^2 respectively. Consequently, all maximum inner circles with a radius of $r < 0.962$ m, which is half of the module diameter, are removed. For the remaining circles, the maximum area covered by PV panels is calculated according to the number of installable PV modules dependent upon the radius (see table A.1 in the appendix).

2.6.3. Annual PV energy yield for best FOR per building and PV energy balancing

Although PV energy yield could be maximized by covering the complete roof with PV panels, this case is very unrealistic due to the monetary investment amount necessary. Therefore, for the optimum scenario 1, only the one FOR with the best energy potential was considered for PV module installation. Thus, the product of GHI, COF (section 2.5.1), and maximum PV module area (section 2.2.2) is generated to predict the annual PV energy yield per FOR, from which the FOR with the highest PV energy yield is selected for each building as the basis for the energy balance prediction. For balancing the PV energy potential, the difference between the average

energy consumption and the building-specific estimated PV electricity generation is formed. For a more realistic scenario 2, the PV energy balancing is performed analogously using only maximum of two PV panels on the best suited FOR.

3. Results

3.1. Structure-from-Motion processing

To achieve the desired coverage of the six defined test areas within Belmopan, due to limited UAV battery capacities, we performed 15 single flights. During these campaigns, a total number of 2.866 images were acquired. One test area was covered by a single flight, for full image-coverage of the other areas, multiple flights were necessary. To prepare the images for SfM processing in Agisoft Metashape, all images were renamed to achieve a consecutive numbering, as well a reference file was compared to provide GPS information on X, Y, and Z position from the EXIF files. The defined image overlap ratio of 70% in along and across-track direction at a flying altitude of 65m above ground resulted in a spatial resolution of the SfM results of 2.0 cm +/- 0.1. We resampled all results to a spatial resolution of 2.5 cm. Additionally, all SfM results were horizontally corrected to the orthorectified WorldView-1 scene from Warth et al. (2020) using a spline interpolation (Franke, 1982) and 50 control points for each test area to ensure the spatial integrity of the datasets. The SfM results cover a total area of 201.2 ha which leads to an image density of 14.2 images per ha at the given flight altitude. Table A.10 in the appendix provides an overview on the SfM processing details.

Using the Agisoft Metashape software, we processed raster DSMs for each study area based on the dense point cloud, calculated from the overlapping aerial imagery using the highest precision settings. In order to generate an nDSM, the dense point cloud was classified into ground points and non-ground points using Agisoft Metashape processes and standard settings. Differencing the interpolated ground point cloud from the DSM in QGIS was done to obtain the nDSM which represents building height information in all six study areas. The spatial resolutions of the elevation-based datasets vary between 1.9 and 2.1 cm within the six datasets.

The orthomosaic datasets of the study areas resulted in a slightly lower spatial resolution 2.2 to 2.4 cm. Therefore, to adapt the spatial resolutions, the datasets were resampled to a 2.5 cm spatial resolution. Slope and aspect of the surfaces are calculated based on the DSM information.

3.2. Electric energy consumption analysis

In order to analyze the residential electric energy consumption, we achieved a dataset, which concludes a cleaned sample size of 190 household interviews. The spatial sampling approach for the interviews resulted in the following interview distribution on the city districts: I: 9.4%, II: 24.2%, III: 21.6%, IV: 17.4%, V: 12,1%, VI: 15,3%. This interview distribution corresponds with the distribution of the detected buildings, as shown in Table 2. 63 interviewees could show bills to validate statements, especially in order to estimate expenses for electric energy. For the statistical analysis, we removed outliers using the two-fold standard deviation as the threshold above and below the arithmetic mean.

Using interview information on yearly electricity consumption and on yearly electricity expenses, the linear regression indicates an average electricity price of 0.42 BZD (see fig. 3), the Pearson's correlation coefficient (Havlicek and Peterson, 1976) of $r = 0.89$, and an $r^2 = 0.81$ show the correlation between the specifications on electricity consumption and electricity expenses and the robustness of the correlation.

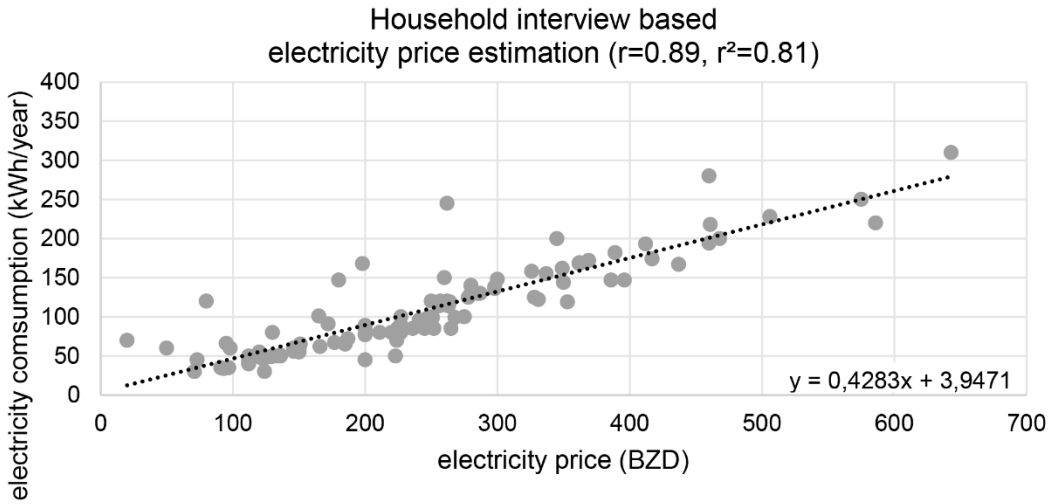

Fig. 3. Linear regression to determine electricity price in Belmopan.

By dividing monthly expenses by 0.42, the monthly household electric energy

consumption is calculated. Multiplying the monthly consumption by 12 results in the annual electricity consumption. The average electric consumption per household in Belmopan is 3,435.6 kWh/year with a standard deviation of 2,011.8, average monthly electricity expenses amount to 124.5 BZD with a standard deviation of 74.4. Considering socioeconomic differences for households in different building types as suggested by Warth et al. (2020), the analysis of electricity consumption considering the building types clearly shows different patterns. Statistics indicate mean annual electricity consumptions of 2,458.5 kWh/year with a standard deviation of 1,152.8 for BT 11, for BT 12 mean annual electricity consumptions of 3,220.7 kWh/year with a standard deviation of 1,765.2. Statistics show mean annual electricity consumptions of 4,042.1 kWh/year with a standard deviation of 2,240.2 for BT 13 and for BT 14 mean annual electricity consumptions of 6,276.2 kWh/year with a standard deviation of 2,766.6 (see Fig. 4).

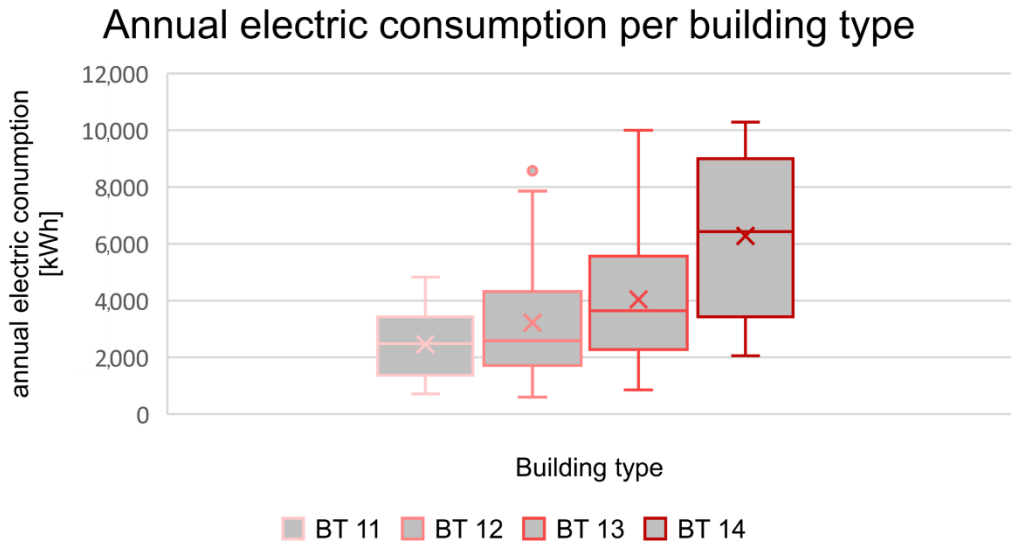

Fig. 4. Boxplots on building type specific electricity expenses.

Due to an insufficient number of interviews for multifamily houses, the analysis is only reliable for single-family houses. BT 21 (multifamily basic) has mean annual electricity consumptions of 3,123.8 kWh/year, based on three interviews. BT 22 (multifamily standard) has mean annual electricity consumptions of 4,257.1 kWh/year from four interviews, BT 23 (multifamily apartment) has one household interview,

411 which specified an annual electricity consumption of 1,428.6 kWh/year.
412 Besides recognizing relations between building types and electricity expenses, there
413 are spatial relations identifiable between city precincts and household electricity
414 expenses. Precincts I and VI show the highest electricity consumption with averages
415 of 4,076.2 kWh/year and 3,765.8 kWh/year respectively. The lowest electricity
416 consumptions are identified in precinct V with mean values 3,072.2 kWh/year.

417 **Table 1**
418 Residential electricity statistics in Belmopan. General overview and statistics in relation with
419 building types and city precincts.

Category	Average household electricity expenses (BZD/month)	Median household electricity expenses (BZD/month)	Average household energy consumption (kWh/year) (assuming 0.42 BZD/kWh)
Belmopan average	124.5 (+/- 74.4)	100	3,435.6
BT 11	98.7 (+/- 70.0)	88	2,458.5
BT 12	115.9 (+/- 65.4)	95	3,220.7
BT 13	141.5 (+/- 78.4)	128	4,042.1
BT 14	219.7 (+/- 96.8)	225	6,276.2
BT 21	109.3 (+/- 46.7)	96.0	3,123.8
BT 22	149.0 (+/- 89.9)	112.5	4,257.1
BT 23	50	50	1,428.6
Precinct I	169.9 (+/- 95.5)	180	4,076.2
Precinct II	107.4 (+/- 60.6)	99	3,648.4
Precinct III	108.6 (+/- 55.6)	88	3,662.2
Precinct IV	113.1 (+/- 58.1)	98	3,301.9
Precinct V	107.4 (+/- 65.2)	80	3,072.2
Precinct VI	147.5 (+/- 64.2)	139	3,765.8

420

421 *3.3. Building footprint adaption*

422 In a first step, the building footprints from Warth et al. (2020) were relocated to
423 remove position inaccuracies. Secondly, each building polygon was manually adapted
424 and reshaped by using the respective orthomosaic for the test area. In total, the UAV
425 mission covers a number of 1,619 buildings, ignoring buildings classified as non-
426 residential use. Table 2 gives an overview of the building numbers in the test areas. In
427 average, the buildings have a 139 m² footprint with a standard deviation of 81,5,
428 which shows a relatively large variation in building footprint sizes. The smallest
429 detected building footprint in Belmopan is 15 m² and the largest footprint is 719 m².

Table 2

Building distribution in the UAV-covered test areas in Belmopan.

I	II	III	IV	V	VI	sum
189	295	449	304	109	273	1619
(11.7%)	(18.2%)	(27.7%)	(18.8%)	(6.7%)	(16.9%)	

3.4. Building type classification

The RF building type classification for Belmopan resulted in a dominance of BT 12 followed by BT 13. As shown in Fig. 5, the percentage distribution is as follows: BT 11: 12.6%, BT 12: 47.4%, BT 13: 29.7%, BT 14: 7.9%, BT 21: 1.4%, BT 22: 0.8%, BT 23: 0.2%. The initial accuracy assessment rates the RF classification with a satisfying overall accuracy of 0.7. The complete confusion matrix is shown in Table 3. Considering the very low number of training and test samples for BT 22, the very low classification accuracy for this class is comprehensible. Ignoring BT 22 in the accuracy assessment, the overall accuracy increases to 0.73. As BT 11 mostly differs by construction materials from other building types, the low accuracies for BT 11 can also be understood. For BT 12, BT 13, and BT 14, which together represent 85.3% of all covered buildings in this study, user's accuracies range between 0.67 and 0.79, and producer's accuracies range between 0.67 and 0.77.

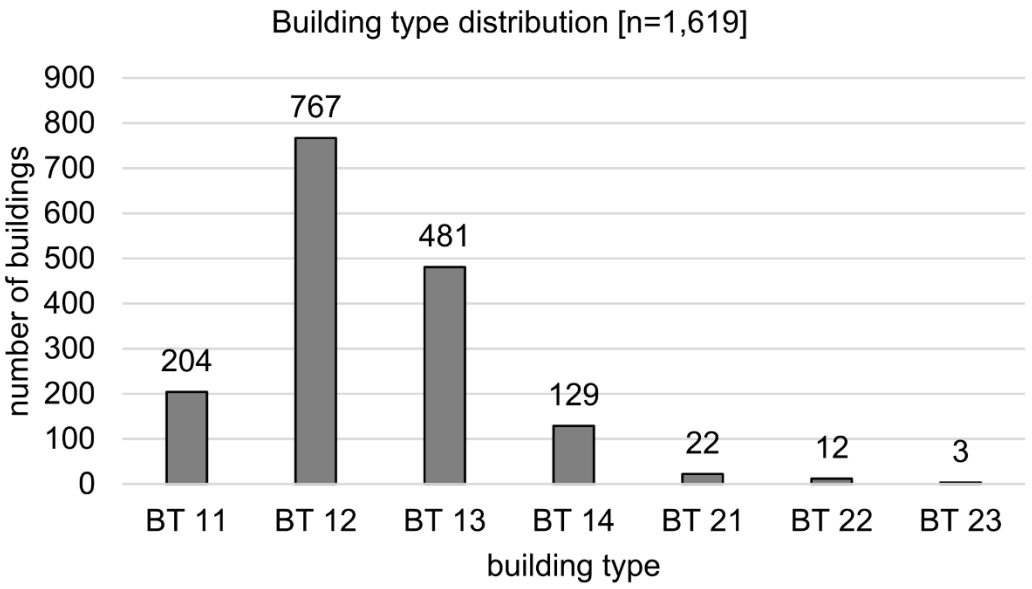

Fig. 5. Resulting building type histogram for Belmopan from Random Forest classification.

Table 3

Confusion matrix to determine the accuracy assessment for the building type classification in Belmopan.

		predicted						
	Building type	**11**	**12**	**13**	**14**	**22**	**sum**	**User's Acc.**
actual	**11**	6	6	1	0	0	13	0.46
	12	6	41	5	0	0	52	0.79
	13	0	6	24	2	0	32	0.75
	14	0	1	4	10	0	15	0.67
	22	0	1	2	1	0	4	0.00
	sum	12	55	36	13	0	116	
	Producer's Acc.	0.50	0.75	0.67	0.77	0.00		OA 0.70

Table 4 shows the ten most important ranked features for the RF classification related to the presented results. The most important classification criteria accordingly is the building footprint, followed by other building footprint related measures. The building height, derived from the nDSM, was ranked importantly as well as roof ridge information such as the number of roof ridges per building and the roof ridge density per building. Apparently, in this study building-specific attributes are sufficient to achieve satisfying classification accuracies.

Table 4

Feature list and ranking for Random Forest building type classification in Belmopan using the Gini inequality index (Menze et al., 2009).

Shape parameters	Gini ineq. index/ Rank	Three-dimensional parameters	Gini ineq. index/ Rank	spatial/distance parameters	Gini ineq. index/ Rank
Building footprint area (A)	0.152 #1	Building height (mean)	0.055 #14	Distance to bus line	0.031 #20
Roof ridge length [sum]	0.142 #2	Building height (median)	0.040 #17	Distance to paved roads	0.031 #21
Building footprint perimeter (P)	0.136 #3	Building height (standard dev.)	0.033 #18	Distance to industry	0.027 #23
Building D/A	0.134 #4	Building height (variance)	0.032 #19	Distance to ring road	0.024 #24
Building maximum distance (D)	0.124 #5	Roof slope (mean)	0.019 #26	Distance to education	0.022 #25

Roof ridge number	0.109 #6	Building density 100m	0.018 #27
Building P/A	0.102 #7	Distance to commercial center	0.014 #28
Roof ridge density [RR number/ A]	0.092 #8	Building density 250m	0.013 #29
Roof ridge length [standard deviation]	0.092 #9	Distance to public institution	0.012 #30
Building footprint corners	0.087 #10	Building density 150m	0.011 #31
rr_angle_stdev	0.081 #11	Building density 200m	0.011 #32
Roof ridge density [sum length/ A]	0.063 #12	Building density 50m	0.010 #33
Roof ridge length [mean]	0.058 #13		
Building shape index	0.044 #15		
shape_P/sqrt(A)	0.044 #16		
shape_D/sqrt(A)	0.030 #22		

Table 5 shows some key characteristics to describe and distinguish building types according to the findings of the study. Accordingly, clear differences can be identified in the building footprint area, building height, and the number of roof ridges.

Table 5

Building type characteristics in Belmopan: Mean values on building footprint area, building height and number of roof ridges.

building type	Area [m²]	Height [m]	rr_number
11 [204]	59.4	2.9	1.2
12 [767]	102.8	3.1	1.5
13 [481]	177.5	3.4	3.4
14 [129]	250.2	4.7	8.4
21 [22]	104.1	2.8	1.3
22 [12]	141.9	5.9	2.9
23 [3]	135.0	4.4	3.7

3.5. Single building photovoltaic potential approximation

The NSRDB raster dataset at Belmopan has spatial resolution of 898 m by 899 m (X and Y direction). The GHI in Belmopan varies between 1,852 and 1,859 kWh/m²/year, spatial statistics on the building footprints show an average GHI of 1,856.4 kWh/m²/year.

The solar processing using SAGA GIS and the UAV-based DSM revealed an optimum roof inclination for PV generation of 17° facing southwards in Belmopan. Zonal statistics based on single fields of roof (FOR) show average FOR inclinations of 23.2° with a standard deviation of 7.19, which indicate a well-fitting roof construction geometry for PV purposes.

3.5.1. Scenario 1: Most suitable field of roof fully fitted with PV panels

The FOR evaluation on the 1,619 buildings, covered by the UAV campaigns, reveals a total number of 4,546 FOR with a radius larger than 0.963 m which meets the required dimensions for PV module installation. As shown in the histogram in Fig. 6, based on FOR area without consideration of insolation characteristics, 50.9% of all FOR are suitable for the installation of 1 – 4 PV panels, another 26.9% of the FOR are suitable to install up to 9 PV panels. Fig. 7 illustrates analysis of the number of PV panels per FOR.

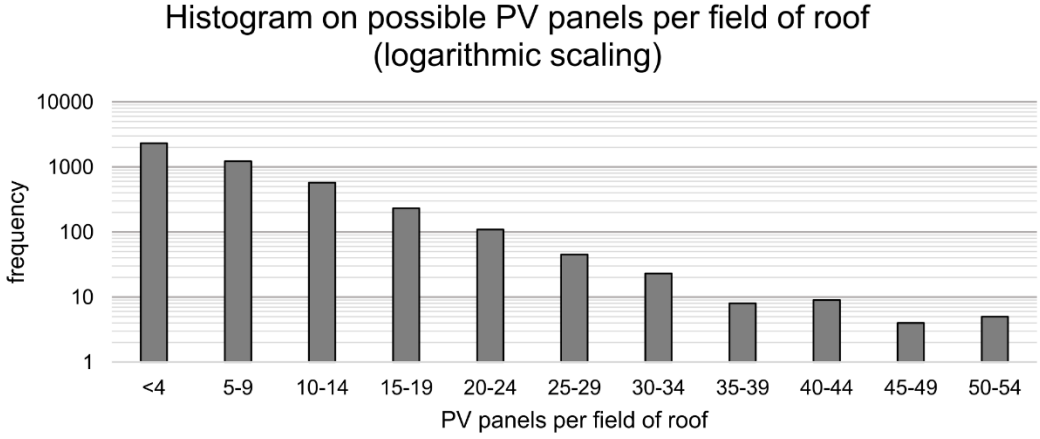

Fig. 6. Histogram of possible PV panels per field of roof in Belmopan.

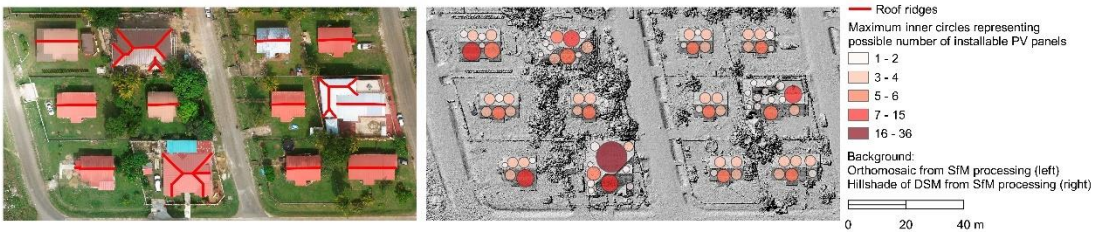

Fig. 7. Results of the SfM processing showing the orthomosaic combined with roof ridges (left) and the hillshade of the DSM combined with information on maximum installable PV panels (right).

The results of the PV energy production estimation, considering the best suited FOR by means of PV energy productivity, using the number of possible PV panels, the GHI, the local insolation factor, and the PR, show that 1,585 of all covered buildings are eligible for PV energy production. Twelve buildings have too large tree coverage to generate sufficient roof and height information, 22 buildings are too small or show too high roof fragmentation to host PV modules. The smallest PV power yield per building with optimal FOR usage is 979 kWh²/year and the building with maximum PV power yield with optimal FOR usage is 127,780 kWh/year. On average, the PV panels on the best-fitted roof can generate an estimated PV power yield per building of 22,965 kWh/year with a standard deviation of 17,949. Fig. 8 shows the histogram for the estimated PV power generation in Belmopan.

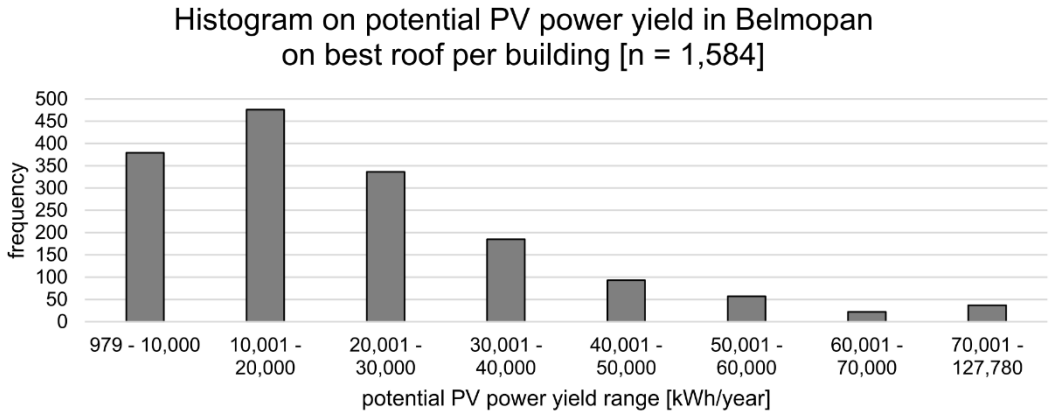

Fig. 8. Histogram on potential PV power yield in Belmopan considering best suited FOR.

The mean values of estimated PV power generation using the best-fitting roof per BT show clear differences in expected power yield (see Table 6). BT 11 assigned buildings are predicted to generate an average of 12,709 kWh/year from solar power,

BT 12 buildings show an increased average of 21,266 kWh/year. BT 13 and BT 14 buildings show similar averages, but also the highest estimated power yields, with 30,390 kWh/year and 30,633 kWh/year respectively. The average estimated PV power generation of the multifamily BT show similar values between 24,583 kWh/year and 26,718 kWh/year, the low number of reference data have to be considered and therefore limit conclusiveness of the statistics. However, general characteristics of PV power generation for multi-family BT can be recognized by these values. Table 6 displays the PV generation statistics for the building types.

Table 6

Average potential PV power generation per building type for the optimal scenario in dependence to building type using reference building type information from data collection campaign.

Building Type	mean estimated PV power generation [kWh/year]	standard deviation estimated PV power generation
11 (n = 38)	12,709	8,014
12 (n = 149)	21,266	13,707
13 (n = 78)	30,390	14,305
14 (n = 41)	30,633	17,019
21 (n = 7)	26,718	9,636
22 (n = 13)	24,983	13,252
23 (n = 2)	24,583	6,919
Total	22,965	17,950

In order to use the findings on PV power generation for urban planning purposes, the data is analyzed spatially. Therefore, the statistics of the estimated PV power generation per city is very insightful. In the individual city districts, there are major differences in average estimated PV power generation per building. The average PV electricity generated per building with 16,046 kWh/year is lowest in district V and highest in district II with 27,063 kWh/year and in district I with 26,949 kWh/year. For complete PV electricity generation characteristics see Table 7.

Table 7

Average potential PV power yield per building using best-fitted roof in dependence to the city district.

City district	mean estimated PV power generation [kWh/year]	standard deviation estimated PV power generation
I (n = 188)	26,949	14,752
II (n = 287)	27,063	19,366

III (n = 440)	24,304	19,794
IV (n = 288)	17,475	15,855
V (n = 102)	16,046	12,004
VI (n = 267)	22,801	17,027

3.5.2. Scenario 2: Maximum two PV panels on the most suitable field of roof

Applying scenario 2, where each roof is equipped with maximum of two PV panels, the 1,584 suitable buildings in average can generate 1,029.2 kWh/year photovoltaic energy with a standard deviation of 133.8.

Building-type related statistics in Table 8 show a range in PV power generation between 885.9 kWh/year for BT 11 and 1,112.0 kWh/year for BT 23, whereby the average PV yield for BT 11 clearly differ from the other building type yields. The differences for the average PV yield related to the city districts is not as distinct, buildings located in district V have an average PV yield of 950.9 kWh/year, whereas buildings in district I have the highest average PV yield of 1,074.3 kWh/year.

Table 8

Average potential PV power yield for scenario 2 with maximum two PV panels on best fitted field of roof.

Building type	mean estimated PV power generation [kWh/year]	standard deviation estimated PV power generation	City district	mean estimated PV power generation [kWh/year]	standard deviation estimated PV power generation
11	885.9	226.5	I	1,074.3	100.2
12	1,030.3	118.4	II	1,051.9	78.9
13	1,071.2	73.8	III	1,007.9	147.5
14	1,073.0	63.1	IV	1,014.0	163.4
21	1,003.9	104.2	V	950.9	181.8
22	1,027.1	87.4	VI	1,057.8	88.8
23	1,112.0	11.5			
Total	1,029.2	133.8			

3.6. PV energy balancing

According to the statistics on per building type, as presented in section 3.2 and in Table 1, we assume the following numbers on electric energy consumption for the PV energy balancing: BT 11: 2,458.6 kWh/year, BT 12: 3,220.7 kWh/year, BT 13:

4,042.1 kWh/year, BT 14: 6,276.2 kWh/year. Even though statistics on multifamily buildings base on very few sample sizes, these mean values are used for the PV energy balancing. For BT 23, the energy consumption is unrealistically low, therefore this value is replaced by the mean value for all buildings in Belmopan. This results in the following values for the multifamily types: BT 21: 3,123.8 kWh/year, BT 22: 4,257.1 kWh/year, BT 23: 3,435.6 kWh/year. As these multifamily buildings together occur only 37 times and therefore have represented 2.3% of all studied buildings, the small sample sizes have to be considered but do not have a major impact on the results.

Values on PV energy production are estimated individually for the single building, as described in section 2.5.

3.6.1. Scenario 1: Most suitable field of roof fully fitted with PV panels

In this optimal scenario, on each building, the most suitable FOR is fully fitted with PV panels to show the potential of PV energy production.

Out of 1,619 buildings, 35 buildings or 2.2% of the studied buildings are not suitable for PV energy production. This is due to FOR areas smaller than PV panel sizes one the one hand and too much foliage coverage by trees on the other hand.

The calculation of scenario 1 in average resulted in a positive PV energy balance of 1,847.2 kWh/year, which is an average PV energy coverage of 148.0% for all residential building types. The PV energy balances range between a deficit of -5,459 kWh/year for a BT14 building with high energy consumption and a low number of installable PV panels, caused by roof complexity, to a positive PV energy balance of 24,546 kWh/year for BT 12 building with comparably low energy consumption and a large and unfragmented roof. 975 out of 1585 buildings, which are suitable for PV panel installation, show positive PV energy balances. 85.6% of all buildings can cover 50% of their energy demand through the scenario 1 setting, 72.9% of the buildings can cover 75% of the energy demand with PV energy and even 60.2% of the studied buildings show a positive energy balance.

Table 9 gives an overview of average PV energy balances per building type and in

spatial relation to city precincts. Even though the standard deviations appear to be large, the mean PV energy balances in part show obvious differences. Unlike the other building types, BT11 has a negative PV energy balance with a mean deficit of -337 kWh/year. With a mean surplus of 1,318 kWh/year, BT 12 has a clearly positive PV energy balance. BT 13 with a mean PV energy balance of 3,489 kWh/year has the highest PV energy balance values. BT 14 with 1,670 kWh/year has distinctively lower PV energy balance, due to the high roof complexity, which prevents large undisturbed FOR. The multifamily building types BT 21, BT 22 and BT 23 in average show comparable surpluses in their PV energy balances of 2,353, 2,814 and 2,125 kWh/year respectively. Even though BT 11 shows negative PV energy balances, PV energy production can cover 86% of the energy consumption of the building type. The coverage ratios for the other building types show similar characteristics as the energy balances. BT 13 with averagely 186% energy surplus can almost produce twice the amount of electric energy as consumed. Due to the high energy consumption statistics in BT 14, the energy surplus is only 127%.

When comparing regional statistics, a characteristic stands out: The eastern city areas (IV and V) show positive PV energy balances, but clearly lower energy balances compared to the other study areas. BT 11 mainly is concentrated in these areas. The highest average PV energy balance has precinct II with 2,814 kWh/year. The standard deviations for the PV energy balances are very high, due to different FOR suitabilities for the single buildings, which are influences by FOR areas and FOR fragmentation.

Fig. ***9*** provides an overview on the statistical distributions of the PV energy balances.

Table 9

PV energy balance statistics for scenario 1 (1st and 2nd column) and scenario 2 (3rd and 4th column) in Belmopan related to building types and spatially aggregated to city precincts. Standard deviations are noted in brackets.

	Scenario 1: maximum number of PV panels on best FOR		Scenario 2: maximum two PV panels on best FOR	
	PV balance [kWh/year]	PV energy coverage [%]	PV balance [kWh/year]	PV energy coverage [%]
total	1,847 (+/- 4,049)	148% (+/- 108)	-2,607 (+/- 903)	29.5 % (+/- 6.5)
BT 11	-337 (+/- 1,930)	86% (+/- 78)	-1,573 (+/- 227)	36.0% (+/- 9.9)

BT 12	1,318 (+/- 3,420)	141% (+/- 106)	-2,191 (+/- 118)	32.0% (+/- 3.7)
BT 13	3,489 (+/- 4,443)	186% (+/- 110)	-2,971 (+/- 74)	26.5% (+/- 1.8)
BT 14	1,670 (+/- 5,528)	127% (+/- 88)	-5,203 (+/- 63)	17.1% (+/- 1.0)
BT 21	3,189 (+/- 2,625)	202% (+/- 84)	-2,120 (+/- 104)	32.1% (+/- 3.3)
BT 22	925 (+/- 2,779)	122% (+/- 65)	-3,230 (+/- 87)	24.1% (+/- 2.0)
BT 23	8,662	352%	-2,324	33.0%
Precinct I	2,353 (+/- 3,442)	161% (+/- 84)	-3,006 (+/- 1,072)	27.8% (+/- 6.3)
Precinct II	2,814 (+/- 4,443)	174% (+/- 117)	-2,601 (+/- 685)	29.5% (+/- 4.5)
Precinct III	2,125 (+/- 4,537)	158% (+/- 128)	-2,664 (+/- 1,011)	29.0% (+/- 6.9)
Precinct IV	837 (+/- 3,385)	117% (+/- 85)	-2,326 (+/- 807)	31.5% (+/- 7.1)
Precinct V	734 (+/- 2,624)	117% (+/- 83)	-2,171 (+/- 863)	32.3% (+/- 9.1)
Precinct VI	1,676 (+/- 3,926)	146% (+/- 99)	-2,712 (+/- 726)	28.9% (+/- 4.7)

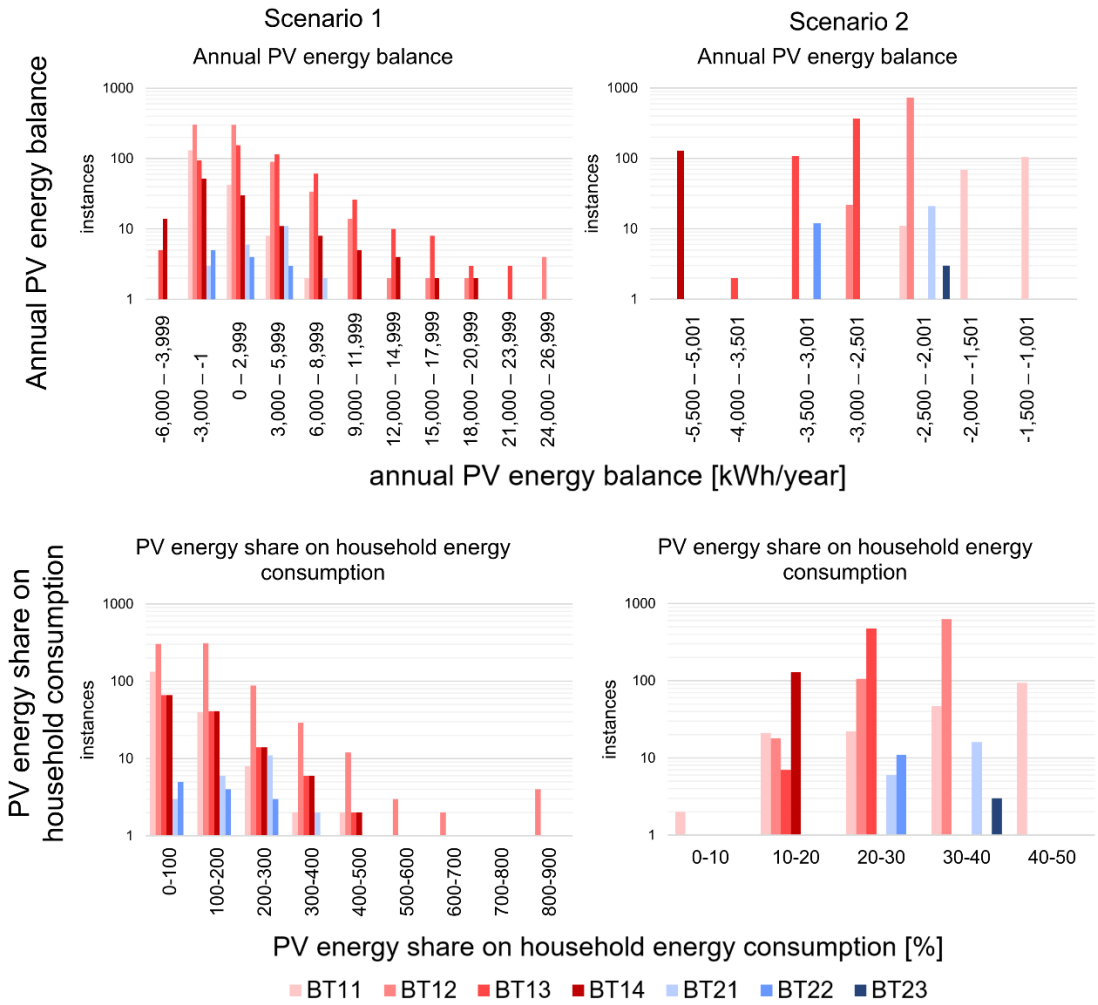

Fig. 9. Histograms on annual PV energy balances and PV energy share on household consumption. The left column displays the scenario 1 results, the right column displays the scenario 2 results.

3.6.2. Scenario 2: Maximum two PV panels on most suitable field of roof

For scenario 2 with two installed PV panels, no building can cover its energy

consumption. Although resulting in an average energy deficit of -2,607.5 kWh, the two-panels scenario enables reaching an average energy coverage ratio of 29.5%. The smallest deficit after PV energy balancing is 1,317 kWh/year for BT 11 with comparably low energy consumption, the largest energy deficit is 5,490 kWh/year for a BT 14 building with high energy consumption. through PV mean PV energy balance is a surplus of 719.2 kWh/year with a standard deviation of 135.7 or 179.8% respectively (see Table 9).

Due to differences in consumption patterns within the different building types, the PV energy balance statistics show quite large differences in the energy balances. BT 14 has the lowest PV energy balance with an energy coverage deficit of -5,203 kWh/year or 17.1% coverage ratio respectively. For single-family building types in scenario 2, BT 11 has the lowest energy coverage deficit of -1,573 kWh/year and the highest PV energy coverage of 36.0%. When considering only two PV per building, the energy coverage ratio obviously is closely related to the energy consumption, as the roof area has no impact in generated PV energy.

These described contrasts in comparison to scenario 1 appear as well, when regarding the regional statistics for Belmopan. The precincts with highest PV energy balances show the lowest PV energy balances with two PV panels and vice versa. The same characteristics occur for the energy coverage ratios, so that the highest energy coverage ratios are statistically achieved in precincts IV and V.

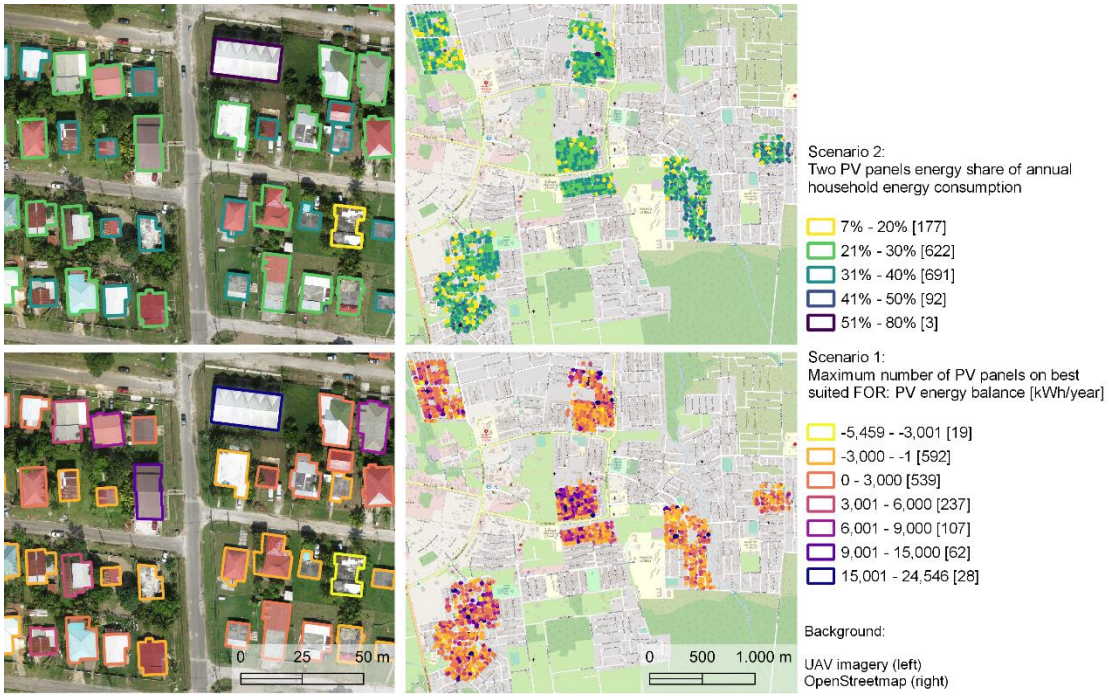

Fig. 10. Map showing PV energy balances on single building scale (left) and on city district scale (right). The upper row shows the two PV panel scenarios, the lower row shows the optimal scenario.

4. Discussion

Even though using an approach that underestimates the number of applicable PV panels per building, this study highlights two main findings. Firstly, the locally adapted building type is a very valuable proxy not only to estimate socio-economic parameters as presented by (Warth et al., 2020), but as well to spatialize electric energy consumption. Secondly, that the city of Belmopan is highly suited for increasing the share PV energy in the energy mix.

Using UAV imagery and derivate information, such as height, enables an increased classification accuracy, in comparison to the approach by Warth et al, (2020) using WorldView-1 and Planet imagery. Many relevant building characteristics and classification parameters, such as the number of building corners or building height can be determined more precisely using UAV data. Other parameters that have strong weight in the RF classification, such as roof ridge information, even cannot be determined based on satellite imagery. Therefore, using UAV data for building type classification has proven to be highly beneficial. In this study, building shape information, building footprint and height information as well as roof ridge

information had the most weights in the RF classification process. This underlines assumptions that three-dimensional data increase the understandability of urban structure (Zhu et al., 2019). In order to operationalize this approach, attention has to be laid on building detection. Accurate building footprint information is the basis and key for the success of the analysis, deep learning approaches promise high suitability in this regard. The increase of the accuracy in order to characterize multi-family buildings needs to be focused in the future, as these building types are very much underrepresented in Belmopan, but are dominating in many other cities.

The presented approach profits from the VHR UAV data. On this spatial scale, the data provide detailed information regarding roof structure which is essential to estimate possible numbers PV panels per field of roof. Although this study shows the potential of the approach, few details have to be considered in data collection and future research as well: Bright sunlight conditions during UAV data collection can cause negative effects in data quality due to high reflectivity on white and metallic roofs, and the estimation of possible number of PV panels is done here very conservatively and has room to be further improved.

By showing the relation between building type and electric energy consumption, the study results highlight the relevance of knowledge on locally adapted building types for urban planning. Not only socio-economic characteristics can be linked to the building type, but specific urban planning relevant information, as shown for electricity consumption. The use of building types to estimate other material flows, such as waste production and water consumption must be further analyzed.

Even though the main objective in planning sustainable energy supply is significantly increase the share renewable energies, in scenario 1 with maximum numbers of PV panels on the best suited FOR, 60.2% of all studied buildings have positive PV energy balances, the average PV energy balance per building is 1,847 kWh/year. This enables covering the annual household energy demand by 148%. In general, buildings with large and undisturbed roof areas achieve the highest PV energy yields. For this reason, BT 12 and BT 13 show the best energy balance statistics. BT 14 with high numbers roof ridges and BT 11 with smaller roof areas and often occurring foliage coverage

show lower energy balances. Based on the results of scenario 1, Belmopan could in theory achieve energy self-sufficiency for the residential sector through PV utilization. The two-panel setting in scenario 2 results in a mean PV energy coverage rate of 29.5% in Belmopan, which is an average deficit of -2,607 kWh/year. In contrast to scenario 1, BT 11 and BT 12 can cover the highest rates of electricity consumption with PV energy with 35.7% for BT 11 and 32.0% for BT 12. BT 14 can only cover 17.1% of its energy demands. These shares directly depend on the energy consumption in the building type. The NSRDB indicates a diurnal climate that leads to constant daily sunshine durations with incoming solar radiation between 6 a.m. and 6 p.m. and between April and August even two hours more (Sengupta et al., 2018). This constant PV electric energy availability enables the coverage of the electrical baseload from fridges, computers, and air conditioning systems. The threshold for roof installed PV panels of 1000 kWh/m²/year (Compagnon, 2004) in Belmopan is far exceeded by 1,856.4 kWh/m²/year. In combination with increases in module efficiencies, large PV electric energy yields can be achieved.

By only presenting the two scenarios, a constellation for complete energy coverage through PV energy can be shown and a constellation to relieve socio-economically weaker groups in BT 11 and BT 12 (compare Warth et al. (2020)) in terms of energy expenses, which suffer most from high energy prices due to lockdown-related increase of residential energy consumption during the COVID pandemic (Belmopan City Council, 2021b). Furthermore, from a planning and policy perspective, the high PV potential in Belmopan allows reducing the large share of energy imports by establishing a decentral and socially-fair PV technology. Therefore, we could show that a PV strategy in Belmopan can contribute to achieve SDG 7 “Affordable and clean energy”, SDG 10 “Reduce Inequalities” and SDG 11 “Sustainable Cities and communities”. Considering Belmopan as capital city, which relocation was caused by climatic effects, the establishment of a PV strategy can act as a beacon function for other cities or countries in the region.

The presented approach is suitable to support urban infrastructure planning, because it enables scenario evaluation: Considering information on building type, FOR area,

FOR suitability and flexible number of PV panels allow testing different settings for urban infrastructure planning and policy development, where the scenarios are only two of many possibilities, as the number of PV panels or the number of FOR can be varied. Presenting two scenarios for Belmopan, on one hand, shows the flexibility of this bottom-up approach but on the other hand, can provide decision-makers different options to develop sustainable urban planning strategies.

Therefore, urban planning can clearly benefit from the findings of this study: Not only enables this approach to assigning electric consumption and PV production values to single buildings, but the bottom-up approach allows to spatially aggregate information to gain information on precinct or city level. Hereby it is possible to characterize city areas in terms of electric energy consumption and PV potential. Knowledge of these parameters enables the implementation of appropriate planning measures and instruments to direct urban development on different scales. As demands for evidence-based planning are more frequently perceptible, this approach can deliver a database for urban planning but as well for PV energy policy development, as specific quantitative values are provided. The more relevant and reliable planning data are available, the better bridges can be built between scientists and practitioners to strengthen cooperation, as demanded by Sapena (2020).

The presented study is an alternative approach to relate electric consumption with a residential building type, instead of grouping buildings by means of thermo-physical parameters. Especially in regions, where energy consumption has irrelevant shares for heating purposes. However, this approach demonstrates particularly clearly that estimation solely based on earth observation techniques, cannot deliver sufficient data. Expert knowledge and survey information is the key to provide accurate data.

Author Contributions

Conceptualization, G.W.; methodology, G.W., A.B., O.A.; validation, A.B., G.W., V.H. O.A., K.F.; formal analysis, G.W.; investigation, G.W.; data curation, G.W., A.B., K.F.; writing—original draft preparation, G.W.; writing—review and editing, G.W., A.B., O.A.; visualization, G.W.; supervision, V.H., O.A.; project administration, V.H.,

O.A.; funding acquisition, V.H., O.A. All authors have read and agreed to the published version of the manuscript.

Appendices

Table A.1

Amount of PV panels per circle in dependence of radius.

Radius [cm]	Number of PV panels (1.650 x 992 mm)	Radius [cm]	Number of PV panels (1.650 x 992 mm)
96.3	1	351.7	18
129.6	2	388.9	22
161.1	3	445.9	30
192.9	4	481.0	36
216.1	6	540.9	45
277.6	10	574.5	52
318.2	14		

Table A.10

SfM processing details for the Belmopan UAV SfM processing.

Test area	Images	Covered area [ha]	Images/ha	Total points (dense cloud)	Points/m^2 (dense cloud)
I	483	29.8	16.1	849,870,712	2,844
II	539	32.6	16.5	978,717,386	2,999
III	779	49.4	15.7	1,840,465,320	3,722
IV	546	49.6	11.0	1,220,806,970	2,459
V	112	9.4	11.9	302,720,407	3,226
VI	407	30.4	13.4	874,278,662	2,873
Total	2,866	201.2	14.2	6,066,859,457	3,012

Declaration of Competing Interest

The authors declare no conflict of interest.

Acknowledgments

This research was funded under the grant no. 01LG1301K by the German Federal Ministry of Education and Research (BMBF) under the project “RapidPlanning”. We acknowledge support by Deutsche Forschungsgemeinschaft and Open Access

Publishing Fund of University of Tübingen.

We thank Dieter Steinbach and Andrea Schultheis from AT-Association for developing and bringing up the idea of deriving planning relevant information with relevance of building types. Many thanks to the Belmopan City Council for their hospitality, as well as for the fruitful and professional collaboration which made this work possible, including the provision of data and the tireless support during our field work. Without the support by the University of Belize, the household surveys would have not been conductible. Last but not least, we are very grateful for the language advising provided by Carolyn Elizabeth Duffy.

References

Agisoft LLC, 2021. Agisoft. https://www.agisoft.com/about/ (assessed 5 April 2021).

Audebert, N., Boulch, A., Randrianarivo, H., Le Saux, B., Ferecatu, M., Lefevre, S., Marlet, R. Deep learning for urban remote sensing.

Bachofer, F., Braun, A., Adamietz, F., Murray, S., d'Angelo, P., Kyazze, E., Mumuhire, A.P., Bower, J., 2019. Building Stock and Building Typology of Kigali, Rwanda. Data 4(3), 105. doi:10.3390/data4030105.

Ballarini, I., Corgnati, S.P., Corrado, V., 2014. Use of reference buildings to assess the energy saving potentials of the residential building stock: The experience of TABULA project. Energy policy 68, 273–284.

Belize Energy Unit, 2020a. Belize - Annual Energy Report - 2016, Belmopan City.

Belize Energy Unit, 2020b. Belize - Annual Energy Statistics Report - 2018, Belmopan City.

Belmopan City Council, 2021a. Belmopan City Council. https://belmopancitycouncil.org/welcome/ (assessed 29 January 2021).

Belmopan City Council, 2021b. Financial effects of the COVID-pademic on households.

Blair, T.L., 1973. Poverty of Planning. TBS The Book Service Ltd, Colchester.

Breiman, L., Friedman, J., Stone, C.J., Olshen, R.A., 1984. Classification and regression trees. CRC press.

Brito, M.C., Gomes, N., Santos, T., Tenedório, J.A., 2012. Photovoltaic potential in a Lisbon suburb using LiDAR data. Solar Energy 86(1), 283–288.

CameraDecision, 2021. Canon S110 Review. https://cameradecision.com/review/Canon-PowerShot-S110 (assessed 15 July 2020).

Chen, Y., Weng, Q., Tang, L., Liu, Q., Zhang, X., Bilal, M., 2021. Automatic mapping of urban green spaces using a geospatial neural network. GIScience & Remote Sensing, 1–19.

Chowdhury, P.K.R., Weaver, J.E., Weber, E.M., Lunga, D., St Thomas, M.L., Rose, A.N., Bhaduri, B.L., 2019. Electricity consumption patterns within cities:

application of a data-driven settlement characterization method. International Journal of Digital Earth.

Compagnon, R., 2004. Solar and daylight availability in the urban fabric. Energy and Buildings 36(4), 321–328. doi:10.1016/j.enbuild.2004.01.009.

Conrad, O., Bechtel, B., Bock, M., Dietrich, H., Fischer, E., Gerlitz, L., Wehberg, J., Wichmann, V., Böhner, J., 2015. System for Automated Geoscientific Analyses (SAGA) v. 2.1.4. Geosci. Model Dev. 8(7), 1991–2007. doi:10.5194/gmd-8-1991-2015.

Doelling, R.J., 2017. PV Modul-Größen im Überblick. https://www.energie-experten.org/erneuerbare-energien/photovoltaik/solarmodule/groesse (assessed 27 November 2020, in German).

Dong, R., Pan, X., Li, F., 2019. DenseU-net-based semantic segmentation of small objects in urban remote sensing images. IEEE Access 7, 65347–65356.

Dronecode, 2019. QGroundControl. Intuitive and Powerful Ground Control Station for the MAVLink protocol. https://github.com/mavlink/qgroundcontrol (assessed 19 November 2020).

[data] Eurostat, 2021. Supply, transformation and consumption of electricity. https://appsso.eurostat.ec.europa.eu/nui/submitViewTableAction.do (assessed 25 June 2021)

Everitt, J.C., 1984. Belmopan, dream and reality: A study of the other planned capital in Latin America. Revista Geográfica, 135–144.

Fenton, P., Gustafsson, S., 2017. Moving from high-level words to local action governance for urban sustainability in municipalities. Current Opinion in Environmental Sustainability(26-27), 129–133. doi:10.1016/j.cosust.2017.07.009.

Franke, R., 1982. Smooth interpolation of scattered data by local thin plate splines. Computers & Mathematics with Applications 8(4), 273–281. doi:10.1016/0898-1221(82)90009-8.

Friesner, J., 1993. Hurricanes and the Forests of Belize.

Guterres, A., 2018. Sustainable cities, human mobility and internationalmigration, New York.

Haklay, M., Weber, P., 2008. Openstreetmap: User-generated street maps. IEEE Pervasive Computing 7(4), 12–18.

Havlicek, L.L., Peterson, N.L., 1976. Robustness of the Pearson Correlation against Violations of Assumptions. Perceptual and Motor Skills 43(3_suppl), 1319–1334. doi:10.2466/pms.1976.43.3f.1319.

Hofierka, J., Suri, M., 2002. The solar radiation model for Open source GIS: implementation and applications 2002.

Huang, B., Zhao, B., Song, Y., 2018. Urban land-use mapping using a deep convolutional neural network with high spatial resolution multispectral remote sensing imagery. Remote sensing of Environment 214, 73–86.

Jazizadeh, F., Taleghani, M., 2016. Towards urban facilities energy performance evaluation using remote sensing. Procedia Engineering 145, 916–923.

Kearns, K.C., 1973. Belmopan: perspective on a new capital. Geographical Review, 147–169.

Kim, S., Koh, B., Park, J., Cheon, D., 2014. Comparative Study on Performance of Grid-Connected Photovoltaic Modules in Tropical Monsoon Climate under Thailand condition. Journal of the Korean society for New and Renewable Energy 10, 39–46. doi:10.7849/ksnre.2014.10.3.039.

Klopp, J.M., Petretta, D.L., 2017. The urban sustainable development goal: Indicators, complexity and the politics of measuring cities. Cities 63, 92–97.

Kottek, M., Grieser, J., Beck, C., Rudolf, B., Rubel, F., 2006. World map of the Köppen-Geiger climate classification updated.

Lang, S., Blaschke, T., 2007. Landschaftsanalyse mit GIS. Ulmer Verlag, Stuttgart.

Li, W., Liu, H., Wang, Y., Li, Z., Jia, Y., Gui, G., 2019. Deep learning-based classification methods for remote sensing images in urban built-up areas. IEEE Access 7, 36274–36284.

Lin, D., Gold, H.T., Schreiber, D., Leichman, L.P., Sherman, S.E., Becker, D.J., 2018. Impact of socioeconomic status on survival for patients with anal cancer. Cancer 124(8), 1791–1797. doi:10.1002/cncr.31186.

Liu, C., Huang, X., Wen, D., Chen, H., Gong, J., 2017. Assessing the quality of building height extraction from ZiYuan-3 multi-view imagery. Remote Sensing Letters 8(9), 907–916.

Malekpour, S., Brown, R.R., Haan, F.J. de, 2015. Strategic planning of urban infrastructure for environmental sustainability: Understanding the past to intervene for the future. Cities 46, 67–75. doi:10.1016/j.cities.2015.05.003.

Martínez, C.I.P., 2015. Energy and sustainable development in cities: A case study of Bogotá. Energy 92, 612–621.

Menze, B.H., Kelm, B.M., Masuch, R., Himmelreich, U., Bachert, P., Petrich, W., Hamprecht, F.A., 2009. A comparison of random forest and its Gini importance with standard chemometric methods for the feature selection and classification of spectral data. BMC bioinformatics 10, 213. doi:10.1186/1471-2105-10-213.

Musse, M.A., Barona, D.A., Rodriguez, L.M.S., 2018. Urban environmental quality assessment using remote sensing and census data. International journal of applied earth observation and geoinformation 71, 95–108.

Pal, M., 2005. Random forest classifier for remote sensing classification. International Journal of Remote Sensing - INT J REMOTE SENS 26, 217–222. doi:10.1080/01431160412331269698.

Poruschi, L., Ambrey, C.L., 2019. Energy justice, the built environment, and solar photovoltaic (PV) energy transitions in urban Australia: A dynamic panel data analysis. Energy Research & Social Science 48, 22–32. doi:10.1016/j.erss.2018.09.008.

pv magazine, 2021. JinkoSolar announces 23.01% efficiency for n-type monocrystalline panel. https://www.pv-magazine.com/2021/01/12/jinkosolar-announces-23-01-efficiency-for-n-type-monocrystalline-panel/ (assessed 9 December 2020).

Reckien, D., Creutzig, F., Fernandez, B., Lwasa, S., Tovar-Restrepo, M., Mcevoy, D., Satterthwaite, D., 2017. Climate change, equity and the Sustainable Development Goals: an urban perspective. Environment and Urbanization 29(1), 159–182.

doi:10.1177/0956247816677778.
Romero Rodríguez, L., Duminil, E., Sánchez Ramos, J., Eicker, U., 2017. Assessment of the photovoltaic potential at urban level based on 3D city models: A case study and new methodological approach. Solar Energy 146, 264–275. doi:10.1016/j.solener.2017.02.043.
Romero-Fiances, I., Muñoz-Cerón, E., Espinoza-Paredes, R., Nofuentes, G., La Casa, J. de, 2019. Analysis of the Performance of Various PV Module Technologies in Peru. Energies 12(1), 186.
Safe Software Inc., 2021. FME Software. Data Integration and Automation. Safe Software. https://www.safe.com/fme/fme-desktop/ (assessed 17 January 2021).
Sanchez-Rodriguez, R., Ürge-Vorsatz, D., Barau, A.S., 2018. Sustainable Development Goals and climate change adaptation in cities. Nature Climate Change 8. doi:10.1038/s41558-018-0098-9.
Sapena, M., Ruiz, L.A., Taubenböck, H., 2020. Analyzing Links between Spatio-Temporal Metrics of Built-Up Areas and Socio-Economic Indicators on a Semi-Global Scale. ISPRS International Journal of Geo-Information 9(7), 436.
Sengupta, M., Xie, Y., Lopez, A., Habte, A., Maclaurin, G., Shelby, J., 2018. The National Solar Radiation Data Base (NSRDB). Renewable and Sustainable Energy Reviews 89, 51–60. doi:10.1016/j.rser.2018.03.003.
[data] Sengupta, M., Xie, Y., Lopez, A., Habte, A., Maclaurin, G., Shelby, J., 2019. The National Solar Radiation Data Base (NSRDB), 3.1.1st ed.
Stark, T., Wurm, M., Zhu, X.X., Taubenböck, H., 2020. Satellite-Based Mapping of Urban Poverty With Transfer-Learned Slum Morphologies. IEEE Journal of Selected Topics in Applied Earth Observations and Remote Sensing 13, 5251–5263.
Statistical Institute of Belize, 2019. Annual Report 2018-19, Belmopan.
Šúri, M., Huld, T.A., Dunlop, E.D., Ossenbrink, H.A., 2007. Potential of solar electricity generation in the European Union member states and candidate countries. Solar Energy 81(10), 1295–1305. doi:10.1016/j.solener.2006.12.007.
Travis, M.R., 1975. VIEWIT: computation of seen areas, slope, and aspect for land-use planning. Department of Agriculture, Forest Service, Pacific Southwest Forest and …
Tu, W., Hu, Z., Li, L., Cao, J., Jiang, J., Li, Q., Li, Q., 2018. Portraying Urban Functional Zones by Coupling Remote Sensing Imagery and Human Sensing Data. Remote Sensing 10(1), 141.
Ullman, S., Brenner, S., 1979. The interpretation of structure from motion. Proceedings of the Royal Society of London. Series B. Biological Sciences 203(1153), 405–426. doi:10.1098/rspb.1979.0006.
United Nations, 2015. Transforming our World: The 2030 Agenda for Sustainable Development, New York.
United Nations, 2018. World Urbanization Prospects: The 2018 Revision, New York.
Vetter-Gindele, J., Braun, A., Warth, G., Bui, T.T., Bachofer, F., Eltrop, L., 2019. Assessment of Household Solid Waste Generation and Composition by Building Type in Da Nang, Vietnam. Resources 8(4). doi:10.3390/resources8040171.

Wan, K.S., Yik, F.W., 2004. Building design and energy end-use characteristics of high-rise residential buildings in Hong Kong. Applied Energy 78(1), 19–36.

Warth, G., Braun, A., Assmann, O., Fleckenstein, K., Hochschild, V., 2020. Prediction of socio-economic indicators for urban planning using VHR satellite imagery and spatial analysis. Remote Sensing 12(11), 1730.

Westoby, M.J., Brasington, J., Glasser, N.F., Hambrey, M.J., Reynolds, J.M., 2012. 'Structure-from-Motion' photogrammetry: A low-cost, effective tool for geoscience applications. Geomorphology 179, 300–314. doi:10.1016/j.geomorph.2012.08.021.

[data] World Bank, 2018. Urban Population. https://data.worldbank.org/ (assessed 19 March 2021).

Yi, Y., Zhang, Z., Zhang, W., Zhang, C., Li, W., Zhao, T., 2019. Semantic Segmentation of Urban Buildings from VHR Remote Sensing Imagery Using a Deep Convolutional Neural Network. Remote Sensing 11(15), 1774.

Zhu, Z., Zhou, Y., Seto, K.C., Stokes, E.C., Deng, C., Pickett, S.T.A., Taubenböck, H., 2019. Understanding an urbanizing planet: Strategic directions for remote sensing. Remote sensing of Environment 228, 164–182.